Master´s in Mechanical Engineering

ExoBike – Mechanical Component Development

Project presented to acquire the Master´s degree in Mechanical Engineering with specialization in Construction and Maintenance of Mechanical Equipment

Author

João Miguel Sousa Santos

Advisors

Luis Manuel Ferreira Roseiro

Coimbra Polytechnic - ISEC

Mechanical Engineering Department

Pedro Miguel Soares Ferreira

Coimbra Polytechnic - ISEC

Mechanical Engineering Department

Coimbra, September 2019

Acknowledgment

This work is co-financed by the European Regional Development Fund (ERDF), through the partnership agreement Portugal2020 – Regional Operation Program CENTRO2020, under the project CENTRO-01-0145-FEDER-00000 SAICT-POL/24013/2016: Exo Bike - Biomechanical Equipment for Restorative Therapy and Rehabilitation.

Dedico este trabalho aos meus pais,

Por me terem permitido frequentar o ensino superior

E me tornar na pessoa que sou hoje.

Obrigado Mãe

Obrigado Pai

Resumo

Muitas das vezes o processo de reabilitação é monótono e desmotivador devido à repetibilidade dos exercícios e falta de feedback ou ferramentas que permitam avaliar o progresso. Assim, tendo em conta que o exercício de bicicleta é muito utilizado para a reabilitação dos membros inferiores, foi criado o projeto ExoBike. De modo a combater tais fatores, a ExoBike consiste numa bicicleta equipada com sensores de força nos principais pontos de interação entre bicicleta e paciente. Assim é possível adquirir dados importantes para avaliar o progresso do paciente, bem como estabelecer metas e ajustar os exercícios conforme as necessidades do paciente. Alem desta componente de aquisição de dados, o projeto ExoBike engloba ainda uma vertente de realidade virtual, que junta com a componente de aquisição de dados, proporciona ao paciente uma experiência mais imersiva, tornando assim a prática de exercício para reabilitação mais divertida e motivadora. Este documento foca-se no desenvolvimento dos dispositivos mecânicos instalados na bicicleta para a aquisição dos dados do paciente. Para tal foi desenvolvido um selim capaz de analisar a postura do paciente, um guiador que caracteriza a força que o paciente realiza com os membros superiores, uns pedais capazes de analisar o movimento de pedalada e uns punhos que adquirem a força de preensão que o paciente é capaz de efetuar. Sendo que as metodologias de aquisição de dados dos dispositivos se baseiam em células de carga, extensometria elétrica por resistência e inteligência artificial. Os dispositivos foram desenvolvidos e otimizados com recurso a programas de desenho computacional, analisados através de métodos numéricos e analíticos, ensaiados através de prototipagem rápida com impressão 3D e produzidos com recurso a máquinas de fabrico subtrativo com controlo numérico. De modo a garantir o correto funcionamento dos dispositivos, estes foram sujeitos a uma serie de calibrações e testes funcionais com grupos de 3, 5 e 31 voluntários para corroborar as metodologias adotadas e avaliar as capacidades das mesmas. Sendo que os dipositivos indicaram uma correlação de 0.7, entre a postura do voluntario e a sua altura, e uma correlação elevada de 0.9 entre a massa do voluntario e a força exercida pelos membros inferiores. Entre outro tipo de correlações, os dipositivos foram ainda capazes de determinar, com uma fiabilidade 95%, o efeito de recalcamento psicológico quando os voluntários foram sujeitos a uma reação de defesa induzida nos membros inferiores. Considerando assim, que as metodologias e dispositivos desenvolvidos se encontram mais do que aptos para o objetivo pretendido de avaliação e monitorização do processo de reabilitação dos membros inferiores com recurso a bicicleta estática.

Abstract

Sometimes the rehabilitation process can be monotonous and demotivating due to the exercise's repeatability and lack of feedback or tool to evaluate the progress. Therefore, considering the high interest in cycling exercise for the lower limb rehabilitation, is created the ExoBike project. In order to fight the enunciated factors, the ExoBike consist in a normal bicycle equipped with force measuring sensors in the main connection points between bicycle and patient. Thus, is possible to acquire relevant data to evaluate the patient progress, settle goals and adapt the exercises to the patient needs. Besides this data acquisition component, the ExoBike project also includes a virtual reality component, which simultaneously with the acquisition one, provides a more immersive experience to the patient, making the rehabilitation exercise practice more interesting and motivating. This document focuses in the development of the mechanical devices, installed on the bicycle, for the data acquisition. Therefore, was developed a bicycle saddle capable to analyse the patient posture, a handlebar able to characterise the force from the upper limbs, pedals capable to characterise the pedalling motion and a bicycle handle to acquire the patient grip force. Thus, the data acquisition methodologies used on the devices developed are based on loadcell, strain gauges and artificial intelligence. The devices were subject to several functional tests with groups of 3, 5 and 31 volunteers to corroborate the adopted methodologies. Results indicate that the devices determine a correlation of 0.7, between volunteers´ posture and high, and a strong correlation of 0.9 between volunteers´ mass and lower limbs force. Among other kinds of correlations, the devices were able to identify the psychological repression effect, with a reliability of 95%, when the volunteers are subject to an induced defence reaction. Therefore, the devices are considered capable to perform the intended goals of evaluation and monitoring.

Index

Index of Figures

Index of Graphs

Index of Tables

Index of Equations

Symbology

mm	- *Millimetres*
Pa	- *Pascal*
N	- *Newtons*
ε	- *Strain*
ºC	- *Degree Celsius*
V	- *Volts*
Hz	- *Hertz*

FEM	- *Finite Elements Method*
FEA	- *Finite Elements Analysis*
CAM	- *Computer-Aided Manufacturing*
CNC	- *Computer Numerical Control*
HSM	- *High Speed Machining*
FDM	- *Fused Deposition Modelling*
PLA	- *Polyacid Lactic*
GUI	- *Graphical User Interface*
HSS	- *High Speed Steal*
RCTT	- *Radial Chip Thinning Theory*

1 - Introduction

The ExoBike project suggests the development of a bicycle which assumes the role of an exoskeleton for the rehabilitation and early diagnostic of injuries and degenerative diseases. The ExoBike structure is based on a normal bicycle frame in which are installed a group of sensors and actuators that interact dynamically with the user. The ExoBike allows the medical professional to adapt parameters in order to meet the patient requirements. The patient movements are monitored through a set of wireless sensors and a virtual reality environment is used to provide a more immersive experience. The system allows the acquisition, storage and processing of the data acquired by the sensors, which can be posteriorly analysed by qualified medical professionals.

The project ExoBike is composed by a multidisciplinary researching team, composed by elements from different engineering fields, namely, Biomedical Engineering, Electrotechnical Engineering, Computer Engineering, Mechanical Engineering and Mathematics. The project has been developed in the Applied Biomechanics Laboratory located in Polytechnic of Coimbra - ISEC, in partnership with two Physiatrists from Centro de *Medicina de Reabilitação da Região Centro – Hospital Rovisco Pais* – CMRRC-HRP, a Social Assistant and a Psychologist from *Centro de Apoio Social de Pais e Amigos da Escola Nº10* – CASPAE and collaboration from Tomar Polytechnic Institute.

The project is organized in different activities. The present work fits in the following different activities within the ExoBike project – mechanical project, legal and ethical guidelines compliance verification, usable and functional system testing, data analysis and project reporting.

The mechanical project activity contemplates the development, production and implementation of sensors and measurement methodologies, as also, the assembly of some mechanical components on the ExoBike.

The legal and ethical guidelines compliance verification activity is performed through the elaboration of a free and informed ethical consent process under the current data protection legislation, the Helsinki Declaration and the World Health Organization relative to the experiments with human beings.

The data analysis activity is performed using the data acquired from a set of functional tests performed with 31 volunteers.

The usable and functional system testing activity is elaborated through an inquiry form answered by each volunteer after performing the functional tests.

The project report activity is made during the project development phase by the elaboration of several scientific papers, of which some have been submitted and some have been published and presented in national and international congresses.

The present document reports the development, test and validations of four different devices, which are installed in strategic spots from the bicycle, able to acquire important rehabilitation data. Those devices consist in an instrumented bicycle saddle capable to analyse the patient posture, an instrumented handlebar to determine the forces exerted by the patient upper limbs, an instrumented pedals able to analyse the force applied by each lower limb and an instrumented bicycle handle capable to determine the patient gripping force.

Therefore, the document has an initial section where the ExoBike project is more deeply explained, the mechanical challenges are presented and is made a contextualization of the technologies used on the device's development. Then, is presented the development of each device individually in more detail, from idealization and design up to manufacturing and calibration. Lastly there are a section where are presented the preliminary functional tests, to warranty that the devices are working properly, and the results from the final functional tests elaborated with the volunteers. In the conclusion section, the author also indicates some improvements issues as guidelines for possible future work development.

2 - ExoBike Project

The physical rehabilitation process relies on the use of traditional gymnastic equipment with adapted exercises in order to meet the patient needs. The monitoring of those exercises, as also, the follow-up and evaluation of the patient progress is performed manually. Thus, the evaluation process is subjective and directly dependent of the medical experience.

The exercises used on the rehabilitation process are monotonous and uninteresting, which results in loss of interest and motivation from the patient. Also, the patient does not have any indication if the exercises are being performed in the correct way, without being from the therapist. Despite the effort from the medical team to provide motivation and real-time feedback to every patient in the room, considering the number of patients to each therapist, is impossible to the therapist being entirely dedicated to each patient.

Several studies indicate that the use of bicycle exercises is benefit for the rehabilitation of musculoskeletal injuries and the treatment of different medical conditions.

Some studies explore the benefits of aerobic exercises, such as cycling exercises, in Coronary Heart Disease (Lei Wang, 2017), Fibromyalgia (Terre, 2010), Depression (Joy, 2013) and Osteoarthritis (McKinney R, 2000), as also the benefits in Post Cerebrovascular Accident patients (Michal Katz-Leurer, 2006) (Peipei Han, 2017).

Studies conducted by Singhal *et al.* (2009) use tissue Doppler imaging and harmonic imaging with newly designed supine exercise platforms for bicycle exercise to facilitate the detection of exercise-induced diastolic dysfunction and pulmonary hypertension. The authors also propose that bicycle exercise echocardiography should be included as part of a comprehensive cardiac evaluation of patients with unexplained exertional dyspnea, due to the superior diagnostic capabilities of this method.

In 2011, a systematic review of the literature related with the benefits of cycling performed by Oja *et al.* (2011), indicate a clear positive relationship between cycling and cardiorespiratory fitness, as also, an inverse relationship between daily cycling exercises and all-cause mortality, cancer mortality, and cancer morbidity.

The emerging and development of technologies have as main purpose the improvement of the society life quality and well-being. Therefore, the technologies in the health sector also tends to evolve and emerge in order to improve the users experience quality, for both the patient and the therapist. The research and development of new physical rehabilitation products is a crucial step to introduce and develop the methods and technologies in this field. Therefore, a technological rehabilitation bicycle is developed – the ExoBike.

The goal of the ExoBike project is the development of an apparatus that enables the assistance during the physical rehabilitation process of lower limbs. This project results in innovative technologies and knowledge produced in the academic domain, which then can be used by the society.

Different studies have been conducted to study the interaction between user and bicycle. Already in 1968, Hoes *et al.* (1968) analyse the force applied on the pedal and crank of an ergometer. The authors have concluded that the force exerted on the pedal is maximum when the pedal is in the front position at about 90º from the vertical line, the passive leg is lifted partly by the active leg and toe-clips pedals are, probably, not always used to pull the pedals.

Studies have been conducted using cine film records with elementary mechanics, in order to study the forces that the bicycle rider applies in the pedals, saddle and handlebar (Soden & Adeyefa, 1979). The authors also compare the results obtained through this methodology with the force measurement values obtained from an instrumented pedal.

Bolourchi and Hull (1985) present a computer-based instrumentation system which measure the seat, handlebar and pedal loads together with the absolute pedal position during cycling exercises. The authors also present results and conclusion based on the data acquired with the system.

In 1993, researchers analysed the applied force on the bicycle saddle, handlebar and pedals during cycling exercise, by three different subjects (Stone & Hull, 1993). The authors also analyse the differences between the seated cycling and standing cycling, concluding that during the standing cycling the maximum normal force applied on the pedals reach substantially higher values, even exceeding the weight of the subject.

Gorka and Jordi (1996) designed a pedal to evaluate the pedalling technique in real conditions. The pedal designs are very similar to the most popular clipless pedals and can be used in road trials such as sprint or climbing, measuring three-dimensional movements. In the results, the authors present the maximum normal force and force distribution along crank revolution.

Studies have been conducted in order to develop a system that allows monitoring the power from a crankshaft whether in laboratory whether in field cycling (Jones & Passfield, 1998). The authors validate the methodology by comparing the results obtained with the results from a standard laboratory cycle ergometer.

In 2005, Bressel and Cronin (2005) has analysed the pressure applied on the bicycle seat in order to reduce seat injuries. The authors used a pressure-sensing mat applied on the bicycle seat and perform the study with male and female participates. The study concludes that work rate and hand position are factors that influence seat pressure, as also, male and female respond differently to the adjustments on those factors.

Chunfu Gao (2009) developed a sensor device to measure the pedal push force. The author used the finite element method to analyse the sensor structural behaviour and optimize strain elements mount position.

Petrona *et al.* (2012) equipped a downhill bicycle with strain gauges at the most significant components, stroke sensors at the suspension and accelerometers at the front axle, in order to collect data in the field. The study relies on the development of methodologies to evaluate the field loads spectra. Thus, the acquired data may be used in the components fatigues life prediction and the peaks values would allow defining the static overload value.

Also, in 2012, to study and understand the human balancing control, a study is conducted to develop an instrumented bicycle system to estimate the bicycle and human pose (Zhang, *et al.*, 2012). The system, developed by the authors, use a force sensor and an inertial measurement unit. In 2013, Yizhai *et al.* (2013) present a computational scheme to estimate the rider trunk pose and the bicycle roll angle using inertial and force sensor with an extended Kalman filter-based sensor fusion. The estimation scheme is extensive experimented on indoor and outdoor riding.

On the next year, Giubilato and Petrone (2014) present a study from the structural behaviour of a bicycle saddle fixation mechanism. In order to perform the experimental stress analysis, the authors used strain gauges. In the results section, the authors compare two different situations, one on road cycling and other on mountain cycling.

Also, studies are performed to measuring the vibration comfort of the cyclist and measuring the load distribution at bicycle components (Vanwalleghem, *et al.*, 2015).

Therefore, the ExoBike project takes advantage of the academic methodologies already developed to study the user interaction with the bicycle, as also develop new methodologies and apply them in the rehabilitation domain.

Authors have already present similar projects (Lee & Jeong, 2018) (Fluet & Deutsch, 2013) (Deutsch, *et al.*, 2013) (Ranky, *et al.*, 2014) (Farjadian, *et al.*, 2013). However, this is an incipient field and every contribution is essential to the development of funded knowledge, in order to create more robust products.

2.1 - Project Description

The ExoBike project is a fusion between different engineering fields. The computer engineering is responsible to develop a virtual environment, as also, a patient and physio therapist software application. The virtual environment provides a motivational atmosphere and real time biofeedback, from the sensors connected to the Exobike. The software applications intent to store the collected data from rehabilitation sessions for posteriorly analysis and progress evaluation. Thus, the patient is more motivated and is able to visualize the rehabilitation progress evaluation, this way the patient is more independent from the physio therapist, which may improve his self-esteem.

The electrotechnical engineering concerns with the development of methodologies to study the patient posture and devices to transmit the data from the bicycle to the software applications. The patient posture determination is based on Inertial Measuring Units sensors, while the data from the ExoBike sensors is transmitted to the software applications through Bluetooth Low Energy with costume electronic circuit boards.

The mechanical engineering works in the development of mechanical components to study the interaction between the patient and the bicycle. The devices consist in electromechanical interfaces installed on the principal contact points between patient and bicycle, namely: saddle, pedals and handlebar. Also, the mechanical engineering is responsible to corroborate the devices developed and perform field functional tests for statistical study. The Figure 2.1 presents a simple illustration of the different components from the Exobike.

Figure 2.1 – ExoBike Components.

This report presents the mechanical engineering components developed for the Exobike project and the functional tests performed to their validation.

As previous referred, several researches have been conducted to study the interaction between human being and bicycle. So, measuring interfaces have been already developed in order to characterize the forces applied on the bicycle saddle, pedals and handlebar. However, those studies are mostly inserted in an academic domain. Despite the studies are not oriented to the rehabilitation domain, those represent a solid background for the development of the required methodologies and devices.

The ExoBike project intents to not only be used in the usual hospital and rehabilitation practice environment, but also in a home environment, warranting a continuous remote monitoring of the patient evolution. This long-term remote monitoring may provide important information to the medical and physiotherapist team. Thus, the project, also intent to accomplish several challenges of an aging society.

The development of this project introduces new technology in the sports and rehabilitation field. As a rehabilitation tool, the Exobike intends to improve the rehabilitation process and achieved results. Thus, contributing to the improvement of the society life quality. In the sports field, the project introduces tools that enable the evaluation of the athletes' technique and can help in the improvement or development of new techniques.

2.2 - Mechanical Components

During the cycling rehabilitation exercises is important to evaluate the patient posture, balance and stability, as also, the way the patient performs the lower limbs cycling movement and the gripping force applied on the handlebar. Those parameters are important rehabilitation indicators, once the rehabilitation process is not focused on the development of muscular mass, but also in providing, the patient, with all the required conditions to perform the quotidian life activities. Also, by analysing the patient grip force is possible to determine if the patient is comfortable or apprehensive, since when the patient is nervous, he tends to grab the handlebar firmly.

Therefore, considering that the main contact points between patient and bicycle are the saddle, the handlebar and the pedals, the mechanical engineering part have been responsible for the development of an instrumented saddle, handlebar, grip device and pedals. The saddle device must be capable of analysing the patient posture and force asymmetries according the sagittal and coronal plane. As, the instrumented handlebar and grip device must be able to study the patient stability and balance. In order to study the balance between the lower limbs, the pedals must be capable of acquiring the force exerted by each one of them, independently, and characterize all the pedalling cycle.

Different methods and options have been considered to develop each measurement interface device, in order to achieve the intended results.

To study the force applied on the saddle, two different methods was considered, a piezoresistive blanket methodology and a structural behaviour loadcell methodology. The piezoresistive blanket methodology foresee the use of a piezoresistive blanket applied in the bicycle saddle surface to acquire the different force values over the surface. The structural behaviour loadcell methodology foresee the use of three loadcells applied under the bicycle saddle to determine the resultant force and its location. The piezoresistive blanket provides more detailed information, since that it indicates de force applied in every point. However, since that the piezoresistive blanket provides more information, it also requires much more data processing than the three loadcells methodology. Furthermore, since that the information from the piezoresistive blanket is more complex, it is harder to the medical team understand the acquired values and get conclusions from the user posture and behaviour. In terms of implementation, the three loadcells methodology are simpler than the piezoresistive blanket, since that the loadcells only need to be bolted to the saddle, while the blanket needs to be installed and fixed, ensuring that it do not moves over the time, to get stable and realistic values. According to the advantages and disadvantages that each methodology represents, is decided to use the structural behaviour loadcell methodology.

Thus, the Instrumented Saddle Device is an instrumented bicycle saddle with three loadcells, which measure the vertical force in three different points, as illustrated in Figure 2.2. The vertical forces are the most significant ones applied on a bicycle saddle. By acquiring the force values applied in three different points is possible to determine force asymmetries on the sagittal and coronal planes during the pedalling movement, which can be used as indicators for the rehabilitation process.

Figure 2.2 – Instrumented Saddle Device.

To study the forces applied on the handlebar, three different methods are considered. The first method consists in the application of a rotating hub and a loadcell in each side of the handlebar. Thus, with the loadcell is measured the applied force, while the rotating hub allow the handle to rotate warranting that the loadcell is always faced to the applied force direction. The second method considered foresee the development of an interface, to apply in each handlebar side, with two built-in loadcells that measure the applied force in two different directions. Therefore, is possible to determine the applied force magnitude and direction. The third method analysed, consists in the installation of two strain gauges, in each handlebar side, to measure the handlebar deformation in two different directions. Thus, assuming that the handlebar operates in the structural elastic domain, through a calibration process is possible to determine the applied force magnitude and direction.

The first method is the simplest one, since that is acquired only one sensor value, in each handlebar side, and that value does not need a processing operation, i.e. the value acquired already correspond to the applied force magnitude. However, this method implies cutting the handlebar to install the loadcell and the rotating hub, as also it introduces some instability to the system utilization, since that the handlebar are free to rotate. The second method is the most complex one, it contemplates the development of an interface with built-in loadcells. The interface has to be designed, analysed and produced. This method also implies cutting the handlebar in order to install the interface. However, since that the interface has built-in loadcells, it is the method with better expected reading values. The third methodology considered is based on the same working principle as the second method. However, instead of use loadcells, are used strain gauges. Thus, is not as evasive as the previous methods considered, since that is not necessary cutting the handlebar. This method is simpler to implement than the second method and more stable during the utilization than the first method. However, is expected that the values acquired from the strain gauges are less precise, that the values from the loadcells in the second method, since that the loadcells have signal stabilization systems and they are easier to calibrate. Considering the advantages and disadvantages inherent to each method considered, is decided to implement the third method, i.e. installation of two strain gauges in each handlebar side.

The Instrumented Handlebar Device consists in a bicycle handlebar equipped with four strain gauges, as illustrated on Figure 2.3. This device determines the force that the rider applies in each side of the handlebar, as well as the force direction angle in the handlebar cross section plane. Both these indicators are relevant to study the user stability, balance and posture.

Figure 2.3 – Instrumented Handlebar Device.

In 1993, Stone *et al.* (1993) had developed a similar methodology to measure the loads that a cyclist applies on the bicycle handlebar during standing treadmill cycling, demonstrating that the strain gauges methodology is viable. Also, the Instrumented Handlebar Device and Instrumented Saddle Device viability are demonstrated in the scientific paper *Identification of forces applied on seat and handlebar from a static bicycle* (Santos, *et al.*, 2019), presented in the *8º Congresso Nacional de Biomecânica*, proven that the used methodology can provide analysable indicators.

The force applied on the pedals is studied through a specific device developed to measure the vertical force applied by the feet in each pedal. According to the results obtained by Stone & Hull (1993), the vertical force is the most significant force applied on the bicycle pedals. Thus, the vertical force can be used as a performance indicator. Two designs have been considered in order to acquire the vertical force applied on the pedal. The first implies the full development a pedal with a built in loadcell, this way is created a robust system with a design very similar to the normal pedals that the patient is used to see. The second design take advantage of a mountain bike pedal cleat mechanism, a planar loadcell is installed on top of the cleat pedal, while the electronic data transmitting board may be installed below the cleat pedal. This way the system is easily installed and uninstalled, as also, it can be easily installed in a normal bicycle for laboratory or field data acquisition.

Considering the peculiarities of each design, is decide to implement the design based on the mountain cleat pedal mechanism due to its versatility and modularity as Illustrated in Figure 2.4.

Figure 2.4 – Instrumented Pedal Device.

The Instrumented Pedal Device already have its working methodology proven on the scientific paper *Development of a Pedal Force Measurement Interface for Rehabilitation Purposes* (Santos, et al., 2019), presented in Instituto Piaget University Campus of Viseu at the International Congress of Health and Well-being Intervention, 2019.

To acquire the gripping force exerted by the user, is developed an Instrumented Grip Device, illustrated in Figure 2.5, with a methodology based on the material elastic domain deformation and electro resistive strain gauges.

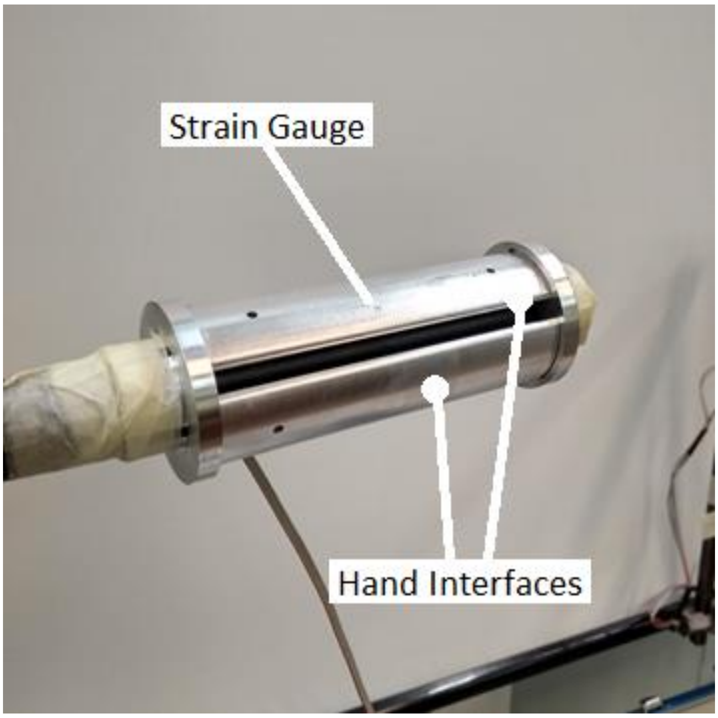

Figure 2.5 – Instrumented Grip Device.

The methodology consists in a beam simply supported in both extremities and two equal loads equally distanced from the beam middle. With this configuration, the beam middle section is only subject to pure flexion and is the location where the displacement is higher, which are two advantages for the strain gauges installation. Thus, the strain gauges provide better quality data, since it reads higher strain values, and the contribution for that values are exclusively from flexion, which simplify the calibration process.

After this introduction to the ExoBike project, the present document is divided in three main sections. The development and production of the electromechanical interfaces, where is explained the development and production process of the instrumented saddle, handlebar, pedals and grip device. The functional tests and data acquisition, where the developed devices are corroborated and a statistical analysis are made in order to study the results obtained from 31 volunteers, through a free and informed ethical consent process. In the end, the conclusion and future work, where the achieved results are commented and possible improvements to the developed devices are stated.

2.3 - Used Technologies

Before entering in the deep details about the development of the electromechanical devices, is presented a brief introduction to the technologies used in the development of the present work, in order to help the reader better understanding the technical terms used through the document.

2.3.1 - Finite Elements Method (FEM)

In Structural Engineering domain, the Finite Element Method (FEM) is used to analyse the stress and deformation state of a solid with a specific geometry and exposed to defined external interactions. The analysis of structures, such as, buildings, bridges and airframes, using FEM is known as Finite Element Analysis (FEA). When a structure is developed, is usual run a sequence of analysis and modifications in order to accomplish an optimal solution that satisfies the functional requirements, regulations and economical limitations (Azevedo, 2003).

The FEM consists of an approximation of complex geometry designs by many small elements that are simple to calculate. By applying the material properties to the elements, it is possible to simulate the designed part. That approximation, created by the small elements, is known as "mesh". As the model is an approximation from the intended design the results are an approximation too. However, a well-tuned element size has an error small enough to be considered insignificant. In order to find the optimal element size, different simulations with different element sizes must be executed. When the elements are too large, there may occur "underfitting", which is when the elements poorly represent the intended geometry. On the other hand, when the elements are too small there may occur "overfitting", which is when elements start to display distorted values that do not represent the reality.

In Structural FEA there are three main types of elements: beam elements, solid elements and shell elements. The beam elements only allow calculations in one dimension, i.e. only simulate traction or compression. They are commonly used to simulate frameworks and trusses systems. The solid elements allow calculations in three dimensions. However, they only calculate the traction and compression over the three axes. They are mostly used to analyse robust geometries. The shell elements also allow calculations in three dimensions, but they do not only calculate the translation component, but also, the rotations over the three axes. However, the shell elements can only be used to simulate thin geometries, i.e. when the length is considerably bigger than the thickness, such as, sheet metal parts.

Considering the elements calculation capability, the shell elements are the ones which provide higher resolution results. Thus, the beam elements are the ones which provide lower resolution. However, as the shell elements provide higher resolution, they require more computation capabilities. Thus, there is a direct relation between resolution and computation capabilities.

2.3.2 - Computer Aided Machining (CAM)

With the advance in technology, the automation of processes had become increasingly a reality. This enable the reduction of waste and production time, while increasing quality and complexity. A product from this evolution are the computer numerical controlled machinery, which make part of Computer-Aided Manufacturing (CAM) domain.

CAM can be defined as the use of computer systems to plan, manage, and control the operations of a manufacturing plant through either direct or indirect computer interface with the plant´s production resources (Groover & Zimmers, 1984).

Computer Numerical Control (CNC) is often used with resource of Computer-Aided Design (CAD) and Computer-Aided Manufacturing software. With CAD is designed a 3D model of the piece that meet the project requirements. Then, the 3D model can be submitted to a Computer-Aided Engineering process, e.g. FEA, or can be directly introduced in a CAM software. This software analyses the 3D model in order to extract all the required functions and commands which enable the CNC machine turns the 3D model into a real workpiece, through a post-processor.

Then, that information can be loaded to the CNC machine post-processor in order to start the manufacturing sequence. This manufacturing process is considerably automated and allow quite fine tolerances, which enable the production of workpieces very similar to the geometry created in the CAD software. Therefore, the benefits of CNC are not only the production process automation, as well as the process repeatability so after confirming the manufacturing sequence, it can be easily repeated since all the initial conditions are kept. Although, CNC machines allow the production of more complex geometries workpieces when compared to the conventional production machines.

The post-processor, which receive the coded instructions and commands, consist in a microprocessor capable of operate and monitor a machine tool accordingly to the loaded information. The processor receives the coded information, interprets how it is meant to be implemented and send signals to the actuators in order to perform the defined physical movements required to produce the workpiece (Anon., 2019).

In CNC milling centres, as the ones used to produce the workpieces developed in the present work, usually follows the workflow: roughing, semi-finishing, finishing.

The roughing phase is to approximate the raw material to the final workpiece geometry. In this phase tolerances are not considered, leaving some extra material on the workpiece, for the finishing process. The main concern is removing the material as quick as possible.

The semi-finishing phase is optional, depending on the required tolerance level. The load derived from the machining process induce flexion on the machine tool, which leads into dimensional errors. The higher the load the greater the deflection will be. The purpose of the semi-finishing phase is reducing the load applied on the tool during the finishing phase by leaving just a thin layer of material that will be removed during the finishing phase.

Finishing phase is the last operation done to a workpiece. This operation implicates small tool load, faster movements and high tool rotation, in order to achieve the required tolerances. When the tool rotation is very high, it is considered High Speed Machining (HSM). If the piece is moved keeping the tool tangent to the workpiece surface it is known as counter milling. Both HSM and counter milling are specific finishing processes that ensure high dimensional accuracy.

2.3.3 - Strain Gauges

The strain gauges are the fundamental sensing element for many types of sensors, such as pressure sensors, load cells, torque sensors, position sensors, among others.

They consist of a pattern of resistive foil encapsulated on a stripe of a backing material, and work based on the principal that the electrical resistance of a foil changes with the stress that the foil is subjected, in a well-defined relation.

When a strip of conductive metal is stretched it becomes thinner and longer resulting in a higher electrical resistance measured on the extremities of the strip. If the strip is compressed, without bucking, instead of stretched, the opposite occurs i.e. the strip becomes thicker and shorter that leads into an overall lower electric resistance. Thusly, the strip can be used to measure physical force by reading its resistance.

The majority of strain gauges resistance range from 30 Ohms to 3 kOhms and are smaller than a postage stamp. Therefore, they are frequently used to measure the stresses on mechanical structures and pieces with research, development, maintenance and optimization intent.

Usually, the strain gauges are connected in a Wheatstone Bridge configuration, which may have a combination of four active strain gauges, two active strain gauges with other two precision resistors or one active strain gauge with three precision resistors.

The configuration with four active strain gauges is denominated Full Wheatstone Bridge, while the configuration with two and one active strain gauges are denominated Half Wheatstone Bridge and Quarter Wheatstone Bridge, respectively. As illustrated on Figure 2.6.

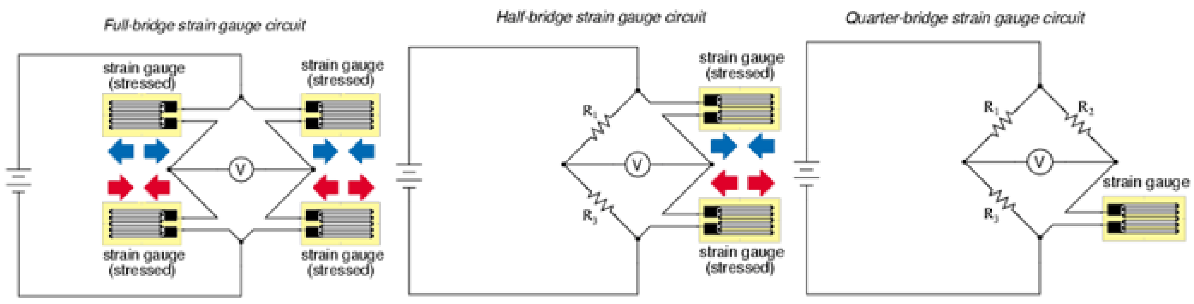

Figure 2.6 – Wheatstone Bridge Strain Gauges Configurations **(Anon., 2018)**

When the Wheatstone Bridge is excited with Direct Current (DC), as deformation is applied to the strain gauge, its resistance varies and unbalance the Wheatstone Bridge, resulting on a small potential difference, in the range of millivolts. This potential difference is amplified and used as output signal.

The relation between the deformation applied to the strain gauge and the resulting potential difference is commonly given by a first-grade equation. Thus, through the equation and the potential difference is possible determine the deformation applied on the strain gauge.

In the case of the Quarter Wheatstone Bridge, the precision resistors are selected in order to warranty that the bridge are symmetrically balanced. Thus, when no force is applied on the strain gauge the voltmeter measure zero potential difference. As the strain gauge is compressed or lengthened, its resistance decreases or increase, respectively. This unbalance the bridge and, consequently, produce a potential difference that is acquired by the voltmeter (Anon., 2018)

2.3.4 - Artificial Neural Networks

The Artificial Neural Networks are mathematical models, inspired in the human biological neural system behaviour. As the Biological Neural Networks, they are composed by simple processing elements designed as neurons or nodes, which are interconnected between them. Each node receives an input signal from other nodes or from an external stimulus, processes it through a transfer function and send an output signal to other neurons or to an external output.

Individually, the neurons do not have a good performance or precision, however together in a network they can achieve impressive results. The Artificial Neural Networks are able to learn from already known cases and then generalize to cases never tested before, is this characteristic who makes Artificial Neural Networks a powerful and interesting tool. They are used in different types of problems especially in forecasting due to their capability of input-output mapping.

An Artificial Neural Network is usually composed by different layers of neurons, an input layer where the external information is received, an output layer where the results are deployed and one or more hidden layers which perform the connection between the input layer and the output layer. The number of input neurons have to be the same of the number of independent variables associated with the problem and the output neurons number have to be the same of the variables wanted to determinate.

As the Biological Neural Network, the Artificial Neural Network have to be trained before try to solve any kind of problem. Training the Artificial Neural Network is the name given to the process of determining the various weights of the connections between the different neurons inside the Artificial Neural Network. The total available data is usually divided into a training set and a test set, the training set is used to determinate the neurons connections weights, through a training algorithm, while the test set is used to measure the Artificial Neural Network performance and precision (Zhang, et al., 1998).

2.3.5 - Addictive Quick Prototyping – 3D printing

Addictive quick prototyping is a technology that consists on successive layers of material placed one above the other, typically polymers, with a specific shape in order to perform a three-dimensional object. There are multiple technologies used for quick prototyping, as is possible to observe in the Figure 2.7.

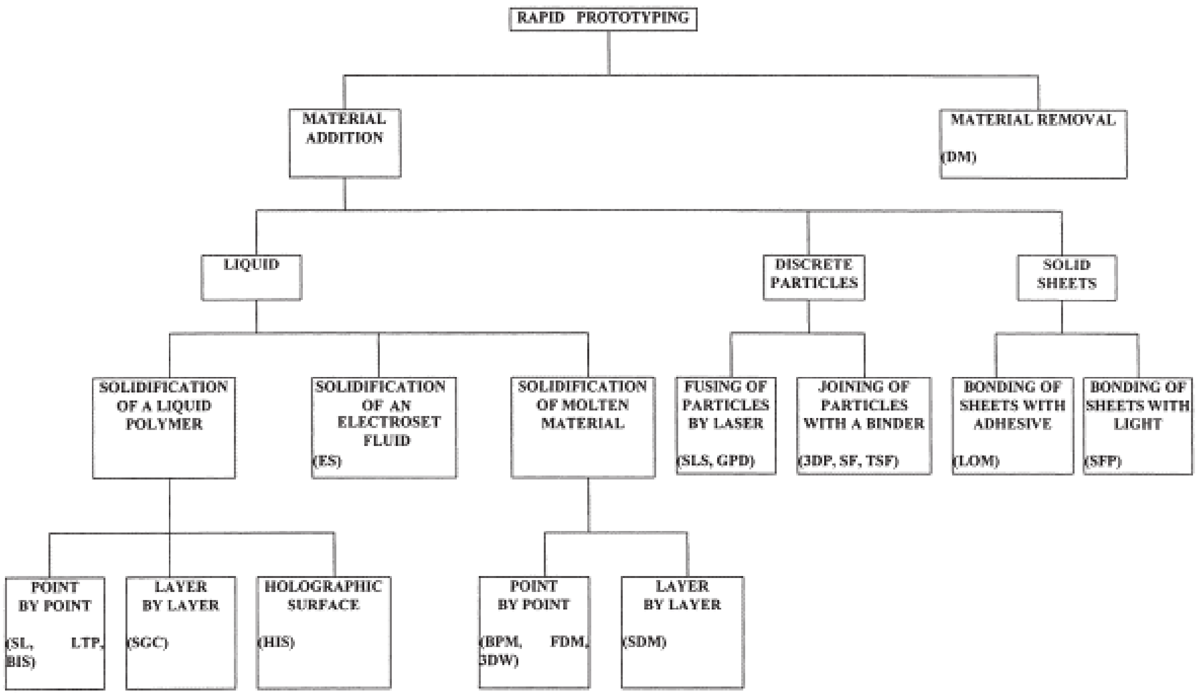

Figure 2.7 – Rapid Prototyping Methods Diagram **(Pham & Gault, 1998)**.

Polymer addictive quick prototyping technology is commonly used to produce parts that perform under low stress, for example electronic components protections, and to verifying the geometry of mechanical parts before producing in more noble materials. This technology is generally faster and more economical than the technologies that allow to work with metal, so the process of iterations before achieving the final geometry for the part is faster and less expensive.

3 - Developed Devices

The development of the Instrumented Saddle, Pedals and Gripe Device follows the workflow presented on the Figure 3.1Figure 3.1 – Devices Development Workflow Diagram. It starts with the idealization of the working principle, pass through a development of a 3D virtual model, the production of a prototype and finalize with the production of the final workpiece. In other hand, since the Instrumented Handlebar do not require the production of new workpieces, its development is based only in the precise application of the strain gauges and the development of the measuring methodology.

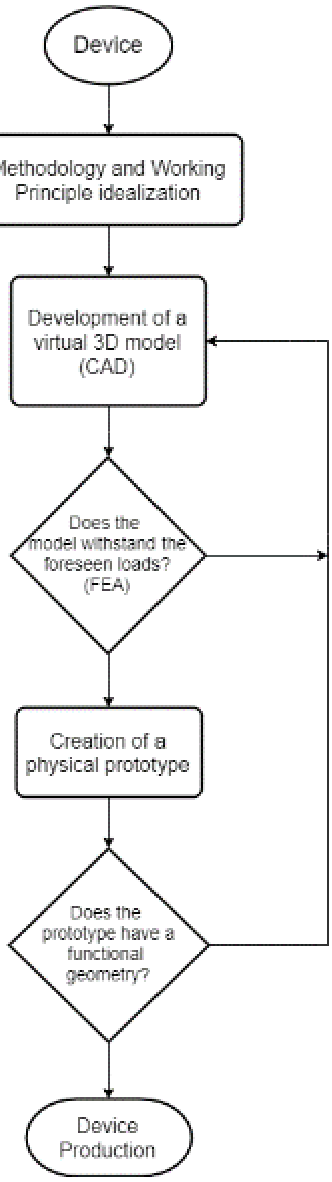

Figure 3.1 – Devices Development Workflow Diagram

The virtual 3D models are developed with the CAD software Solidworks. With the 3D model is possible to get a first impression of the device idea in a three-dimensional environment, which facilitate the detection of design errors and collision situations. The devices are designed taking into consideration the location and mechanical fixations mechanisms present on the bicycle, in order to take advantages of the fixation mechanisms and to minimize the interference with the patient.

To optimize the devices structural behaviour, design optimization studies are performed, with Solidworks, to minimize the workpieces mass, while warranting that a minimal safety factor of 2 are present. However, taking into consideration different factors, such as, strength, stiffness and production process, lead into the selection of designs distinct from the ones achieved by the optimization study.

The structural behaviour of the final designs is analysed with resource to the Finite Elements Method. Each device is analysed with a FEA model on the Solidworks Simulation software and other on the MSC Nastran/Patran software. Then, by changing the elements refining properties and compare the displacement and stress values, is performed a mesh convergence study in order to validate the results provided by each FEA model.

Once that the virtual 3D models of the devices are determined and validated, the required parts are prototyped, with 3D printing, to also validate the geometry in the real environment context.

After confirming that the designs withstand the foreseen loads imposed by the operation conditions and that the geometry are ergonomic and does not interfere with the patient, the devices designs are ready to be produced. The production process is made with resource to a conventional lathe, a FDM 3D printer and CNC milling machines, as also, Mastercam software to create the CNC milling codes and Flashprint software to create 3D printing codes.

3.1 - Instrumented Saddle Device

The Instrumented Saddle Device consist in two aluminium plates, three loadcells, a bicycle saddle and a bicycle post connection mechanism. The two aluminium plates are hold together by the three loadcells, the saddle is installed above the upper plate and the bicycle post connection mechanism is installed under the lower plate. This way, all the vertical loads that are applied on the saddle must pass through the loadcells, warranting that is acquired the most relevant data to study the patient interaction with the saddle. Despite there are three force components on a saddle interaction, namely vertical, longitudinal and transversal, the most significative one is the vertical component, since is in this direction that the patient apply the majority of is weight. Therefore, the vertical component is the most important and provide the enough information for the project purposes.

The developed bicycle post mechanism allows to change the Instrumented Saddle Device inclination, as also, to tune the saddle forward and backwards. With this mechanism, the device can be tuned in order to better answer the patient ergonomic needs, as also, being applied in any bicycle with a standard post connector.

All the Instrumented Saddle Device components result in an overall high of 113mm, which can be easily corrected by tuning the bicycle post high. The section where the loadcells are applied is covered with a black fabric for aesthetic proposes and to avoid loadcells damage, as illustrated in Figure 3.2.

Figure 3.2 – Instrumented Saddle Device

The three loadcells are disposed in a triangular form with two in the rear part of the saddle and one on the front part, as illustrated in Figure 3.3. Through this positioning system is possible to obtain the vertical force applied on the saddle, its magnitude and distribution in the three locations. The resultant force magnitude is the sum of the values from the three loadcells. The difference between the two rear loadcells allow to identify the asymmetry relatively to mediolateral direction (according to sagittal plane), and the difference between the front load cell and the sum of the rear ones can be observed as the asymmetry in anteroposterior direction (according to the coronal plane). The Figure 3.3 illustrate the global dimensions of the saddle considered and the relative positioning of the loadcells.

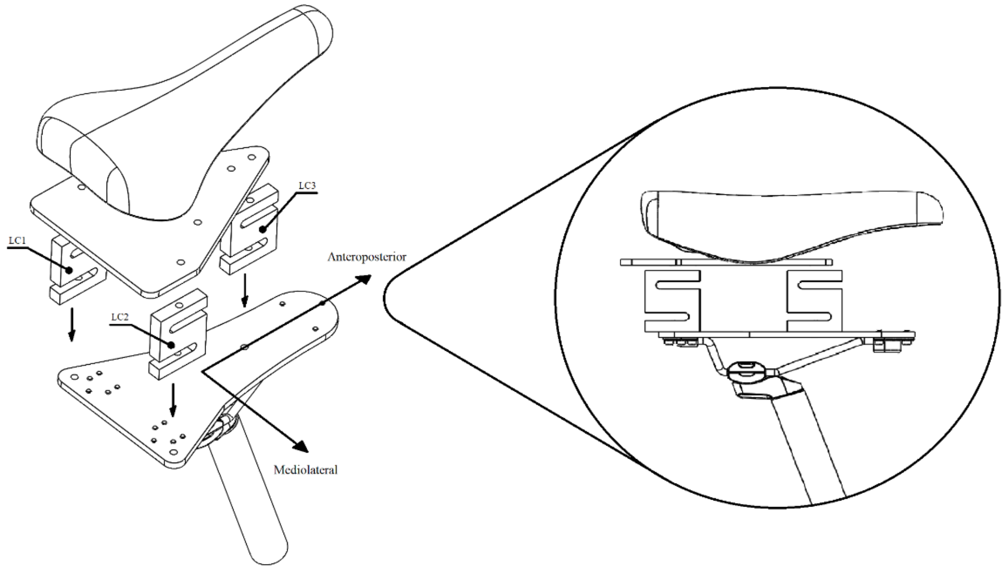

Figure 3.3 – Instrumented Saddle Device Schematics

3.1.1 - Design

The design of the Instrumented Saddle device split in two major parts, the Loadcells Interfaces and the Saddle Post Connector, which are analysed individually.

As pre-requirements, the saddle set should withstand the weight of the user during the different possible movements of the cycling exercise. As an additional requirement, the workpieces should be able to manufacture with the materials already available in the facilities, in order to minimize the waiting time.

The Loadcells Interfaces part design are based in two 6 mm thick 7075 alloy aluminium plates, that was available in the materials warehouse. The plates are shaped in a way that do not interfere in the user movements or comfort, as is possible to observe on Figure 3.4. One provides the connection between the saddle and the loadcells, the other provides the connection between the loadcells and the Saddle Post Connector.

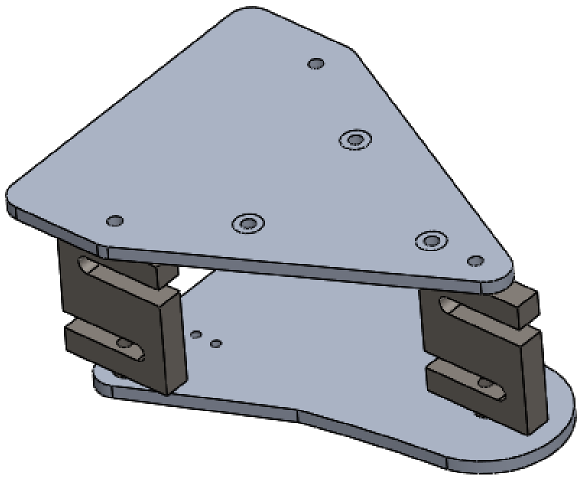

Figure 3.4 – Loadcells Interface

For the Saddle Post Connector are presented and analysed three different options made of two different designs, which are represented in Figure 3.5 (a) and Figure 3.5 (b) that will be referred as Uninterrupted Design and Interrupted Design, respectively. The first option study the Uninterrupted Design made out of Poly Acid Lactic (PLA) through the 3D printing technology Fused Deposition Modelling (FDM). The second option take the same design as the previous one but produced in 7075 alloy aluminium. The third option study the Interrupted Design with the connectors in 7075 aluminium and the rods in 304 alloy stainless steel.

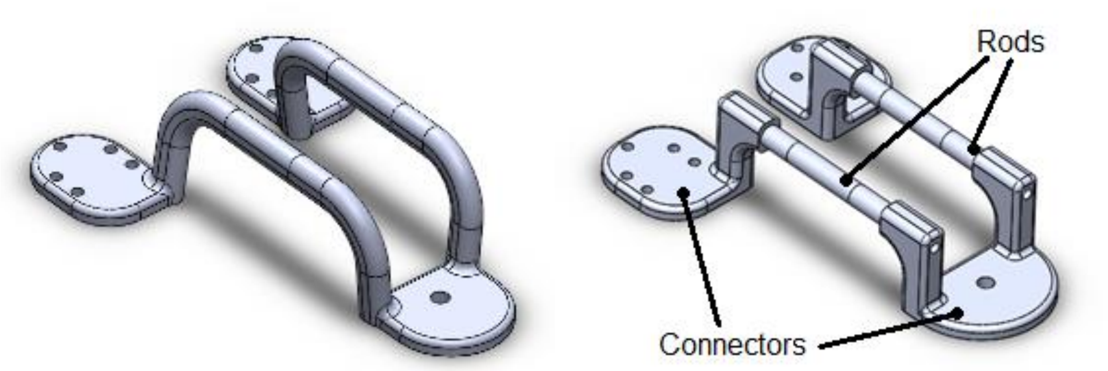

Figure 3.5 – (a) Uninterrupted Design on the left and (b) Interrupted Design on the right

3.1.2 - Numerical Models

The study of the structural behaviour, relatively to the foreseen loads, of the Instrumented Saddle device components are made with FEA. The studies are performed in two different softwires, Solidworks and MSC Nastran/Patran, in order to verify and cross validate the achieved results.

3.1.2.1 - Loadcells Interface

The expected worst-case scenario is when the user is entirely supported on the saddle i.e. the user is applying all his weight in the saddle, with no feet on the pedals neither the hands on the handlebar. In 2018, Stephen Gill (2019) indicate 91.72 kg as the higher average weight in North America, which, as indicated in the paper, is the country with the higher average weight, according to the author. Thus, in order to simplify and be on the safety side, the load magnitude considered on the FEA is 1000N, approximately 101.97 kg. The mechanical properties used to perform the FEA are an elastic modulus of 72 GPa, a Poisson ratio of 0.33 and a yield strength of 505 MPa, which are the properties for the aluminium alloy 7075 present on the Solidworks materials properties database.

Considering the plates geometry, it suggests the use of shell elements. The plates are 6 mm thick, 150 mm width and 175mm long, which give a thickness/length relation of 25 and 29, respectively. Thus, considering the thickness/length relation, it suggests the use of thick shell elements. However, the relation is close to the solid element's domain (thickness/length < 20). Therefore, the device is analysed with both kind of elements. With the Solidworks software is analysed a shell elements FEA model and a solid elements FEA model. While with the MSC Nastran/Patran software is only analysed a solid elements FEA model.

In the Solidworks software the Loadcells Interface are simulated together, in other words, the FEA model is simulated as an assembly. In order to simulate the Loadcells Interface in the Solidworks as an assembly, several connection and boundary conditions are applied. Therefore, since that the Loadcell Interface is composed by different independent metallic parts, the contact between the components is defined as no penetration for the solid elements FEA model, i.e. the different bodies do not can pierce each other. However, in the shell elements model that components interaction is not possible to use since that the model do not provide stable values. Thus, in the shell elements FEA model the components contact are defined as bonded. The connection between the loadcells and the plates are made using virtual pins instead of bolts. Despite the bolts make a better representation of the real work condition, these also represent a much more complex FEA model. Thus, considering that the bolts in the real assembly do not need to be very tight, the use of virtual pins do not represent a significative less realistic FEA model.

To simulate the connection between the Loadcells Interface and the Saddle Post Connector, a boundary condition is applied in the faces, that touch each other, restricting the elements translation to only two directions, i.e. the faces cannot leave the plane where they are inserted, as illustrated in Figure 3.6 (a). Another boundary condition is applied in the holes where the Loadcell Interface and the Saddle Post Connector are bolted together, restricting the elements translation to the rotation around one axis, as if it were a hinge, illustration in Figure 3.6 (b).

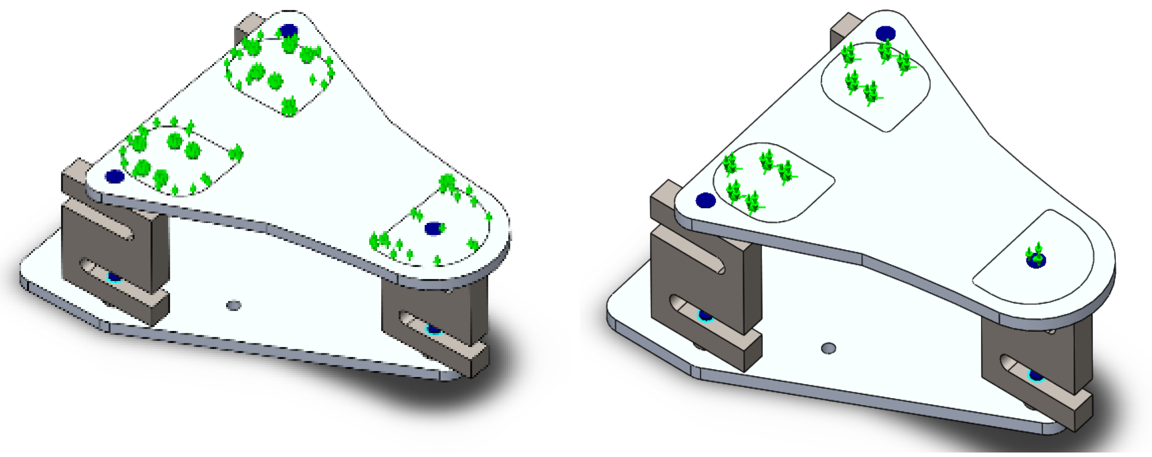

Figure 3.6 – (a) Faces with translation restricted on one direction on the left and (b) Hole with hinge boundary restriction on the right

As the loadcells structural behaviour are not required to be analysed and to make a simpler, but still realistic FEA model, those are analysed as rigid bodies, i.e. bodies with a simpler stiffness matrix that do not deform.

In the Solidworks FEA model, the load condition is applied where the bicycle saddle contact with the upper plate. To apply this condition are created an area around the saddle holes which represent the contact surface between the saddle and the plate, as illustrated in Figure 3.7. The 1000N, previously mentioned, are equally distributed in all the three areas.

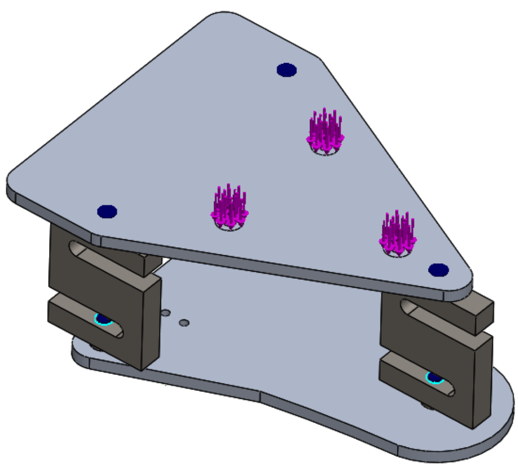

Figure 3.7 – Solidworks load condition application areas

Thus, since the FEA models are fully defined and constricted is possible to create the mesh and solve the matrix in order to analyse the model results. In the Solidworks solid elements FEA model, soft springs are added to stabilize the model and the solver used to solve the matrix is the Direct Sparse Solver. In the Solidworks shell elements FEA model, the solver used are also the Direct Sparse Solver, however, soft springs are not necessary to use for model stabilization.

In the left side of the Figure 3.8 is represented the von Mises stress dispersion over the solid elements FEA model, while on the right is represented the displacements dispersion. Thus, is possible to observe the Loadcells Interface behaviour to the foreseen loads.

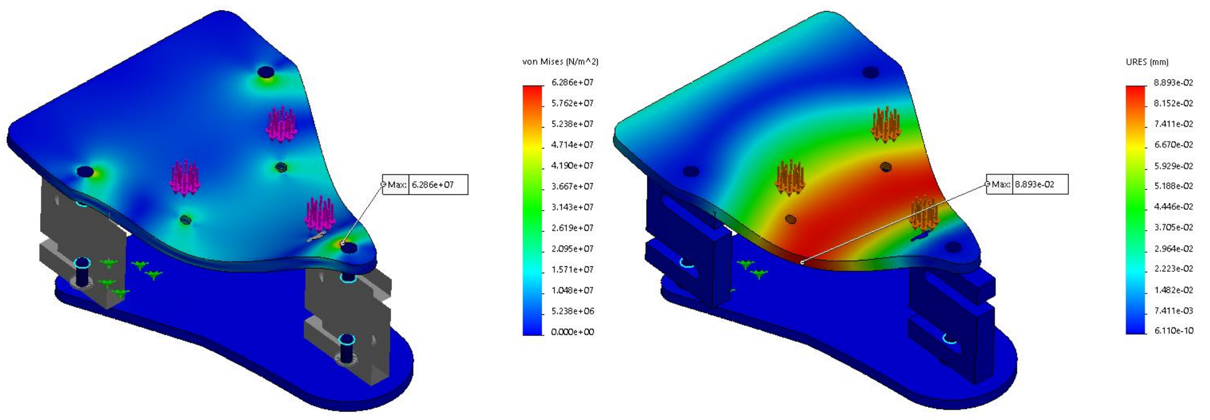

Figure 3.8 – (a) Stress dispersion on the left and (b) displacement dispersion on the right

By solving the FEA model with different mesh elements size is obtained the convergence study Graph 3-1 Relative Displacement Error and Graph 3-2 Relative Stress Error, where on the abscissa axis is represented the number of elements present on the model and on the ordinate axis is displayed the relative error from the model. The relative error (FEAerror) is calculated from the FEA results (Ares) relatively to the results from the previous FEA (Pres), using the Equation 1.

$$\text{FEAerror} = \frac{\text{Ares} - \text{Pres}}{\text{Ares}} \cdot 100$$

Equation 1 - FEA relative error

Both graph, Graph 3-1 Relative Displacement Error and Graph 3-2 Relative Stress Error, suggest that the mesh converge, since that the relative displacement error tend to a value below 0.4% and the relative stress error tend to a value below 1.2%. As shown in Appendix A.1 is possible to affirm that the stress value tends to 65 MPa and the displacement value tend to 0.089 mm, indicating a factor of safety of 7.77. Therefore, is considered that the FEA model which better represent the reality is the model with 232022 elements.

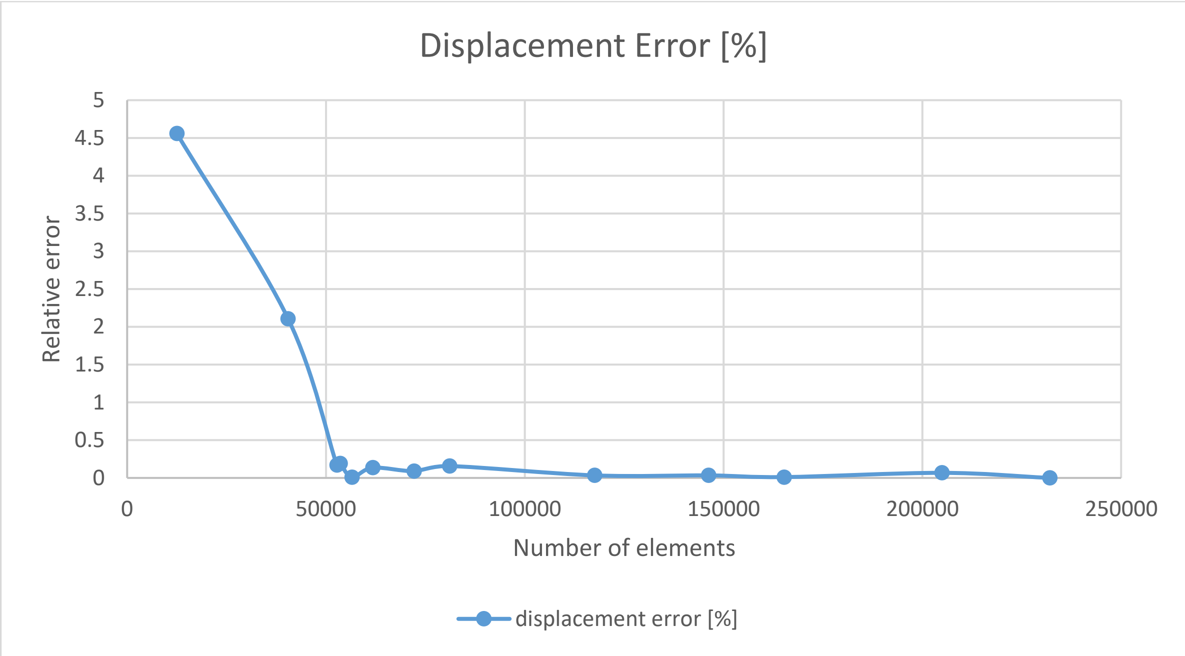

Graph 3-1 Relative Displacement Error

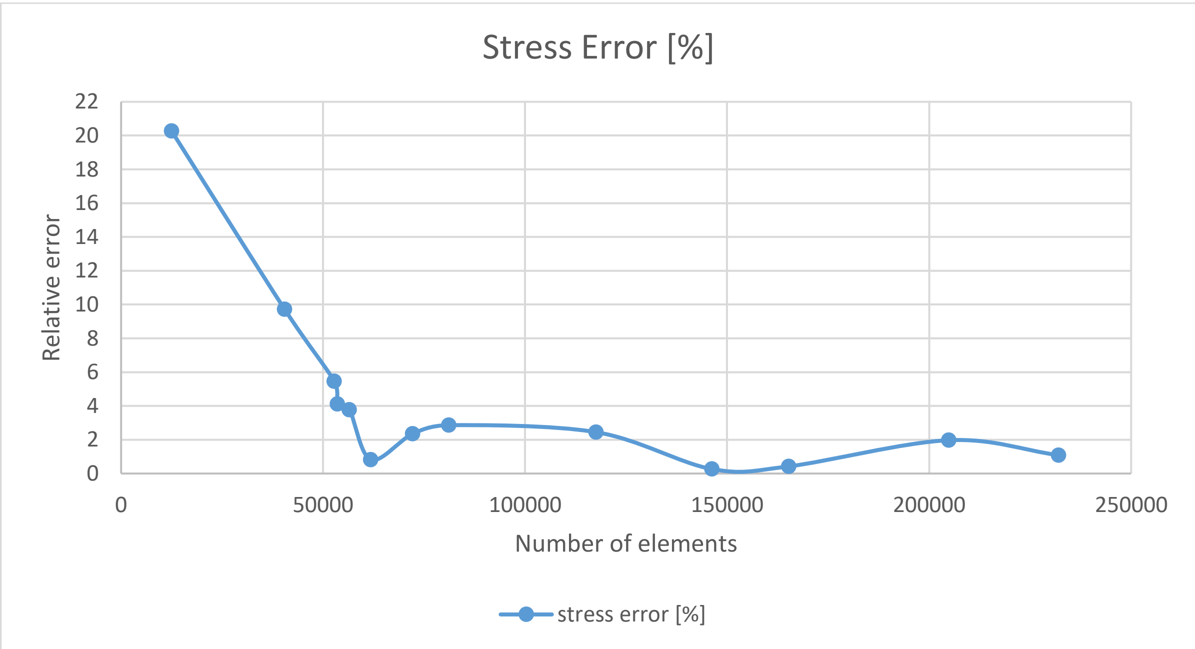

Graph 3-2 Relative Stress Error

As expected, the Solidworks shell elements model display a similar behaviour to the solid elements model, as illustrated in Figure 3.9. This figure represents the von mises stress and the displacements over the FEA model.

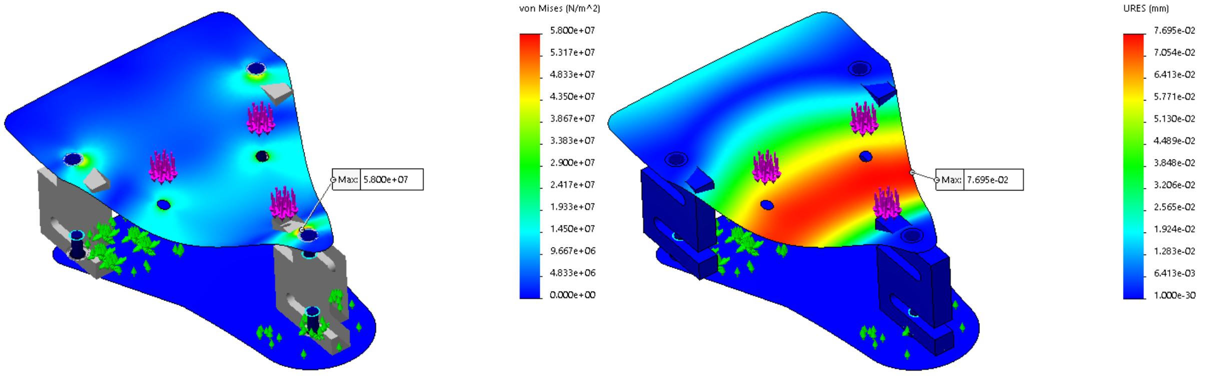

Figure 3.9 – (a) Stress dispersion on the left and (b) displacement dispersion on the right

From the values resultant from the shell elements mesh convergence present in Appendix A.2 is possible to affirm that the model tends to a stress value of 60 MPa and a displacement value of 0.077 mm, indicating a factor of safety of 8.42. Thus, is concluded that the FEA model which better represent the reality is the model with 23797 elements.

In the Pastran-Nastran software, each plate is simulated individually, creating a FEA for each plate. To simulate the interaction between the lower plate with the Post Connector and the interaction between the upper plate with the loadcells, a boundary condition is defined in the contact areas, restricting the elements translation to only two directions, i.e. the contact faces cannot leave the plane where they are inserted, as represented in Figure 3.10. In the holes where the plates are connected with bolts, a boundary condition is defined to restricting the elements translation in to two directions, i.e. the holes cannot translate axially to the cylindrical geometry, simulating the restrictions imposed by the bolts, as illustrated on Figure 3.11.

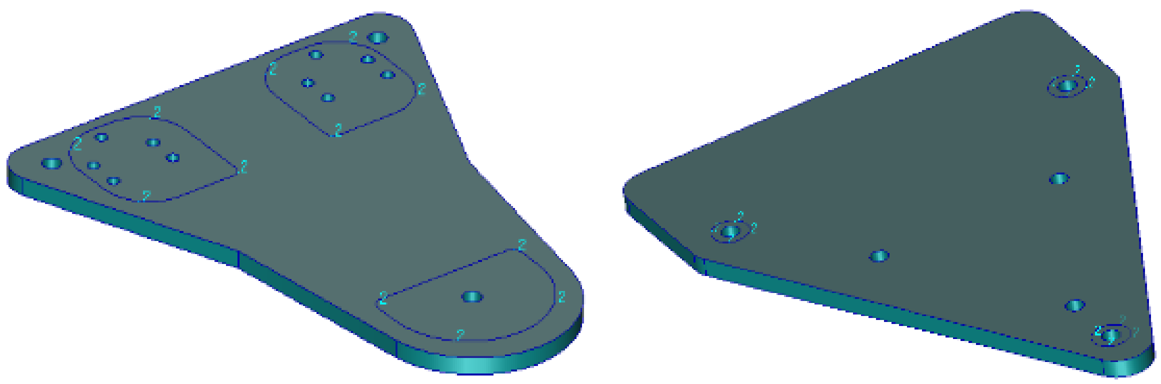

Figure 3.10 – Contact faces boundary condition

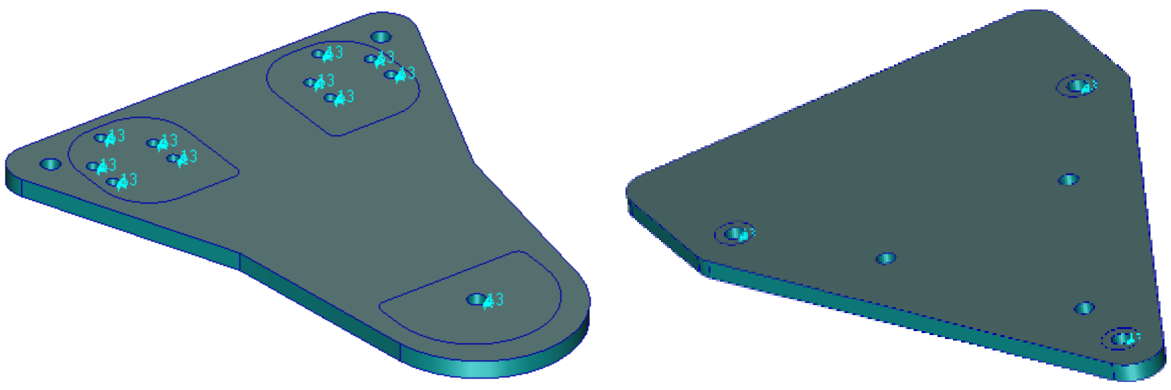

Figure 3.11 – Holes boundary condition

In the MSC Nastran/Patran upper plate model, similarly to the Solidworks model, a force boundary condition is defined where the bicycle saddle interacts with the plate. While in the MSC Nastran/Patran lower plate model, the force boundary condition is applied where the loadcells interact with the plate. Since that the lower plate fully support the upper plate, the 1000N that are defined to the upper plate FEA model, are also defined to the lower plate FEA model, as represented in Figure 3.12.

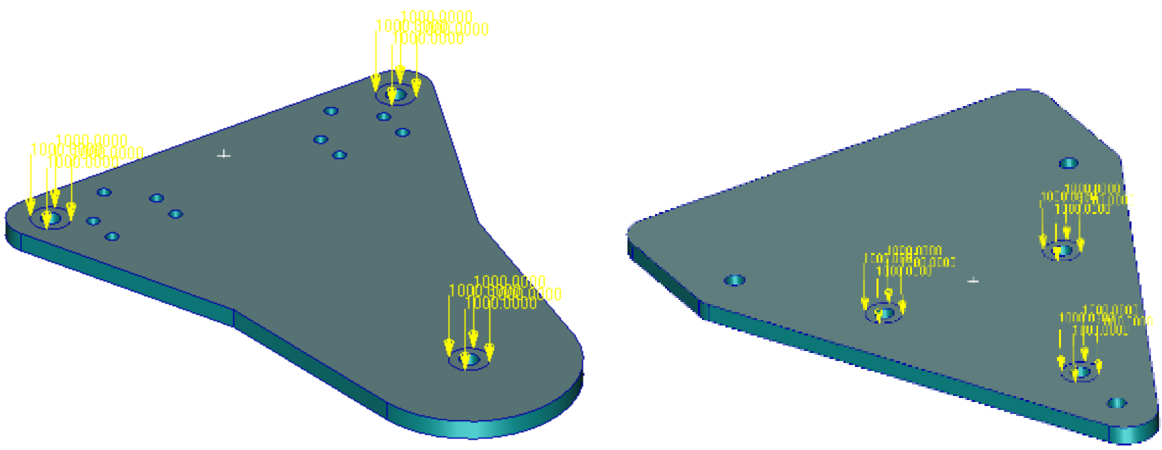

Figure 3.12 – MSC Nastran/Patran load condition application areas

In the Figure 3.13 is shown the upper plate stress dispersion, on the left, and the displacement dispersion, on the right. Through this illustration is possible to understand the upper plate behaviour relatively to the foreseen loads.

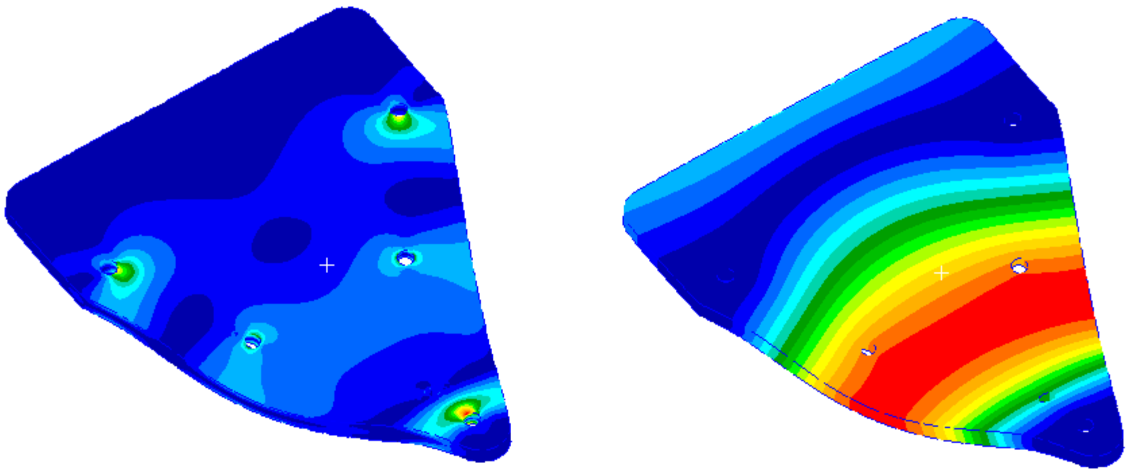

Figure 3.13 – (a) Stress dispersion on the left and (b) displacement dispersion on the right

Despite the relative displacement error do not achieve the 0.4%, the relative stress error goes below 1.2%, Appendix A.3, the FEA model tends to stabilize, since the increase of elements result in a decrease of the relative error in both graphs. Therefore, the MSC Nastran/Patran upper plate FEA model with 52112 elements is considered stable and is conclude that the stress value tends to 11 MPa and the displacement tends to 0.00055 mm, indicating a safety factor of 45.91.

The MSC Nastran/Patran lower plate model cannot be considered stable. From the Appendix A.4, despite the relative error graphs indicates a slight convergence, is observable that both the stress values and the displacement values do not tends to stabilize. Therefore, the results from the MSC Nastran/Patran lower plate FEA model are not considered. However, in the Figure 3.14 is shown the von Mises stress and displacement dispersion over the model.

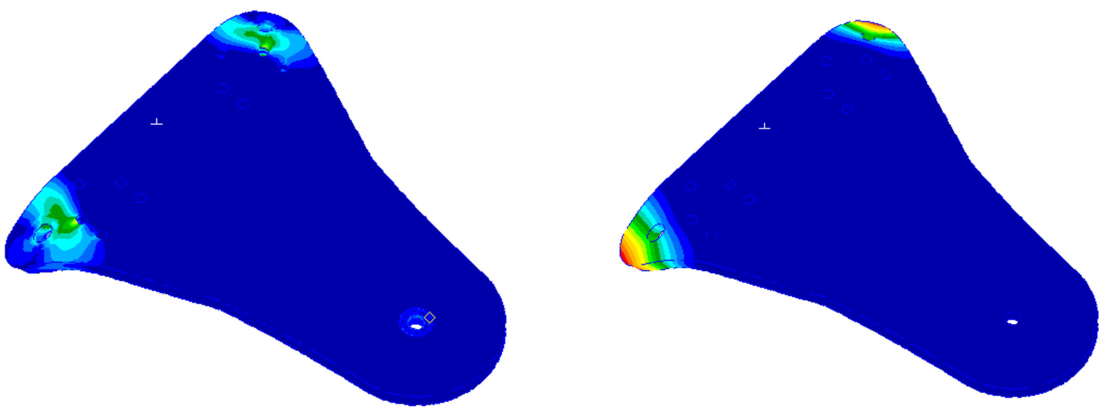

Figure 3.14 – (a) Stress dispersion on the left and (b) displacement dispersion on the right

Comparing the obtained values from the mesh convergence studies is decided to assume the values provided by the Solidworks solid elements FEA model, as the most accurate ones. This FEA model indicate the higher values for displacement and stress, therefore, is the most conservative model, which represent higher safety. The Solidworks solid elements model also achieve better mesh convergence results by having the lower relative error values and is the model which better represent the reality by using the components contacts as no penetration, instead of bonded as the Solidworks shell elements FEA model does.

3.1.2.2 - Saddle Post Connector

The Saddle Post Connector makes the connection between the bicycle post and the Loadcells Interfaces. Thus, to ensure that the Saddle Post Connector can withstand the further stresses, by do not enter the material plastic deformation domain, and warranty the user safety, are performed a static analysis in the same conditions of the Loadcells Interface. To this end, the Saddle Post Connector FEA are performed with a foreseen load of 1000 N.

As previously announced, there are three analysed options. In all the three options, the FEA are performed using solid kind elements. However, as the designs have different details and small rounded areas, the number of elements and mesh properties must be well tuned to reliably represent the geometry in these areas, in order to do not get distorted results due to underfit.

Despite the geometric differences between the two different designs, Interrupted Design and Uninterrupted Design, both have the same fixations methodology. Thus, the boundary conditions applied to simulate those fixations are the same in the Interrupted Design Saddle Post Connector and in the Uninterrupted Design Saddle Post Connector. Both in the MSC Nastran/Patran and the Solidworks, the connection between Saddle Post Connector and the Loadcell Interface is simulated by applying a boundary condition in the faces that contact with the Loadcell Interface, restricting the elements translation to two directions, i.e. the faces cannot leave the plane where they are inserted, as illustrated in Figure 3.15.

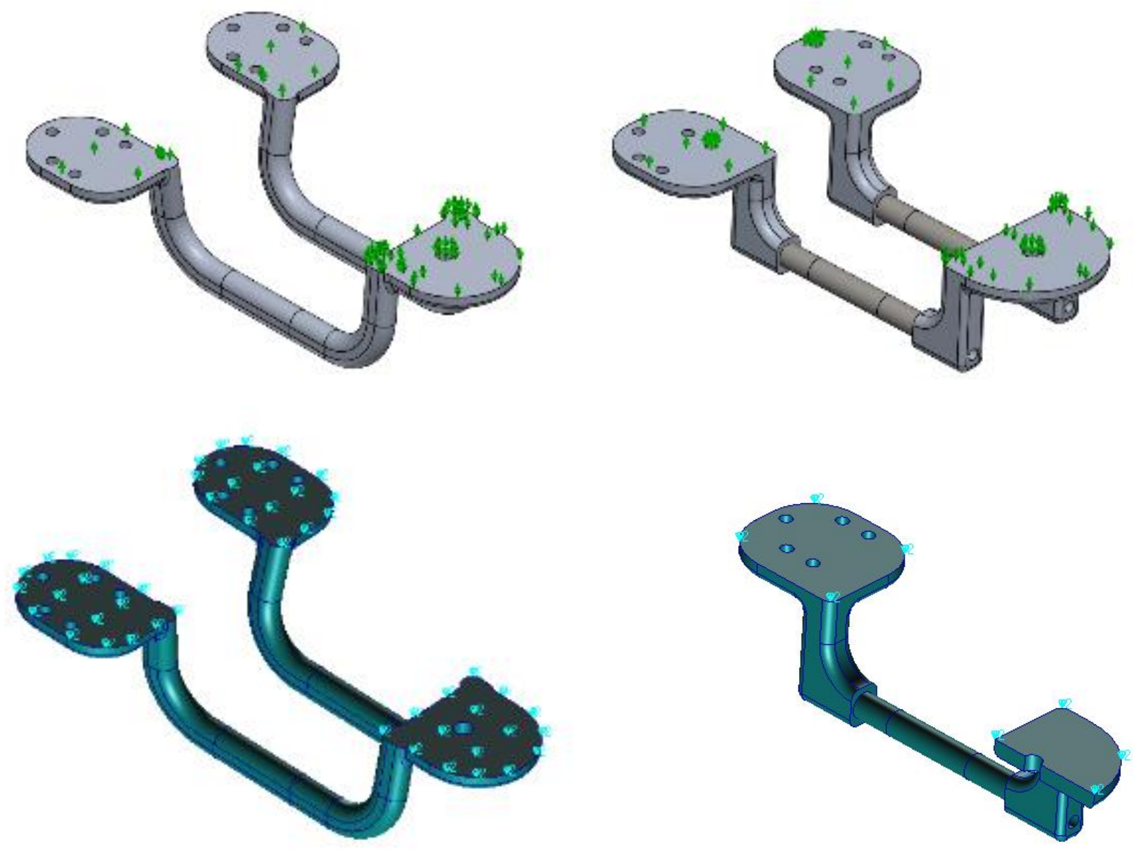

Figure 3.15 – Contact faces boundary condition

In the Solidworks, to represent the bolting connections between the Saddle Post Connector and the Loadcell Interface, a boundary condition is applied in the holes that join the two parts, restricting the elements translation to the rotation around one axis, as if it were a hinge, illustration in Figure 3.16. In the MSC Nastran/Patran, the bolting connections are simulated by a boundary condition which restrict the elements translation in to two directions, i.e. the elements inside the holes cannot translate axially to the cylindrical geometry, simulating the restrictions imposed by the bolts, also illustrated in Figure 3.16.

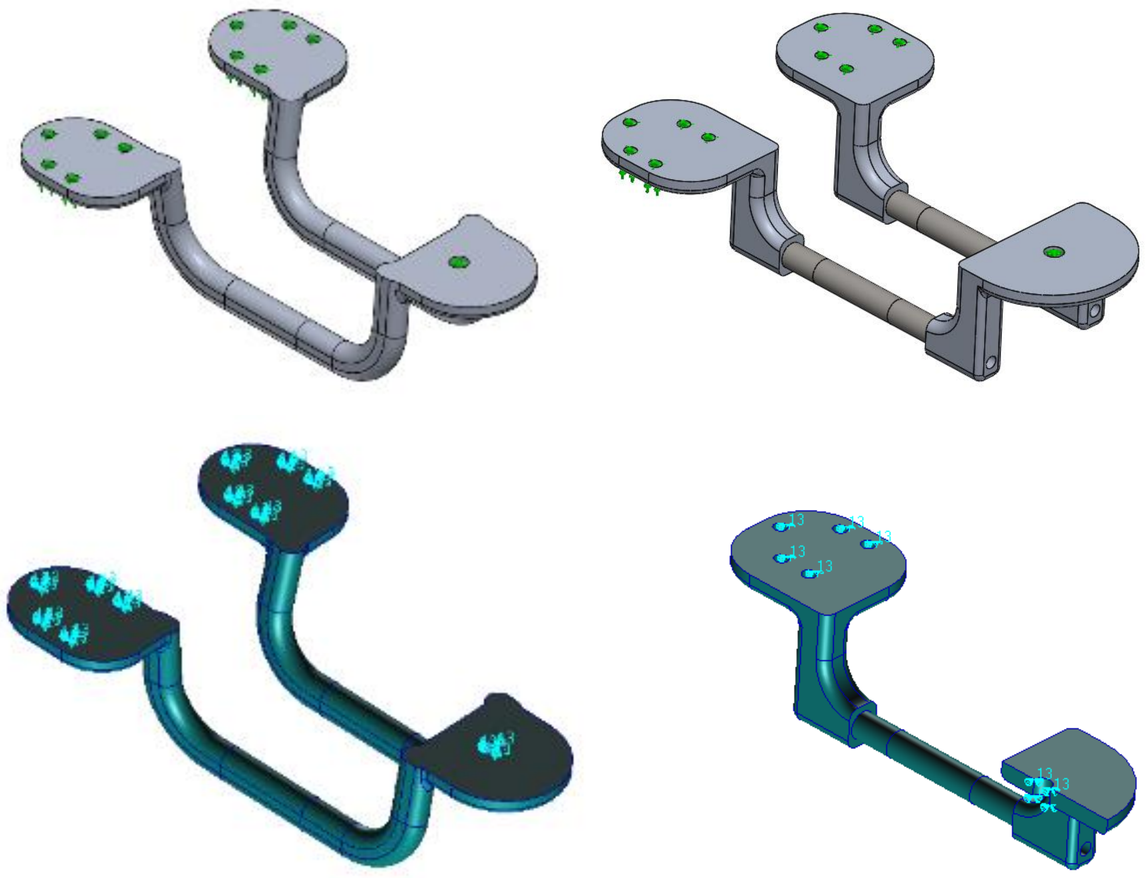

Figure 3.16 – Holes boundary condition

As the post connection mechanism tight on both rods, a boundary condition is defined, in both Solidworks and MSC Nastran/Patran software, to do not let the rods move apart one from each other, as illustrated on Figure 3.17, thus the FEA models have a better representation of the reality.

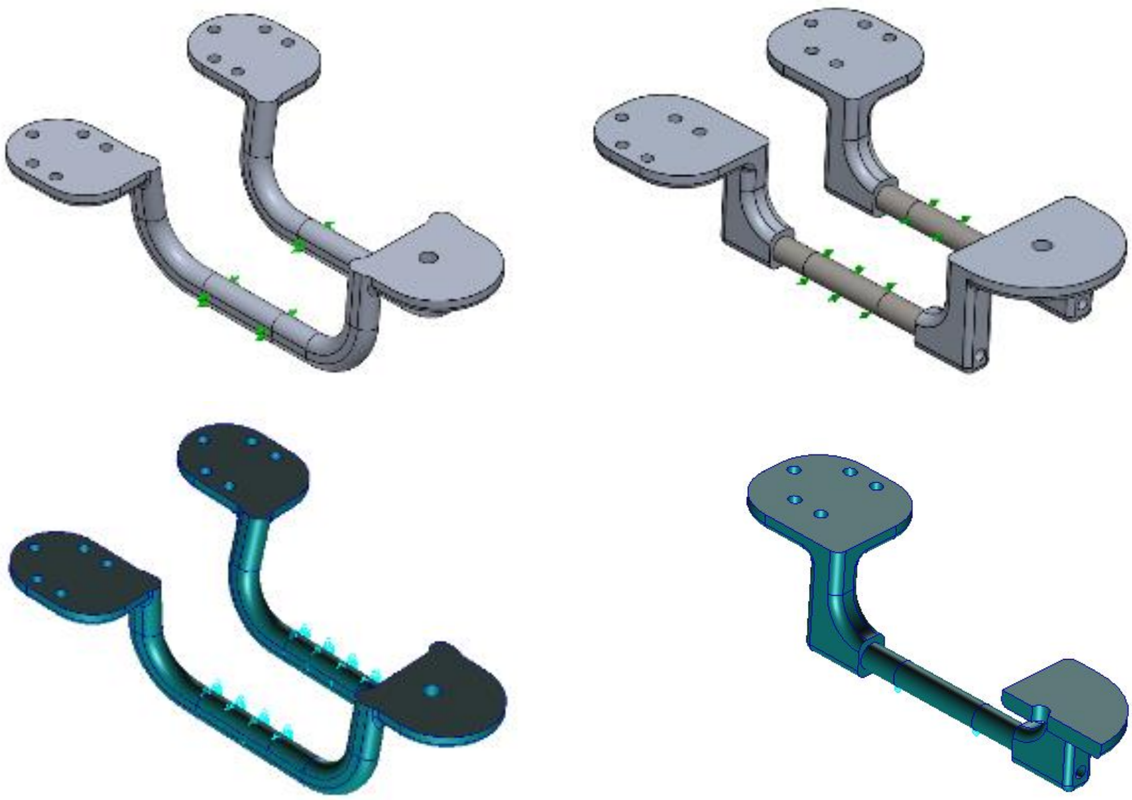

Figure 3.17 – Connection mechanism boundary condition

The first and second option use the Uninterrupted Design which consist in only one part. However, the third option use the Interrupted Design which are composed by five different pieces. Thus, to simulate the five pieces simultaneously the components contact condition must be defined. Considering that the pieces are not welded neither shrink fitted and the material used in its manufacturing do not have rubber like elasticity, the components contact cannot be defined as bounded neither allowing penetration. Thus, the components contact that are used to perform the Solidworks FEA is the no penetration contact type, i.e. the different bodies do not can pierce each other, and in the MSC Nastran/Patran is used the deformable contact type, this contact type allow the bodies to deform accordingly to the materials properties defined, providing more realistic results.

In the MSC Nastran/Patran Interrupted Design model a symmetry boundary condition is used, as illustrated in Figure 3.18. Thus, the computational power required to solve the FEA is substantially decreased.

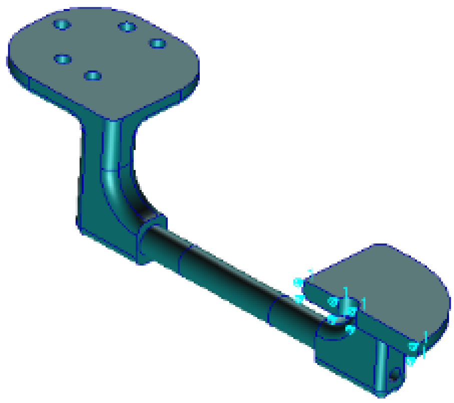

Figure 3.18 - Symmetry boundary condition

The load condition in both Uninterrupted Design and Interrupted Design are applied where the post connection mechanism contact with the Saddle Post Connector. To apply the load condition a split line is used to define the contact surface between the Saddle Post Connector and the post connection mechanism, as illustrated in Figure 3.19. The foreseen 1000 N are equally distributed on both Saddle Post Connector rods.

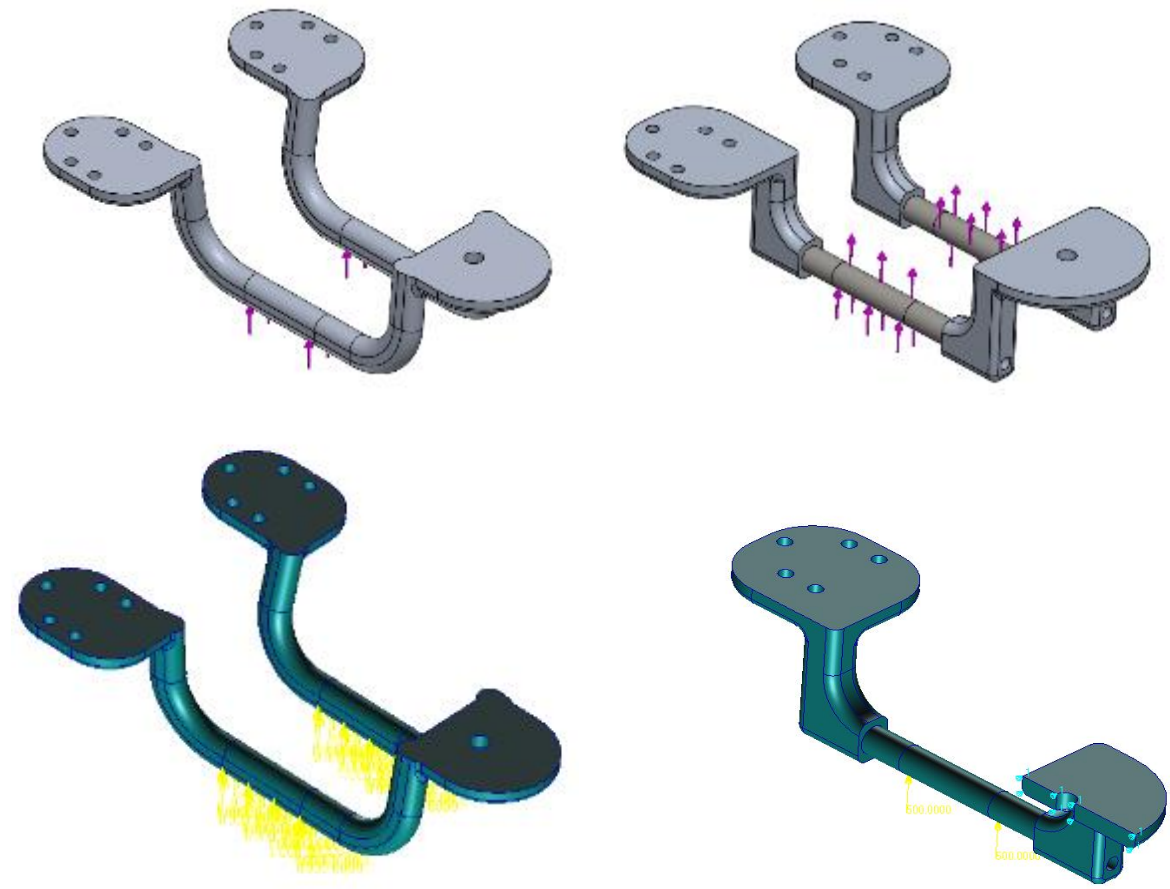

Figure 3.19 – Load condition application areas

Once that all the different FEA models are fully defined and constricted is possible to create the mesh and solve the models, to analyse the different results obtained from each option. The Solidworks FEA models are performed with the FFEPlus solver, while the Patran FEA models are performed with Natran.

The first option foresees the use of the Uninterrupted Design made of PLA by the FDM additive manufacturing technology. As the FDM technology places successive layers of material one on top of the other, this technology usually confers an anisotropic or orthotropic behaviour to the material. Considering the Z axis as the axis perpendicular to the deposited layers plan, the mechanical property through this axis is different from the properties from the X and Y axes. This phenomenon due to the interlayer adhesion of the material, since that the layers are placed one on top the other through the Z axis, i.e. in an interrupted way. While through the X and Y axis they are placed in an uninterrupted way. According to Chacón *et al*. (2017) research, the print settings influence the final piece properties and behaviour, where layer high is the print setting which more influence the mechanical properties of the material. Taking this property into account, the study of the this first option are done considering a print setting of 100 µmm layer high and 100% infill, while as mechanical properties are considered an anisotropic PLA material with 72 MPa of yield strength, an elastic modulus of 3.9 GPa and a Poisson ratio of

0.33 on the X and Y axis. To the Z axis are considered 30 MPa of yield strength, 3.8 GPa of elastic modulus and 0.33 of Poisson ratio.

Thus, the stress values are analysed individually in every spatial direction, since that the material do not have the same behaviour in every direction. The study of this option is performed only with the Solidworks software.

In the Figure 3.20 is presented the stress distribution over the model, in every direction, i.e. vertical, longitudinal and transversal. On the left is shown the stress over the longitudinal direction, i.e. the x axis, on the right is the stress over the vertical direction, i.e. the z axis, and on the bottom is shown the stress over the transversal direction, i.e. the y axis.

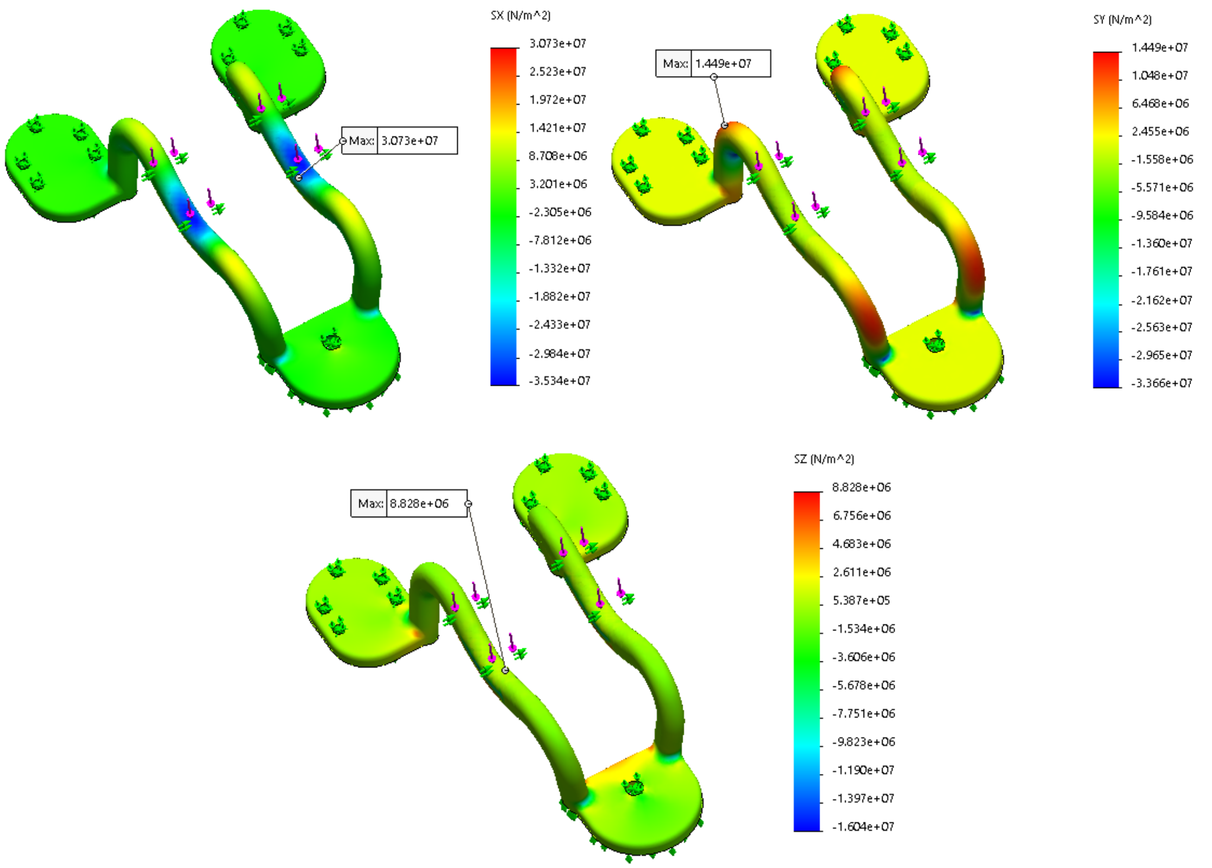

Figure 3.20 – (a) Longitudinal stress dispersion on the left, (b) vertical stress dispersion on the right and (c) transversal stress dispersion on the bottom

On the Appendix A.5 are present the results from the mesh convergence. The FEA model with 69113 elements is considered a good representation of the reality and from his results is considered a maximum stress value of 30.6 MPa over the X axis, which indicate a safety factor of 2.35, and over the Z axis are considered a stress value of 14.5 MPa, which indicate a safety factor of 2.07. Relatively to the Y axis is secure to affirm that the stress value are below 11 MPa, which indicate a safety factor of 6.55.

In the second option is studied the Uninterrupted Design manufactured with a CNC milling machine, subtractive technology. This technology does not significantly interfere with the aluminium alloy 7075 mechanical properties. The 7075 aluminium have a wide elastic domain, high yield strength and good machinability properties. These characteristics confer, not only, flexibility and mechanical resistance, to the Uninterrupted Design, as also confer manufacturing advantages due to its machinability properties. The mechanical properties used for the FEA are the properties for the aluminium alloy 7075 present on the Solidworks materials properties database. Therefore, since the aluminium alloy have the same properties in every direction, isotropic material, the material properties used to perform the FEA are an elastic modulus of 72 GPa, a Poisson ratio of 0.33 and a yield strength of 505 MPa.

The Figure 3.21 indicate the von Mises stress and displacements dispersion over the Solidworks FEA model. This way is possible to understand the structural behaviour of the device.

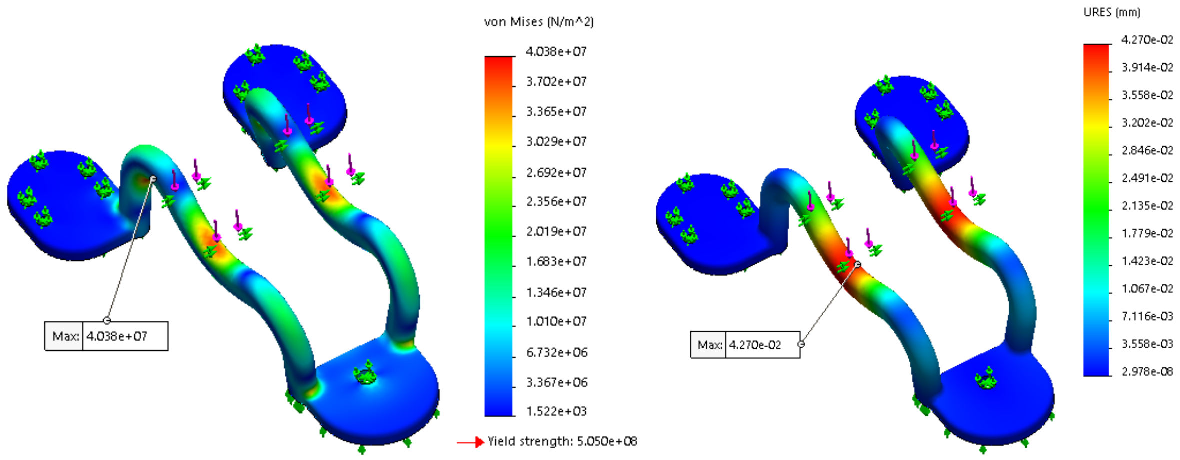

Figure 3.21 – (a) Stress dispersion on the left and (b) displacement dispersion on the right

From the Appendix A.6, where is presented the mesh convergence results, is considered that the FEA model with 72788 elements provides a good representation of the reality and is observable that the stress value tends to 40.6 MPa, indicating a safety factor of 12.44.

In the Figure 3.22 is presented the von Mises stress and displacement dispersion provided from the MSC Nastran/Patran FEA model.

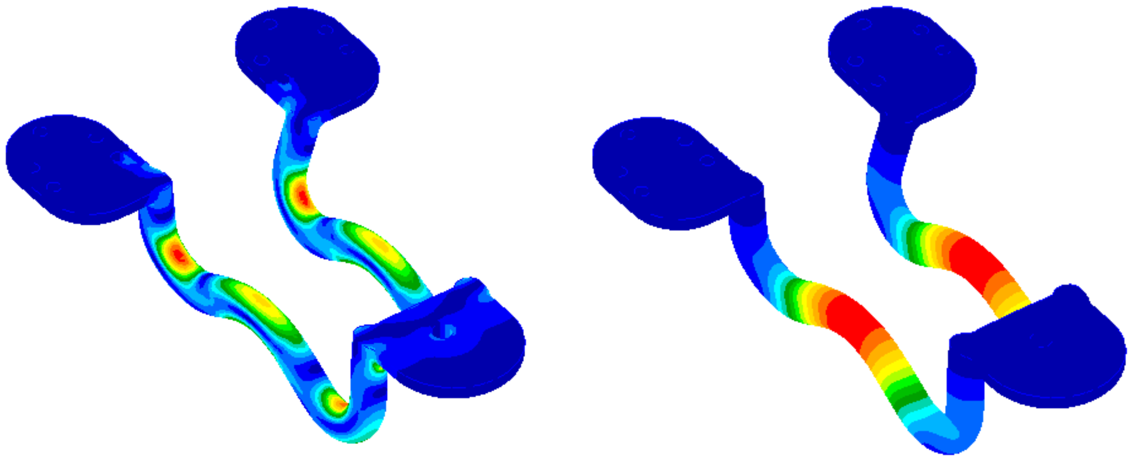

Figure 3.22 – (a) Stress dispersion on the left and (b) displacement dispersion on the right

According to the data from the Appendix A.7 is concluded that the results provided by the MSC Nastran/Patran FEA model are stable and reliable. Therefore, is possible to conclude that the stress value tends to 45 MPa and the displacement to 0.0018 mm, indicating a safety factor of 11.22.

The third option foresee the use of the Interrupted Design. This design is composed by different components, three 7075 aluminium alloy parts and two 304 inox steel rods. All the components are produced with subtractive technology, the aluminium parts through a CNC milling machine and the rods through a lathe machine. The aluminium parts make the connection between the Loadcells Interface and the rods, while the rods make the connection between the aluminium parts and the post fixing mechanism. By splitting the design in different components, the waste of material is minimized, and by introducing the inox steel rods in the critical area the workpiece robustness increase. The FEA are performed with all the components together as an assembly. The 7075 aluminium alloy and 304 inox steel mechanical properties used to perform the FEA are the properties present in the Solidworks material database. For the 304 inox steel the properties are an elastic modulus of 190 GPa, a Poisson ratio of 0.29 and a yield strength of 206.8 MPa. The 7075 aluminium alloy properties have already been presented above.

The Figure 3.23 shown the von Mises stress dispersion, on the left, and the displacement dispersion, on the right, provided by the Solidworks FEA model. Thus, is easily understood the device behaviour when subjected to the expected load.

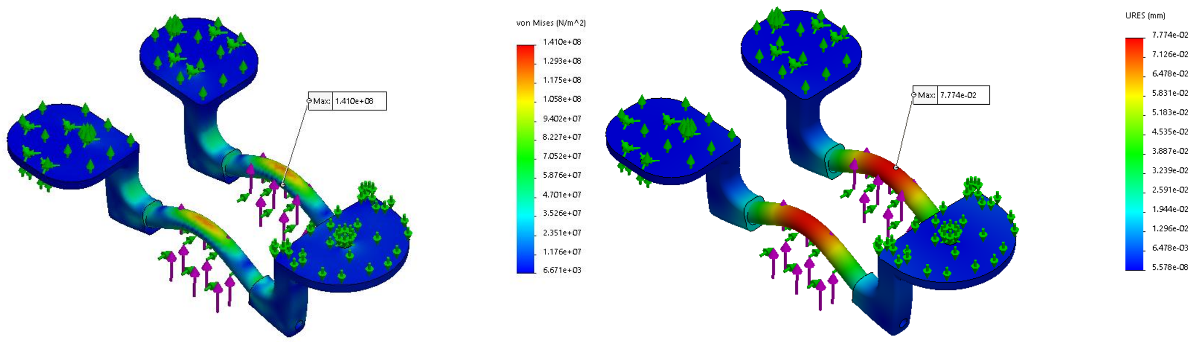

Figure 3.23 – (a) Stress dispersion on the left and (b) displacement dispersion on the right

In the Appendix A.8 is presented the data related to the Solidworks FEA model mesh convergence study. Due to the despair values from the last three points in the graphs, is considered that those points are in the overfitting domain. Between the 60000 and the 70000 elements the FEA modal indicates to be stable, however, considering the data from the Appendix A.8 is assumed a stress value of 72.8 MPa, in order to be in the safety domain. Considering the model with 66419 elements and that the higher tension occurs in the 7075 aluminium parts, this stress value indicates a safety factor of 6.94.

In the Figure 3.24 is presented the stress and displacement dispersion indicate by the MSC Nastran/Patran FEA model, which is analysed with a symmetry boundary condition.

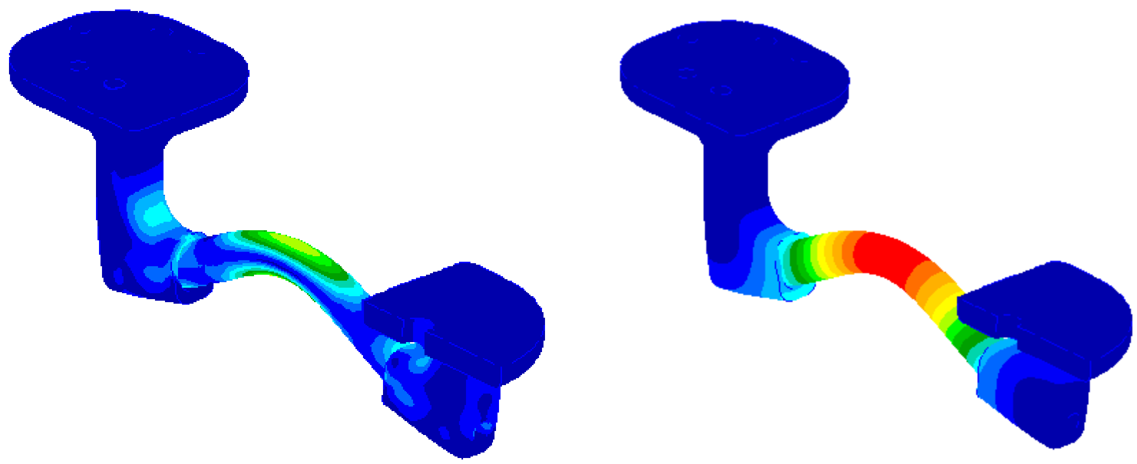

Figure 3.24 – (a) Stress dispersion on the left and (b) displacement dispersion on the right

Considering the values from the FEA model with 45961 elements, presented on the Appendix A.9, is possible to conclude that the stress value tends to 100 MPa and the displacement value to 0.0013 mm, indicating a safety factor of 5.05.

Analysing the results from the three different options is possible to conclude that the first option is the one with lower production coast, in other hand is the option with a lower safety factor of

2.07. The second option is the one with a higher safety factor of 11.22, in contrast is the one with higher production coast too. The third option still have a very satisfying safety factor of 3.47, a lower production coast and a lower production waste material, when compared with the second option.

Comparing the results from the Uninterrupted Design and Interrupted Design is concluded that the Uninterrupted Design is the most optimized one. However, depending on the application requirements, sometimes there are influential factors, such as production coast, production time or available resources, which are important to take in consideration during the decision-making process.

3.1.3 - Manufacturing

The parts from the Instrumented Saddle Device are made with resource to numerically controlled milling machines and a conventional turning lathe.

The Lower Plate, from the Loadcell Interface, is made from a 6 mm thick 7075 aluminium alloy plate. The stock plate is held to the CNC milling table with clamps and machined with 2D milling cycles. The first machining operation is drilling the holes in the middle of the workpiece, taking advantage from the stock material that is around the part to hold the workpiece with the clamps, as illustrated in Figure 3.25. This way is ensured a bigger clearance area in the middle of the workpiece. The holes that are to thread for M4 are drilled with a 3.3 mm drill and the holes that are to assemble the loadcells are drilled with a 6 mm drill. All the holes are made with peck drill cycles, cutting 1,5 mm in each cycle.

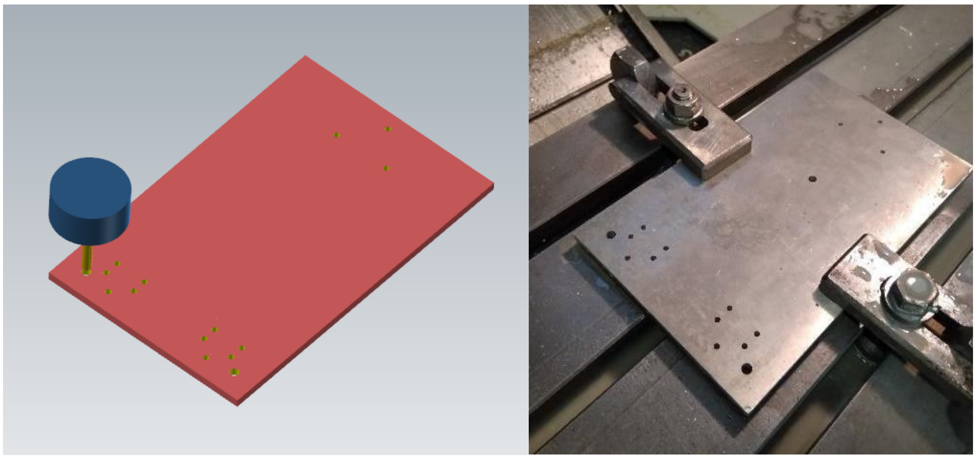

Figure 3.25 – Drilling CAM cycle on the left and workpiece clamped to the worktable on the right

Then, since that the clamps are holding the workpiece from the sides, a 10 mm 4 flutes HSS milling toll is used to machining the front and the rear geometry from the part, as illustrated in Figure 3.26 (a). Thereunto, contour milling cycles are used to cut 1 mm depth in each pass and the lead in and lead out tool path is extended 7,5 mm, in order to avoid surface imperfections. After, the workpiece is held, with clamps, in the front and rear part to machine the sides geometries, also with contour milling cycles with the 10 mm HSS milling tool, as illustrated in Figure 3.26 (b). To avoid accidents and injuries, the pieces that can be throw by the machine should be clamped to the worktable too.

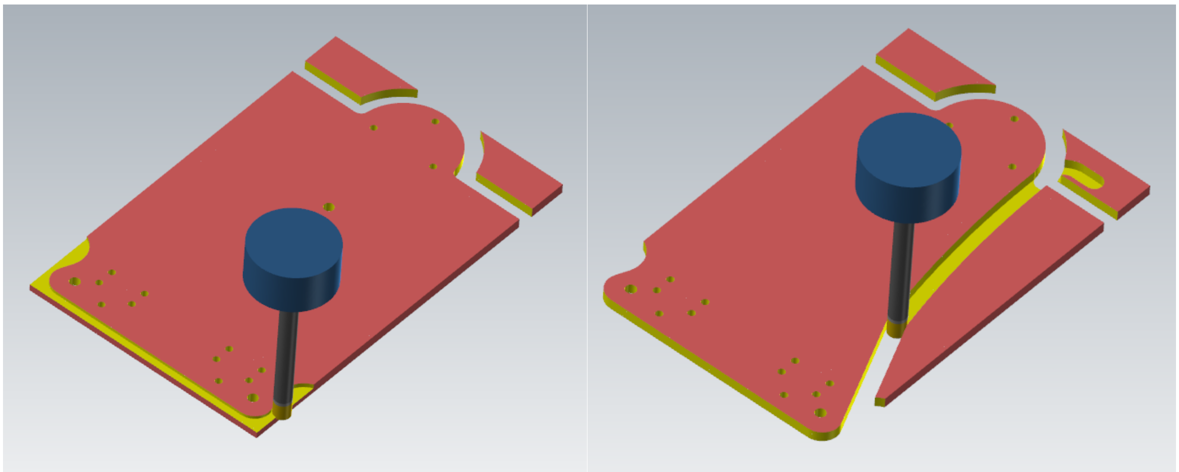

Figure 3.26 – (a) Workpiece rear end milling cycle on the left and (b) workpiece side milling cycle on the right

After the machining process, the part is sanded with sandpaper, by hand, to eliminate sharp edges and the threads are opened, also by hand.

The Upper Plate, from the Loadcell Interface, is machined with 2D milling cycles while the 6 mm 7075 aluminium stock plate is clamped to the CNC milling machine worktable. As on the Lower Plate, the first machining cycle is drilling the holes, illustrated in Figure 3.27, taking advantage from the outer part material to hold the workpiece. In the Upper Plate, all the holes are made with the 6 mm drill and peck drill cycles, cutting 1,5 mm each cycle.

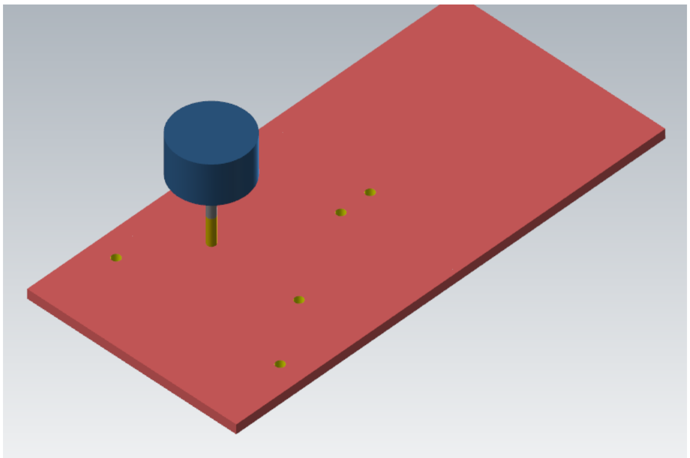

Figure 3.27 – Drilling CAM cycle

In the second operation is applied a contour cycle to mill the rear part of the workpiece, as illustrated in Figure 3.28 (a), and in the third operation the workpiece is clamped from the rear side and is machined the front geometry with a contour cycle too, as illustrated in Figure 3.28 (b).

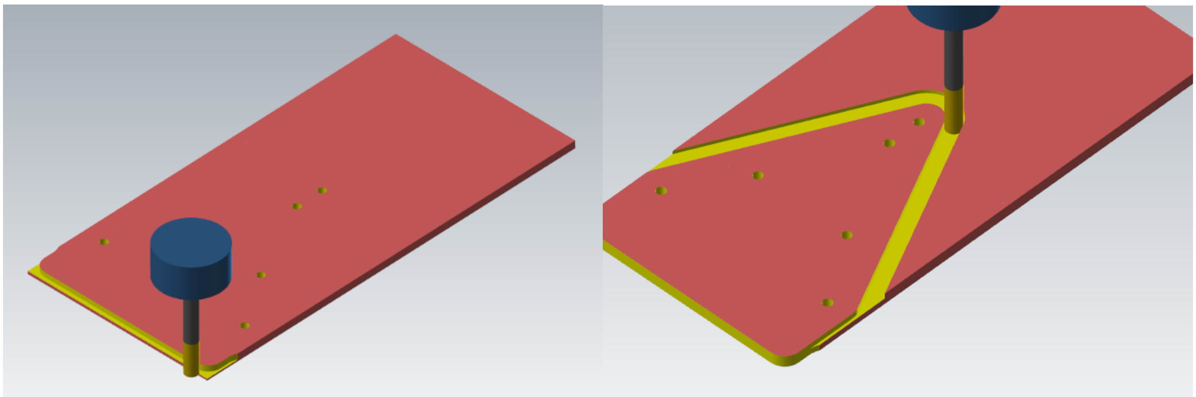

Figure 3.28 – (a) Workpiece rear end milling cycle on the left and (b) workpiece sides and front milling cycle on the right

The contour cycles are performed with a 10 mm 4 flutes HSS milling tool, with 1 mm cutting depth in each pass and with a tool path extension of 7,5 mm in the tool lead in and lead out paths to avoid surface imperfections. The pieces of material that can be throw during the machining process are clamped, to the worktable, to avoid accidents, as shown in Figure 3.29.

Figure 3.29 – Waste pieces clamped to the worktable

As finishing process, the Upper Plate workpiece is sanded with sandpaper to remove sharping edges and avoid injuries during the assembling and working process.

The Interrupted Design for the Saddle Post Connector is composed by five separated parts, two stainless steel rod, one aluminium front fixation workpiece and two aluminium rear fixation workpieces, as illustrated in Figure 3.30.

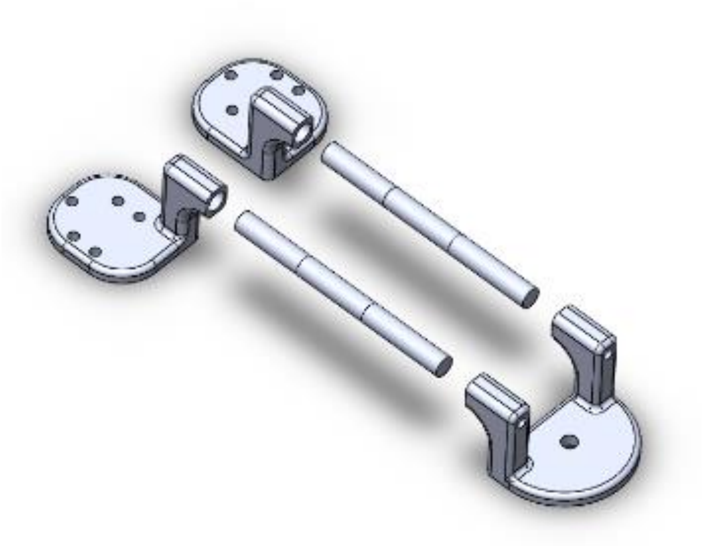

Figure 3.30 - Interrupted Design Saddle Post Connector exploded view

To machine the two stainless steel rods, an 8 mm 304 stainless steel calibrated rod are used as stock material. The rods are cut with 4 mm of excess material in a mechanical saw. Then, with the conventional lathe, the surface on one end of the rods are faced, the edges are chamfered and the 3.3 mm hole are opened. After that, the other end of the rods is faced until the required rod length is achieved, the edges are also chamfered and the other 3.3 mm hole are opened. Lastly, the 3.3 mm holes are threaded to M4 threads by hand.

The aluminium parts are machined by planes, i.e. the workpieces are machined with 3D milling cycles and, in order to be able to machine all the geometry, the milling machine work plane is changed, as exemplified in Figure 3.31.

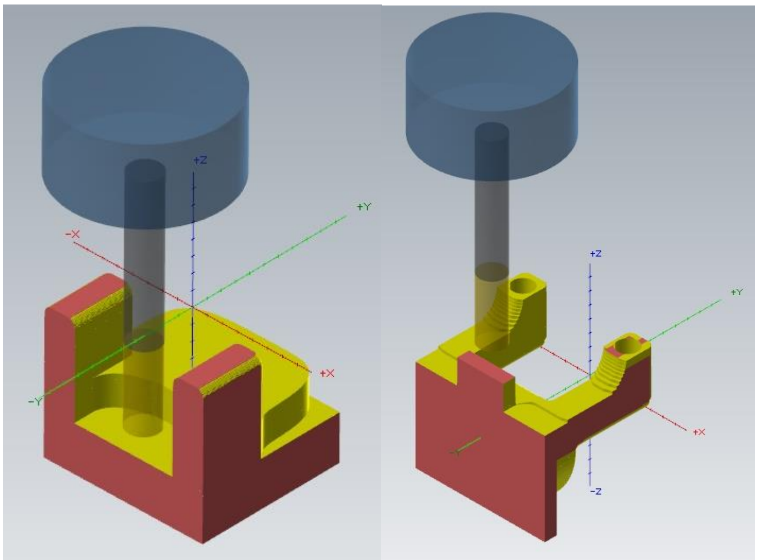

Figure 3.31 – On the left is the first work plane and on the right is the second work plane

The three parts are machined from 7075 aluminium alloy. To mill these parts are used Radial Chip Thinning Theory or dynamic milling technics. The RCTT use all the tool cutting length, reduce the lateral effort, dissipate the cutting heat on the chip and maximize the volume of material removal. With this technic the tool life increase because it is subject to lower efforts and temperatures, the machine wear is lower due to the lower efforts evolved, warranty better tolerances since that the tool deflection is reduced and improve the productivity due to the higher volume of material removal (Ferreira, 2018).

In some parts of the workpieces is possible to observe tool vibration, as shown in Figure 3.32. This vibration is due to the use of a small diameter tool with a big length out of the tool holder. However, although knowing that this is not the most correct procedure, it is the way that enable the machine to achieve those geometries.

Figure 3.32 - Tool vibration imperfections

The vibration can be avoided with the use of thermic or hydraulic tool holders and with smaller geometry approximation steps. However, this represents a much more complex and time consumption process. Considering the required demand and the workpieces operation conditions is conclude that those imperfections are not relevant to workpieces proper operation.

The Uninterrupted Design for the Saddle Post Connector is only produced with addictive manufacturing, since that its productions with subtractive manufacturing it is not viable. Due to its geometry, it requires a big stock material whose 95.9% is waste material and a lot of roughing time, which represent a lot of tool wear.

Therefore, the Uninterrupted Design Saddle Post Connector is manufactured in PLA with FDM technology. The workpiece is produced upside down, as illustrated in Figure 3.33, with a nozzle temperature of 215 ºC, a bed temperature of 50 ºC, 3 outside shell layers, 4 bottom/top shell layers and 100% infill.

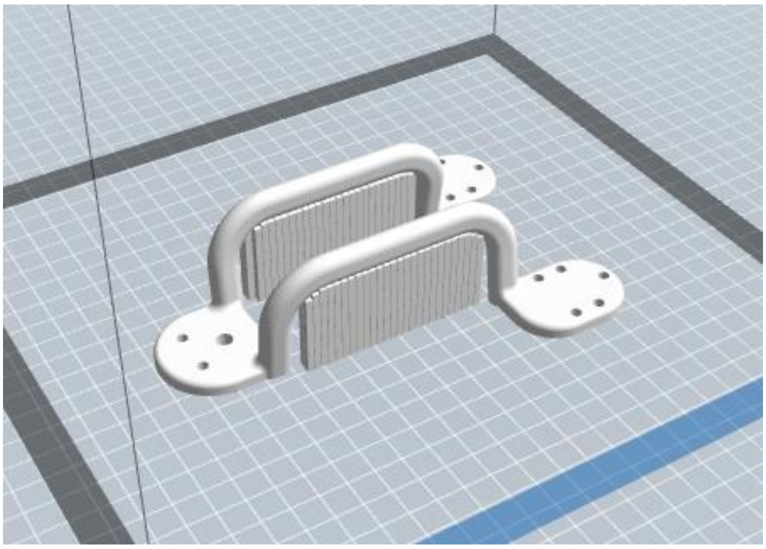

Figure 3.33 - Uninterrupted Design Saddle Post Connector Flashprint software

After the workpiece is printed, the support material is removed and the imperfections are sanded with sandpaper. The PLA is a hygroscopic material that lose its mechanical properties by absorbing the environmental humidity. Taking that into account, a coat of Barbot varnish are applied to prevent the PLA Saddle Post Connector humidity absorption and preserve its mechanical properties.

3.1.4 - Calibration

Since the sensitivity from the loadcell sensor was not supplied in the datasheet present in the Appendix A.10, it is needed to determinate. For that a laboratory setup are prepared to obtain the needed characteristics from the sensor, Figure 3.34.

Figure 3.34 - S type loadcell calibration laboratory setup

In the setup, one side of the loadcell are fixed to the upper part of a test stand, while in the other side of the loadcell are applied a traction force with calibrated masses, that goes from 0 N to 198.07 N (10 kg more 100 N). During the test are acquired the different values of the loadcell deformation, through the increasing and decreasing of the traction force, as illustrated on Appendix A.1.

With this laboratory setup are acquired the sensor sensitivity. Since the loadcell have a maximum allowed force of 100 kg (980,67 N), the determination of the sensor sensitivity, i.e. relation between the sensor response and the input signal, should be done by covering all its range, or at least, until the expected maximum during operation. However, the maximum load applied on the loadcell are 198,07 N due to laboratory restrictions and safety issues. Nevertheless, the relation between deformation and applied force is translated by a first-degree equation, the Hooke Law. Thus, is possible to extend the sensitivity acquired during the experimental setup to the entire sensor range, since that do not enter in the sensor plastic domain. Thus, the sensitivity value used in the data acquisition application is 0.6577με/N.

3.2 - Instrumented Handlebar Device

The Instrumented Handlebar Device is composed by four 350 Ω HBM 1-LY13-3/350 electro resistive strain gauges installed on a bicycle handlebar from the brand "Prototype", as illustrated on Figure 3.35, each handlebar side have two strain gauge applied 90º apart from each other. With this strain gauges configuration is possible to acquire the deformation in two well-known directions. Thus, is possible to develop methodologies to identify the force magnitude and direction. This device uses a metaheuristic artificial neural network methodology to determine the force that the rider applies in each side of the handlebar, as well as the force direction angle in the handlebar cross section plane. Both these indicators are relevant to study the user stability, balance and posture.

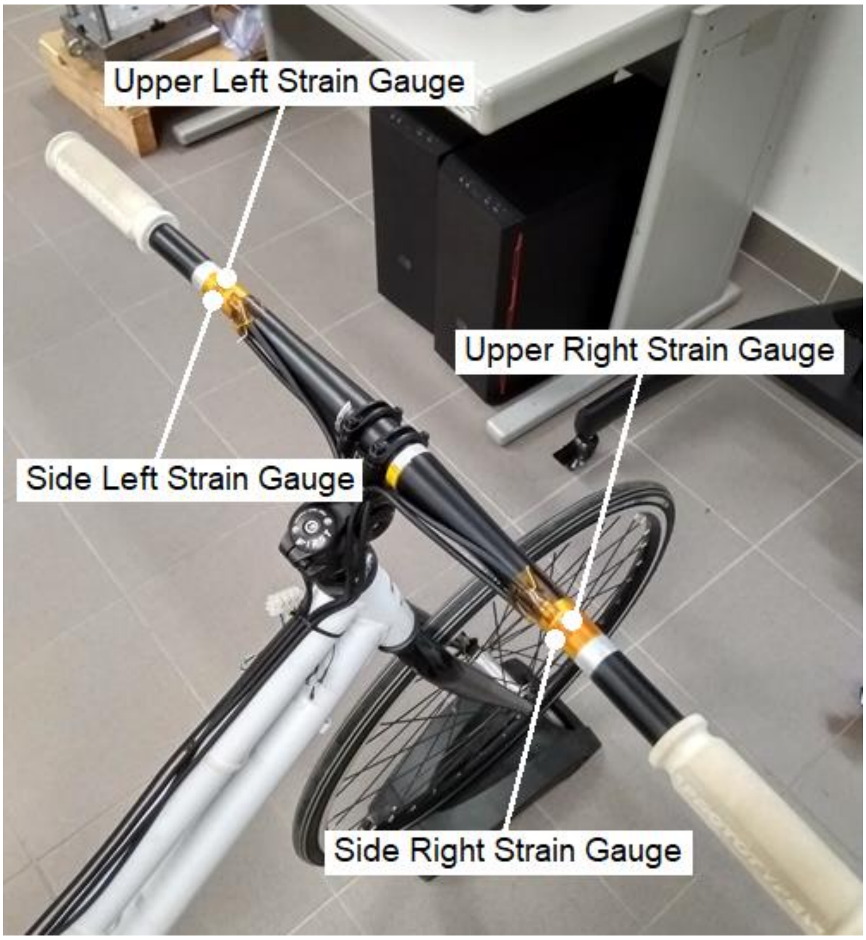

Figure 3.35 - Instrumented Handlebar Device

3.2.1 - Strain Gauge Application

Before the strain gauge application is necessary determinate the application spot. To determine the spot different factors must be taking in consideration, such as, deformation range and operations conditions. Higher deformation represents better reading values, however, the strain gauge should not deform more than 1500 με, to do not damage it. In other hand, relatively to the operations conditions, higher humidity and temperature should be avoid.

After determinate the application zone, the surface must be prepared in order to ensure that the strain gauge is applied in the raw material and have no interference from oxides, grease or surface protective materials. For that the surface is sanded and chemically treated. The strain gauge should be manipulated with tweezers to avoid contamination by hands grease and applied with a cyanoacrylate glue. During the glue curing process, a hydrostatic force is applied on the strain gauge, this force can be done using the fingertip. In Figure 3.36 is illustrated the material used in strain gauge application.

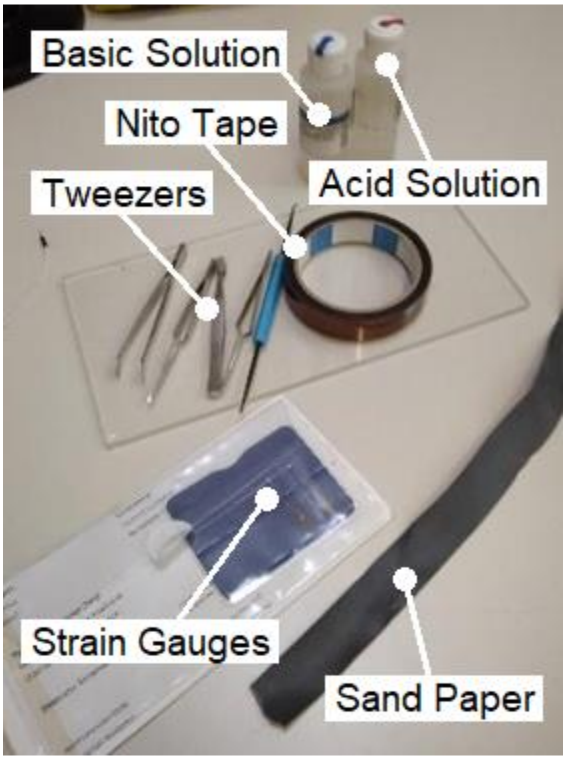

Figure 3.36 - Strain gauge application material

In order to determine the strain gauge application spot, analytic and FEA methods are used to identify the handlebar area which suffer higher deformation. As the handlebar do not have always the same cross-section, the analytic method analyses the two most adverse cases. The first case is where the momentum is higher, near the handlebar fixation mechanism, the second case is where the momentum is higher for the section with lower inertia, near the cross-section change. Taking in account that the handlebar has constant mechanical properties, i.e. constant value of Young Modulus, according to the Hooke law, the higher deformation occurs where the tension is maximum, i.e. the higher deformation occurs in the cross-section change area, as indicated in the analytical calculus present in Appendix B.1.

With the software Solidworks a finite elements model was developed to analyse the handlebar structural behaviour. A thin shell elements FEA model was implemented, since that the handlebar wall thickness are more than 60 times thinner compared to its length. As the handlebar is symmetrical in the middle, only half the handlebar is modelled and a symmetry constriction are used, this way the model is lighter and the results are equally accurate. As load condition are used a 1000 N force applied in the extremity of the handlebar, the obtained results are shown in Figure 3.37.

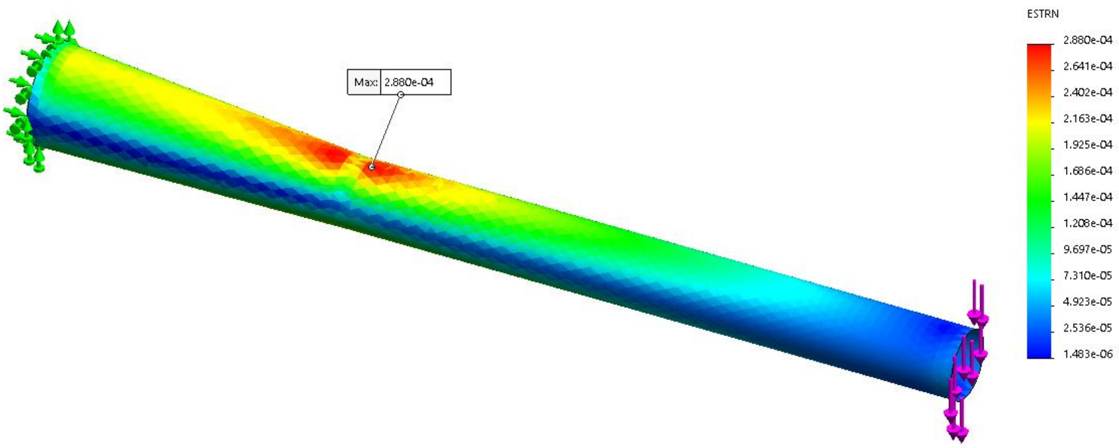

Figure 3.37 - Handlebar FEA model

Through the FEA is cross validated the results from the analytical method, relatively to the place where the handlebar deformation is higher. Considering that in higher deformation zone the strain gauges are not subjects to the heat and humidity that can come from the user hands or expected external factors, that is the optimal zone to apply the gauges.

However, with the FEA is possible to get the predicted strain value that the strain gauges will be subjected to. With an applied force of 1000N the strain gauges will be subjected to 347.2 $\mu\varepsilon$, which is a very low value. Thus, before the strain gauge application the handlebar is fragilized by spinning it in a mechanical lathe and using sandpaper, as shown in Figure 3.38. With this method is avoided the production of tension concentration geometries, that would be created with the lathe tool, and this process act as the oxide cleaning and sanding process needed to the strain gauge application.

Figure 3.38 - Handlebar fragilization

To warranty that the strain gauges are glued in the exact position and 90º apart each other, a template is made out of paper with the spaces for the strain gauges, as shown in Figure 3.39. This way is ensured that the HBM 1-LY13-3/350 strain gauges are correctly placed and ready to be glued with a Loctite cyanoacrylate glue. In the Appendix B.2 are presented the strain gauge datasheet.

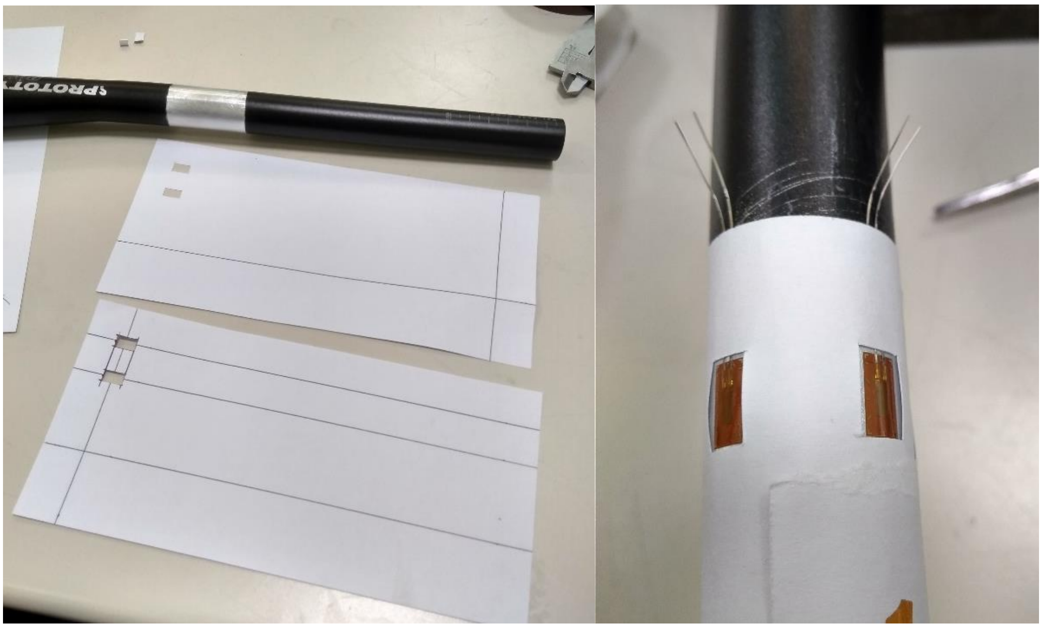

Figure 3.39 - Strain gauge installation with paper template

Each strain gauge is using a quarter Wheatstone Bridge configuration. However, to get better values from the sensors, they are connected with a three wires quarter-bridge circuit. Therefore, two electric wires are soldered in one strain gauge terminal, while only one wire is soldered to the other terminal. During the wires soldering is necessary pay attention to do not let the strain gauge terminal in contact with the metal surface, this will result in a short circuit and the measurement unit will not get correct values from the sensor.

3.2.2 - Calibration

The Instrumented Handlebar Device have two strain gauges installed in each side. Each pair of strain gauges is used to identify the force magnitude and direction, applied in each handlebar extremity. Thus, each pair of strain gauges is calibrated individually. Therefore, an inverse problem methodology is used to study the strain gauges response to well-known force magnitudes and directions. By understanding the system response, through an inverse methodology, is possible to predict the applied force characteristics based on the strain gauges output values.

To acquire the datasets needed to study the both strain gauges systems, a laboratory setup is made. This setup consists on an instrumented handlebar, a calibrated S-type loadcell, a group of calibrated masses, a NI 9219 National Instruments acquisition board, a NI cDAQ-9174 National Instruments chassis and a LabView data acquisition application. The instrumented handlebar is fixed to a test stand as if it were a bicycle, the masses are used to apply the force on the handlebar extremity, the calibrated loadcell are used to determine the force magnitude and with the Nacional Instruments hardware and LabView application is acquired simultaneously the values from the strain gauges and the loadcell, as illustrated in Figure 3.40. Using this method is acquired a variety of different force magnitudes for the same direction. Therefore, the process is repeated for 0º, 30º, 45º, 60º, and 90º of force direction, that are interchanged by rotating the handlebar on the fixation mechanism. The same methodology is replicated on the other handlebar extremity. With this setup is acquired a dataset of 600 different patterns for each handlebar side.

Figure 3.40 - Strain gauges calibration laboratory setup

To predict the applied force direction and magnitude based on the strain gauges output response, two methodologies are considered and developed using the data acquired with the laboratory setup. An analytical method and a metaheuristic method based on artificial neural networks.

The analytic method is based on trigonometry, since that the strain is measured in two different plains that are 90º apart each other, as represented in Figure 3.41, the trigonometry and vectors rules are applicable. Thus, by a vectorial sum is possible to join the strain from both planes and determine the resultant strain applied on the handlebar. Considering that the handlebar deformation is in the elastic domain, the materials elastic properties are applicable. Therefore, the resultant strain and the applied force are related through a proportional relation. Thus, using the acquired data, this proportional relation is determined. Thereunto, the relation between the resultant strain and the applied force are determined for all the dataset patterns and then the median value is selected as the proportional relation between the resultant strain and the applied force. The median value is used instead of the mean value in order to eliminate outlier values.

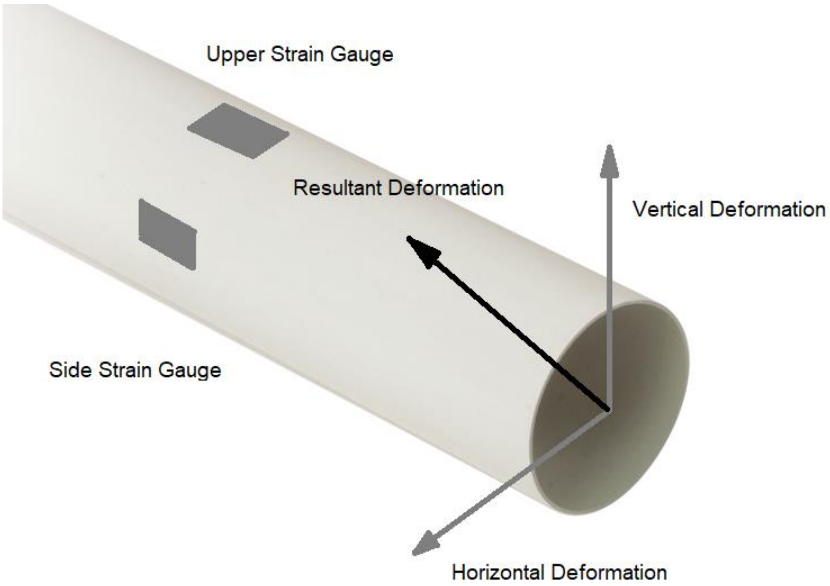

Figure 3.41 - Strain gauges application zone and work methodology

To determine the force angle, since that the strain values are measured in two 90º apart different plains and considering this values as adjacent and opposite sides of a trigonometric triangle, is possible to apply the arctangent formula to estimate the applied force direction. However, the strain gauges are not in the same referential used to experimentally measure the applied force direction. Thus, a correction constant is needed, to translate the trigonometric referential into the experimental one. Therefore, the difference between the trigonometric referential and the experimental referential are determined for every dataset pattern and then the median value is selected as the referential correction constant.

During the development of this methodology are identified some outlier values on the dataset. The outlier values identified are mostly located in patterns where the applied force is very low or even null. In this force magnitude, the deformation readied by the strain gauges are very low, therefore, any systematic measurement error or interference have a high impact on the output values, consequently in the force and direction predictions too. Considering this phenomenon, the values with an applied force below 5 N are rejected.

Thus, determining the relative error (Rerror) from the predicted value (Pval) relatively to the real value (Rval) acquired with the loadcell, as indicated in Equation 2, this analytic methodology achieved a relative error of 34.22% in the force magnitude identification and a relative error of 100% in the force direction identification. However, the force direction identification 100% error is due to the fact of a part of the dataset pattern being acquired for 0º angle. Therefore, by ignoring this untrue phenomenon, is determined a force direction identification error of 41.39%.

$$\text{Rerror} = \frac{\text{Pval} - \text{Rval}}{\text{Pval}} \cdot 100$$

Equation 2 - Prediction relative error

3.2.3 - Artificial Neural Network

The neural network methodology is developed with MATLAB software. Two neuronal networks are needed do develop, one for each side of the handlebar. From the 600 different patterns acquired with the laboratory setup, 5 are taken apart for further accuracy tests. The remaining 595 patterns are divided in 70% for neuronal network training, 15% for test and the last 15% for cross validation, which means that 417 patterns are used to train the network. Thus, the number of connections between the neuronal network neurons should be lower than the number of patterns used to the training process, in order to avoid overfitting.

Therefore, taking the referend in account, a MATLAB script is developed to optimize the neuronal network. The optimization process is made by performing all the possible network configuration, by: switching the transfer functions between the tangent sigmoid, logarithmic sigmoid and pure line; switching the training algorithm between the Levenberg-Marquardt, Bayesian Regularization, BFGS Quasi-Newton, Resilient Backpropagation, Scaled Conjugate Gradient, Conjugate Gradient with Powell/Beale Restarts, Fletcher-Powell Conjugate Gradient, Polak-Ribiére Conjugate Gradient and One Step Secant; and changing the number of neurons in each of the two layers, never exceeding the 417 neurons connections. After the optimization, each possible configuration is classified according to the performance values obtained. From this classification is picked up the three best configurations which are net255_1, net168_2 and net237_1, present on Table 1.

Network Name	Number Neurons 1º hidden layer	Number Neurons 2º hidden layer	Tansfer Function 1	Tansfer Function 2	Tansfer Function 3	Training Function	Performance
net255_1	6	47	logsig	tansig	purelin	Levenberg-Marquardt	6.28E-5
net168_2	28	12	tansig	logsig	tansig	Bayesian Regularization	7.04E-5
net237_1	13	25	purelin	tansig	purelin	Levenberg-Marquardt	7.28E-5

Table 1 - Artificial neural network top three configurations

Thus, according to the values present on the Table 1 is decided to use the configuration net255_1. Considering that the methodology used in the other side of the handlebar is the same, the system response and behaviour is similar. Therefore, a neural network is trained, for the right handlebar side, using the same neural network configuration used in the left. Through all this process is achieved a performance of 6.76E-5 for the right side and a performance of 6.28E-5 for the left, with the training evolution represented on Graph 3-3, respectively, right and left side.

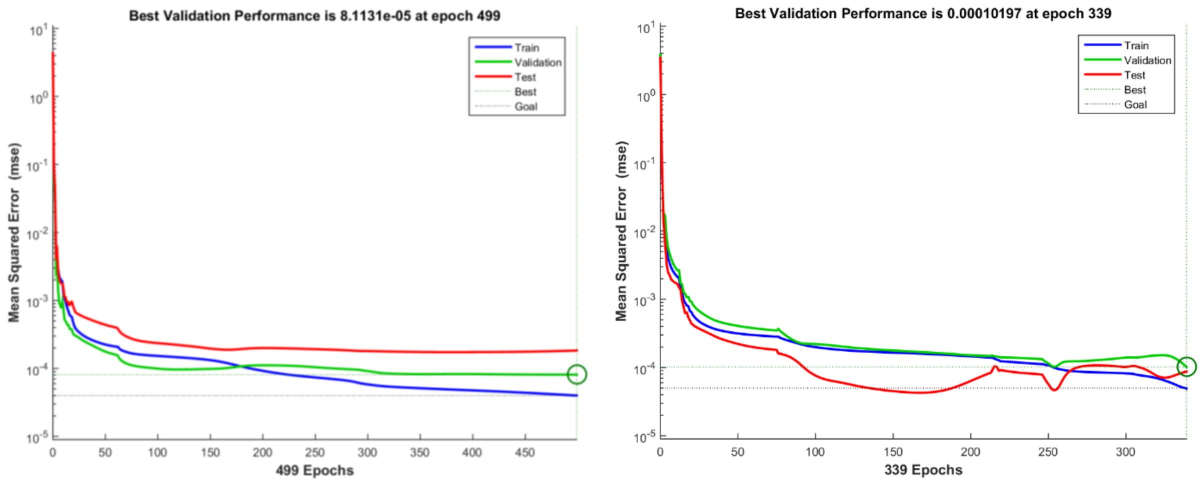

Graph 3-3 On the Left (a) training evolution for the right handlebar side and on the right (b) training evolution for the left handlebar side

On Table 2 are presented the comparation between the values predicted with the artificial neural networks and the values withdrawn from the dataset before the creation of the networks. The relative error (Rerror) is calculated from the predicted value (Pval) with the artificial neural network relatively to the real value (Rval), using the Equation 2 as previous for the analytic methodology.

Right handlebar side developed neural network

Angle	Force	Predicted Angle	Predicted Force	Relative Angle Error	Relative Force Error
0	162.58	-2.6472	155.2669	100	4.710019
30	134.60	29.8064	137.1973	0.649525	1.893113
45	111.81	35.9026	118.81	25.33911	5.89176
60	164.27	59.6969	172.0433	0.507732	4.518223
90	70.69	90.2173	72.4832	0.240863	2.473953

Left handlebar side developed neural network

Angle	Force	Predicted Angle	Predicted Force	Relative Angle Error	Relative Force Error
0	84.12	-0.10857	84.07985	100	0.047752

30	83.37	29.87957	82.43609	0.403051	1.13289
45	141.74	45.13347	142.4407	0.295723	0.491924
60	60.87	59.89961	59.98624	0.167597	1.473271
90	18.82	90.16724	19.00955	0.185478	0.99713

Table 2 - Artificial neural networks predictions and relative errors

The neural network from the right side predict the force direction with an error of 25.34% and the force magnitude with an error of 5.89%, while the neural network from the left side predict the force direction with an error of 0.40% and the force magnitude with an error of 1.47%.

Comparing the results from the analytic methodology and the artificial neural network methodology, the neural network methodology provides better results with lower prediction error either in angle or force magnitude prediction. The impressive results, obtained from the left side neural network, demonstrated the capabilities of the methodology used. However, the relative error associated to the prediction of the force direction on right side, still higher than the tolerable. Thus, the methodology is only considered viable to predict the force magnitude applied on the Instrumented Handlebar Device.

3.3 - Instrumented Pedals Device

The instrumented Pedals Device, Figure 3.42, is a modular device, which measure the vertical force exerted by the patient lower limbs and can be used independently from the rest of the ExoBike project.

Figure 3.42 – Instrumented Pedals Device

This device is composed by a planar loadcell, Vetek 202WA, which has a Zeray ZP-108S mountain bike clipping system in one of the sides and an aluminium plate on the other, where the foot is placed, as illustrated in Figure 3.43. With this method the device is easily installed in any bicycle with mountain bike clipping pedals, for indoor or outdoor purposes. In the ExoBike project the bicycle is equipped with Shimano PD-M520 mountain bike clipping pedals.

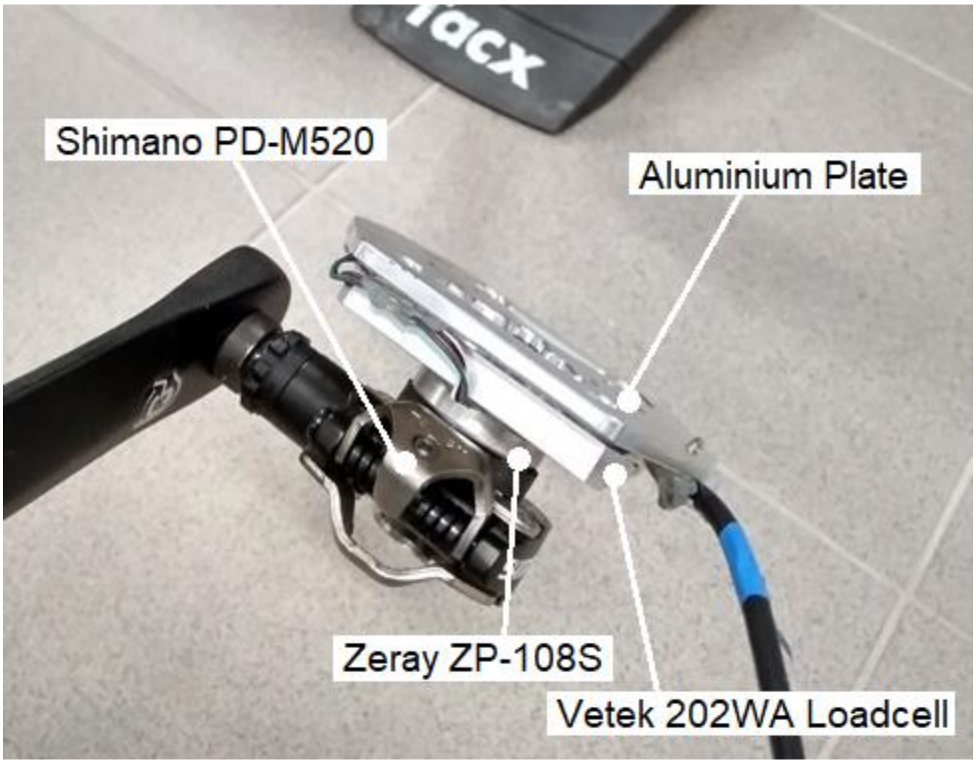

Figure 3.43 – Instrumented Pedals Device installed and with legend

The foot is placed on the aluminium plate and by applying force on this plate, the loadcell that is beneath reads the applied force value. Those values are transmitted to an acquisition board which is connected to a computer. The connection between the loadcells and the acquisition board are made by wires attached to the user lower limbs, in order to prevent the wires to wrap around the pedals.

Due to the aluminium plate geometry, it also enables the use of clipping shoes through a metallic interface. Ensuring a better fixation and correct positioning of the foot on the device, as illustrated on Figure 3.44.

Figure 3.44 - Clipping Shoe Interface on the left and the Clipping Shoe Interface installed on the Foot Interface on the right

The Instrumented Pedal Device have an overall distance from the pedal centre rotation of 37 mm, as represented in Figure 3.45 (a), compared to the 14 mm of a normal bicycle pedal, as represented in Figure 3.45 (b).

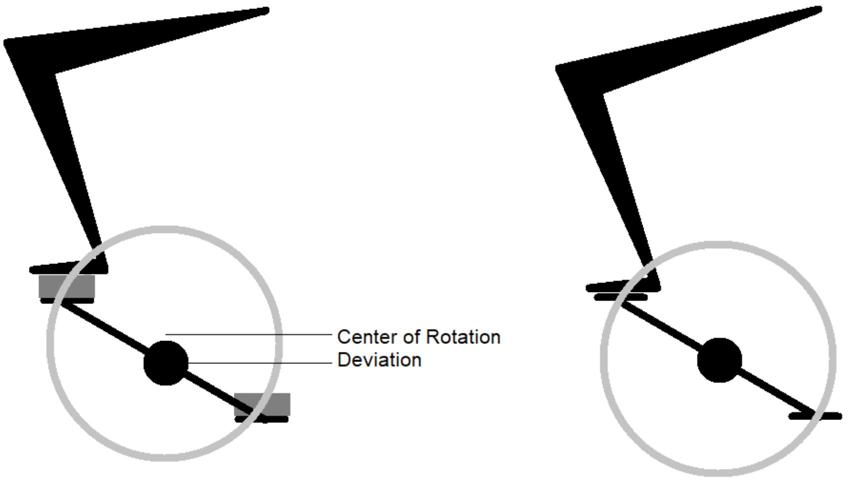

Figure 3.45 - (a) Pedalling cycle with the Instrumented Pedal Device on the left and (b) Pedalling cycle with a normal pedal on the right

Taking this into account, the pedal rise 23 mm, as illustrated in Figure 3.45, however, it can be easily corrected by raising the bicycle saddle in 23 mm too. In other hand, since that the distance between the force application region and the pedal centre of rotation is larger, than in a normal bicycle pedal, the Instrumented Pedal Device is more unstable. However, with the use of clipping shoes, this condition is not noticed.

3.3.1 - Design

The design of the Instrumented Pedal device is composed by two main components. These components are designed taking in consideration the loadcell dimensions, in order to warranty the loadcell proper operation and keep the overall height as lower as possible. An extra third component is developed so it can be installed in the device and create an interface that allow the use of mountain clipping shoes.

As main goal, the developed pedal device must withstand the force inherent to the cycling exercise. As an additional goal, the device should be as comfortable and ergonomic as possible, so that the acquired values are as real as possible, too. Like the previous device, Instrumented Saddle Device, the workpieces should be able to manufacture with the materials already available in the warehouse, in order to minimize the waiting time.

As represented in Figure 3.46, the Cleat Interface provide the connections between the clipping mechanism and the loadcell. While the Foot Interface is assembled in the other end of the loadcell and work as interface between the user foot and the loadcell. A gap of 2mm between the components and the loadcell allow it to deform and acquire proper values.

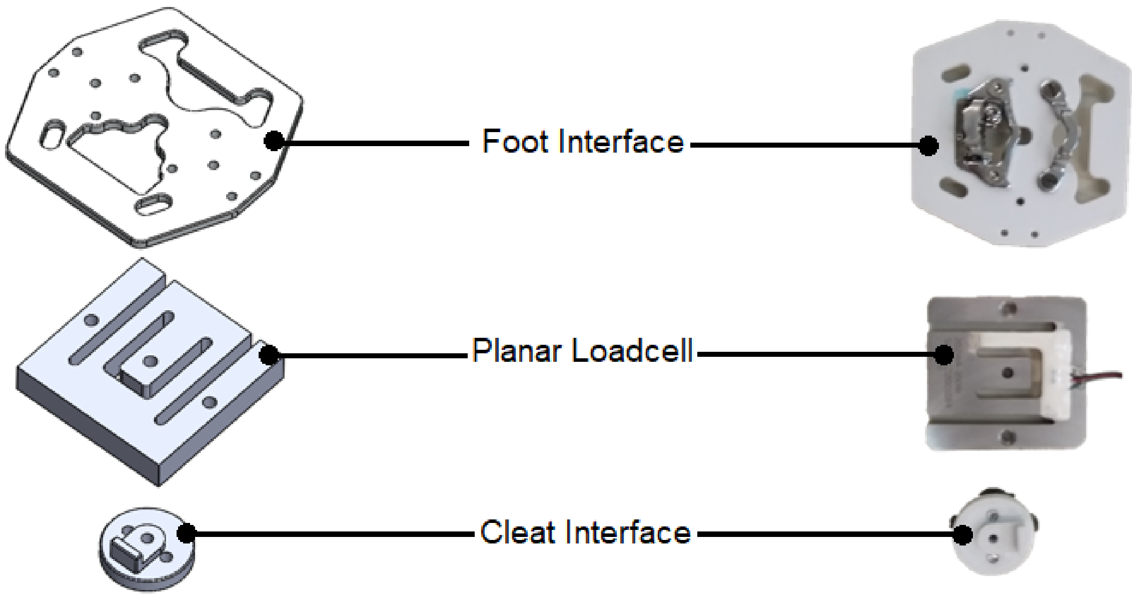

Figure 3.46 - Exploded view on the left with the respective prototype on the right

In order to produce the components with materials stocked in the warehouse, the Foot Interface is machined in 6082 aluminium alloy, while the Cleat Interface and Clipping Shoe Interface are machined in 7075 aluminium alloy.

3.3.2 - Numerical Models

To verify that the Instrumented Pedals Device withstand the foreseen loads are performed a static analysis of the worst-case scenario. The studies are performed considering the user entirely supported on one pedal, i. e. the user is applying all his weight in the pedal. Taking, again, in consideration the study by Stephen Gill (2019) which indicate 91.72 kg as the higher average weight and in order to simplify and be on the safety side, the load used on the FEA is 1000N, approximately 101.97 kg.

The Foot Interface 6082-T6 aluminium mechanical properties are acquired from the Makeitform website (MakeItForm, 2019). Thus, the mechanical properties used are a Poisson ratio of 0.33, an elastic modulus of 69 GPa and yield strength of 270 MPa. The Cleat Interface are made in 7075 aluminium alloy, the same material used in the Instrumented Saddle Device parts. This material has an elastic modulus of 72 GPa, a Poisson ratio of 0.33 and a yield strength of 505MPa.

The Cleat Interface and the Foot Interface are studied separately. Thus, being two studies of individual bodies there are no needed the use of connectors or components contact settings. In the Foot Interface FEA models, the elements on the surface that contact with the planar loadcell are restricted to translation in only two direction, i.e. the elements cannot leave the plane surface where they are inserted. While the elements inside the hole where the bolt pass, to connect the Foot Interface with the loadcell, are restricted with a hinge boundary condition, i.e. the elements only can translate around the hole axis, as illustrated in Figure 3.47.

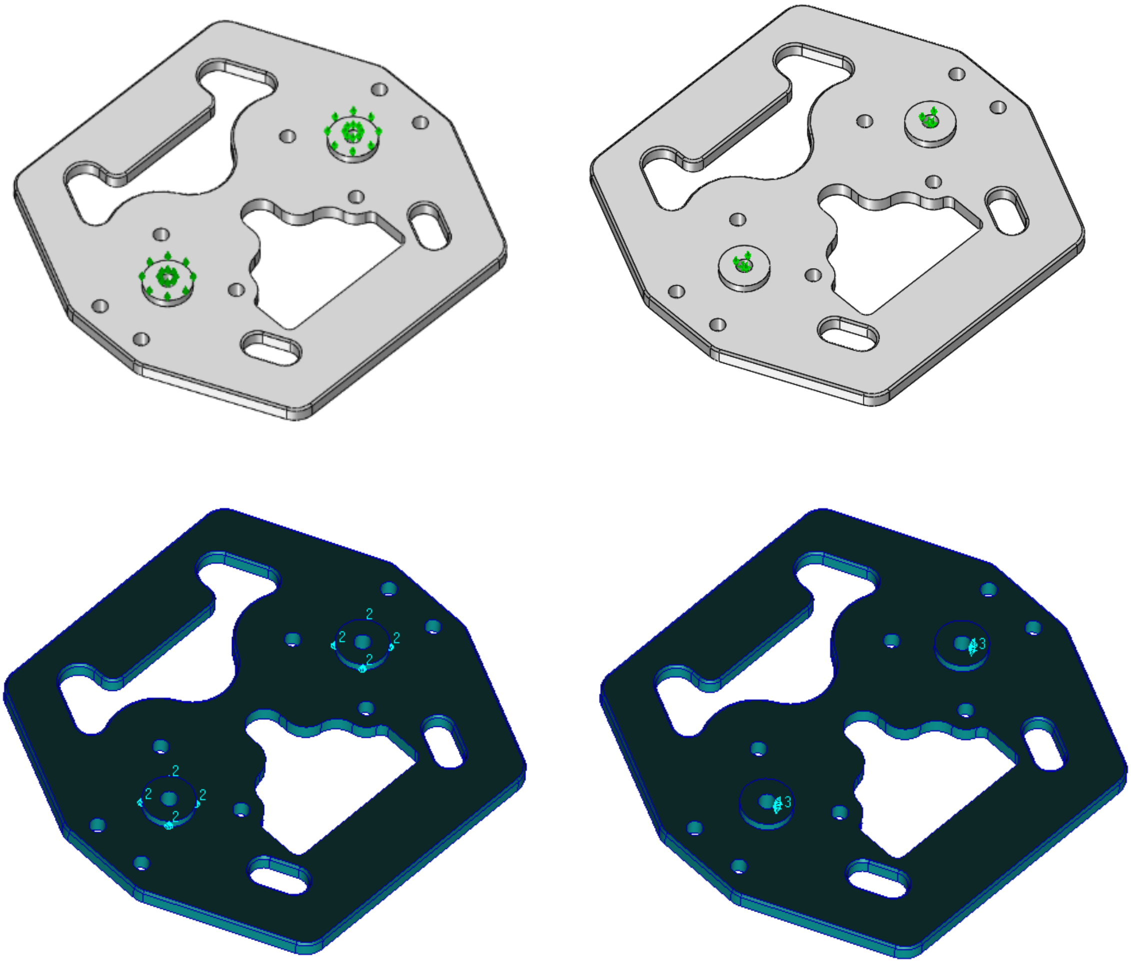

Figure 3.47 – Contact surfaces boundary condition on the left and holes boundary conditions on the right

In the Cleat Interface FEA models, the elements on the surface that contact with the clipping pedal mechanism are restricted in one direction, i.e. the elements cannot leave the plane surface where they are inserted. In other hand, the elements inside the holes used to assemble the cleat mechanism are restricted with a hinge condition, i.e. the elements only can translate around the hole axis, as illustrated in Figure 3.48.

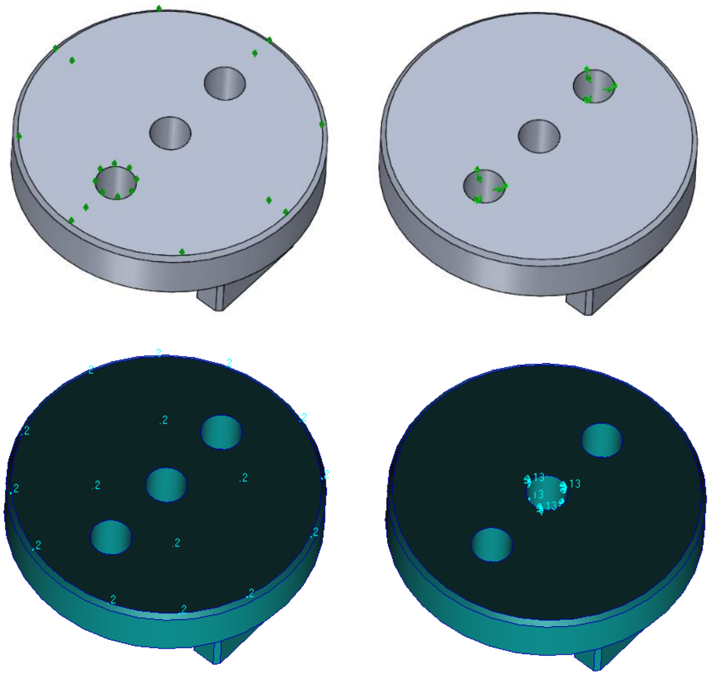

Figure 3.48 - Contact surfaces boundary condition on the left and hole boundary condition on the right

Both in the Foot Interface FEA models and the Cleat Interface FEA models are applied a vertical load of 1000N. In the Foot Interface, the load condition is applied in the planar surface which contact with the user foot. While in the Cleat Interface, the load condition is applied in the surface where the planar loadcell contact with the workpiece, as illustrated in Figure 3.49.

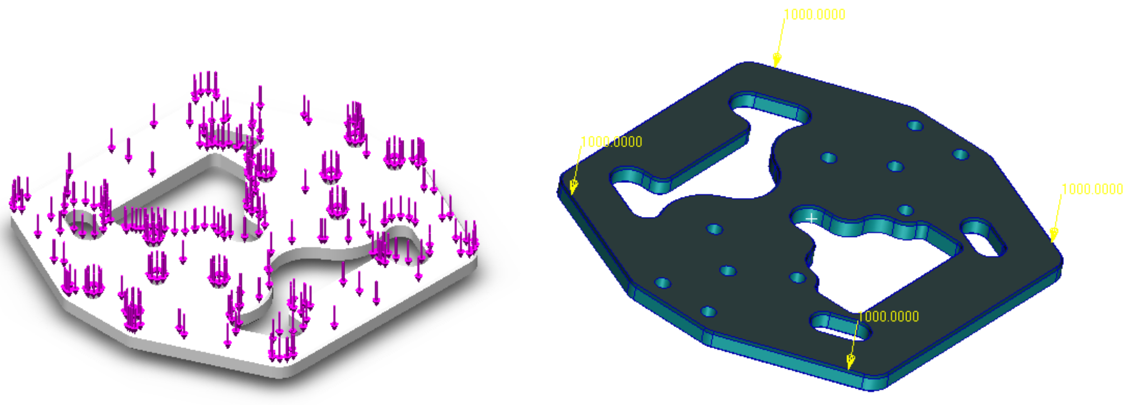

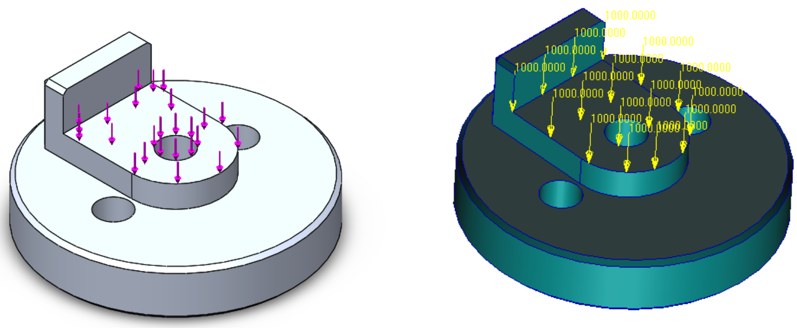

Figure 3.49 - Load conditions application areas

The Figure 3.50 show the implication that the load condition introduces in the Solidworks Foot Interface FEA model, by displaying the stress and displacement scattering over the model.

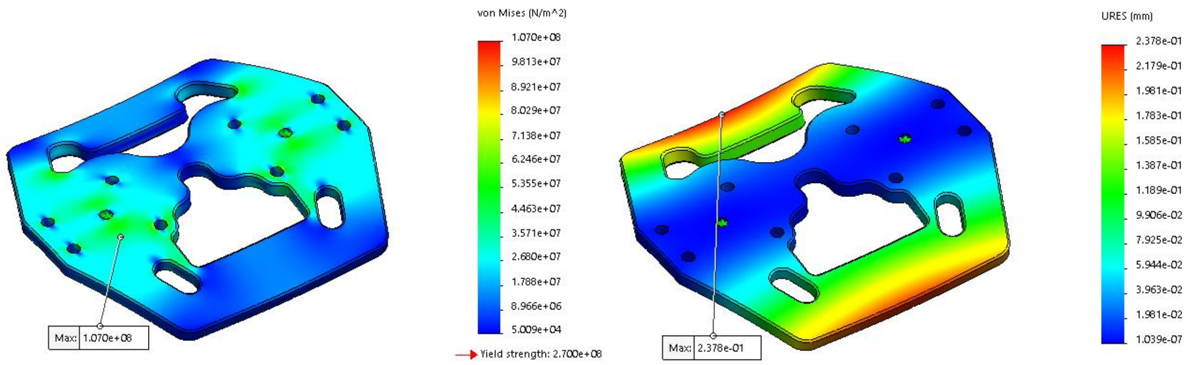

Figure 3.50 – (a) Stress dispersion on the left and (b) displacement dispersion on the right

By analysing the graphs present in the Appendix C.1, is possible to conclude that the FEA model with 40241 elements provide the better mesh convergence values, thus, this is the model which better represent the reality. It is also possible to affirm that the stress tends to a value below 100 MPa and the displacement tend to a value below 0.238 mm, indicating a factor of safety of 2.7.

In the Figure 3.51 is presented the stress and displacement dispersion over the Solidworks Cleat Interface FEA model. On the left is presented the stress dispersion and on the right is presented the displacement dispersion,

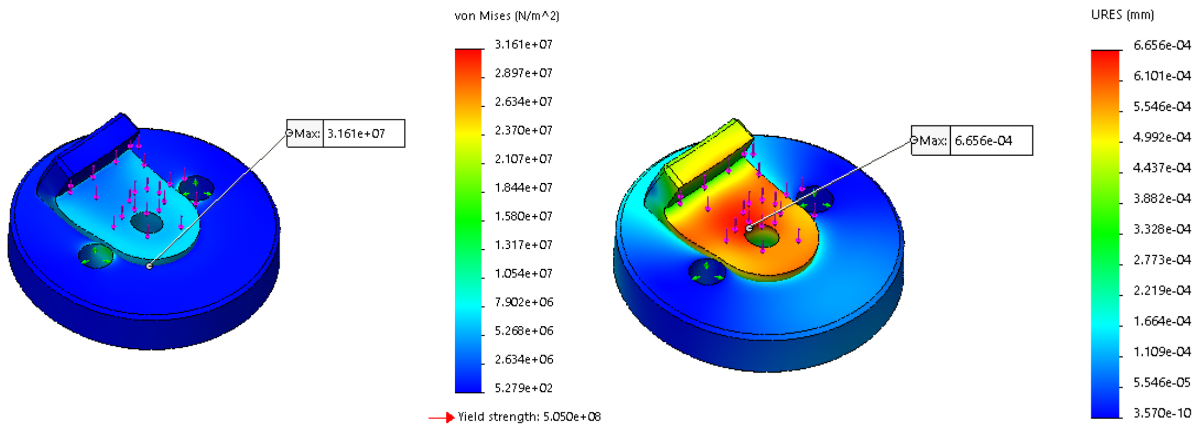

Figure 3.51 – (a) Stress dispersion on the left and (b) displacement dispersion on the right

The values present on the Appendix C.2 suggest that the FEA model with 150992 elements is a good representation of the reality and conclude that the model tends to a stress value of 18 MPa and a displacement value of 0.000665 mm, indicating a factor of safety of 28.1.

The MSC Nastran/Patran Foot Interface FEA model mesh convergence study is not conclusive, since the study do not indicate a model stabilisation. Therefore, this FEA model is not considered for the Foot Interface design validation. However, the mesh convergence graphs are present in the Appendix C.3 and the stress and displacement scattering are represented on the Figure 3.52.

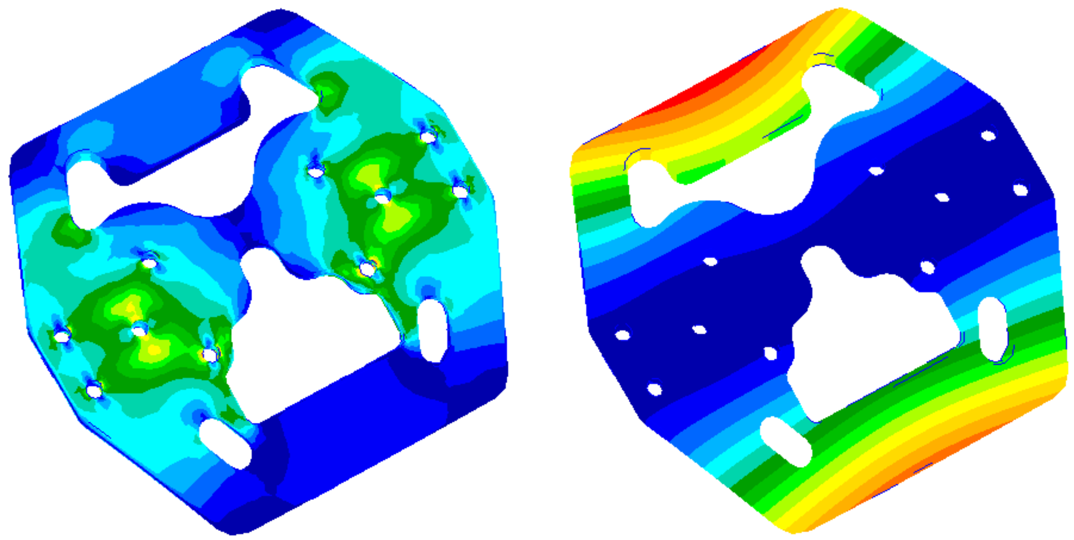

Figure 3.52 – (a) Stress dispersion on the left and (b) displacement dispersion on the right

The Figure 3.53 illustrate the Cleat Interface MSC Nastran/Patran model behaviour to the foreseen loads. Illustrating the stress and displacement distribution all over the FEA model.

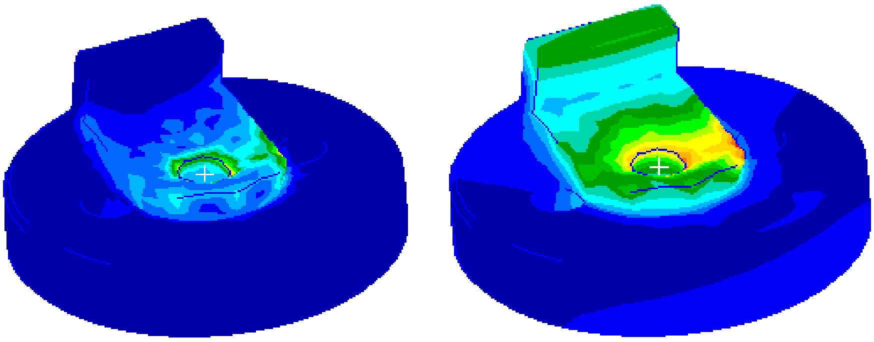

Figure 3.53 – (a) Stress dispersion on the left and (b) displacement dispersion on the right

Considering the results in the Appendix C.4 is possible to affirm that the FEA model with 88674 elements is a satisfactory representation of the reality and that the stress value is below 30 MPa and the displacements value below 0.00003 mm, indicating a safety factor of 16.83.

Considering the results obtained from the Foot Interface FEA models and the Cleat Interface FEA models mesh convergence, even that the results from the MSC Nastran/Patran models and the Solidworks Foot Interface model do not have stable values, is possible to conclude that the Instrumented Pedal Device will withstand the foreseen loads with a factor of safety of 2.7, which is a satisfying value considering the operating environment.

Since that the pedals device are subject to a dynamic pulsating load, over the pedalling cycles, also the study of fatigue damage is required. However, since that the higher value of stress, present on the workpieces, are lower than the material fatigue limit stress, presented on Graph 3-4, is concluded that the workpieces are in the infinite fatigue life domain.

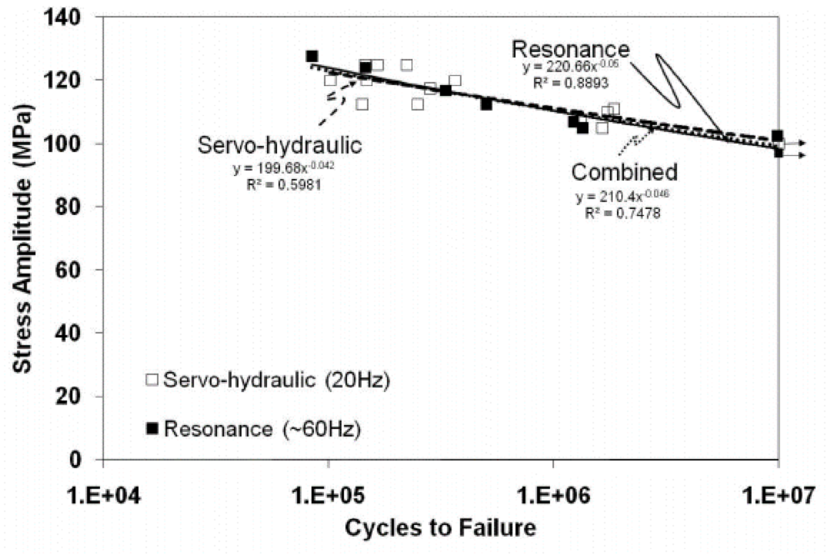

Graph 3-4 Aluminium Alloy 6082 S-N curve (Nanninga, 2008)

3.3.3 - Manufacturing

Considering that the Instrumented Pedal Device integrate a cleat on one end, to install the pedals on mountain bicycle cleat pedals, and on the other end it integrate a mountain bicycle cleat mechanism, all the system are prototyped with 3D printing to verify that all the integrant parts of the device operate in the proper way, before its production in aluminium. The parts are printed in a Flashforge Guider II FDM 3D printer with 80% infill, three outside shell layers and four bottom/top shell layers, as illustrated in Figure 3.54. Thus, the parts have enough strength to perform experimental tests to the methodology and help analysing if any modification is needed.

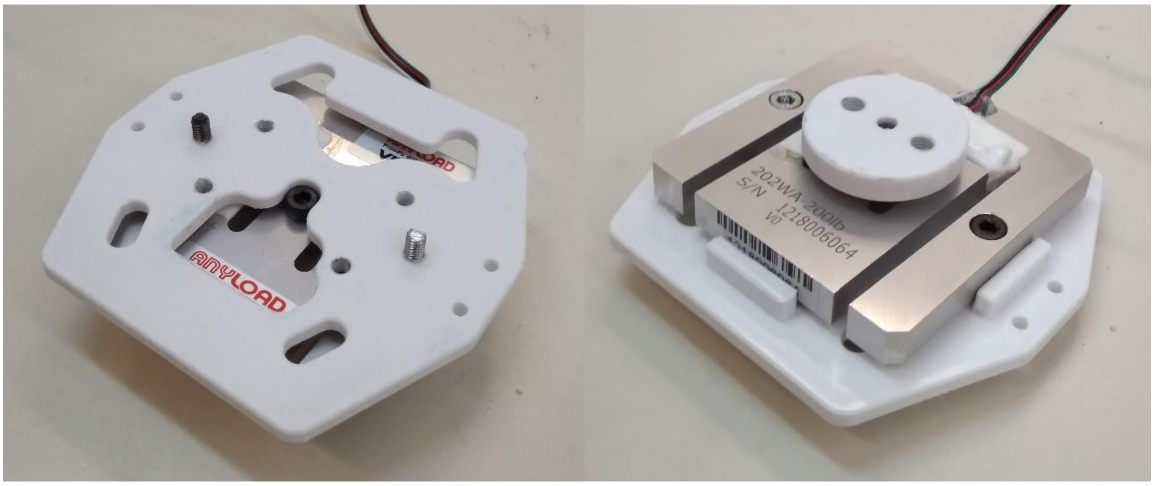

Figure 3.54 – Instrumented Pedal Device 3D printed prototype

The parts from the Instrumented Pedal Device are produced with a 5-axis CNC milling machines. The machining of the Cleat Interface is made with two different clamping positions. On the first clamping position, a 4 flutes 10 mm endmill is used to rough the excess of material from the workpiece. Then, a waterline and a horizontal 3D cycles are used to trim the workpiece to the correct dimensions. Then, an 8 mm chamfer tool is used to chamfer the workpiece sharp edges, which can cause injuries, with 2D contour cycles. A 3.25 mm and a 4.25 mm drills are used to drill the holes with peck drill cycles, cutting 1 mm of material in each cycle. The 3.25 mm hole is treaded to M4 thread and the 4.25 mm holes are threaded to M5 thread, both by hand. The M5 holes are used to install the mountain bicycle cleat, while the M4 hole is used to fix the planar loadcell.

On the second clamping position the workpiece is milled to the correct height with the 10 mm endmill and 2D facing cycles. Also, the sharp edge resulting from the facing cycle are trimmed with the chamfer tool and a 2D contour cycle.

The Foot Interface workpiece is also produced with two clamping positions. In the first clamping position is used RCTT technics by applying 2D dynamic milling cycles, with a 10 mm endmill, to rough the stock material around the workpiece and, with a 4 mm endmill, to rough the stock material inside the workpiece pockets, as illustrated in Figure 3.55.

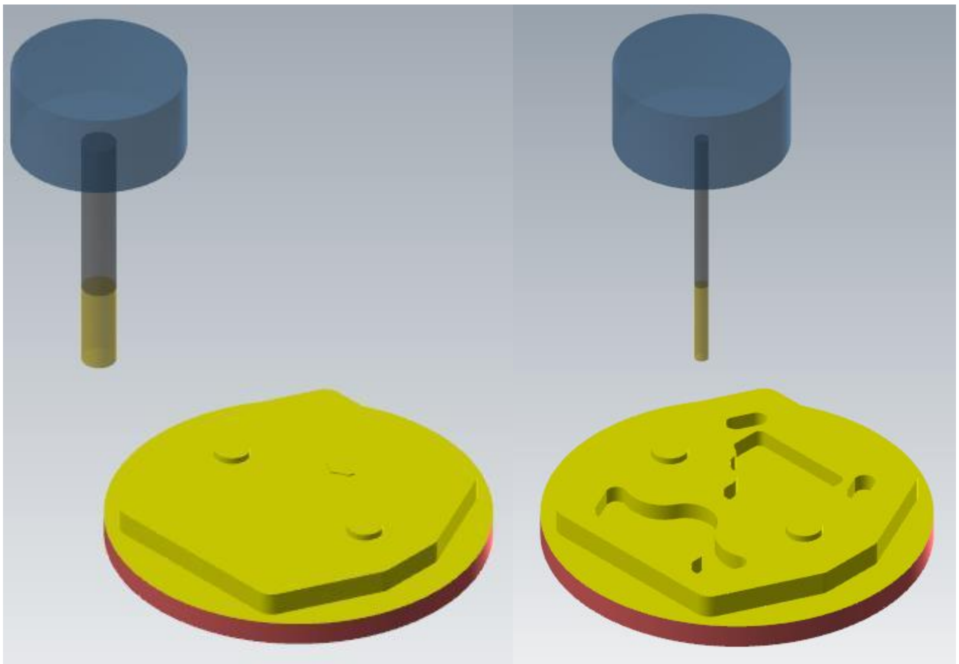

Figure 3.55 – Cycles made with the 10 mm tool on the left and cycles made with the 4 mm tool on the right

Then, still in the first clamping position, is applied horizontal and ramp cycles in order to trim the workpiece to the final dimensions, peck drill cycles to drill the 3.25 mm holes and 2D contour cycles to trim the sharp edges with an 8 mm chamfer tool.

In the second clamping position the workpiece is flipped upside down. Thus, 2D facing cycles are performed, with the 10 mm endmill, to trim the workpiece to the correct dimension and 2D contour cycles are applied to chamfer the sharp edges, which can cause injuries, with the 8 mm chamfer tool.

To manufacture the Clipping Shoe Interface is used 2D RCTT dynamic milling cycles, during the rough process. Since that this technic maximize the material removal rate, it reduces the production time. In the workpiece finishing process is used a 10 mm endmill with a facing cycle and a ramp cycle, to trim the remaining material in the upper face and around the workpiece, respectively. Then, peck drill cycles are applied to drill the 4.25 mm holes.

After, the part is flipped and a facing operation, with the 10 mm endmill, is applied to trim the workpiece to the correct dimension, as illustrated in Figure 3.56.

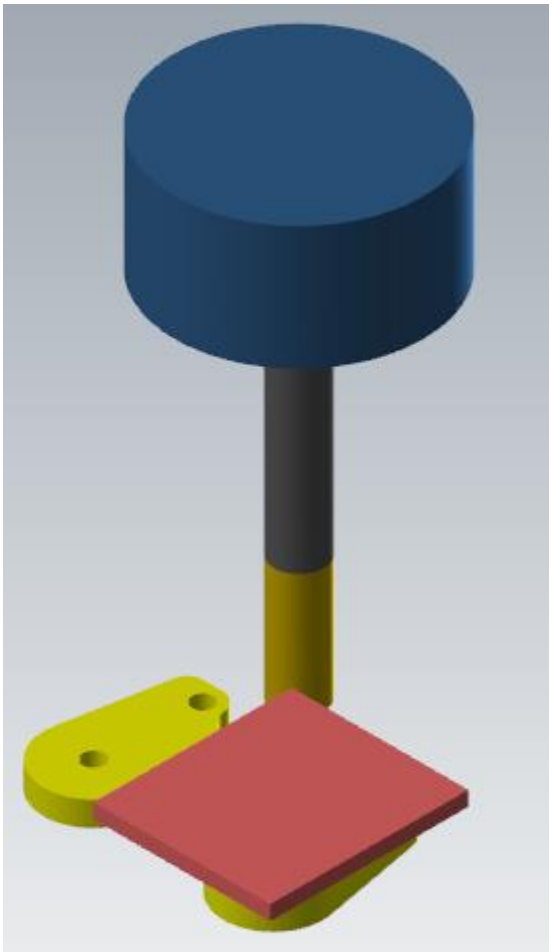

Figure 3.56 - Final facing operation

3.3.4 - Calibration

The Vetek 202WA loadcell datasheet, Appendix C.5, do not supply the sensor sensitivity that correlates the force and the loadcell deformation neither the sensitivity that correlates the voltage variation and the force applied on the sensor. Thus, in order to determine the two characteristic curves needed, a laboratory setup is created. The laboratory setup created consist in fixe on side of the loadcell to a test stand and apply a traction force on the other side, which increase and decrease gradually, from 0 to 227.1 N. As illustrated in Figure 3.57.

Figure 3.57 - Vetek 202WA calibration laboratory setup

By acquiring the loadcell deformation value, over the traction force application is possible to elaborate the first graph present on the Appendix C.6, which concerns to the relation between force and deformation. Since the voltage reading are very tiny and instable, small force increment are not noticeable. Thus, only two measurement are made, one without load and other with a mass of 83kg, resulting in the second graph present on the Appendix C.6. These graphs represent the two sensitivity curves needed to the data acquisition applications.

The proper loadcell sensitivity calibration should cover all the sensor range, which goes from 0 N to 889.64 N, with several intermediate values. Although, the loadcell have a linear response, which means that is possible to extend the acquired sensitivity line to the entire sensor range. Thus, for the relation between the force (N) and loadcell deformation (με) is used a sensitivity of 0.9806 N/με and for the relation between the force (N) and the voltage (V) variation is utilised a sensitivity of 198524 N/V with a systematic error of 397.05 N.

3.4 - Instrumented Grip Device

The Instrumented Grip Device consists in four measuring workpieces disposed around a handlebar, as illustrated in Figure 3.58. Those workpieces are hold in place by two supports, on in each side, and allow the measurement of the force applied, independently, on each workpiece. The sum of the forces applied in the workpiece represent the gripping force exerted by the patient on the device. The force value applied in each workpiece is determined through a strain gauge applied on the interior of the device.

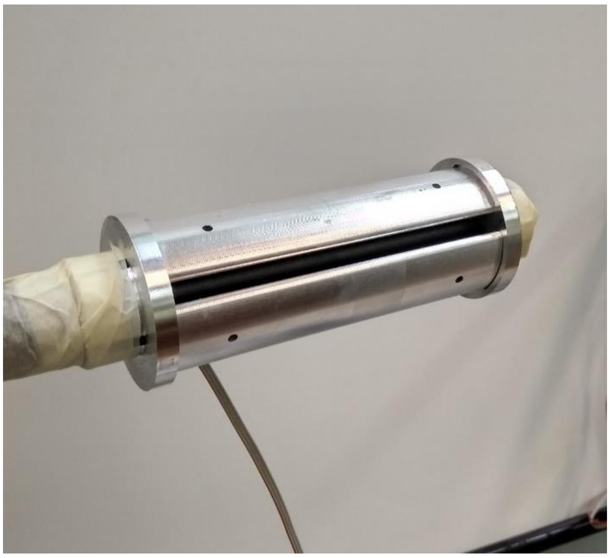

Figure 3.58 - Instrumented Grip Device

All the Instrumented Grip Device parts are developed considering the resultant device diameter, in order to keep the handle as ergonomic as possible. The total diameter of the device is 40 mm, which according to Kong and Lowe (2005) is a comfortable diameter for maximum grip force exertions, as observable in the Graph 3-5.

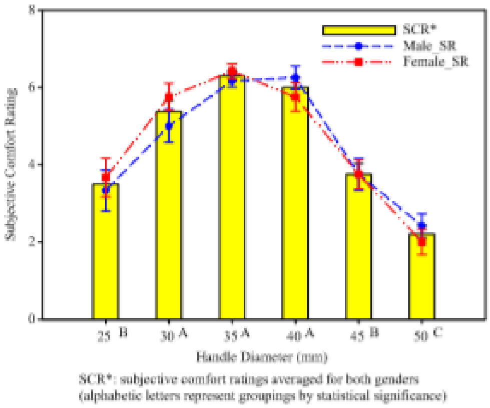

Graph 3-5 Relation between comfort rating and handle diameter (Kong & Lowe, 2005)

3.4.1 - Design

The design of the Instrumented Grip Device split in three different workpieces, the Mount, the Blade and the Instrumented Rod. The Instrumented Rod is the measuring component from the device, it consists in a calibrated rod instrumented with a strain gauge installed in the middle of the length. The Blade work as interface between the user hand and the Instrumented Rod, thus, the device is more ergonomic and avoid possible interferences between the user and the instrumented components, such as, the body temperature. The role of the Mount is to keep the different parts together in the right place, while allowing the clearance needed for the proper operation of the device.

The Mount holds four Blades and four Instrumented Rods around the handlebar, as illustrated in Figure 3.59.

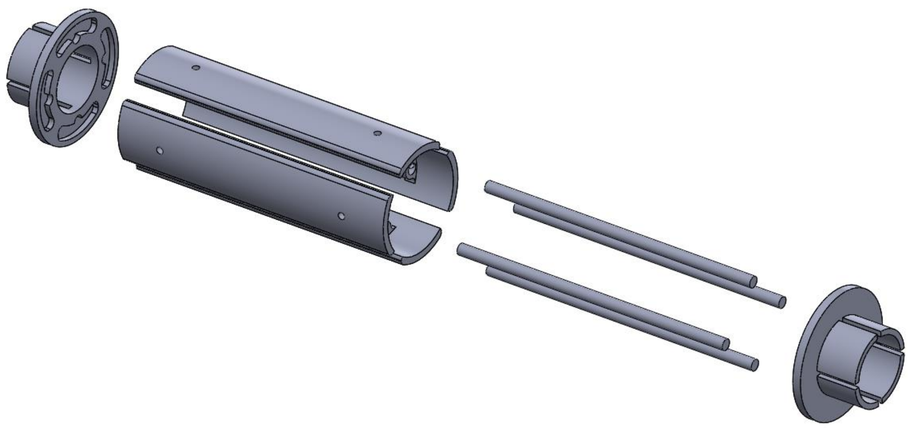

Figure 3.59 - Instrumented Grip Device exploded view

As main goal the Instrumented Grip Device must withstand the user griping force and still deform the enough to provide satisfactory strain gauges values. In order to minimize the waiting time, the Mount and the Blade are produced in 7075 aluminium alloy while the Instrumented Rod are made from 304 stainless steel, which are materials already available in the materials warehouse.

The Instrumented Rod dimensioning is made through analytic calculus. According to Kong and Lowe (2005), for a handle with a diameter of 40 mm the maximum force registered is about 400 N. However, the grip force will not be equally distributed by the four Instrumented Rods, i.e. some rods will suffer higher stress than others, and the bicycle handle is not only subject to the grip force, it is also subject to the user supporting force. Therefore, the Instrumented Rods are dimensioned for a foreseen force of 700 N in total, in other words, 175 N on each rod. On each rod extremity is considered a support reaction force, since that the Instrumented Rod is supported by a Mount in each side. The Blade contacts with the Instrumented Rods on two points equally distanced from the rod ends, as illustrated in Figure 3.60. This way, the area where the strain gauge is installed, is under pure flexion.

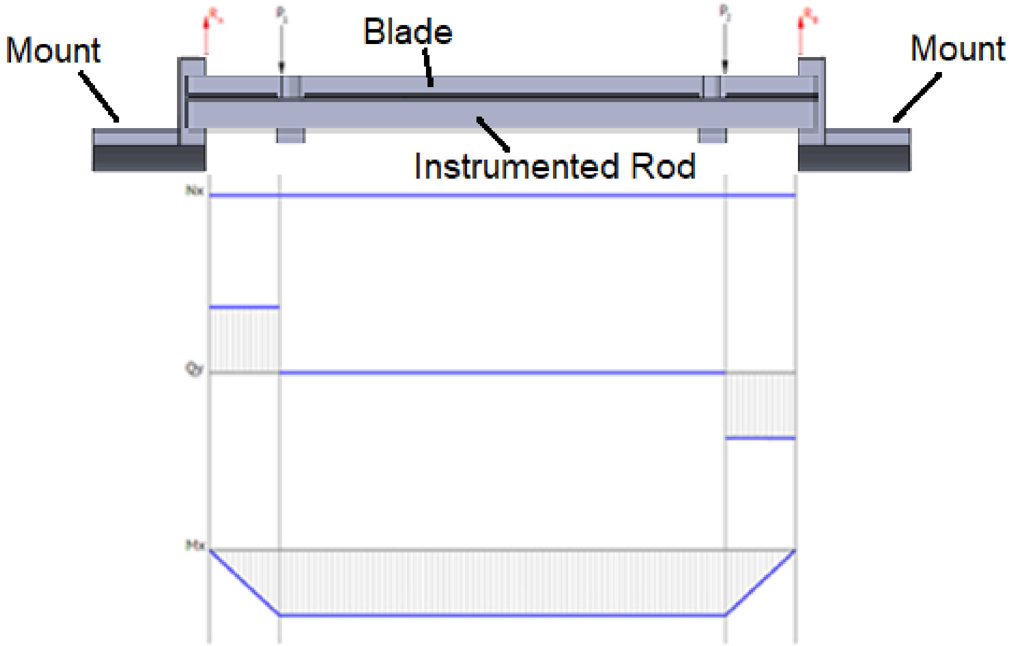

Figure 3.60 - Forces distribution schematic

Considering the 304 stainless steel properties and that the strain gauges should not suffer a deformation higher than 1500 με, is determined that the Instrumented Rod maximum stress cannot exceed 200 MPa.

Thus, solving the calculus is determined a relation between the Instrumented Rod diameter and positioning of the Blade – Instrumented Rod contact point. Considering factors such as strain gauge enough installation clearance and overall device volume, is determined that the 4 mm diameter rod meets the imposed requirements. The analytical calculus is present in Appendix D.1.

3.4.2 - Numerical Models

Once that the measuring component are dimensioned to withstand a total force of 700 N, a FEA static analysis is performed to demonstrate that the remaining parts of the device can withstand the same working condition, i.e. a total force of 700 N or 175 N in each Blade and Instrumented Rod. In order to allow the Instrumented Rod to freely deform, a 0.2 mm clearance are used between the Mount and the rod. This way is ensured that the Instrumented Rod deform as expected in the reality and the results from the FEA are more reliable.

The Mount and the Blade are made from 7075 aluminium alloy and the Instrumented Rods from 304 stainless steel, the same materials used on the Instrumented Saddle Device and the

Instrumented Pedal Device. Therefore, the same mechanical properties are used, i.e. a 0.33 Poisson ratio, a 72 GPa of elastic modulus and a 505 MPa of yield strength for the 7075 aluminium alloy and 0.29 Poisson ratio, a 190 GPa of elastic modulus and a 206.8 MPa of yield strength for the 304 stainless steel.

The Instrumented Grip Device FEA models are performed as an assembly with solid elements. However, since that the FEA models are studied as an assembly, additional caution must be taken in the components contact areas to warranty that the elements nodes match, in order to create a more stable FEA model.

The Instrumented Grip Device geometry is based on a circular pattern composed by four Blades and Instrumented Rods. Therefore, since that the device have two axes of symmetry, is possible to simulate only one fourth of the Instrumented Grip Device, by applying symmetry boundary conditions, as illustrated on Figure 3.61. Thus, the computational power required to solve the FEA are substantially decreased. In the MSC Nastran/Patran an extra symmetry axis are added, as represented on Figure 3.61.

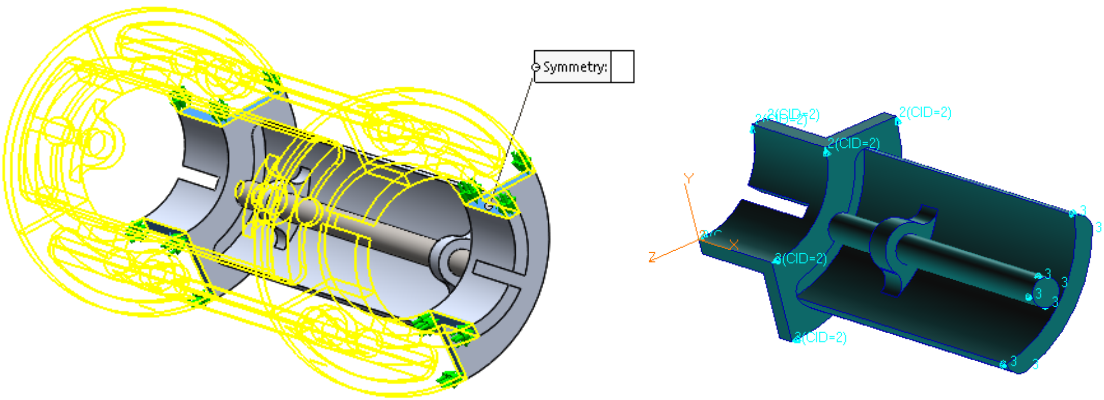

Figure 3.61 - Symmetry boundary conditions

The Mounts extremity are fixed to the handlebar with clamps, i.e. the Mounts cannot translate along the handlebar neither rotate. Thus, in the area where the Mount contact with the handlebar, a fixed geometry boundary conditions are applied in FEA models to represent this phenomenon, i.e. the solid elements in this area cannot translate in any direction, as illustrated in Figure 3.62.

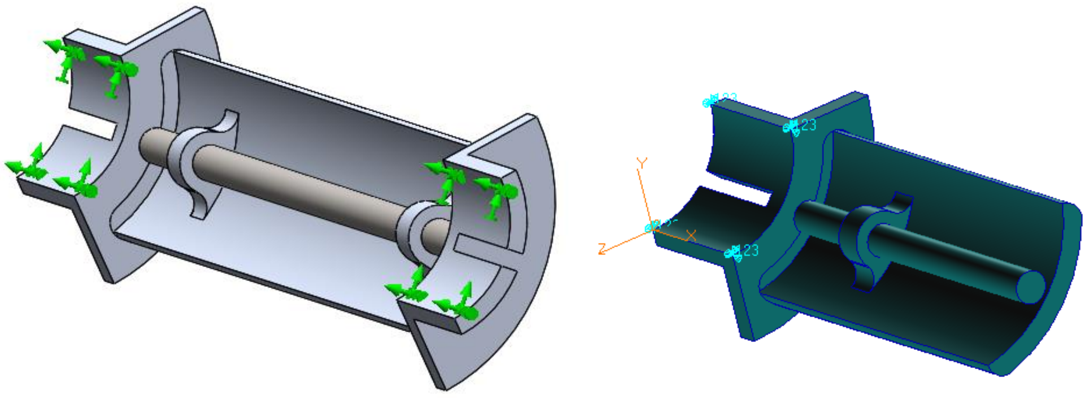

Figure 3.62 - Fixed geometry boundary conditions

Once that the Instrumented Grip Device is studied as assembly and is composed by different independent metallic parts, a component contact condition must be defined. Considering that the components are clipped and need clearance to move and deform, the components contact used in the Solidworks FEA is the no penetration contact type, i.e. the bodies cannot pierce each other. In the MSC Nastran/Patran FEA is used the deformable contact type, this contact type allows the bodies to deform accordingly to the materials properties defined.

The load condition in the Instrumented Grip Device is applied on the outside of the Blade, where the user hand is supposed to grab, as illustrated in Figure 3.63. As the Soliworks FEA model only represent a fourth of the device, the load applied is also a fourth of the total force considered, i.e. 175 N that is a fourth of the total 700 N considered as the maximum force applied on the device. In the MSC Nastran/Patran FEA model is only considered 87.5 N, since that the FEA model only represent half of the real Blade, as represented in Figure 3.63.

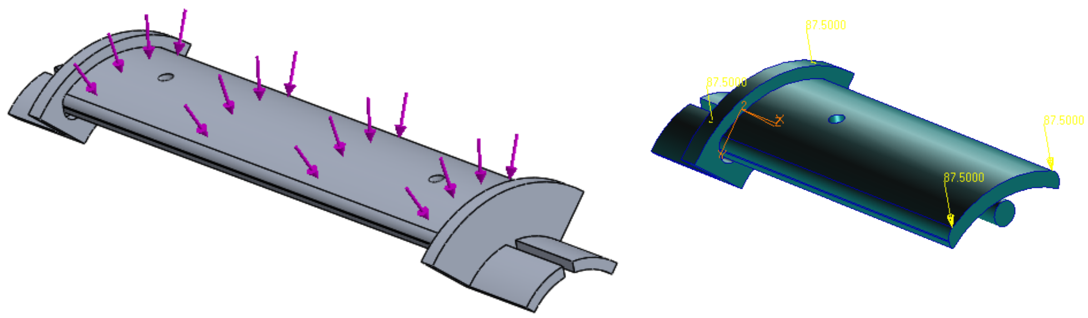

Figure 3.63 - Load condition applied area

In the Figure 3.64 is represented the stress dispersion, on the right, and the displacement dispersion, on the left, from the Solidworks FEA model. The figure suggest that the higher stress value occur on the Mount workpiece, where the Instrumented Rod contact.

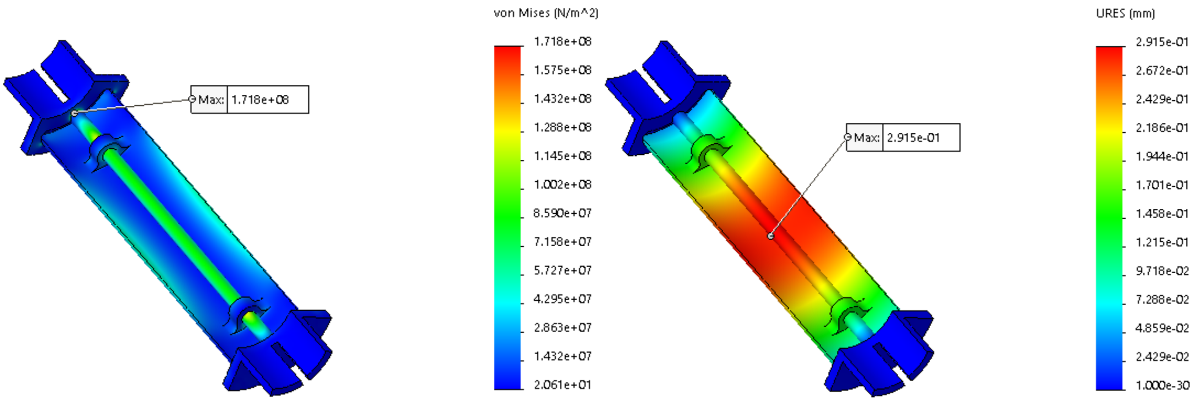

Figure 3.64 – (a) Stress dispersion on the left and (b) displacement dispersion on the right

Through the results present on Appendix D.2, is possible to affirm that the FEA model with 264442 elements is the model which display better convergence values and that the stress tends to a value of 180 MPa. Noting that the higher stress value occurs on the Mount, which is produced in 7075 aluminium, is verified that the Instrumented Grip Device have a safety factor of 2.81.

The Figure 3.65 shown the stress and displacement dispersion over the MSC Nastran/Patran FEA model. However, as opposed to the Solidworks model, it suggests that the higher stress value occur on the Blade workpiece instead of the Mount.

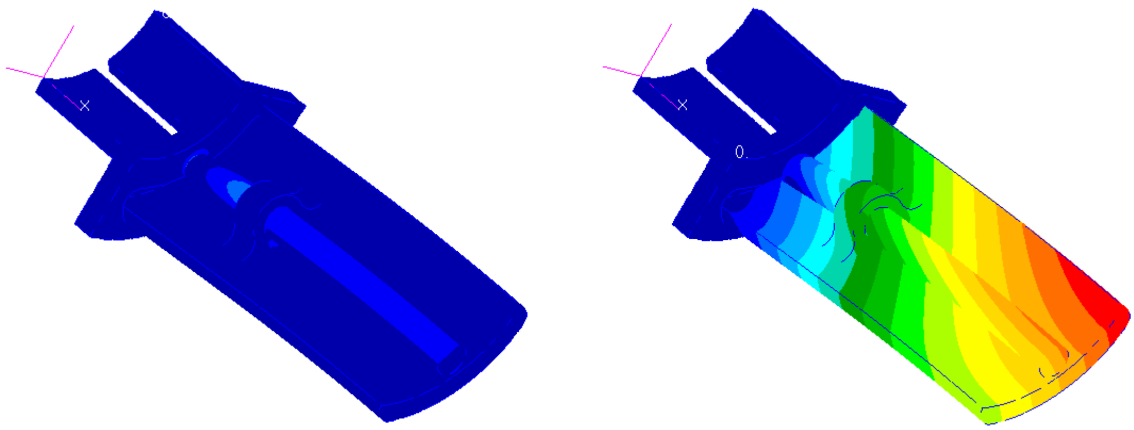

Figure 3.65 – (a) Stress dispersion on the left and (b) displacement dispersion on the right

From the MSC Nastran/Patran Instrumented Grip Device FEA model mesh convergence study is elaborated the graphs present in Appendix D.3. The relative displacement error demonstrates that the FEA model tens to stabilize, since the error tends to decrease with the increase of elements number and in some sections of the graph the displacement error is below 1%.

However, the stress values present on the Appendix D.3 indicate that the stress value do not tend to stabilize, despite the displacement error indicates the opposite. This phenomenon can indicate the presence of a Hertzian point. Therefore, the result obtained with the MSC Nastran/Patran FEA model cannot be considered.

Considering the results obtained from the Solidworks Instrumented Grip Device FEA model mesh convergence is possible to conclude that the device will withstand the foreseen loads with a safety factor of 2.81, which considering the working conditions is very satisfactory.

3.4.3 - Manufacturing

In total, the Instrumented Grip Device are composed by 10 parts: 2 Mounts, 4 Blades and 4 Instrumented Rods. The Instrumented Rods are cut from the calibrated 304 stainless steel rod and then finished with a grinder. The Mounts and the Blades are machined from 7075 aluminium alloy with a 5-axes milling machine.

The Mounts are produced with two different clamping positions. At the first position the two required Mounts are machined at the same time, for that a 4 flutes 10 mm endmill is used to rough the excess of material from the workpieces. Then, the same 10 mm endmill and ramp contour cycles are used to trim, the outside geometry and the inside Mount hole, to the final dimensions. Afterwards, a 3 mm endmill, also with ramp contour cycles, is used to open the pockets where the Blades and the Instrumented Rods will be assembled, as illustrated in Figure 3.66 (a). On the second clamp position the two Mounts are separated and machined individually. For the rough process are used a 3 mm endmill and a 10 mm endmill with a 2D high speed milling cycle and a ramp contour cycle, respectively. Lastly, the 3 mm endmill is used with a pocket cycle to machine the slots, as illustrated in Figure 3.66 (b)

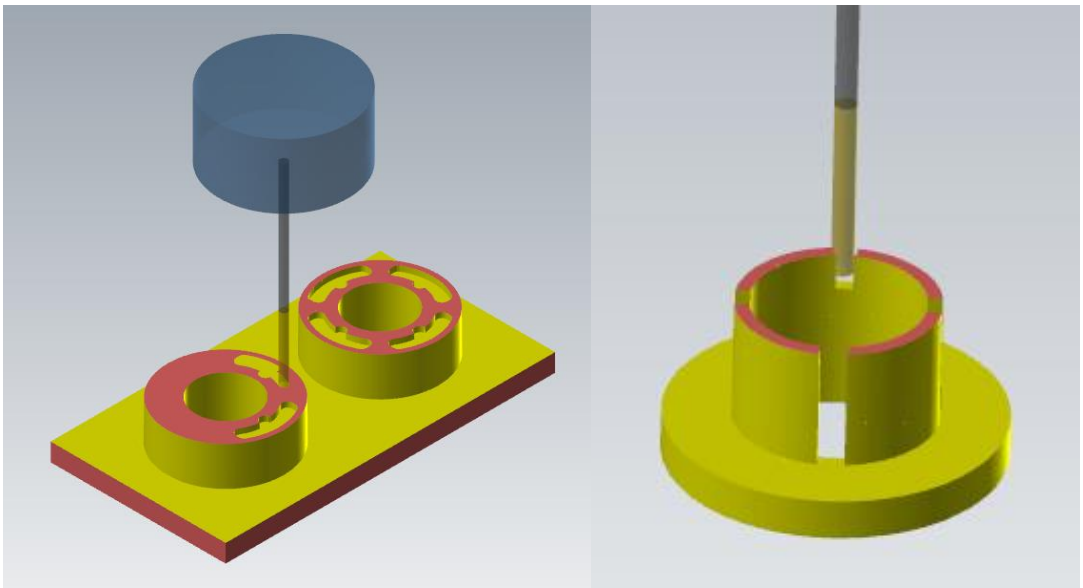

Figure 3.66 – (a) Pocket cycles with the endmill on the left and (b) slot milling with the endmill on the right

The Blades are machined with three clamping positions, since that the in the first clamping position the workpieces are machined by planes, i. e. the workpieces are machined with 3D milling cycles and the milling machine work plane is changed.

In the first clamping position a 10 mm 4 flutes endmill are used, with facing and contour cycles, to rough the excess material around the workpiece. Then, a 2.5 mm drill is used, with peck drill cycles, to drill the holes where would be used pins to hold the Instrumented Rod in place, as represented on Figure 3.67 (a). Lastly, a 4 mm drill is used, also with peck drill cycles, to drill the holes where the Instrumented Rod would be assembled.

The Second clamping position use a 4 mm endmill, with a dynamic milling rough cycle, to rough the inside of the Blades, where are located the Instrumented Rods supports. Then, a 3 mm ball endmill is used, with scallop, raster and flowline cycles to finish the inside surface of the Blades, as represented in Figure 3.67 (b).

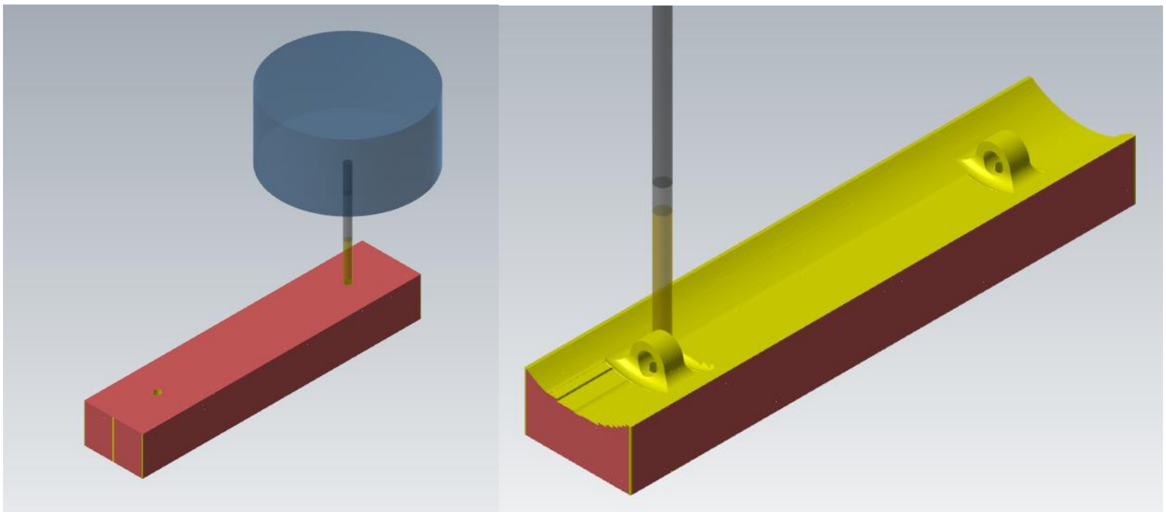

Figure 3.67 – (a) Peck drill cycles on the left and (b) Raster cycle with the ball endmill on the right

Due to the workpiece complex geometry and in order to facilitate the third clamping position, a support is produced in the Flashforge Guider II. The support is a negative of the Blade inside surface. Thus, the Blade can correctly fit in the 3D printed support and the Instrumented Rod supports can be used to hold the Blades during the third clamping position machining, as illustrated in Figure 3.68.

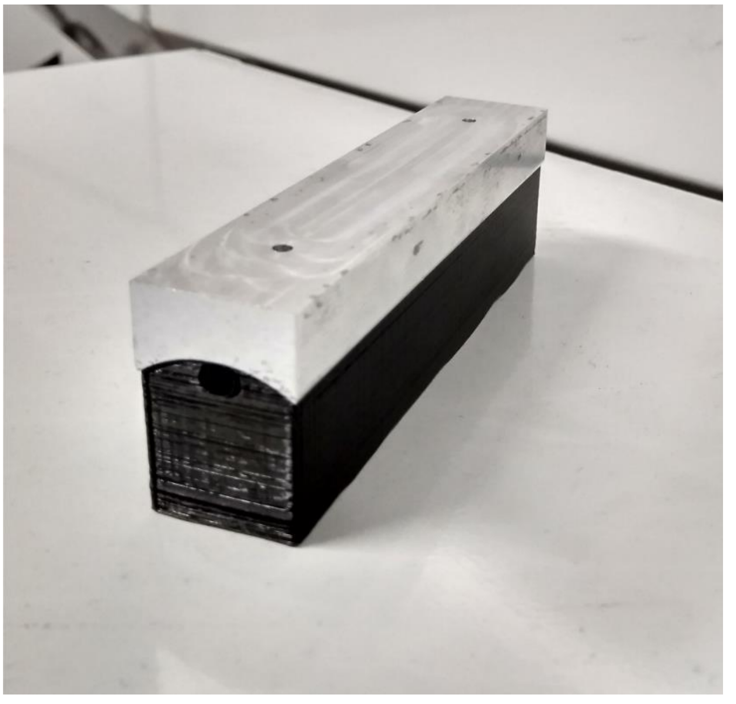

Figure 3.68 - 3D printed support with a half-machined Blade

In the third clamping position a 5 mm flat endmill is used, with a dynamic milling cycle, to rough the workpiece and then a 4 mm ball endmill is used, with flowline cycles, to finish the Blades outside surface, as represented in Figure 3.69.

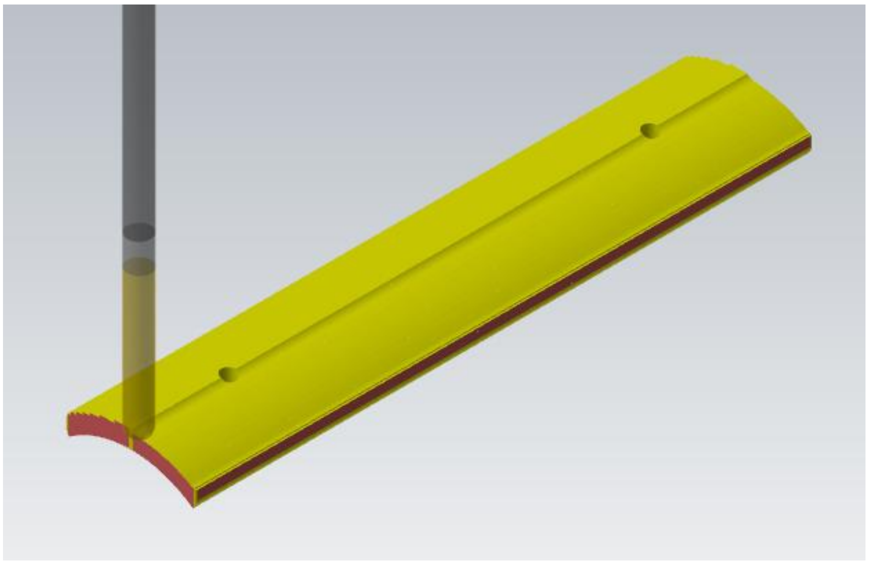

Figure 3.69 - Flowline cycle with the ball endmill

After the machining process, the workpieces are paper sanded by hand to ensure that all the dangerous sharp edges are trimmed.

4 - Functional Tests

All the developed devices are subject to a preliminary functional test, to confirm if the devices are working as expected and to test the data acquisition systems. This process is made to warranty that the systems are working properly before the final functional tests made with a larger number of volunteers.

4.1 - Preliminary Functional Tests

In the Preliminary Functional Tests, some devices are tested individually, while some are also tested simultaneously. These tests are performed in order to make a pre-validation of the developed devices and methodologies, in this phase is still possible to modify the devices if they are not working as expected.

The first preliminary functional test is made to evaluate the data from the Instrumented Saddle Device and the Instrumented Handlebar Device. This test has been made with 5 healthy volunteers, with an average age of 23.2 years and with stature from 1.72m to 1.91m. The data acquisition is made through National Instruments NI9219 boards and a NI cDAQ-9174 chassis, with an acquisition frequency of 3 Hz during approximately 200 seconds, where the first and last 30 seconds are excluded to do not consider the pedalling starting and stopping motion. Thus, is elaborated the graph from the Appendix E.1, which represent the Instrumented Saddle Device behaviour, over the test duration time, for each volunteer.

Analysing the graphs is possible to observe that the Instrumented Saddle Device indicate a higher value, in the front loadcell compared to the other loadcells, for the volunteer 1, 4 and 5, which also are the volunteers with lower stature. Considering that all the volunteers perform the tests with the same bicycle configuration, the volunteers with lower stature need to lean more forward to grab the handlebar, when compared with the volunteers with higher stature (volunteers 2 and 3). Thus, the volunteers with lower stature (volunteers 1, 4 and 5) while apply higher load on the front loadcell from the Instrumented Saddle Device, which is possible to observe on the data from this device. Therefore, is concluded that the Instrumented Saddle Device can loyalty acquire valuable data about the patient posture.

The graphs from the Appendix E.2 represent the data from the handlebar. In this phase the artificial neural network is not developed. Thus, is only possible to observe the deformation suffer by each strain gauge. However, that information is enough to achieve some conclusions and validate the veracity of the values from the strain gauges.

The volunteers with higher stature (volunteers 2 and 3) present a higher deformation on the upper strain gauges, which is expected, since these volunteers have a higher angle between the arms and the handlebar horizontal plane, as illustrated in Figure 4.1.

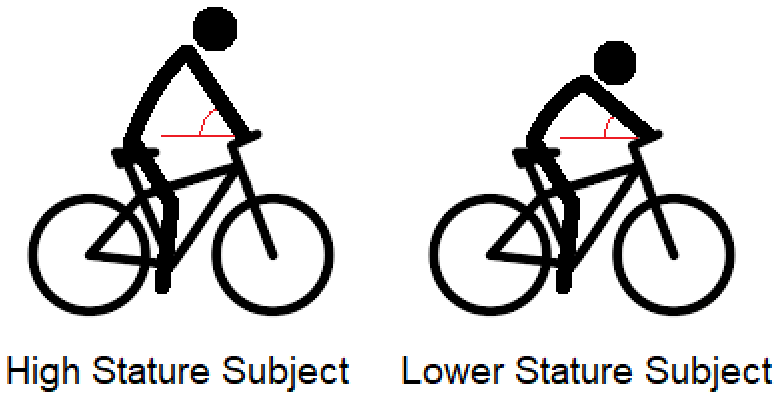

Figure 4.1 – Diagram with a small and a high stature person on a bicycle

Therefore, is considered that the values acquired from the Instrumented Handlebar also represent reliable data about the volunteer posture.

In the second preliminary functional test is acquired the data from the Instrumented Saddle Device, the Instrumented Handlebar Device, as also, the Instrumented Pedals Device. This way is tested the Instrumented Pedals Device data acquisition system, as also, the repeatability of the conclusions from the Instrumented Saddle Device and the Instrumented Handlebar Device.

The test is performed with 3 healthy volunteers, with an average age of 25.3 years and high from 1.72 m to 1.90 m. The data from the devices are acquired with 3 National Instruments NI9219 boards, one to each device, and a NI cDAQ-9174 chassis. As acquisition frequency is defined 3 Hz and the acquisition process is made during approximately 90 seconds.

This preliminary test also studies functional test methodologies, which intend to be applied during the Final Functional Tests. Such as, performing two acquisition section with each volunteer, one with the volunteer pedalling in normal conditions and other one where the volunteer pedals with a simulated defence reaction, induced by a strange object inside one of the volunteer's shoes. The other functional test methodology studied consist in only start the acquisition process after the volunteer have already started the pedalling motion and achieved a stationary regime pedalling motion. This way is not necessary exclude the initial and final parts of the acquired data, as it was done on the first preliminary test.

In the second preliminary test, from the data acquired with the Instrumented Saddle Device and the Instrumented Handlebar Device is achieved the same conclusions as in the first preliminary test, which somehow ends up corroborating the results from those devices. The acquired data from the Instrumented Pedals Device are present in the Appendix E.3, to each volunteer correspond two graph, one graph acquired during the pedalling in normal conditions and other with the induced defence reaction.

By analysing the data acquired, in both sections, from the volunteers 2.2 and 2.3 is possible to conclude that the Instrumented Pedals Device are performing as expected and are sensitive enough to detect the induced defence reaction. When the volunteers are subject to the discomfort of the object inside the shoe, the volunteers tend to exert less effort with that foot in order to do not hurt itself, which can be compared to the discomfort induced by a lesion. Therefore, is considered that both the Instrumented Pedals Device and the functional test methodologies studied, with this preliminary functional test, are corroborated.

The third preliminary functional test is performed to evaluate the data provided by the Instrumented Grip Device. After the manufacturing of the workpieces, from the device, are noticed some miss alignment in the blades holes where the instrumented rods are supposed to be assembled. Thus, the Instrumented Grip Device prototype is not able to be assembled as planned, i.e. the instrumented rods are not possible to assemble. However, some aspects are possible to study, such as ergonometric and fixation mechanism.

Despite the Instrumented Rods are not installed, one of the Blades are instrumented with a 350 Ω HBM 1-LY13-3/350 strain gauge and connected to a Vishay Micro-Measurements P3 Strain Indicator and Recorder, as illustrated on Figure 4.2. This way is studied the viability of directly instrument the Blade instead of the rods, eliminating the need of Instrumented Rods.

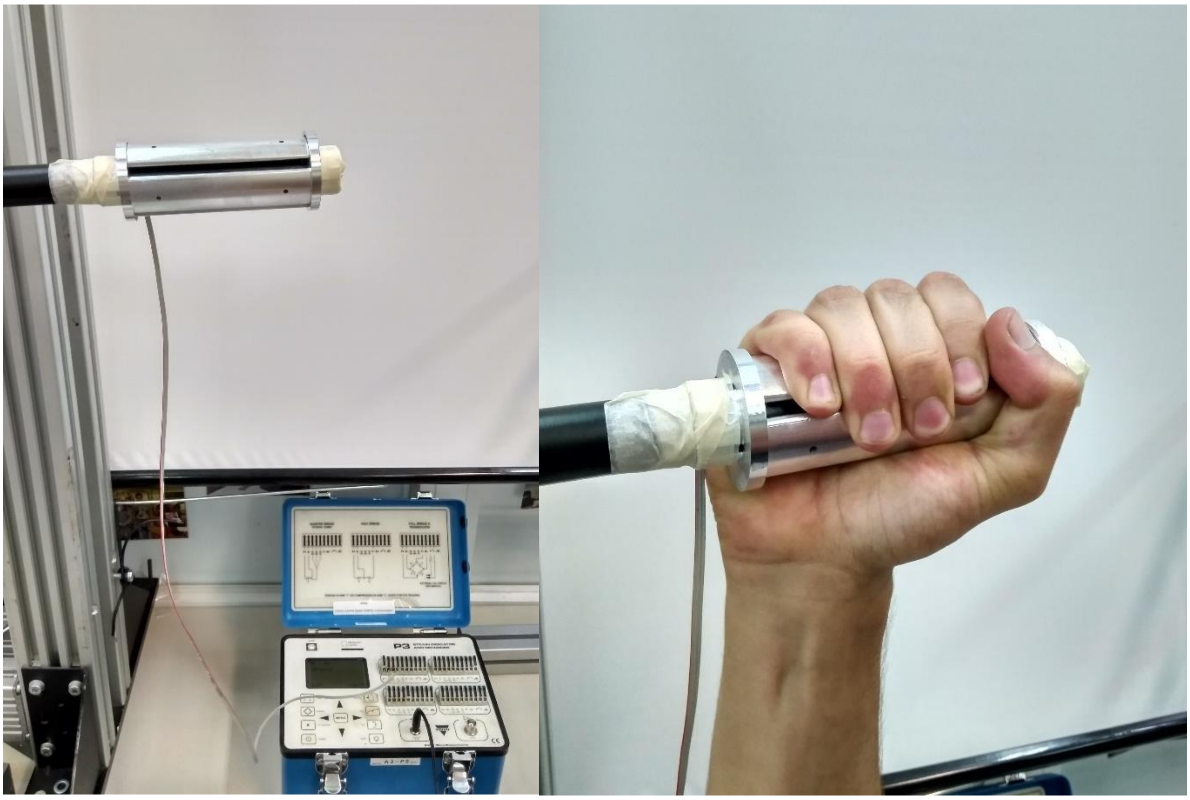

Figure 4.2 - Instrumented Grip Device laboratory setup

The preliminary functional test is realized with 3 volunteers, each volunteer performs the maximum grip force possible and the higher value is registered. In the Appendix E.4 is represented the maximum deformation, on the inside Blade surface, applied by each volunteer.

The test demonstrate that is possible to determine the gripping force applied on the device through the Blade. This way the Instrumented Rods are not necessary, which drastically reduce the number of components required from 10 to 6, as also simplify the methodology complexity. A simpler methodology is a more reliable methodology. However, since that the maximum value acquired is too low to warranty quality results, is conclude that the actual Blade is too stiff for the intended purpose. Therefore, in order to eliminate the Instrumented Rods necessity, the Blades must be fragilized to acquire higher deformation values and warranty higher quality results.

4.2 - Final Functional tests

Since the Instrumented Saddle Device, the Instrumented Handlebar Device and the Instrumented Pedals Device are working properly, they are used to perform a set of Final Functional Tests with a group of 31 volunteers. The Final Functional Tests intend to explore the systems capabilities as also corroborate the repeatability of the data acquired, from the devices over an extensive use.

The data from the Instrumented Saddle Device and the Instrumented Handlebar Device are acquired, with a frequency of 2 Hz through two National Instruments NI 9219 boards mounted on a NI cDAQ-9174 chassis. The three loadcells from the Instrumented Saddle Device are connected to one NI 9219 board in a full Wheatstone bridge configuration, while the four strain gauges from the Instrumented Handlebar Device are connected to the other NI 9219 board in a quarter Wheatstone bridge configuration. The data acquisition of the Instrumented Pedals Device is made with a frequency of 40 Hz through a NI 9219 board connected to a NI WLS 9163 chassis. This chassis allows a higher acquisition frequency, which is important to analyse and characterize the volunteers pedalling motion. While the loadcells from the Instrumented Pedals Device are connected to the NI 9219 boards in a full Wheatstone bridge configuration.

The NI cDAQ-9174 and NI WLS 9163 chassis connect the NI 9219 boards to a LabView application. This application provides biofeedback through a GUI with real-time acquired data and also enable the recording of the data, as illustrated on Figure 4.3.

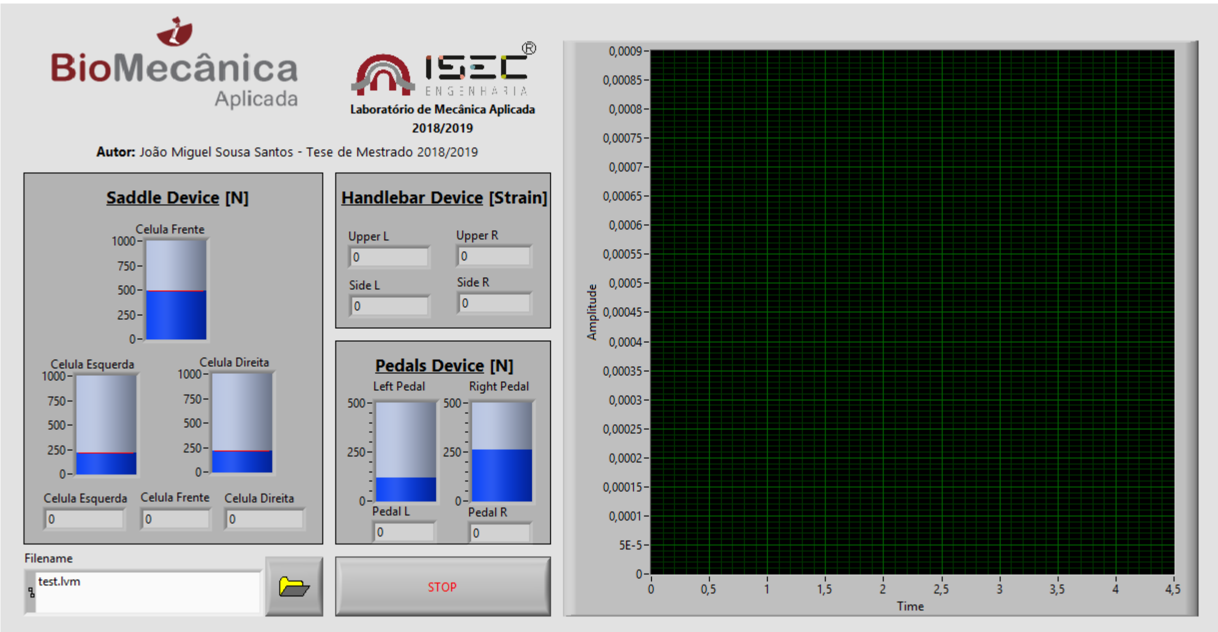

Figure 4.3 - LabView developed GUI

After the data acquisition, the data from the Instrumented Handlebar Device pass through a post processing script in MATLAB. This script contains the developed artificial neural networks and is utilized to convert the raw data from the strain gauges into the desired processed data.

An ethical procedure is elaborated under the data protection legislation, the Declaration of Helsinki and the World Medical Association referent to the experiments with human beings. The ethical procedure has been approved by the Coimbra Polytechnic Institute Ethical Department and an informed, free and clarified consent is assigned by every involved volunteer. By assigning this document the volunteer agrees with the data acquirement and an alphanumeric code is attribute to anonymize the acquired data.

Before the volunteer start the data acquisition in the ExoBike with the Instrumented Saddle Device, Instrumented Handlebar Device and Instrumented Pedals Device, are acquired several biometric values, such as, gender, age, dominant side, high, mass, body mass index, fat percentage, muscle percentage, visceral fat and resting metabolic kilocalories. Then the volunteers make 2 minutes of treadmill at 2 km/h and with 0 % of inclination to warm-up.

All the volunteer makes two section of data acquisition, one in normal conditions and other one with an induced defence reaction, caused be a strange object inside the shoe. Each section has a duration of approximately 170 seconds, resulting in a total of 340 seconds of data acquired from each volunteer. The volunteer pedal at a constant and comfortable rate. During the data acquisition the volunteer have access to the LabView GUI program in order to evaluate the biofeedback level and usefulness.

After the data acquisition process with the devices, the volunteer answer to a query to register some additional data about the volunteer's injuries history, riding bicycle experience and level of defence reaction induced by the strange object in the shoe.

In the query that the volunteers answer after the experiment, are also some questions where the volunteers give a classification from 1 to 10 about the GUI developed for the data acquisition and biofeedback. The questions are related with the GUI intuitiveness and visual aspect, in order to determine if the interface is pleasant and useful for its finality, provide bio feedback. There are four questions related to specific aspects and one final question for a global evaluation of the software application, the classification is present on the Table 3.

Property	Overall Classification
Visual aspect	7.63
Usefulness	8.50
Intuitiveness	8.47
Biofeedback quality	8.53
Global evaluation	8.31

Table 3 – GUI overall evaluation

From the values present on the table above is concluded that the Graphical User Interface, developed for acquire and display the data, accomplish the intended goals with great success.

The data acquired over the Final Functional Tests are analysed with two different statistic software tools, the Microsoft Excel software and the IBM SPSS software. In the Microsoft Excel, is studied all the data set acquired from each volunteer to evaluate the volunteer´s behaviour over the experiment time. In the IBM SPSS, is processed the mean values acquired from the devices to each volunteer, with this software intends to stablish correlations between the acquired data in order to corroborate the devices, with a larger volunteer's sample, and search for biometrical valuable conclusions.

With the Microsoft Excel analysis is studied the volunteer´s pedalling motion. As is possible to observe in the Graph 4-1, with an acquisition rate of 40 Hz is possible to characterize the pedalling motion cycle. Both pedals indicate a sinusoidal wave, one symmetric to the other. When one pedal is in the descending movement, the other is in the ascending movement. Thus, in order to introduce power in the transmission system, the volunteer apply more force during the descending movement, than during the ascending one. As the pedals are 180º apart each other and continuously rotating, alternating between the descending and ascending movement, that generate two symmetric sinusoidal waves of force over the time. The values from the left pedal indicate some interference, which may have been caused by a magnetic field once that the loadcells are very sensitive to this kind of interference and an electric motor are installed on the ExoBike.

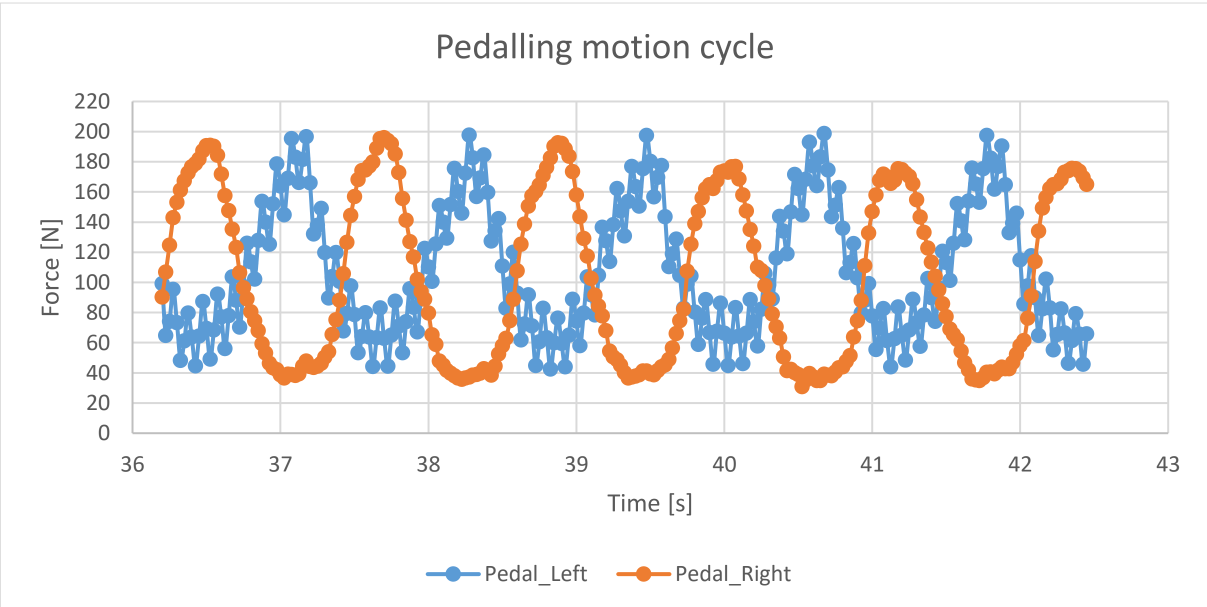

Graph 4-1 Volunteer PSG_25 pedalling motion cycle

Analysing the Graph 4-1 is possible to identify a perturbation on the maximum and minimum regions. This perturbation coincides with the moment when the volunteer changes the force exertion limb, i.e. when stop making effort with one leg and start making with the other. This demonstrate the level of detail possible to acquire with the Instrumented Pedals Device, which shown to be significantly detailed.

Afterwards, are presented several comparisons, also with the Microsoft Excel. One comparison studies the influence of cycling practice frequency on the volunteer pedalling cycle and posture behaviour. Other compares the data from two male volunteers with distinct high, in order to study the posture and pedalling cycle implications. Also, a comparison is made between two volunteers with similar background but from different genders and at the end is compared the same volunteer with and without the induced defence reaction. As the data acquired from the handlebar strain gauges are manly out of the expected range, the artificial neural networks and the analytic method developed for the Instrumented Handlebar Device cannot provide reliable values. Therefore, the data from this device is studied considering the direct values from the strain gauges.

To study the influence of cycling practice frequency, are compared the data acquired from the volunteer, which practice cycling exercise with more frequency and the data from the volunteer, that stop practice cycling exercise at longer time. The graphs on the Appendix E.5 represent the data acquired from the volunteer PSG_25, which practice cycling exercise four times per week. The graphs from the Appendix E.6 shown the data from a volunteer that stop practice cycling exercise 9 years ago, volunteer PSG_02. Both volunteers are from the same gender, male, and are the extremes which concerns to cycling practice frequency.

By analysing the data from the Instrumented Pedals Device, for both volunteers, is possible to conclude that the volunteer with more cycling experience have a more consistent and homogeneous pedalling motion. The volunteer with less cycling practice has a more irregular pedalling motion, since the values from the Instrumented Pedals Device have more fluctuation. The data acquired with the Instrumented Saddle Device demonstrate that the volunteer PSG_25 has a more stable posture, i.e. the device indicate less values fluctuations, which can be related with the regular cycling practice and experience, since that the volunteer with less cycling practice demonstrate more unstable Instrumented Saddle Device values.

The second comparison take concern about the influence of the volunteers high in the posture. For that, the data acquired from two volunteers are considered, a volunteer with 1.90 m of high and other one with 1.64 m, both from the male gender. The graphs from the Appendix E.7 represent the data acquired from the volunteer PSG_19, which is the volunteer with 1.90 m high. The data from the volunteer with 1.64 m, PSG_12, is presented on the Appendix E.8.

By analysing the data from the Instrumented Pedals Device is concluded that both volunteers have a pedalling motion stability identical. However, by analysing the data acquired with the Instrumented Saddle Device, is noticed that the volunteer PSG_12, i.e. the volunteer with lower high, present a higher value in the front loadcell, as already suggested in the second preliminary functional test. Is also noticed that the values from the right and left loadcell of the Instrumented Saddle Device are more balanced in the volunteer PSG_19 than in the volunteer PSG_12. This phenomenon can indicate a bad posture habit or any kind of decompensation.

The third comparison is made with two similar volunteers from different genders, the PSG_01 from the female gender and the PSG_08 from the male gender. Both volunteers have 26 years, same dominate side, identical cycling practice frequency and identical stature with 1.62 m for the female gender volunteer and 1.77 m for the male volunteer. The data concerning to the PSG_01 are presented in the Appendix E.9, while the data from the PSG_08 are shown in the Appendix E.10.

From the data acquired with the Instrumented Pedals Device is possible to observe that the volunteer from the female gender have a more consistent pedalling motion, since there are less values fluctuation. On the other hand, the volunteer PSG_08 indicate better balance between the forces exerted by the right and left limb, i.e. the forces are more similar in magnitude. The data acquired with the Instrumented Saddle Device indicate higher value fluctuations on the male gender volunteer, while on the female volunteer it indicates much lower fluctuations. Which indicate that the volunteer PSG_01 have a more stable posture than the volunteer PSG_08, as also, that the volunteer PSG_08 have a higher ankle movement amplitude during the cycling exercise than the volunteer PSG_01.

The fourth comparison is made to study the influence of the defence reaction induced by the strange object inserted inside the volunteer´s shoe. Therefore, are analysed the data acquired, from the volunteer PSG_08, with the Instrumented Pedals Device in both sections, with and without the object. The first graph from the Appendix E.11 take concern of the acquired data without the object, while the second graph from the same appendix is from the acquisition section with the object.

From the data present in the graphs above is possible to observe that, with the introduction of the defence reaction on the right foot, the maximum force exerted by the right limb decrease, while the minimum force remains almost the same. Indicating that the level of discomfort generated by the induced defence reaction are proportional to the force exerted by the limb, as expected, the higher is the force exerted, the higher is the pain felt by the volunteer.

The analysis performed with the Microsoft Excel demonstrate interesting results and help corroborating the methodologies developed for the Instrumented Saddle Device and the Instrumented Handlebar Device. However, thereafter are presented the analysis and studies performed with the IBM SPSS software.

With the IBM SPSS software are analysed the mean values acquired, by each sensor, in each section. Analysing the acquired data in its entirety, is possible to observe, with 95% of reliability, that the right pedal indicates a difference between the values from the tests performed with the induced defence reaction and the tests performed in normal conditions. In the Table 4 are present the paired differences between several sensors in the normal conditions section and in the induced defence reaction section.

		Paired Differences				
					95% Confidence Interval of the Difference	
		Mean	Std. Deviation	Std. Error Mean	Lower	Upper
Pair 1	Loadcell_Pedal_Left_01 - Loadcell_Pedal_Left_01P	-,9318	4,9570	,8763	-2,7190	,85538
Pair 2	Loadcell_Pedal_Right_01 - Loadcell_Pedal_Right_01P	-1,9280	5,0851	,8989	-3,7614	-,0946
Pair 3	Loadcell_Left_01 - Loadcell_Left_01P	,58012	20,0566	3,5455	-6,6511	7,8113
Pair 4	Loadcell_Right_01 - Loadcell_Right_01P	1,9870	15,0440	2,6594	-3,4369	7,4110
Pair 5	Loadcell_Front_01 - Loadcell_Front_01P	-1,3971	20,4969	3,6234	-8,7869	5,9929
Pair 6	Strain_Left_Upper_01 - Strain_Left_Upper_01P	,00000328	,0000317	,00000561	-,00000817	,0000147
Pair 7	Strain_Left_Side_01 - Strain_Left_Side_01P	-,00000212	,0000194	,00000343	-,00000911	,00000487
Pair 8	Strain_Right_Upper_01 - Strain_Right_Upper_01P	,00000316	,0000271	,00000479	-,00000660	,0000129
Pair 9	Strain_Right_Side_01 - Strain_Right_Side_01P	-,00000327	,0000204	,00000361	-,0000106	,00000410

Table 4 - Full volunteers set paired differences

If the interval between the inferior a superior limit of the confidence interval includes the zero, it means that the mean values of the compared variables may be equal. In other hand, if the interval does not include the zero, means that the mean values of the compared variables are not equal with a reliability of 95%. Therefore, analysing the Table 4, is concluded that the mean force applied on the right pedal are influenced with the presence of the induced defence reaction. Contrarily, the same is not observed on the left pedal. Therefore, considering the disproportionate between the number of lefties and right-handed volunteers and in order to identify a similar relation on the left pedal, the data set are divided accordingly to the volunteers dominate side. As observed on the Graph 4-2, the presence of the left-handed volunteers may not be high, but is perceptible, which may be influencing the results.

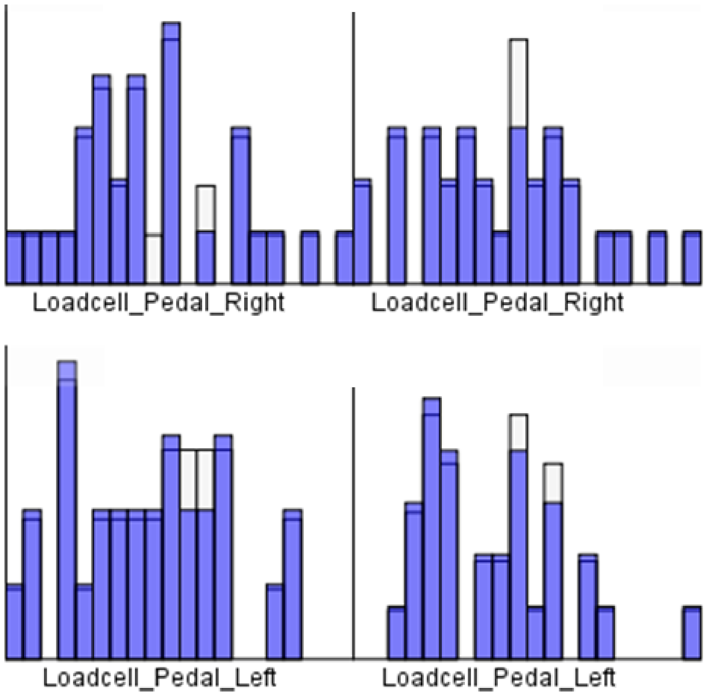

Graph 4-2 Comparison between datasets with and without the left-handed volunteers

Only two volunteers are left-handed, thus, is not rewarding perform a paired difference analysis for this group. Therefore, a paired difference analysis is performed for the right-handed group comparing the Instrumented Pedals Device and Instrumented Saddle Device values, the results are present on the Table 5.

		Paired Differences				
		Mean	Std. Deviation	Std. Error Mean	95% Confidence Interval of the Difference	
					Lower	Upper
Pair 1	Loadcell_Pedal_Left_01 - Loadcell_Pedal_Left_01P	-,7882	4,8105	,8783	-2,5844	1,0081
Pair 2	Loadcell_Pedal_Right_01 - Loadcell_Pedal_Right_01P	-2,0580	4,9998	,9128	-3,9249	-,1910
Pair 3	Loadcell_Left_01 - Loadcell_Left_01P	-,1959	18,9892	3,4669	-7,2866	6,8948
Pair 4	Loadcell_Right_01 - Loadcell_Right_01P	3,1182	13,6271	2,4880	-1,9702	8,2067

Table 5 - Right-handed volunteers paired differences

Once again, the right pedal does not contain the zero in the confidence interval, i.e. the left pedal still does not indicate influence of the induced defence reaction. Thus, is decided to split the data set of right-handed volunteers accordingly to the side in which the defence reaction is induced, i.e. try to find a influence on the force applied on the right pedal when the defence reaction is induced of the right foot and try to find a influence on the force applied on the left pedal when the defence reaction is induced on the left foot, the results are presented on the Table 6 and Table 7.

		Paired Differences				
		Mean	Std. Deviation	Std. Error Mean	95% Confidence Interval of the Difference	
					Lower	Upper
Pair 1	Loadcell_Pedal_Left_01 - Loadcell_Pedal_Left_01P	-1,9487	4,8193	1,1689	-4,4266	,5291
Pair 2	Loadcell_Pedal_Right_01 - Loadcell_Pedal_Right_01P	-2,3294	5,3703	1,3025	-5,0906	,4317
Pair 3	Loadcell_Left_01 - Loadcell_Left_01P	1,7163	19,8212	4,8074	-8,4748	11,9074
Pair 4	Loadcell_Right_01 - Loadcell_Right_01P	-,5186	15,8368	3,8410	-8,6611	7,6239

Table 6 - Right side induced defence reaction influence paired differences

		Paired Differences				
		Mean	Std. Deviation	Std. Error Mean	95% Confidence Interval of the Difference	
					Lower	Upper
Pair 1	Loadcell_Pedal_Left_01 - Loadcell_Pedal_Left_01P	,2207	5,0187	1,2958	-2,5586	2,9999
Pair 2	Loadcell_Pedal_Right_01 - Loadcell_Pedal_Right_01P	-1,4731	4,8868	1,2618	-4,1793	1,2331
Pair 3	Loadcell_Left_01 - Loadcell_Left_01P	-,7076	20,9376	5,4061	-12,3024	10,8873
Pair 4	Loadcell_Right_01 - Loadcell_Right_01P	4,8267	14,0799	3,6354	-2,9705	12,6239

Table 7 - Left side induced defence reaction influence paired differences

This time, none of the paired differences are conclusive. In other words, the confidence interval from the paired differences analysis, either for the group of volunteers with the defence reaction on the right or on the left foot, does contain the zero, i.e. is not identified an influence of the defence reaction on the force applied on the pedal. Thus, since that is not achieved conclusive results with the data set including all the volunteers regardingless the injuries track record, is decided to study the induced defence reaction influence on the volunteers that have lower limbs injuries track record. Therefore, a paired differences analysis is performed between the volunteers, with lower limbs track record, with and without the induced defence reaction. In the Table 8 is present the results from the analysis for the Instrumented Pedals Device and the Instrumented Saddle Device sensors.

		Paired Differences				
		Mean	Std. Deviation	Std. Error Mean	95% Confidence Interval of the Difference	
					Lower	Upper
Pair 1	Loadcell_Pedal_Left_01 - Loadcell_Pedal_Left_01P	-2,3043	4,4650	1,0244	-4,4564	-,15223
Pair 2	Loadcell_Pedal_Right_01 - Loadcell_Pedal_Right_01P	-2,4397	4,6153	1,0588	-4,6642	-,2152
Pair 3	Loadcell_Left_01 - Loadcell_Left_01P	7,0113	19,8007	4,5426	-2,5323	16,5550
Pair 4	Loadcell_Right_01 - Loadcell_Right_01P	3,6531	15,4486	3,5442	-3,7929	11,0991

Table 8 - Lower limbs injuries track record paired differences

From the results on Table 8 is concluded that the values, from the Instrumented Pedals Device, of the volunteers with injuries track record are different in normal conditions and with the induced defence reaction condition. When comparing the results from the paired differences study performed to the full volunteers set, in the Table 4, with the study performed to the volunteers set with lower limbs injuries track record, in the Table 8, is perceptible that the volunteers with injuries track record are more sensitive to the induced defence reaction. This phenomenon may be due to psychological repression, i.e. as the volunteers have already witnessed a lower limb injury, the mind automatically associates the induced defence reaction with an injury, changing the volunteer´s behaviour unconsciously.

The results achieved with the paired differences on IBM SPSS demonstrate important conclusions either at physical or psychological level, which must be considered during the rehabilitation process.

Also, other conclusions are possible to achieve from the correlations resulting from the SPSS analysis.

As expected, since the volunteer are supported with both hands on the handlebar, the values from the strain gauges applied on the right side have a moderately strong correlation with the values from the strain gauges applied on the left side. The analysis indicates a correlation of 0.6 between the strain gauges applied on the upper side of the handlebar and a correlation of 0.7 between the strain gauges applied on the sider surface, as present in the Table 9.

		Strain_Left_Upper	Strain_Left_Side	Strain_Right_Upper	Strain_Right_Side	High	Mass	BMI	% Fat	% Muscle	RM kcal	Visceral Fat
Strain_Left_Upper	Pearson Correlation	1	,0	,6	-,4	,5	,5	,3	-,2	,2	,5	,2
Strain_Left_Side	Pearson Correlation	,0	1	,4	,7	-,4	-,5	-,2	-,0	-,0	-,4	-,2
Strain_Right_Upper	Pearson Correlation	,6*	,4	1	-,1	,3	,2	,0	-,4	,4	,4	,1
Strain_Right_Side	Pearson Correlation	-,4	,7	-,1	1	-,6	-,7	-,3	-,1	,0	-,5	-,2

Table 9 - Instrumented Handlebar Device correlations

The side strain gauges have an inverse moderated correlation with the high, mass, body mass index and RM kilocalories. Which means that the volunteers with higher and bigger stature exert less force in the handlebar horizontal direction. In other hand, the upper strain gauge indicates a direct moderated correlation with the same factors. Meaning that the volunteers with higher and bigger stature exert more force in the vertical plane of the handlebar, than the ones with lower stature.

Both mass and RM kilocalories have a strong direct correlation of 0.7 with the values from the left and right loadcells of the saddle, while the volunteers´ high have a moderate correlation with the left loadcell of 0.5 and a strong correlation with the right loadcell of 0.7, as presented in Table 10. Since these loadcells are applied on the rear part of the Instrumented Saddle Device, this means that the volunteers with bigger stature applies more load on the loadcells installed on the back part of the saddle. The front loadcell indicate an inverse moderate correlation with the volunteers high and muscle percentage of -0.4, as also, a direct correlation with the fat percentage of also 0.4. Which somehow ends up validating the conclusions stated above from the correlation of the right and left loadcells.

		Loadcell _Left_01	Loadcell_ Right_01	Loadcell_ Front_01	High	Mass	BMI	% Fat	% Muscle	RM kcal	Visceral Fat
Loadcell_ Left_01	Pearson Correlation	1	,8	-,6	,5	,7	,4	,0	,1	,7	,5
Loadcell_ Right_01	Pearson Correlation	,8	1	-,6	,7	,7	,3	-,1	,2	,7	,3
Loadcell_ Front_01	Pearson Correlation	-,6	-,6	1	-,4	,0	,3	,4	-,4	-,2	,3

Table 10 - Instrumented Saddle Device correlations

The left and right side loadcells have an inverse correlation of -0.6 with the front loadcell, indicating that when the volunteer applies more force on the two rear loadcell, decrease the force applied on the front loadcell.

The mean force applied on the Instrumented Pedals Device demonstrate positive correlations with the volunteer´s high, weight, body mass index, RM kilocalories and visceral fat, as also, a weak negative correlation with the muscle percentage, as presented on Table 11, which lead to the conclusion that the volunteers with lower physical condition and bigger stature apply more load on the bicycle pedals. However, the useful force transmitted to the system are identical to the others volunteers, i.e. the volunteers are supporting more body weight on the pedals, than the volunteers with better physical condition.

		Loadcell _Pedal_ Left_01	Loadcell _Pedal_ Right_01	High	Mass	BMI	% Fat	% Muscle	RM kcal	Visceral Fat
Loadcell_Pedal _Left_01	Pearson Correlation	1	1	,6	,9	,6	,2	-,2	,7	,5
Loadcell_Pedal _Right_01	Pearson Correlation	1	1	,6	,9	,6	,3	-,2	,6	,5

Table 11 - Instrumented Pedals Device correlations

Taking in to account the data acquired with the functional tests and the correlations achieved with the statistical analysis, the experiment is considered a success by achieve the intended goals. The Instrumented Saddle Device methodology developed enable the study of the patient posture and asymmetries over the sagittal and coronal plane, the Instrumented Pedals Device allow the fully characterisation of the pedalling motion cycle and the Instrumented Handlebar Device, despite the artificial neural network overflow, have a successful strain gauge methodology, since is possible to study the patient stability and posture even only through the raw data from the strain sensors. The instrumented Grip Device, despite not been evaluated in the Final Functional Tests, the analysed methodology demonstrates a high potential, in the acquisition of the patient gripping force, during the Preliminary Functional Tests.

5 - Conclusions

Considering all the development process of the devices, from the idealization to the conception and validation, all the devices are considered successful. Even that some devices do not function as expected, they achieve the intended goals stablished previously.

The ExoBike project compelled to the use of a vast set of technologies, software and knowledge. From CAD modelling, with Solidworks software for the development of the virtual 3D models, to analytical material strength calculus and computer aided engineering methods, with Solidworks Simulation and Patran-Nastarn. From rapid prototyping, with FDM 3D printers, to final products manufactured in CNC machines, with Mastercam software. From National Instruments electronic boards configuration to the development of data acquisition software with Labview programming. From field experiments and statistical analysis, with MS Excel and IBM SPSS software tools, to MATLAB programming and artificial neural networks development. Also passing through electronic sensors installation and calibration, such as loadcells and strain gauges, with soldering skills.

Some of the skills was already acquired while others were acquired during the development process of the devices, which allowed the development of a strong practical skill component. As the Exobike project is a multidisciplinary project which integer different engineering fields, such as electronics, informatics and mechanics, the involvement on the project results into a global perception of the interconnections between the different areas. Which was essential to streamline the communication between the researching team members and to introduce synergies in the project development. All these factors have a strong influence in the developed devices presented.

The methodologies idealized and developed for the Instrumented Saddle Device and the Instrumented Pedals Device are a complete success, since the devices work exactly as expected. Relatively to the Instrumented Handlebar Device, despite the artificial neural network developed suffer overflow during the Final Functional Test data acquisition, the device is considered successful through the raw data from the strain gauges. In other hand, the Instrumented Grip Device is not possible to validate, however, the preliminary functional tests performed indicate that the direct blade instrumentation methodology demonstrate a high viability.

The development of this ExoBike components results in several outcomes. The publication and presentation of two congress articles, one (Santos, *et al.*, 2019) presented in the 8th Portuguese Congress of Biomechanics (CNB2019) and the other (Santos, *et al.*, 2019) in the Health and Well-Being Intervention International Congress 2019, as also the submission of a journal paper to the Portuguese Association of Experimental Stress Analysis (APAET) that, at the present date, is waiting for approval. Also, a resume has been submitted to the 16th International Symposium on Computer Methods in Biomechanics and Biomedical Engineering and the 4th

Conference on Imaging and Visualization. Furthermore, the Exobike project has been presented in two national television programs, the *Produtos Portugueses de Saúde* from the channel *Saúde Mais* and the *Portugal em Direto* from the channel *Rádio e Televisão de Portugal*.

Despite the outstanding results achieved by every developed device there is always place for improvement. The FDM 3D printed Saddle Post Connector demonstrated promising capabilities during the Preliminary Functional Test. The workpiece withstands the foreseen loads very successfully, as demonstrated on the FEA performed. However, is very fragile to lateral unexpected impacts. This property may be circumvented with the use of a different polymer on the manufacturing process and/or improvements on the CAD design. Considering the cost production of this workpiece, with this technology, this development demonstrates high reliability. It would be also interesting studying the possibility of incorporating the post connection mechanism in the lower Loadcells Interface plate. Relatively to the Instrumented Handlebar Device, since that the range of values acquired from the right strain gauges are different from the ones acquired from the left and that the same phenomenon occurred when the handlebar was instrumented with the 120 Ω strain gauges, leads to the conclusion that the values range difference are caused by handlebar structural inconsistence. Therefore, the system robustness would be improved with the substitution of the strain gauges for calibrated loadcells. Regarding the Instrumented Grip Device, in order to use the blades as measuring component, despite the rods as initially considered, they must be fragilized to provide better quality values. By removing the rods is highly decreased the device assembly complexity, keeping its functionality. Since that the Instrumented Grip Device foresee the use of four strain gauges equally distanced each other around the handlebar, its values could be used simultaneously or in substitution of the Instrumented Handlebar Device strain gauges values, as inputs on the artificial neural network. Thus, increasing the input neurons of the neural network, is expected to improve its robustness and reducing the prediction error. Relatively to the Instrumented Pedals Device, developing a method to reduce the device overall high is beneficial, since that the actual high cause a minor instability to the pedalling motion.

Considering the overall results, the developed Instrumented Saddle Device, Instrumented Handlebar Device and Instrumented Pedals Device are designated capable to be used in rehabilitation environment. The provide data are veridical and reliable for rehabilitation follow-up, real-time monitorization and patient motivation improvement.

Bibliography

Álvarez, G. & Vinyolas, J., 1996. A New Bicycle Pedal Design for On-Road Measurements of Cycling Forces. *Journal of Applied Biomechanics,* pp. 130-142.

Anon., 2018. [Online] Available at: https://www.allaboutcircuits.com/textbook/direct-current/chpt-9/strain-gauges/

Anon., 2019. [Online] Available at: http://www.cnc.com/what-is-computer-numerical-control-cnc/

Azevedo, Á. F. M., *MÉTODO DOS ELEMENTOS FINITOS.* Proto: Faculdade de Engenharia da Universidade do Porto. 2003.

Bolourchi, F. & Hull, M. L., 1985. *Measurement of Rider Induced Loads During Simulated Bicycling.* Greeley, USA, J. Terauds, J. N. Barham, pp. 178-198.

Bressel, E. & Cronin, J., 2005. Bicycle seat interface pressure: reliability, vaidity, and influence of hand position and workload. *Journal of Biomechanics,* pp. 1325-31.

Chacón, J., Caminero, M., García-Plaza, E. & Núñez, P., 2017. Additive manufacturing of PLA structures using fused deposition modelling: Effect of process parameters on mechanical properties and their optimal selection. *Materials and Design,* pp. 143-157.

Deutsch, J. E. et al., 2013. Feasibility of Virtual Reality Augmented Cycling for Health Promotion of People Post-Stroke. *Journal of neurologic physical therapy.*

Farjadian, A. B. et al., 2013. *VRACK: Measuring Pedal Kinematics During Stationary Bike Cycling.* Seattle, Washington USA, IEEE.

Ferreira, P., 2018. *Tecnologias de Fabrico.* Coimbra: s.n.

Fluet, G. G. & Deutsch, J. E., 2013. Virtual Reality for Sensorimotor Rehabilitation Post-Stroke: The Promise and Current State of the Field. *Current Physical Medicine and Rehabilitation Reports,* pp. 9-20.

Gao, C., 2009. *Study on the Sensor for the Pedal Push Force of Bicycle.* Beijing, China, IEEE, pp. 977-980.

Gill, S., 2019. *Is there an average weight for men?.* [Online] Available at: https://www.medicalnewstoday.com/articles/320917.php

Giubilato, F. & Petrone, N., 2014. Stress analysis of bicycle saddles structural components during different cycling conditions.. *Procedia Engineering,* pp. 636-641.

Groover, M. P. & Zimmers, E. W., *CAD/CAM: Computer-Aided Design and Manufacturing.* Michigan: Prentice-Hall. 1984.

Hoes, M. J. A. J. M., Binkhorst, R. A., Smeekes-Kuyl, A. E. M. C. & Vissers, A. C. A., 1968. Measurement of forces exerted on pedal and crank during work on a bicycle ergometer at different loads. *Internationale Zeitschrift für angewandte Physiologie einschließlich Arbeitsphysiologie,* p. 33–42.

Jones, S. L. P. & Passfield, L., 1998. The dynamic calibration of bicycle power measuring cranks. *Engineering of Sport,* pp. 265-274.

Joy, S., 2013. Exercise Benefits Patients With Depression. *American Journal of Nursing,* p. 67.

Kong, Y.-K. & Lowe, B. D., 2005. Optimal cylindrical handle diameter for grip force task. *International Journal of Industrial Ergonomics,* pp. 495-507 .

Lee, Y. & Jeong, J., 2018. Design and Implementation of Monitoring System Architecture for Smart Bicycle Platform. *Procedia Computer Science,* pp. 464-469.

Lei Wang, D. a., 2017. Exercise Benefits Coronary Heart Disease. *Exercise for Cardiovascular Disease Prevention and Treatment,* pp. 1 - 7.

MakeItForm, 2019. *6082-T6 Aluminum.* [Online] Available at: https://www.makeitfrom.com/material-properties/6082-T6-Aluminum

McKinney R, A. R., 2000. Exercise benefits patients with osteoarthritis. *The Physician and Sportsmedicine,* pp. 71-72.

Michal Katz-Leurer, I. S. O. K. a. Z. D., 2006. The influence of early cycling training on balance in stroke patients at the subacute stage. Results of a preliminary trial. *Clinical Rehabilitation,* pp. 398-405.

Nanninga, N. E., 2008. *High cycle fatigue of AA6082 and AA6063 aluminum extrusions* , s.l.: Michigan Technological University.

Oja, P. et al., 2011. Health benefits of cycling: a systematic review. *Scandinavian Journal of Medicine & Science in Sports,* p. 496–509.

Peipei Han, W. Z. L. K. Y. M. L. F. L. J. H. Y. X. C. L. H. L. W. X. Y. M. K. a. Q. G., 2017. Clinical Evidence of Exercise Benefits for Stroke. *Exercise for Cardiovascular Disease Prevention and Treatment* , pp. 131-151.

Petrone, N., Giubilato, F., Giro, A. & Mutinelli, N., 2012. Development of instrumented downhill bicycle components for field data collection. *Procedia Engineering,* pp. 514-519.

Pham, D. & Gault, R., 1998. A comparison of rapid prototyping technologies. *International Journal of Machine Tools & Manufacture,* pp. 1257-1287.

Ranky, R. G. et al., 2014. Modular mechatronic system for stationary bicycles interfaced with virtual environment for rehabilitation. *Journal of NeuroEngineering and Rehabilitation.*

Santos, J. et al., 2019. *Development of a Pedal Force Measurement Interface for Rehabilitation Purposes.* Viseu, s.n.

Santos, J. et al., 2019. *Identification of forces applied on seat and handlebar from a static bicycle*. Unhais da Serra, Covilhã, UA Editora, pp. 119-120.

Singhal, S., Yousuf, M. A., Weintraub, N. L. & Shizukuda, Y., 2009. Use of Bicycle Exercise Echocardiography for Unexplained Exertional Dyspnea. *Clinical Cardiology,* pp. 302-306.

Soden, P. D. & Adeyefa, B. A., 1979. Forces applied to a bicycle during normal cycling. *Journal of Biomechanics*, pp. 527-541.

Stone, C. & Hull, M. L., 1993. Rider/Bicycle Interaction Loads During Standing Treadmill Cycling. *Journal of applied biomechanics*, pp. 202-218.

Terre, L., 2010. Does Exercise Benefit Fibromyalgia?. *American Journal of Lifestyle Medicine* , pp. 410 - 412.

Vanwalleghem, J., Baere, I. D., Loccufier, M. & Paepegem, W. V., 2015. Dynamic calibration of a strain gauge based handlebar force sensor for cycling purposes. *Procedia Engineering,* pp. 219-224.

Zhang, G., Patuwo, B. E. & Hu, M. Y., 1998. Forecasting with artificial neural networks: The state of the art. *International Journal of Forecasting,* pp. 35-62.

Zhang, Y., Chen, K. & Yi, J., 2013. Rider Trunk and Bicycle Pose Estimation With Fusion of Force/Inertial Sensors. *IEEE Transactions on Biomedical Engineering,* pp. 2541 - 2551.

Zhang, Y., Liu, F., Trkov, M. & Yi, J., 2012. *Rider/Bicycle Pose Estimation with IMU/Seat Force Measurements.* Kachsiung, Taiwan, IEEE, pp. 2541- 2551.

Appendix

Appendix A – Instrumented Saddle Device

Appendix A.1 – Loadcell Interface Solidworks Solid Mesh Convergence

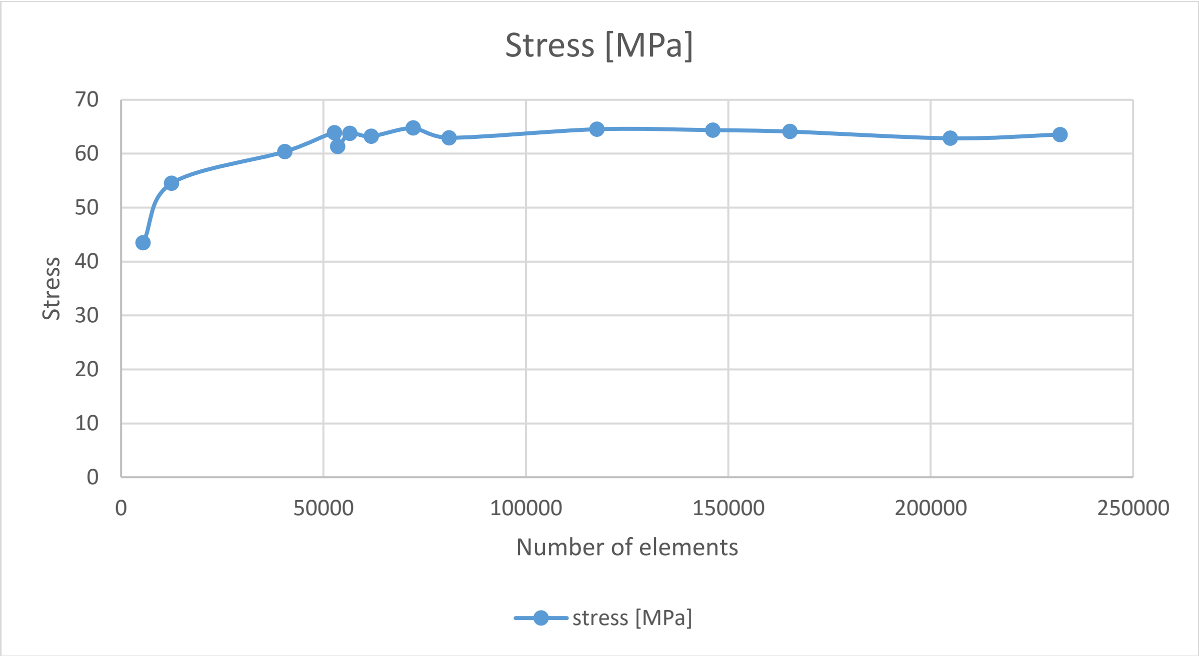

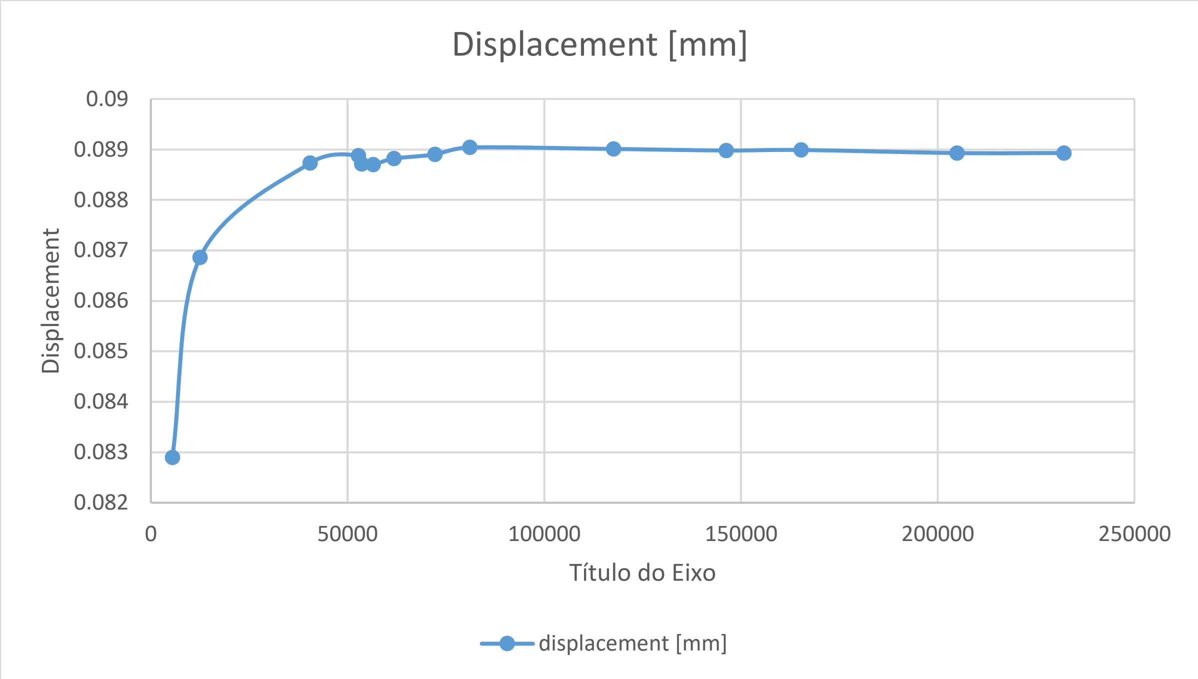

Appendix A.2 – Loadcell Interface Solidworks Shell Mesh Convergence

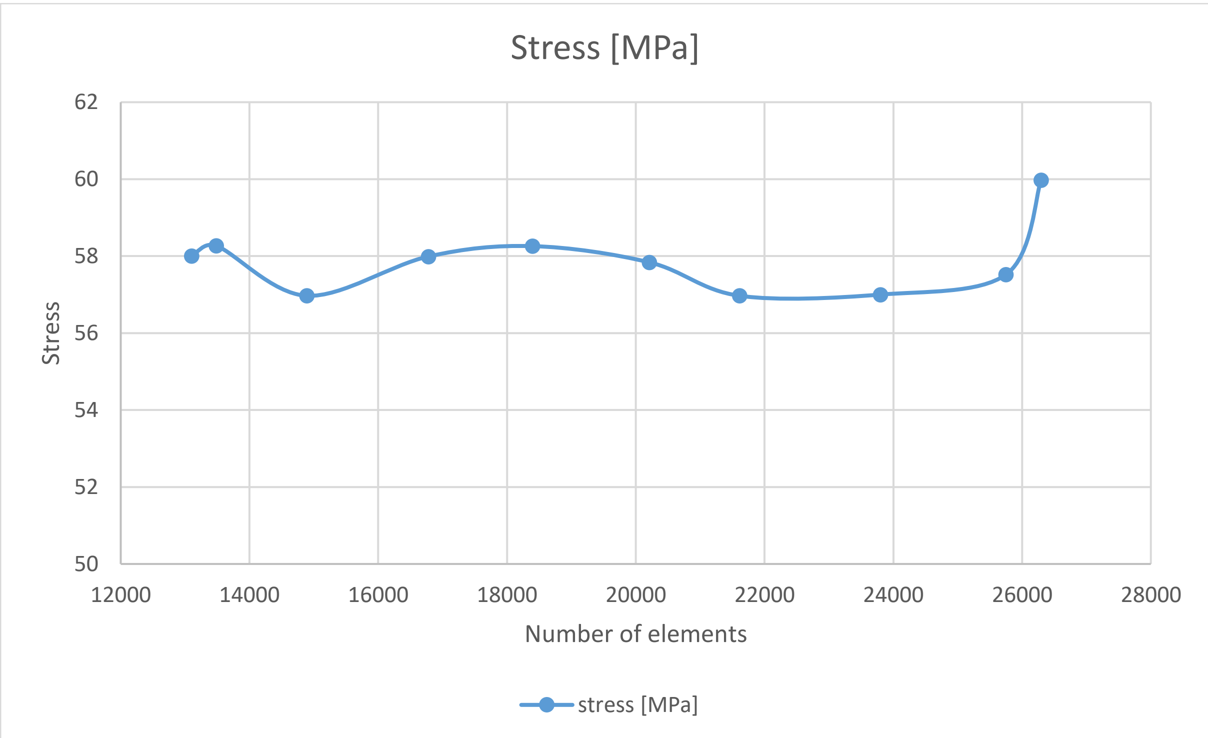

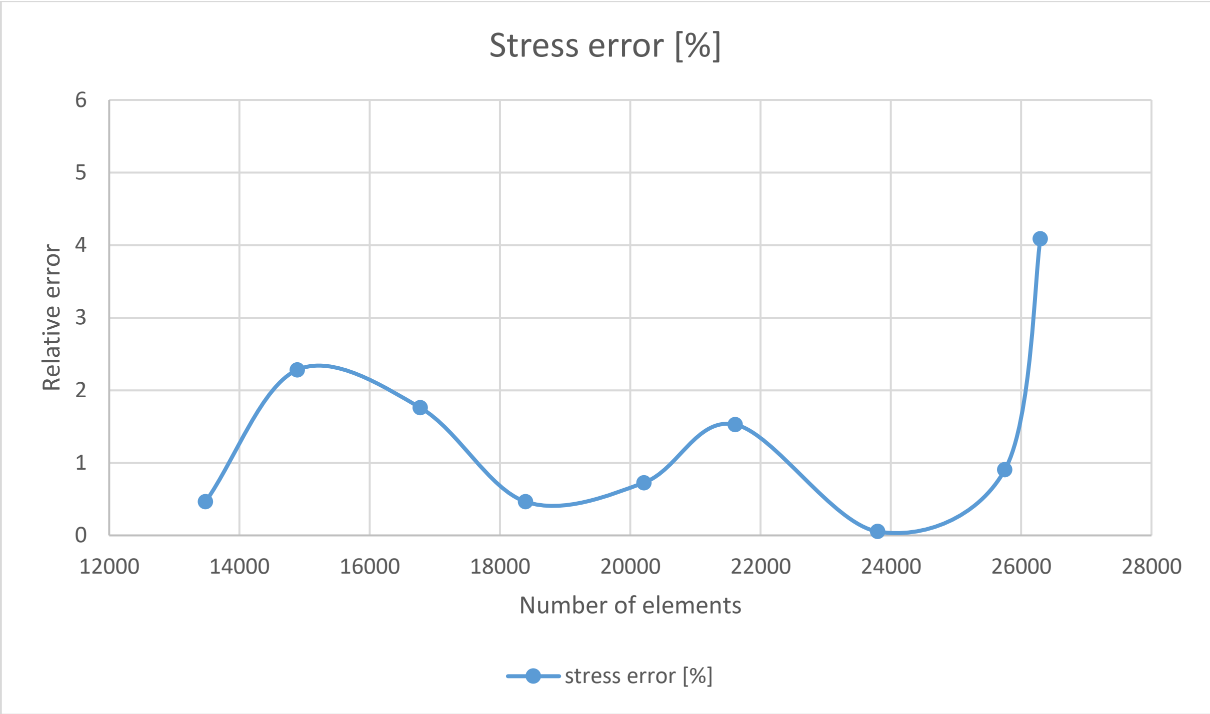
Stress error [%]
6
5
4
3
2
1
0
Relative error
12000
14000
16000
18000
20000
22000
24000
26000
28000
Number of elements
stress error [%]

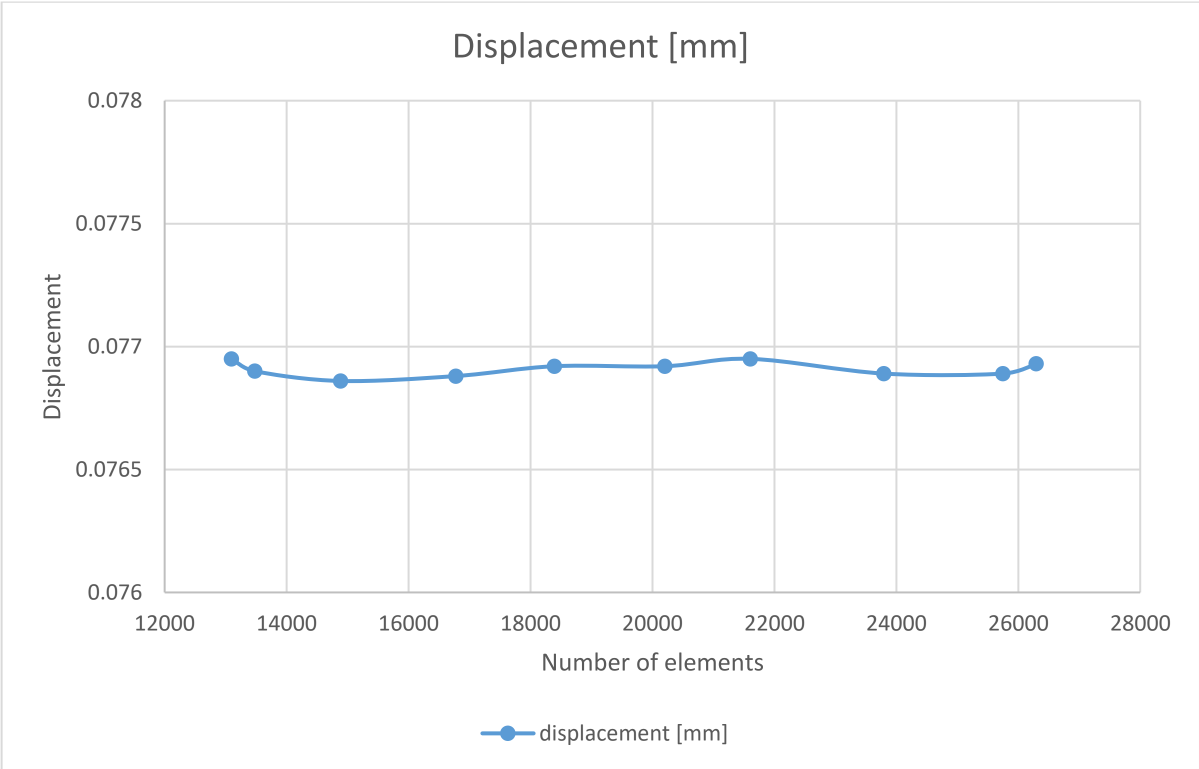
Displacement [mm]
0.078
0.0775
0.077
0.0765
0.076
Displacement
12000
14000
16000
18000
20000
22000
24000
26000
28000
Number of elements
displacement [mm]

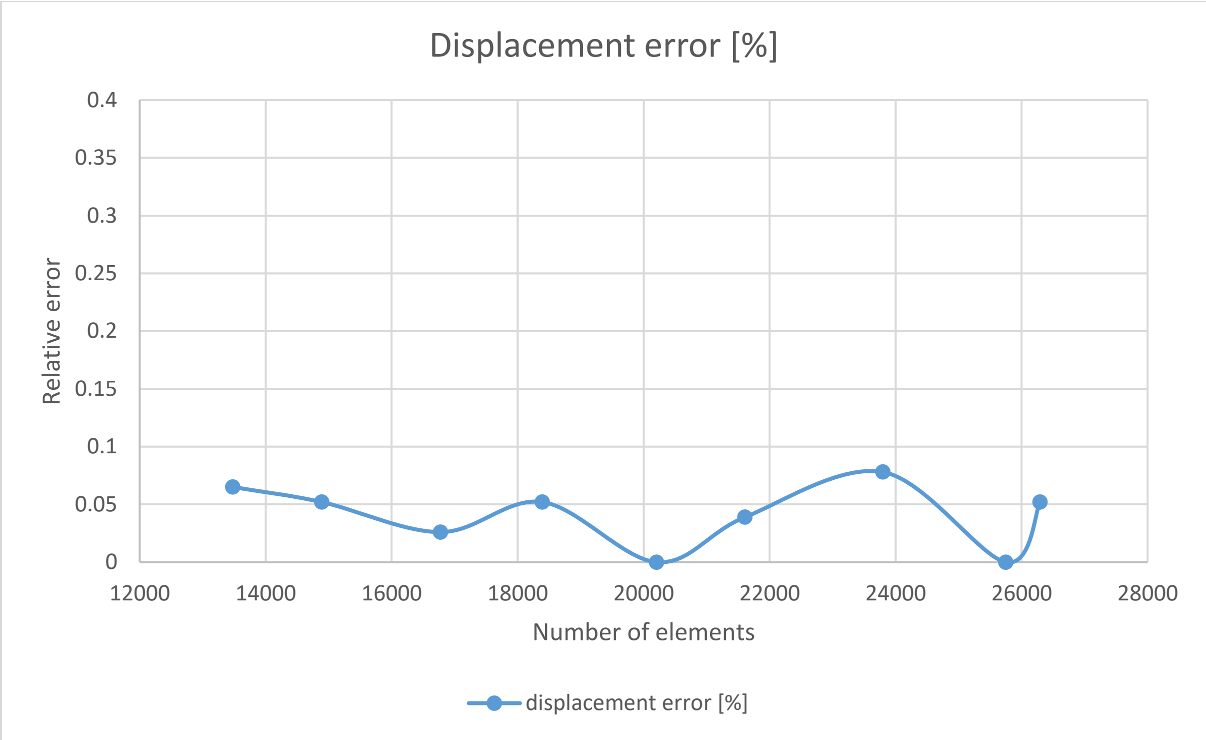
Displacement error [%]
Relative error
0.4
0.35
0.3
0.25
0.2
0.15
0.1
0.05
0
12000
14000
16000
18000
20000
22000
24000
26000
28000
Number of elements
displacement error [%]

Appendix A.3 – Loadcell Interface MSC Nastran/Patran Upper Plate Solid Mesh Convergence

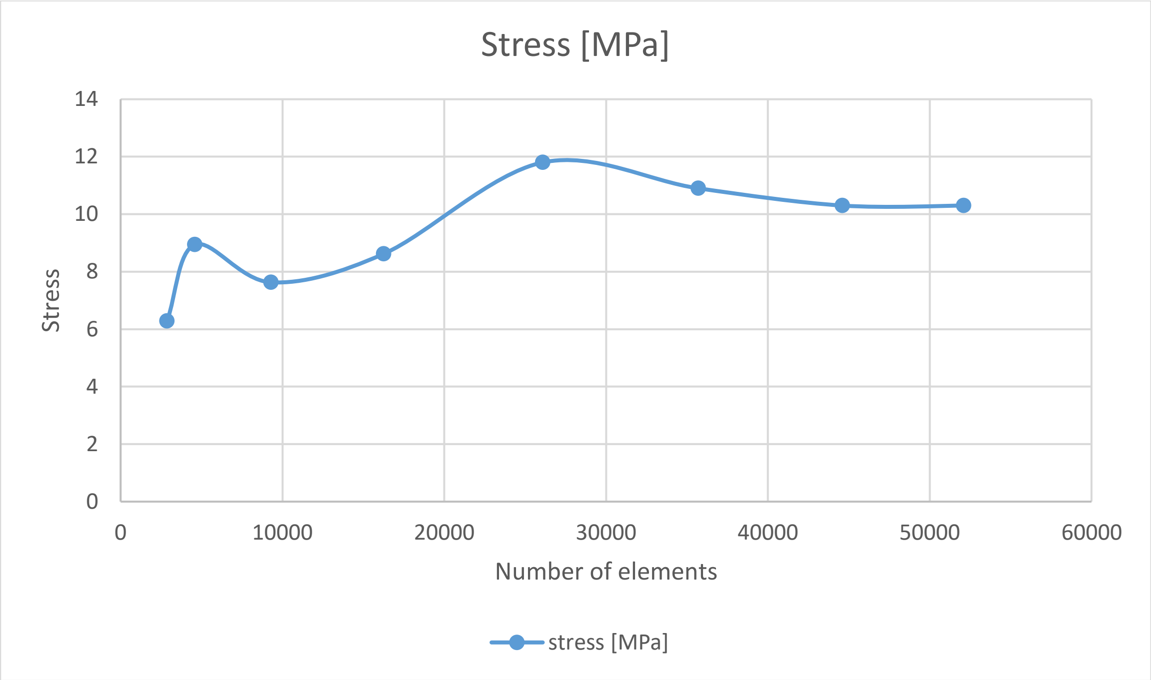

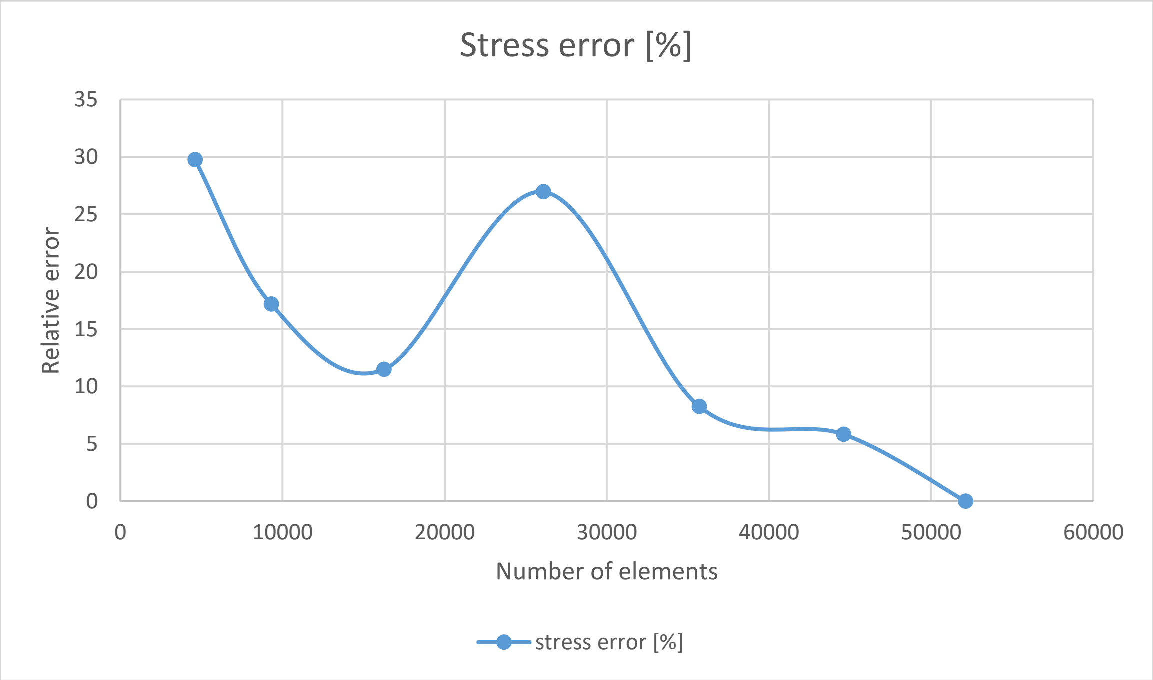

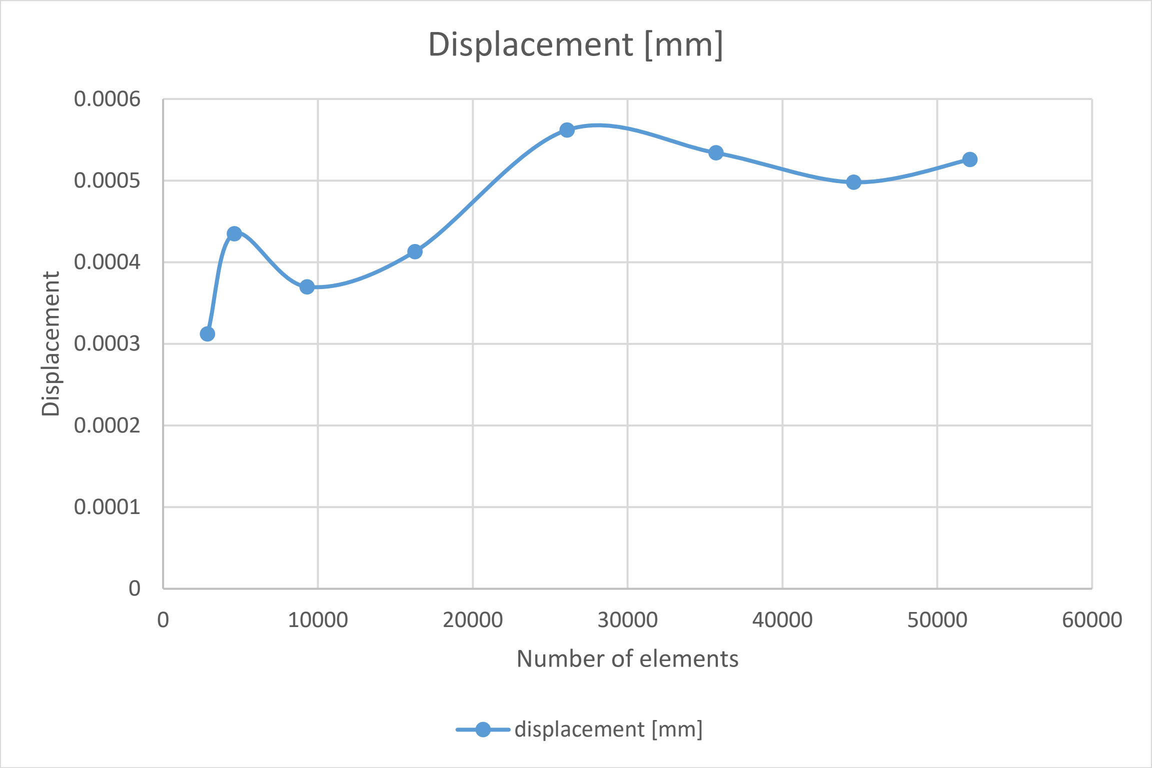
Displacement [mm]
0.0006
0.0005
0.0004
0.0003
0.0002
0.0001
0
Displacement
0
10000
20000
30000
40000
50000
60000
Number of elements
displacement [mm]

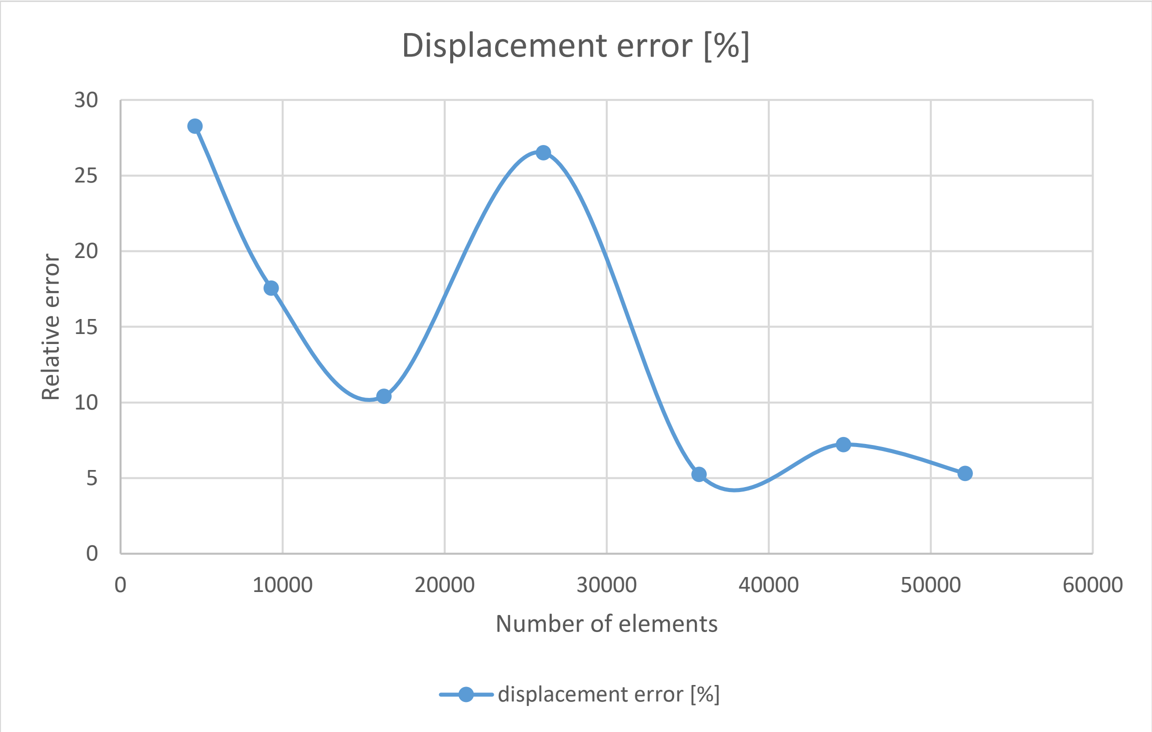
Displacement error [%]
30
25
20
15
10
5
0
Relative error
0
10000
20000
30000
40000
50000
60000
Number of elements
displacement error [%]

Appendix A.4 – Loadcell Interface MSC Nastran/Patran Lower Plate Solid Mesh Convergence

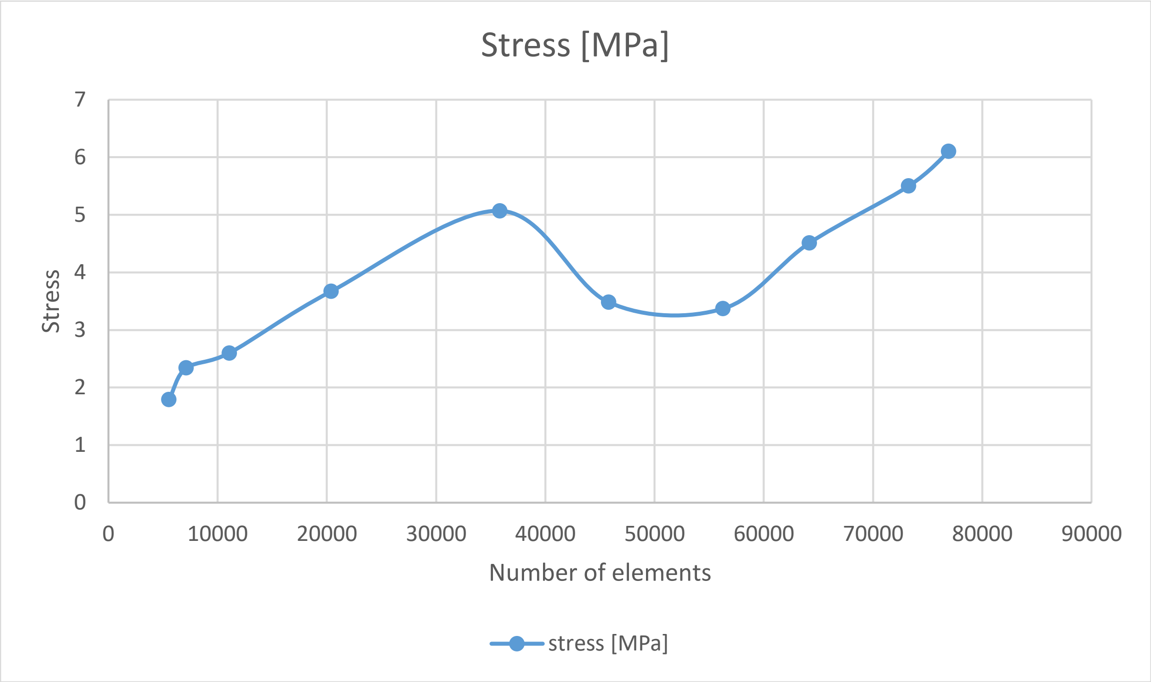

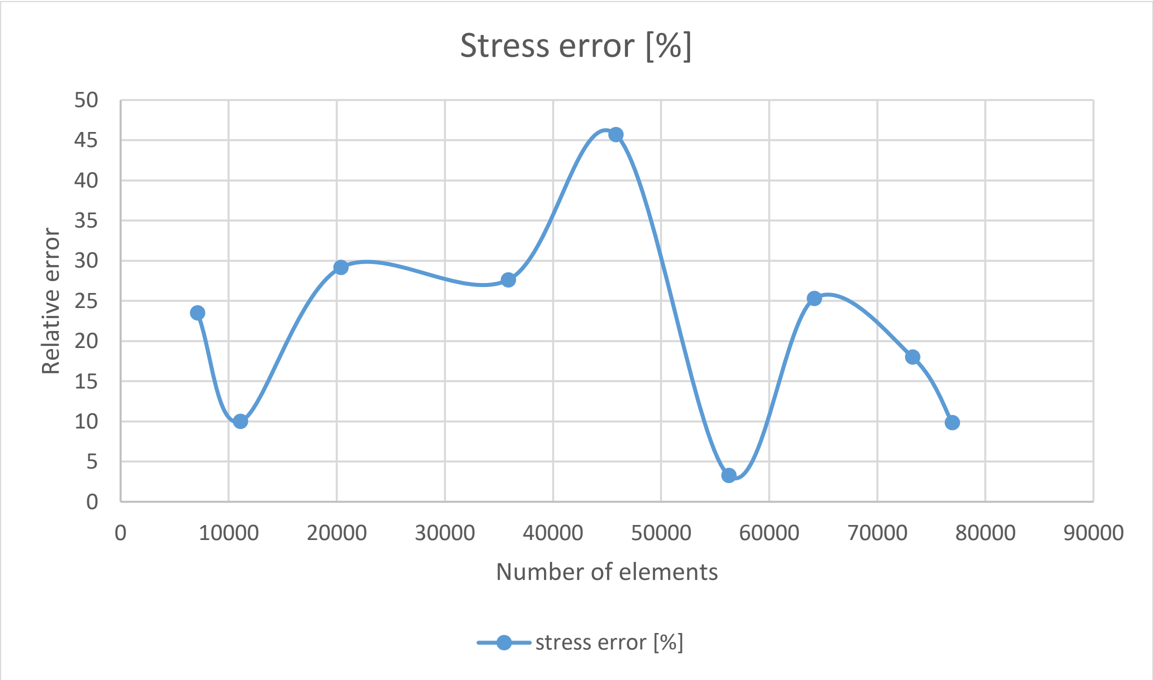

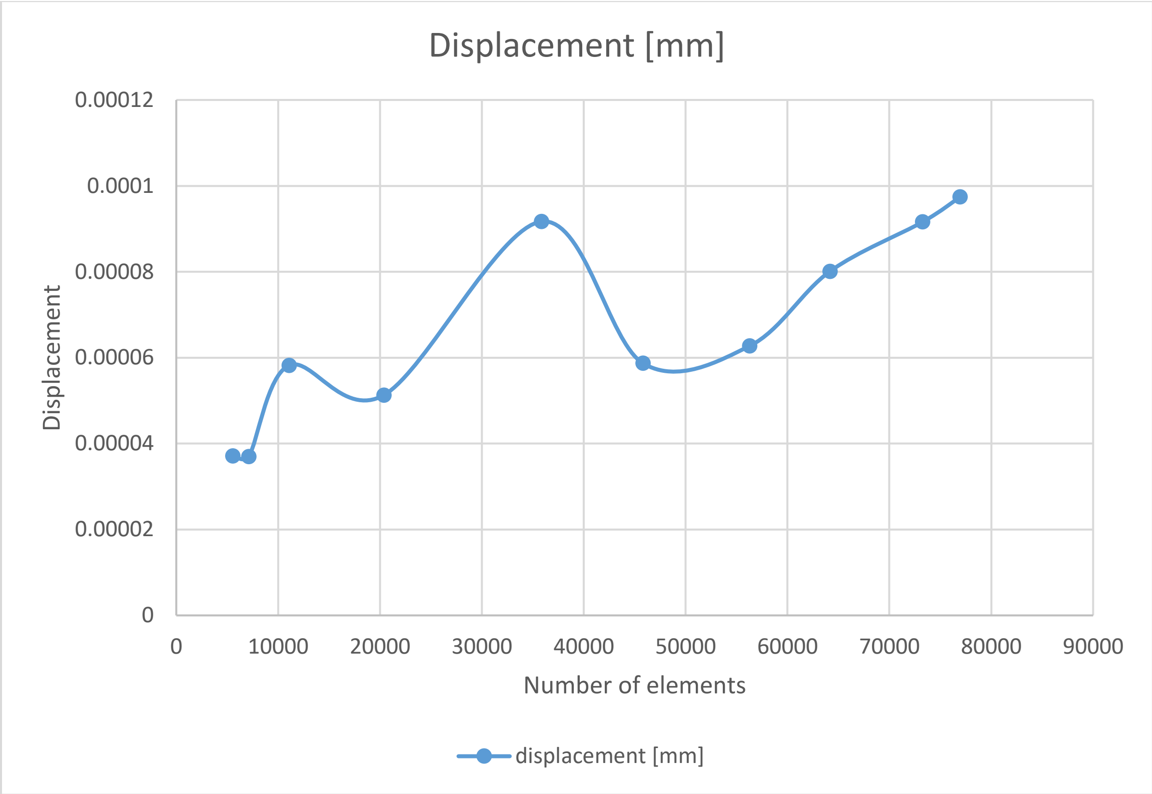

Displacement [mm]
0.00012
0.0001
0.00008
0.00006
0.00004
0.00002
0
Displacement
0
10000
20000
30000
40000
50000
60000
70000
80000
90000
Number of elements
displacement [mm]

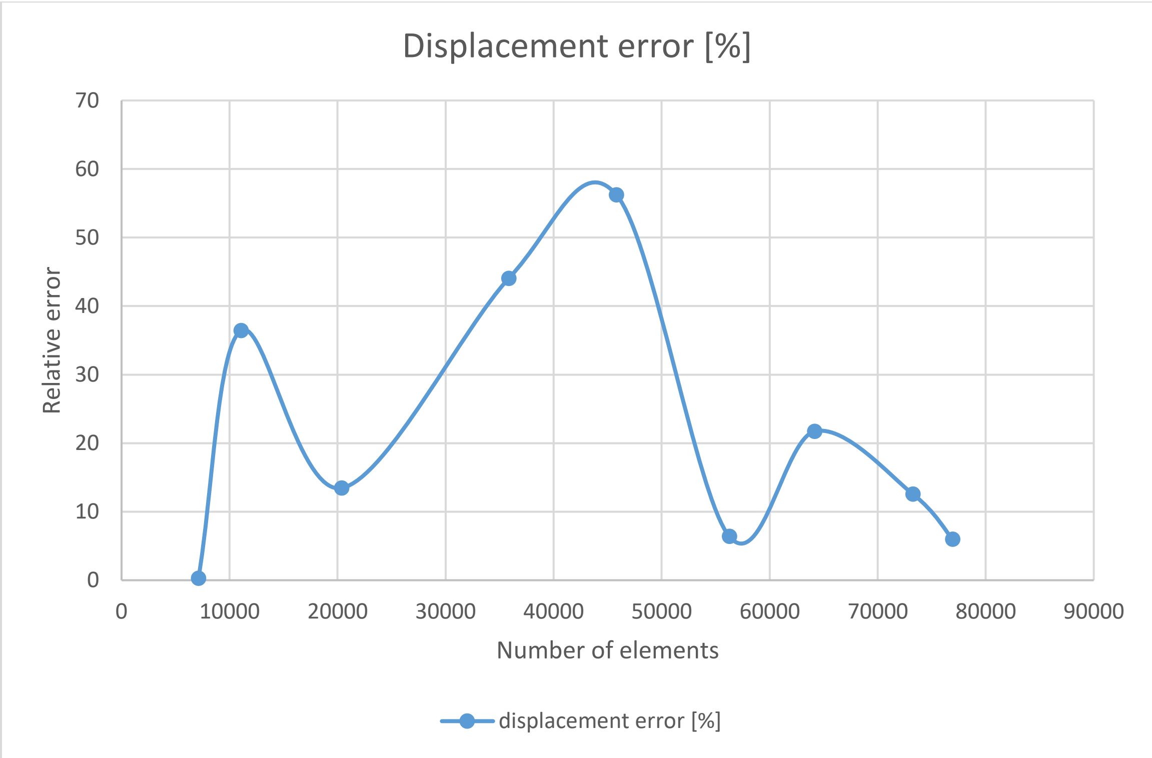

Displacement error [%]
70
60
50
40
30
20
10
0
Relative error
0
10000
20000
30000
40000
50000
60000
70000
80000
90000
Number of elements
displacement error [%]

Appendix A.5 – Saddle Post Connector Solidworks Mesh Convergence – Option 1: Uninterrupted Design 3D printed PLA

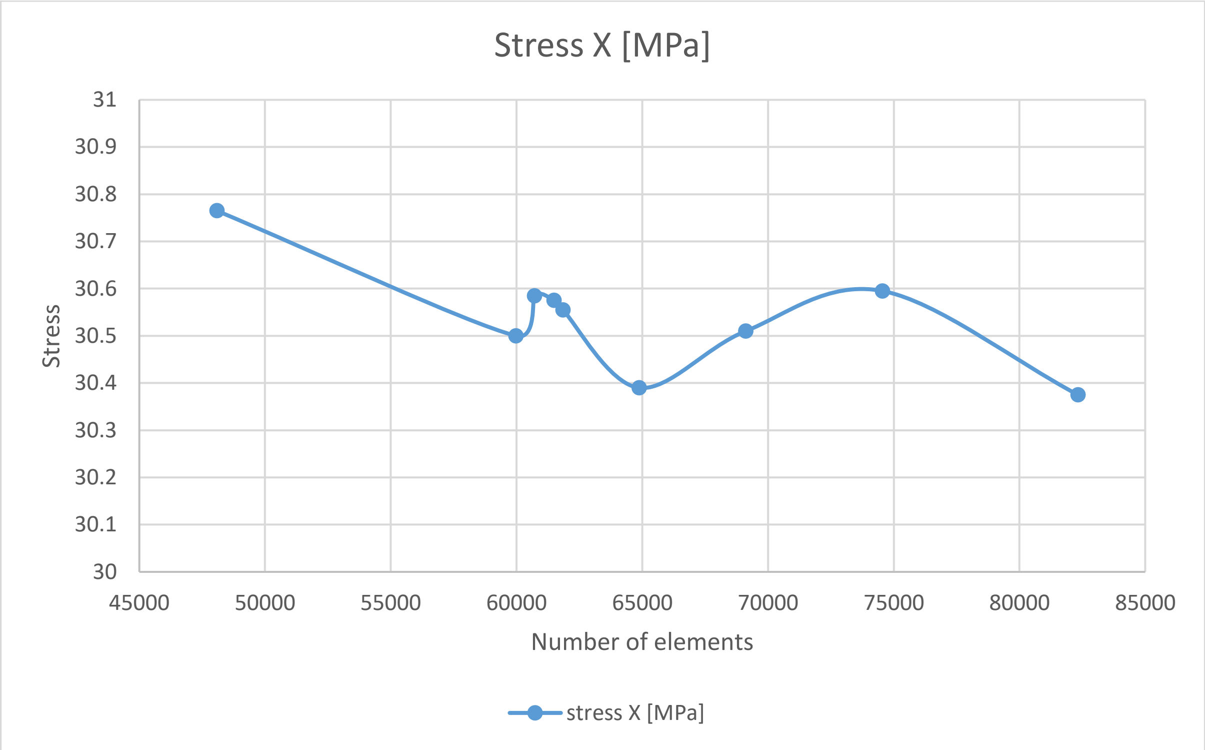

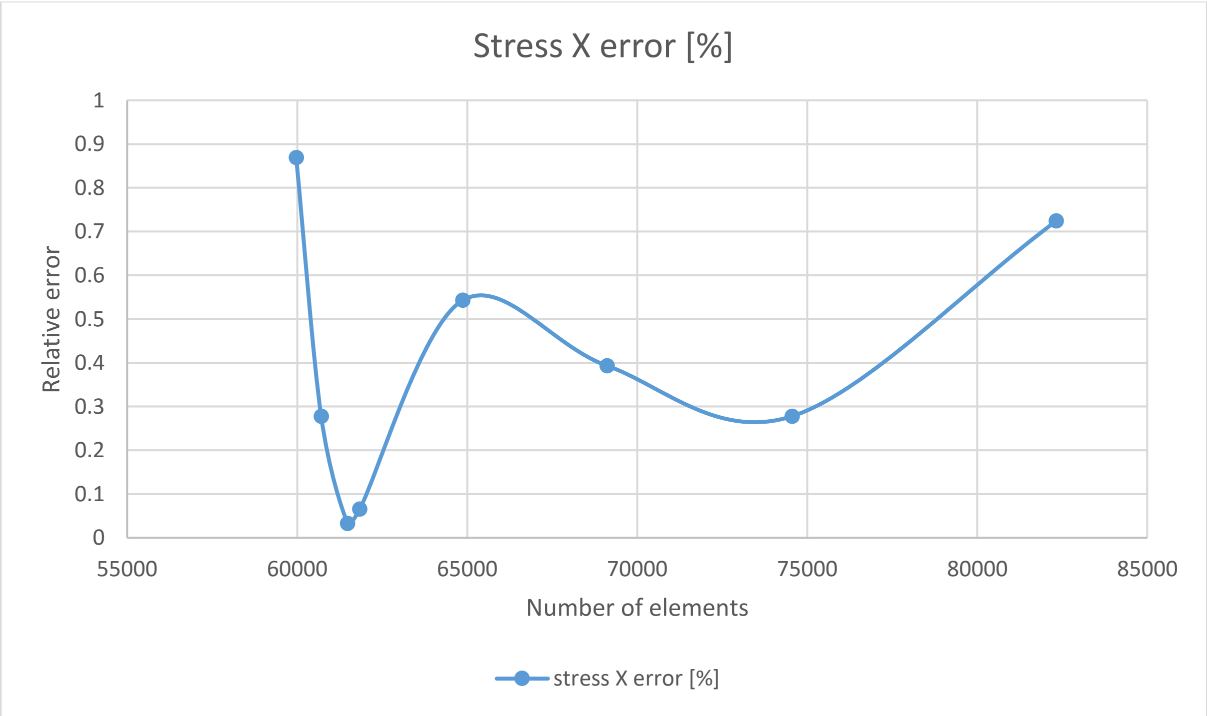

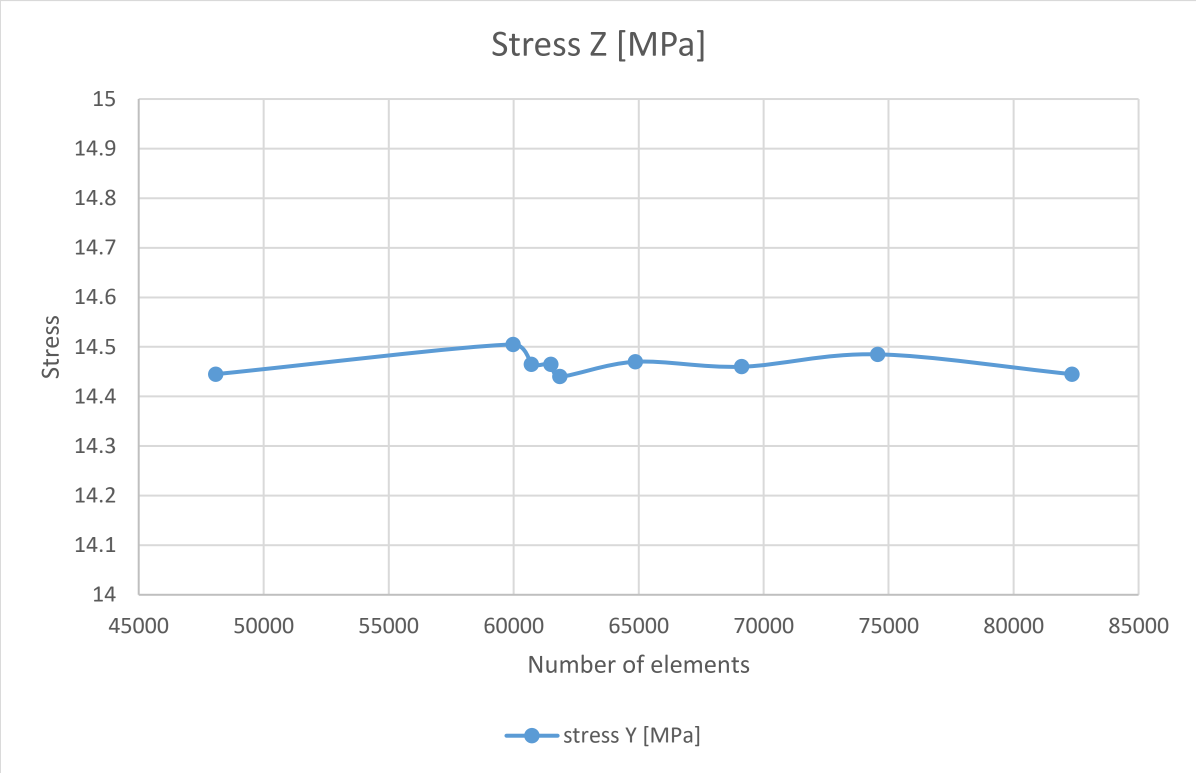
Stress Z [MPa]
Stress
15
14.9
14.8
14.7
14.6
14.5
14.4
14.3
14.2
14.1
14
45000
50000
55000
60000
65000
70000
75000
80000
85000
Number of elements
stress Y [MPa]

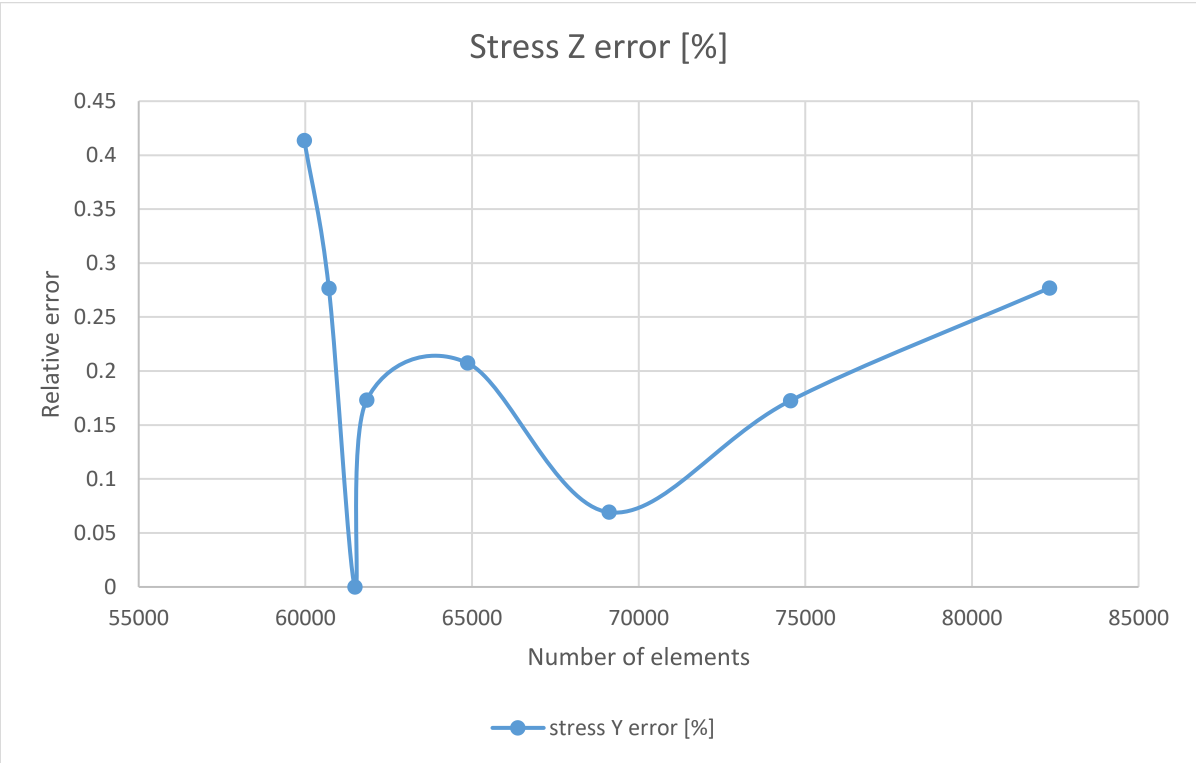
Stress Z error [%]
Relative error
0.45
0.4
0.35
0.3
0.25
0.2
0.15
0.1
0.05
0
55000
60000
65000
70000
75000
80000
85000
Number of elements
stress Y error [%]

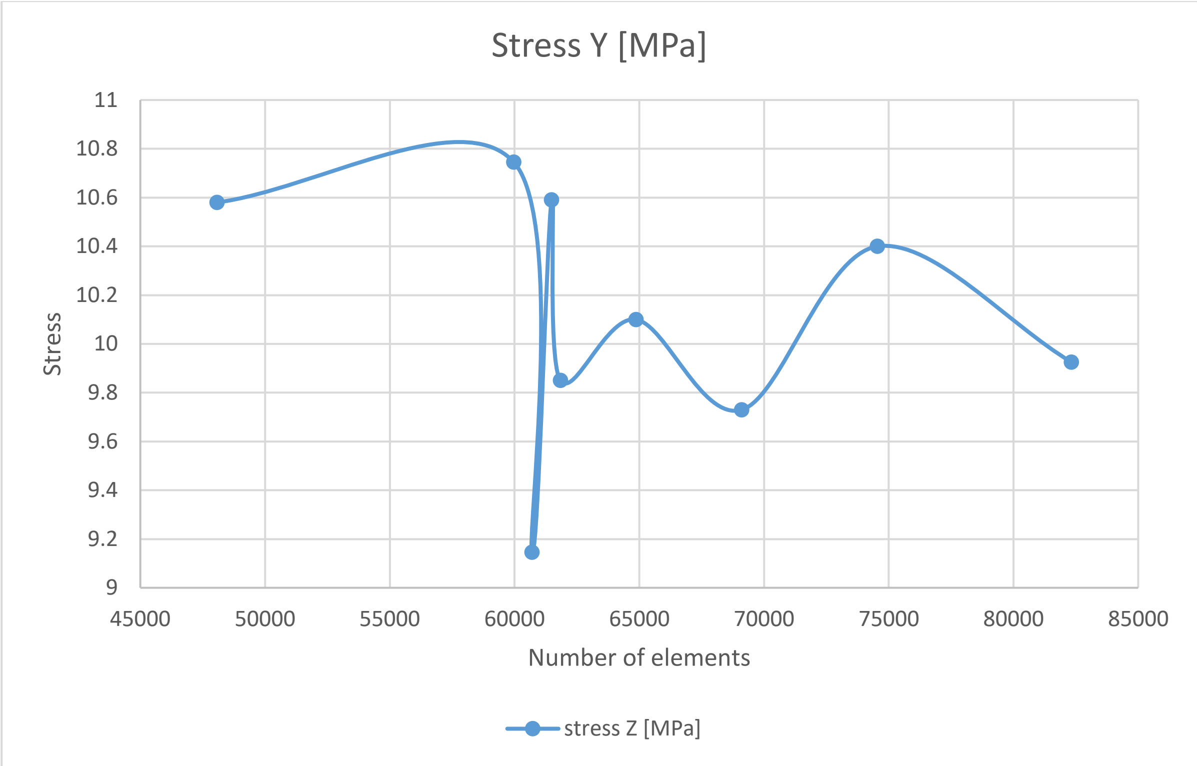
Stress Y [MPa]
Stress
11
10.8
10.6
10.4
10.2
10
9.8
9.6
9.4
9.2
9
45000
50000
55000
60000
65000
70000
75000
80000
85000
Number of elements
stress Z [MPa]

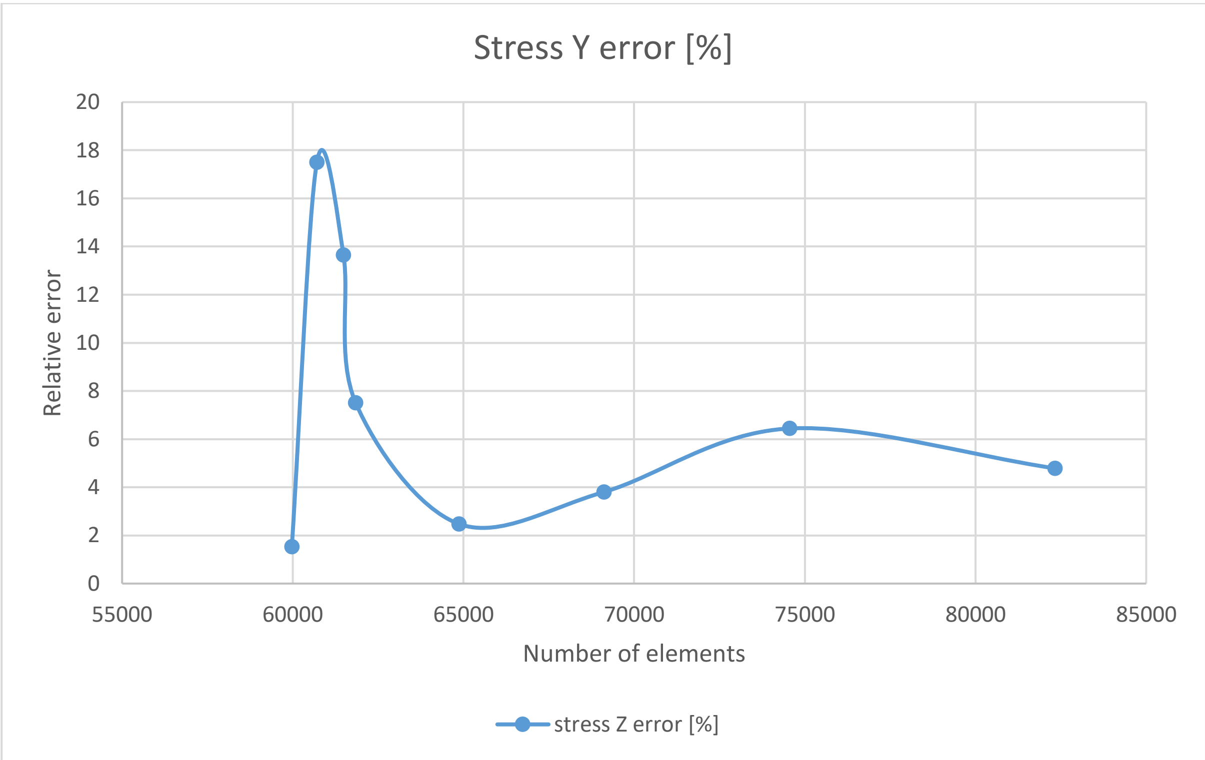
Stress Y error [%]
Relative error
20
18
16
14
12
10
8
6
4
2
0
55000
60000
65000
70000
75000
80000
85000
Number of elements
stress Z error [%]

Appendix A.6 – Saddle Post Connector Solidworks Mesh Convergence – Option 2: Uninterrupted Design 7075 Aluminium

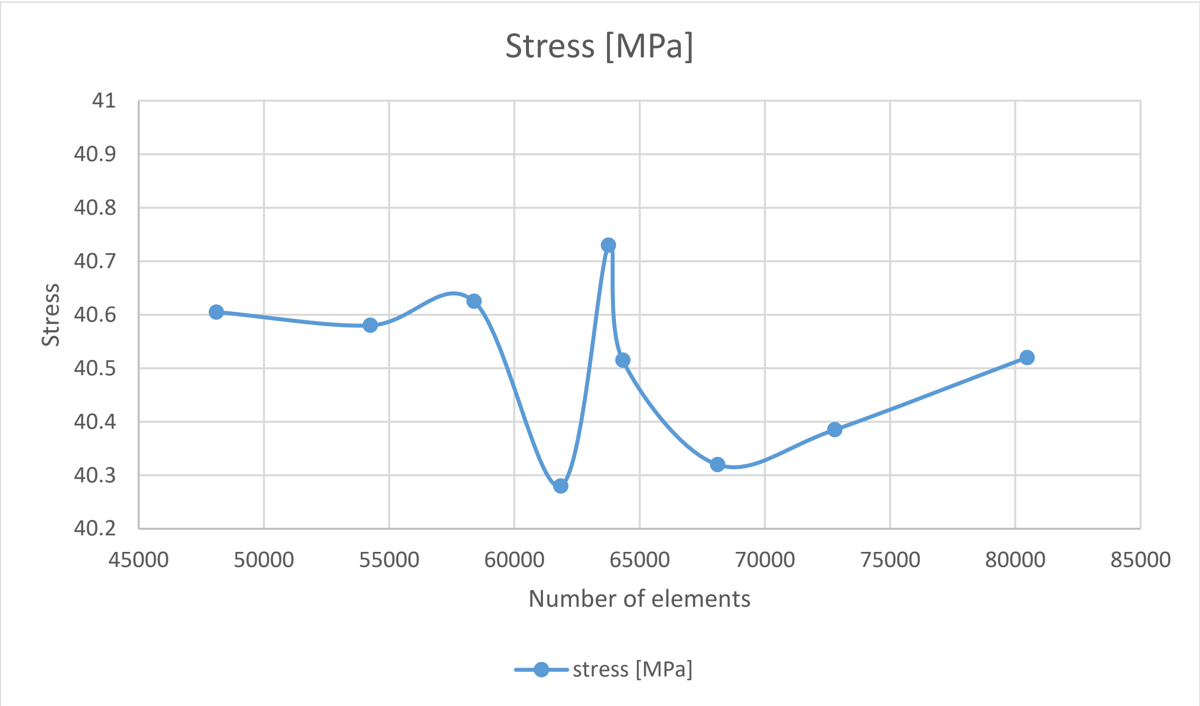

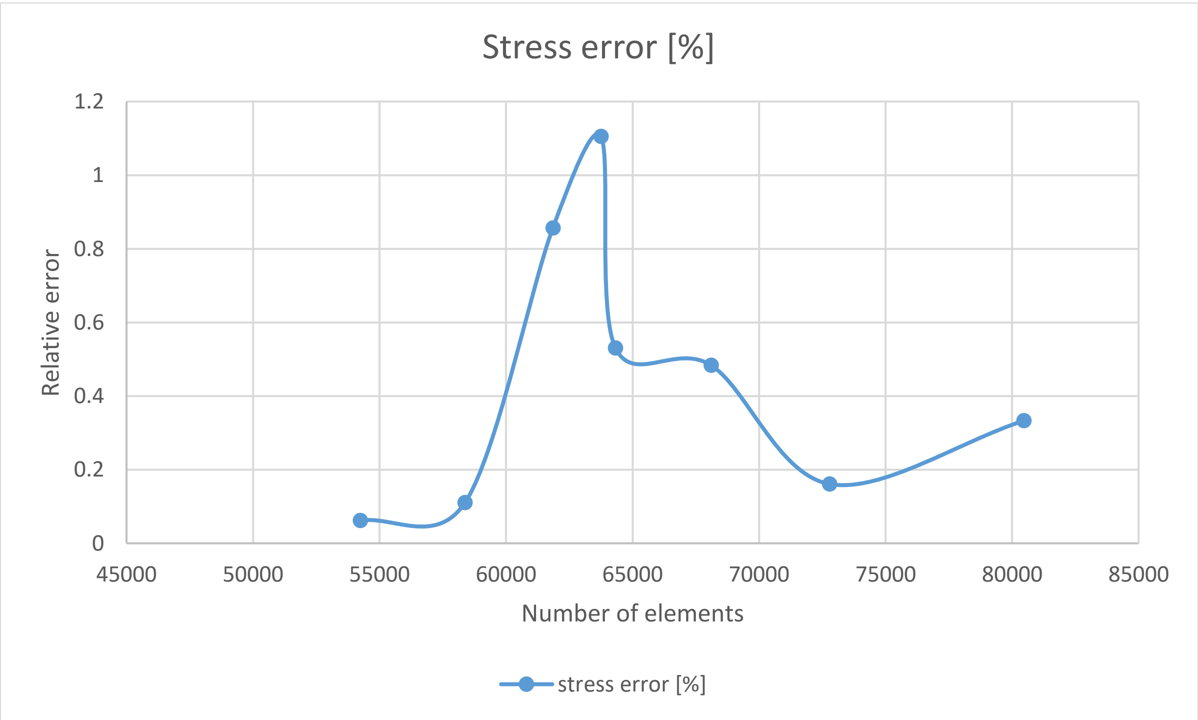

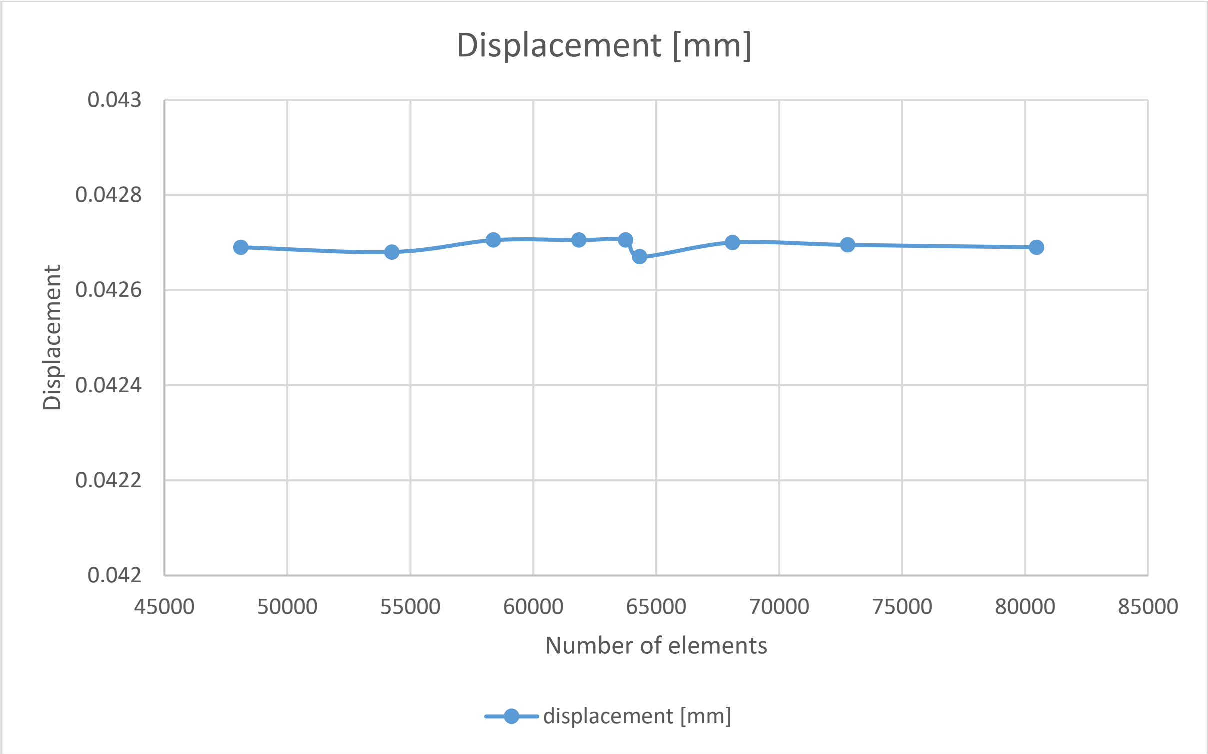

Displacement [mm]
0.043
0.0428
0.0426
0.0424
0.0422
0.042
Displacement
45000
50000
55000
60000
65000
70000
75000
80000
85000
Number of elements
displacement [mm]

Displacement error [%]
0.4
0.35
0.3
0.25
0.2
0.15
0.1
0.05
0
-0.05
-0.1
Relative error
45000
50000
55000
60000
65000
70000
75000
80000
85000
Number of elements
displacement error [%]

Appendix A.7 – Saddle Post Connector MSC Nastran/Patran Mesh Convergence – Option 2: Uninterrupted Design 7075 Aluminium

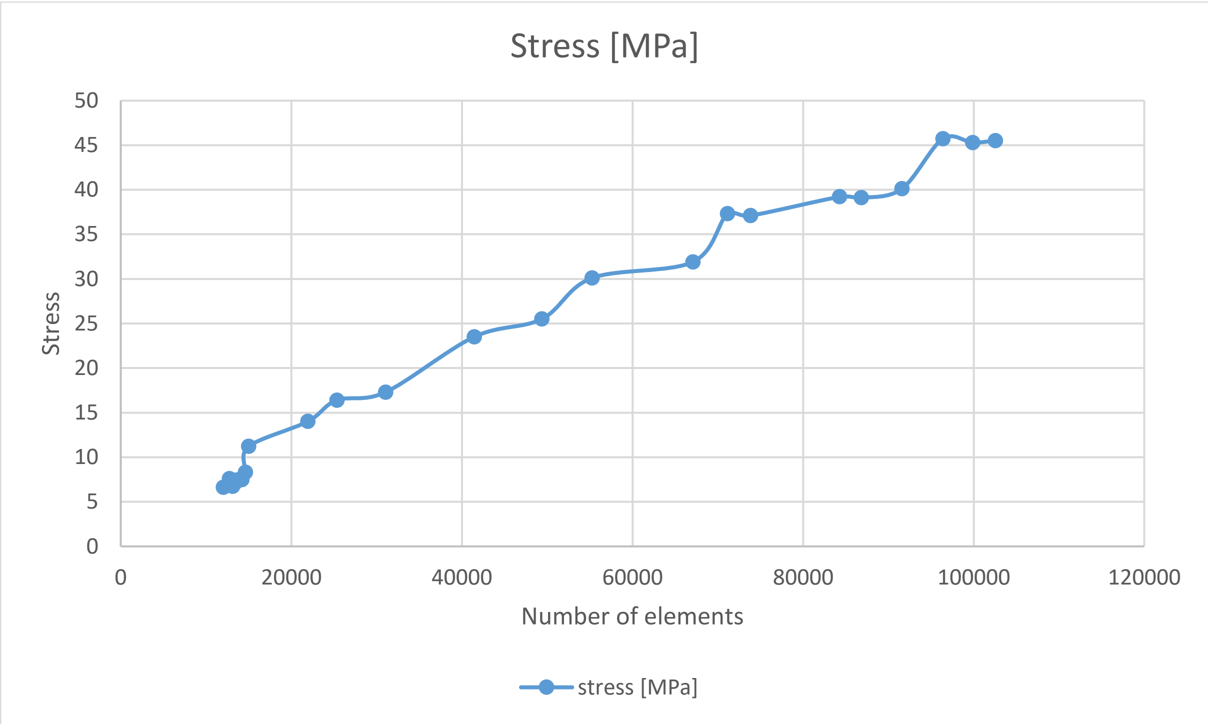

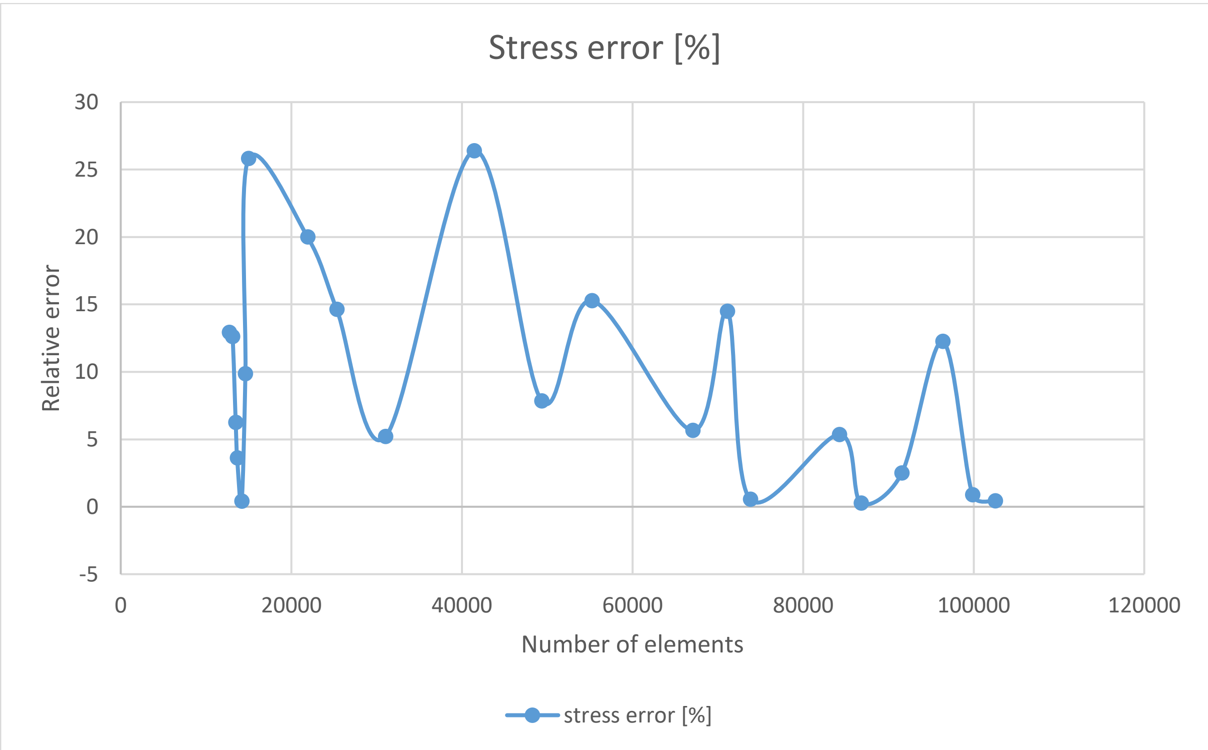

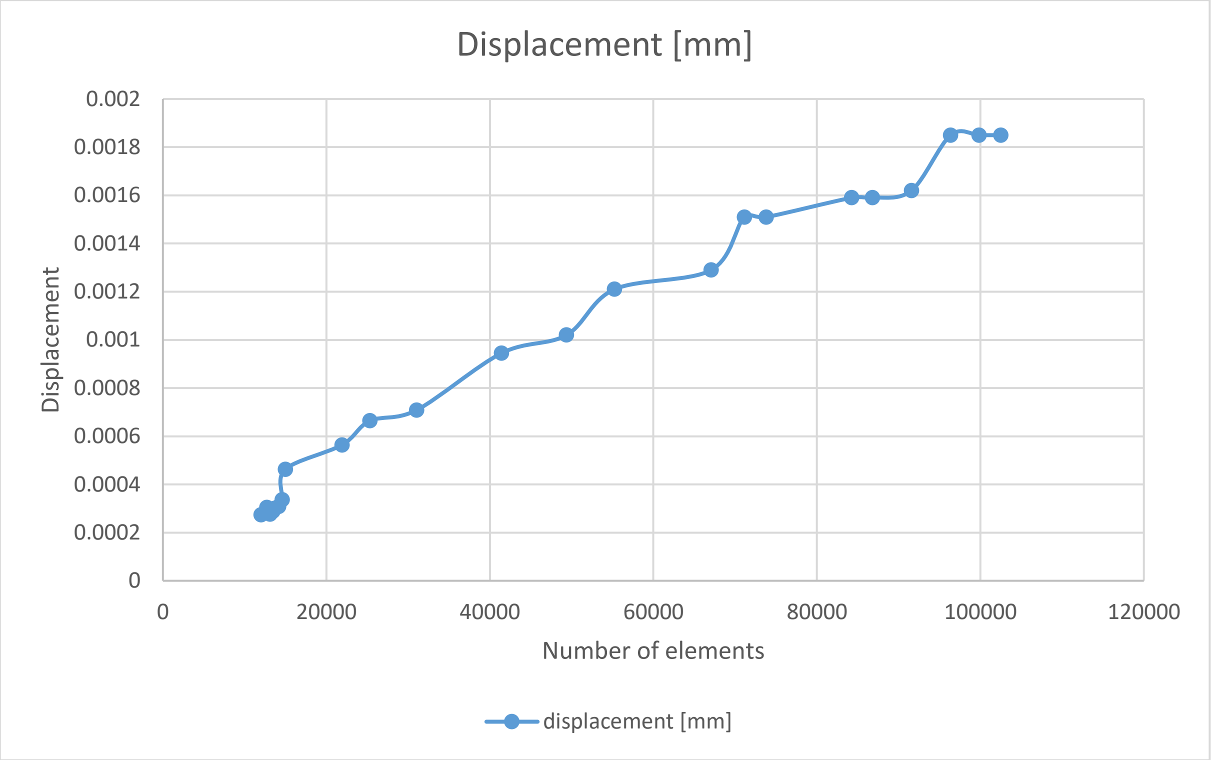
Displacement [mm]
Displacement
0.002
0.0018
0.0016
0.0014
0.0012
0.001
0.0008
0.0006
0.0004
0.0002
0
0
20000
40000
60000
80000
100000
120000
Number of elements
displacement [mm]

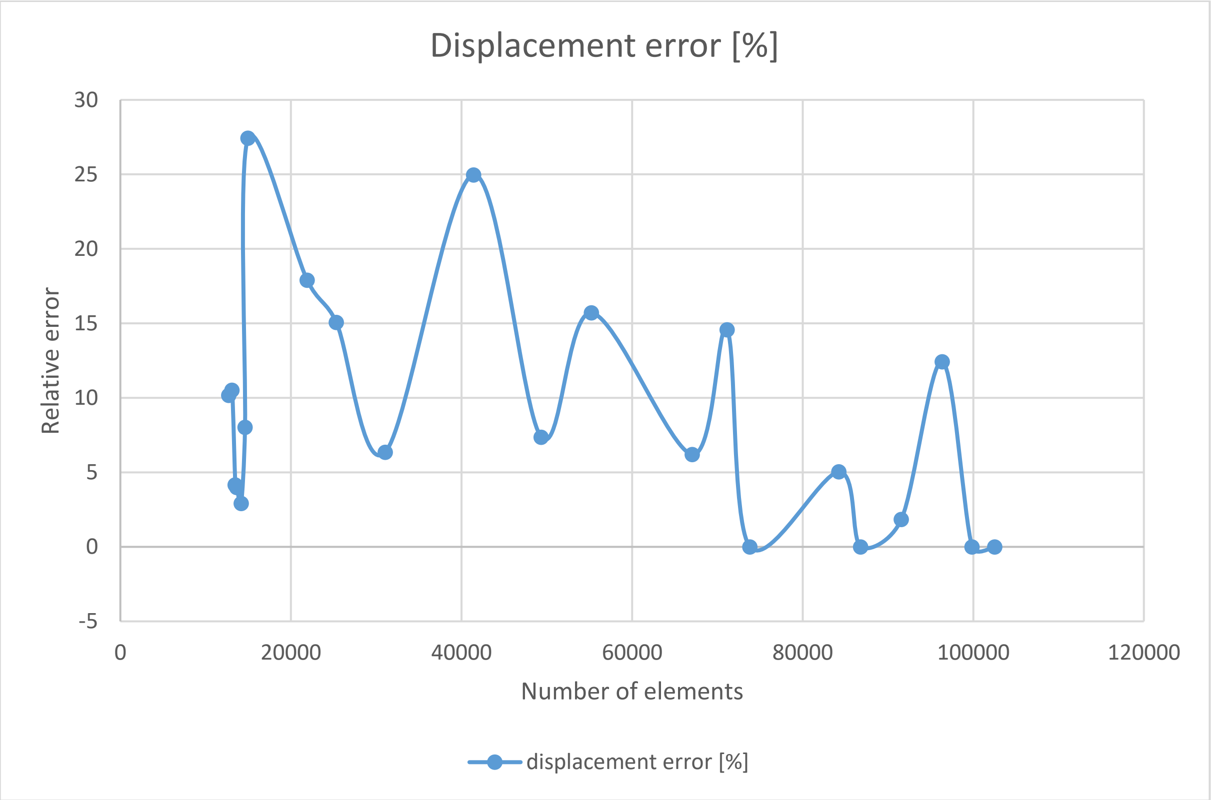
Displacement error [%]
Relative error
30
25
20
15
10
5
0
-5
0
20000
40000
60000
80000
100000
120000
Number of elements
displacement error [%]

Appendix A.8 – Saddle Post Connector Solidworks Mesh Convergence – Option 3: Interrupted Design 7075 Aluminium and 304 Stainless Steel

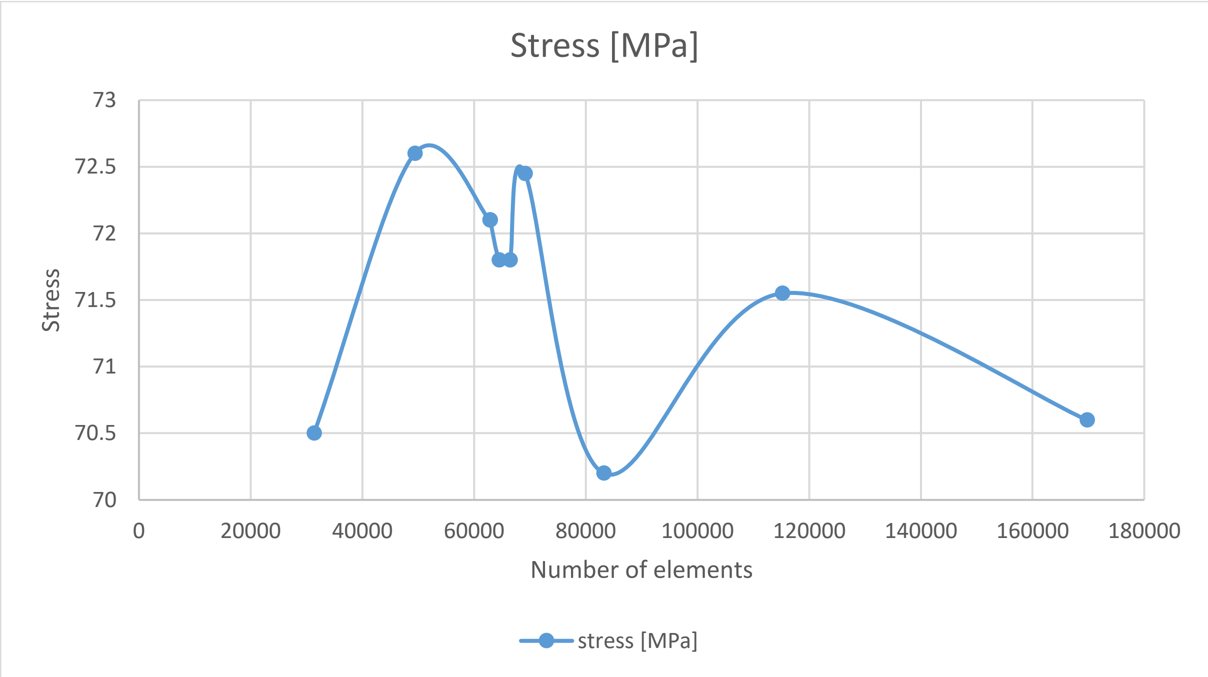

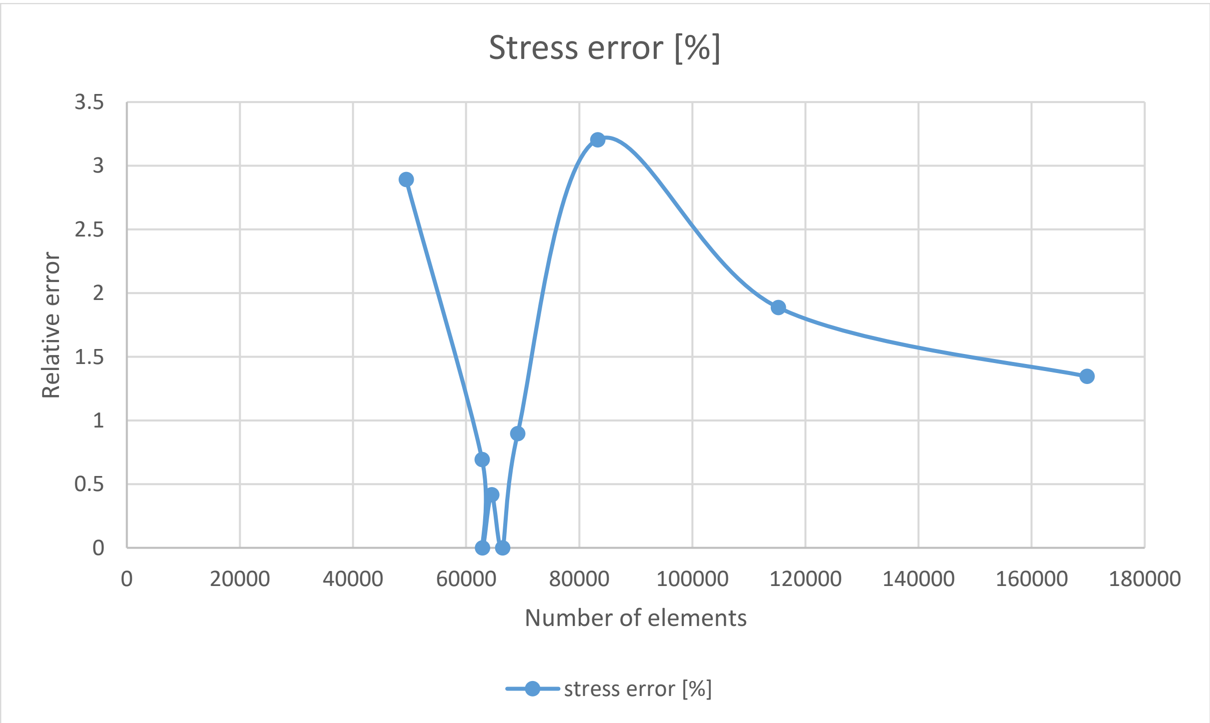

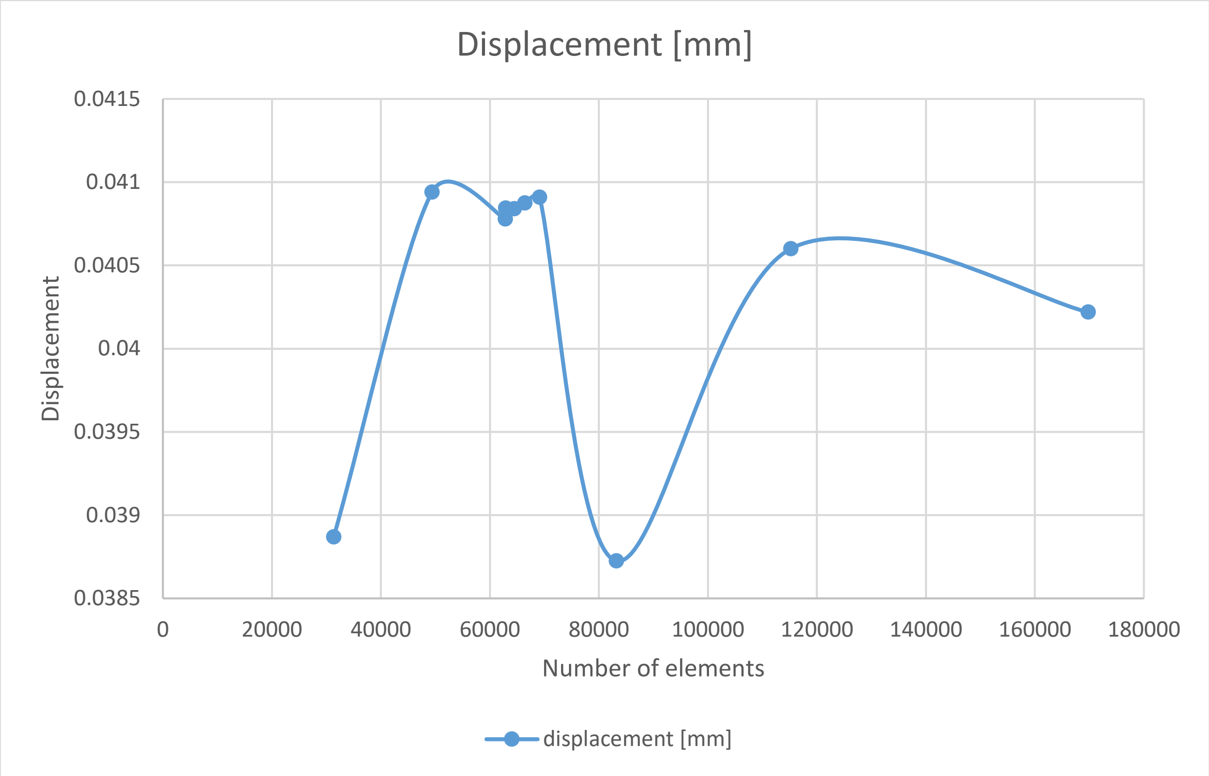
Displacement [mm]
0.0415
0.041
0.0405
0.04
0.0395
0.039
0.0385
Displacement
0
20000
40000
60000
80000
100000
120000
140000
160000
180000
Number of elements
displacement [mm]

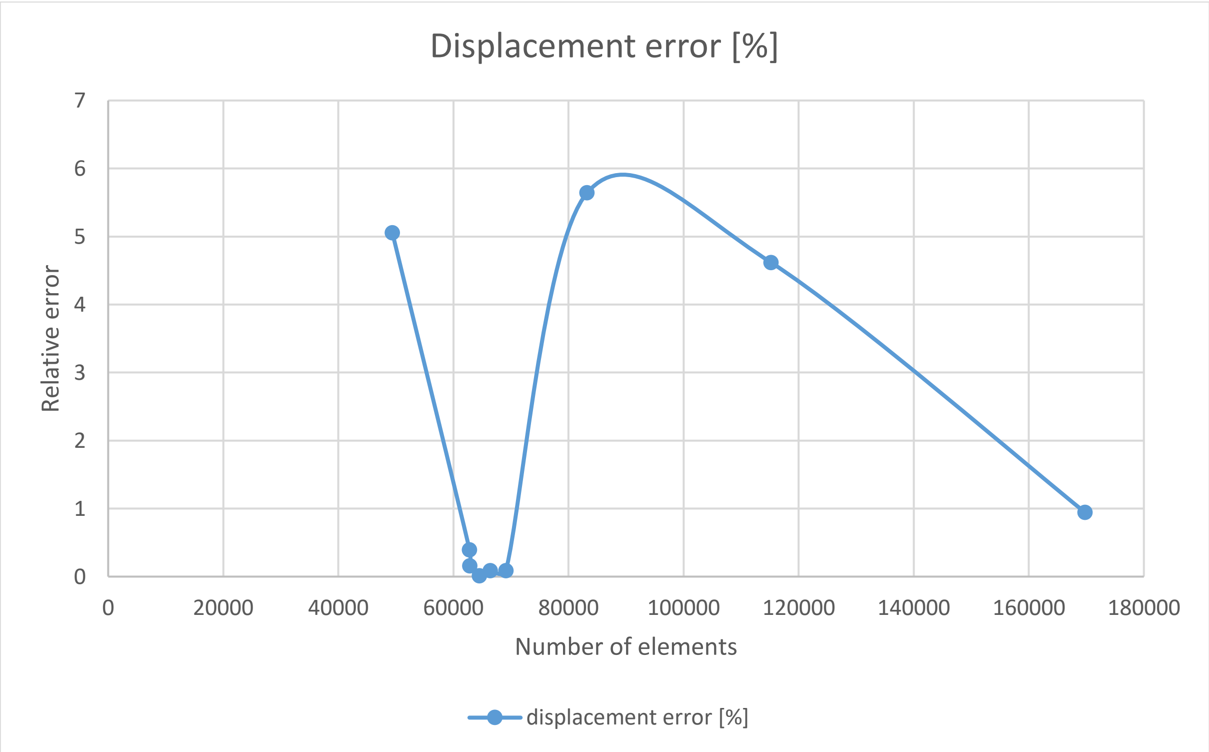
Displacement error [%]
7
6
5
4
3
2
1
0
Relative error
0
20000
40000
60000
80000
100000
120000
140000
160000
180000
Number of elements
displacement error [%]

Appendix A.9 – Saddle Post Connector MSC Nastran/Patran Mesh Convergence – Option 3: Interrupted Design 7075 Aluminium and 304 Stainless Steel

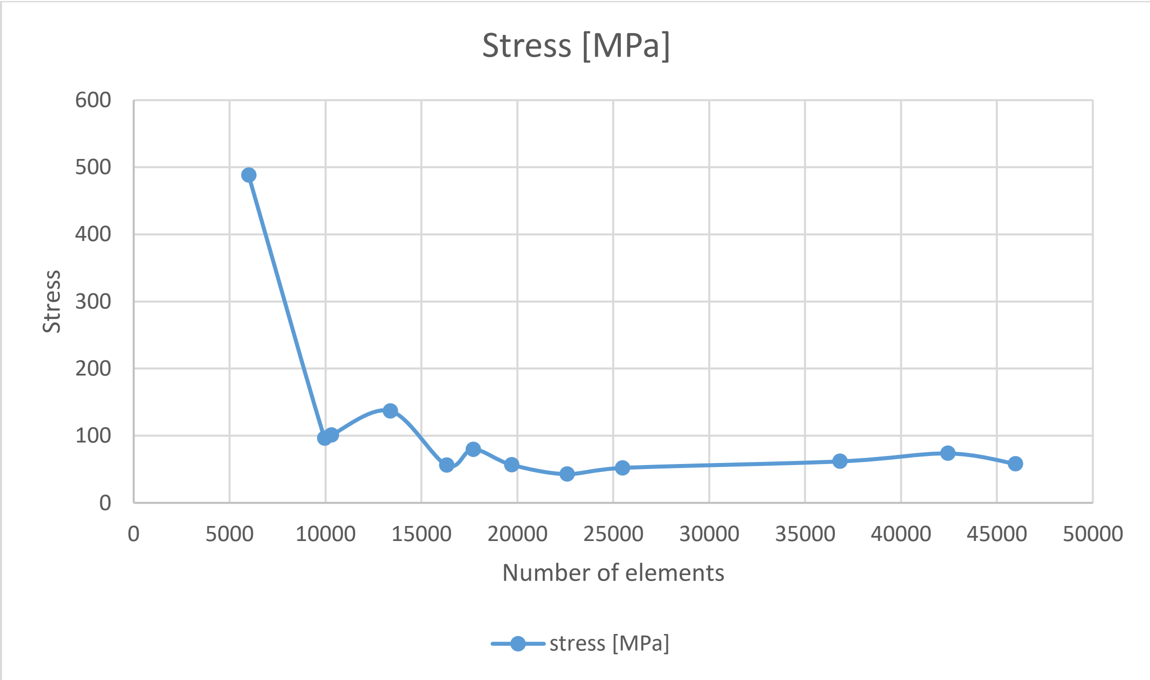

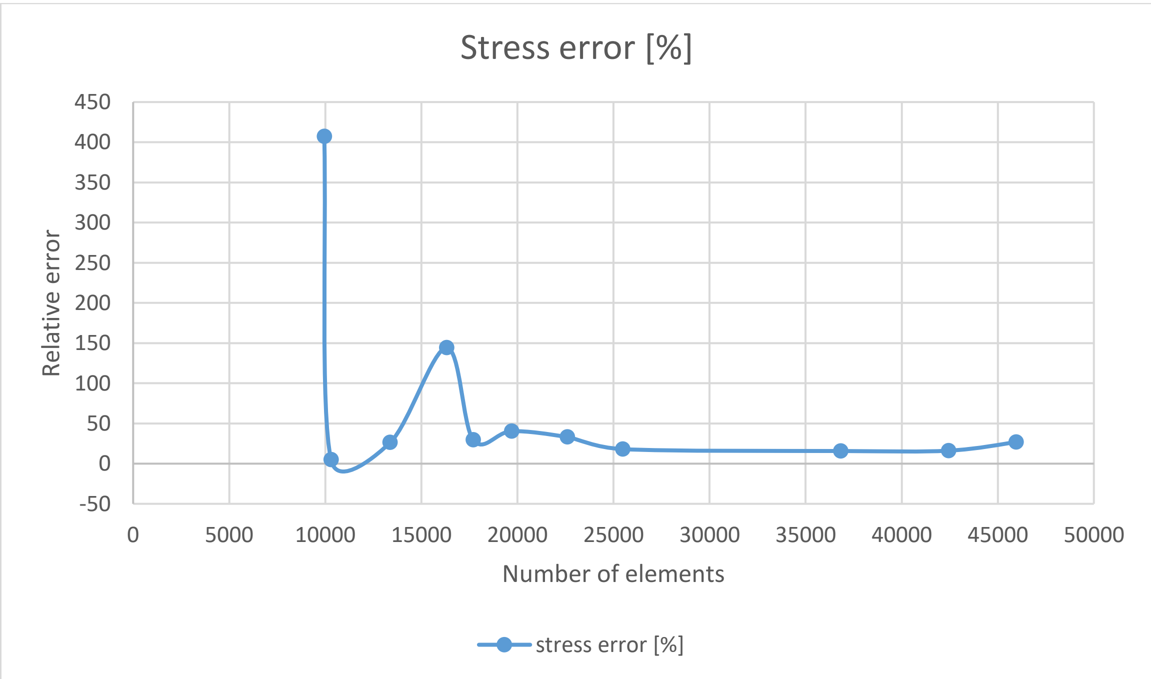

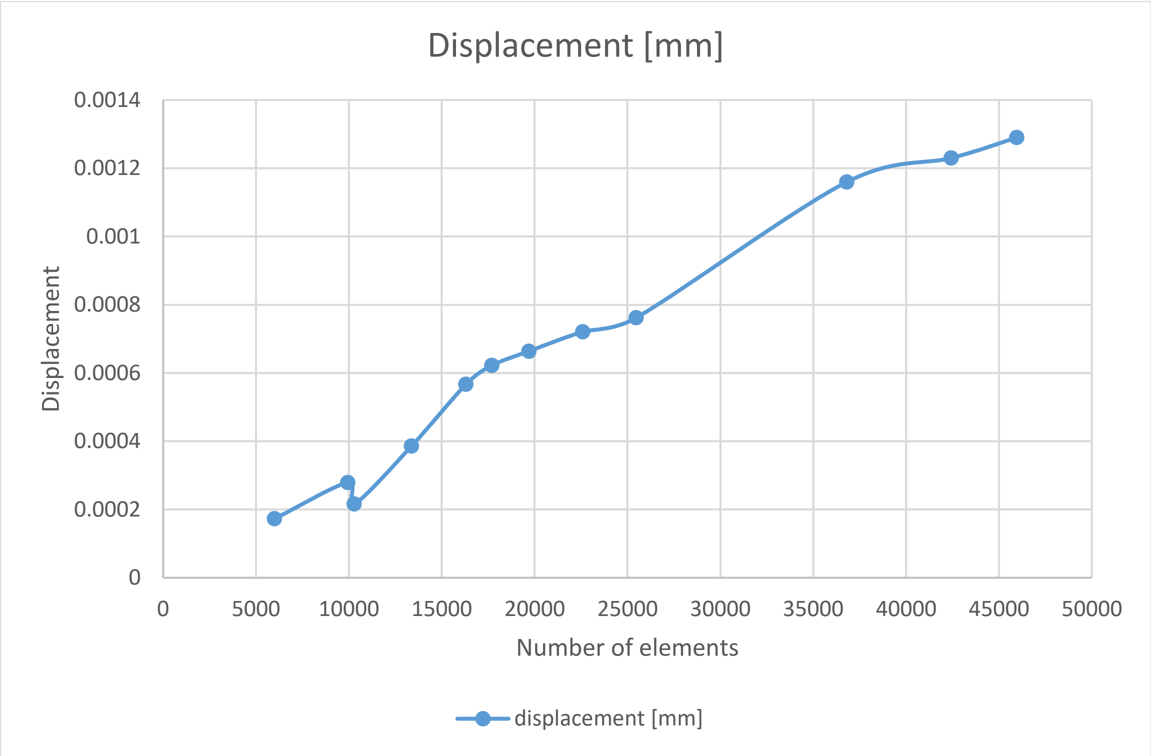
Displacement [mm]
0.0014
0.0012
0.001
0.0008
0.0006
0.0004
0.0002
0
Displacement
0
5000
10000
15000
20000
25000
30000
35000
40000
45000
50000
Number of elements
displacement [mm]

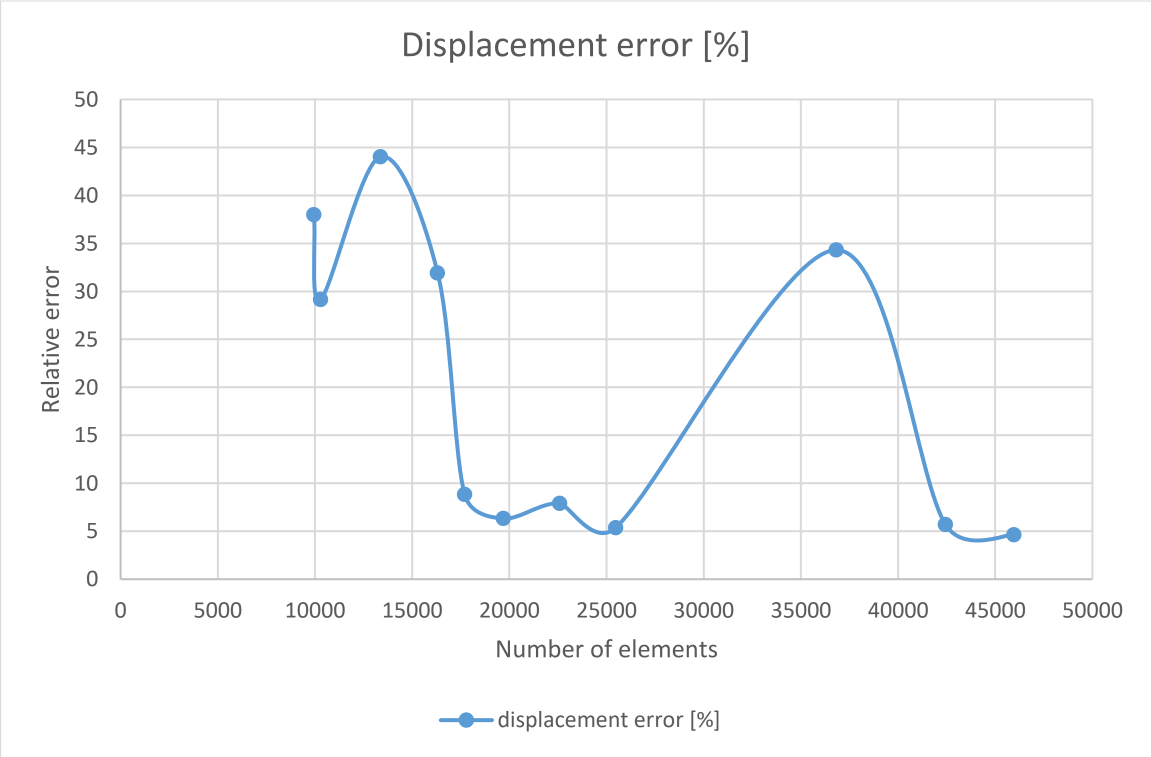
Displacement error [%]
50
45
40
35
30
25
20
15
10
5
0
Relative error
0
5000
10000
15000
20000
25000
30000
35000
40000
45000
50000
Number of elements
displacement error [%]

Appendix A.10 – Saddle Loadcell Datasheet

Certificate

Produt: LOAD CELL   Precision: 0.02%F.S

Model: 3138-100kg   Inspection Date: April05.2016

No: 1525

Specifications

Rated Output	mv/v	3.0020
Non-linearity	%F.S	0.014
Hysteresis	%F.S	0.010
Repeatability	%F.S	0.012
Creep	%F.S/30min	0.017
Temp.effect on zero	%F.S/10℃	0.019
Temp.effect on span	%F.S/10℃	0.018
Zero balance	%F.S	±1
Input impedance	Ω	350±5
Output impedance	Ω	350±5
Insulation resistance	MΩ	≥5000(50VDC)
Recommended excitation voltage	VDC	9~12
Allowed excitation voltage	VDC	5~18
Compensated temp.Range	℃	-10℃~+40℃
Operating temp.Range	℃	-20℃~+55℃
Safe overload	%F.S	120
Ultimate Overload	%F.S	150
Connection	Excitation: ☑red:+ ☑black:– ☐yellow:–	
	Signal: ☑green:+ ☐blue:+ ☑white:–	
Q.C:	Checker:	

Appendix A.11 – Loadcell Calibration

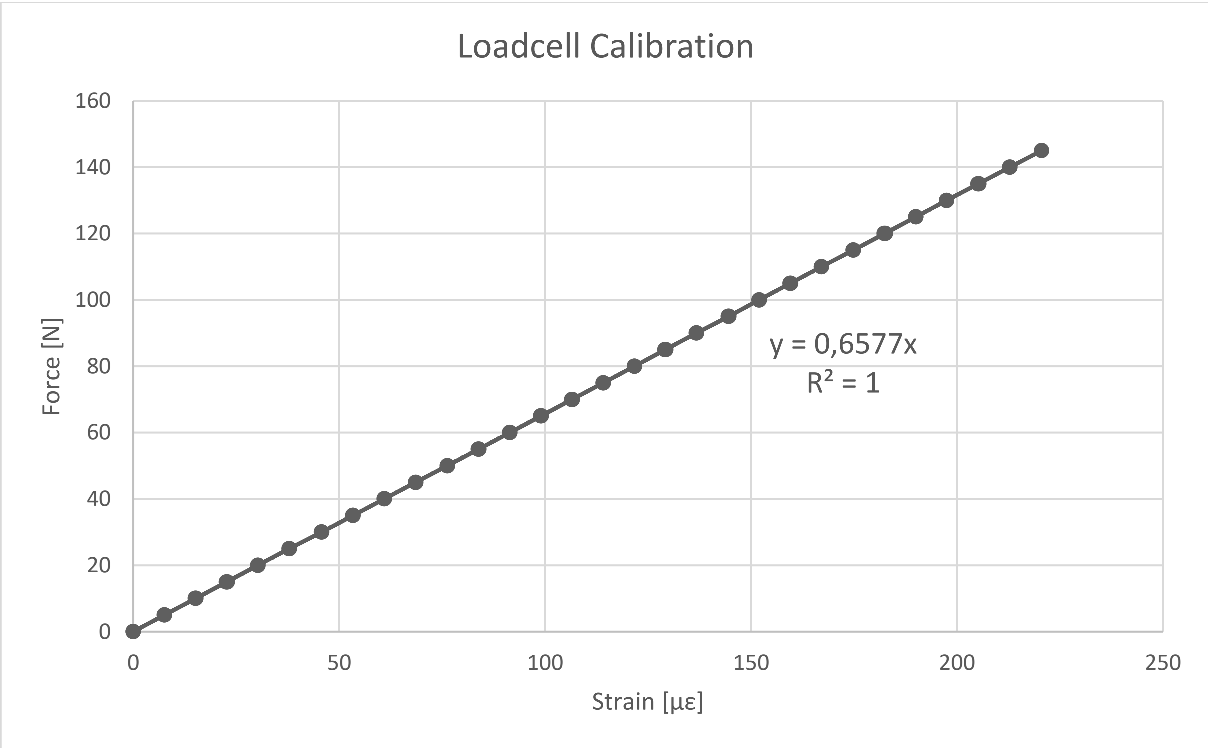

Appendix B – Instrumented Handlebar Device

Appendix B.1 – Strain Gauges Application Zone

$$\sigma = \frac{M_f \cdot y_{max}}{I}$$

$$\sigma = E \cdot \varepsilon$$

same material (E = const.)

$$\therefore \uparrow \sigma = \uparrow \varepsilon$$

$$I_0 = \frac{\pi r^4}{4}$$

Case 1:

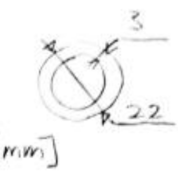

$$M_f = F \times 200 \text{ [mm]}$$

$$I_{Total} = I_O - I_o$$

$$= 11\,499{,}01 - 3216{,}99$$

$$= 8\,282{,}02 \text{ mm}^4$$

$$\sigma = \frac{F \times 200 \times 11}{8\,282{,}02} \Leftrightarrow \sigma = F \cdot 0{,}2656$$

Case 2:

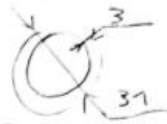

$$M_f = F \times 300 \text{ [mm]}$$

$$I = 45\,333{,}23 - 19\,174{,}76$$

$$= 26\,158{,}47 \text{ mm}^4$$

$$\sigma = \frac{F \times 300 \times 15{,}5}{26\,158{,}47} \Leftrightarrow \sigma = F \cdot 0{,}1778$$

So, with the same force (F), the handlebar suffer higher tension (σ) in the location case 1. Higher tension (σ) means higher deformation (ε) too.

Appendix B.2 – Strain Gauges Datasheet

HBM

Dehnungsmessstreifen
Strain gages
Jauges d'extensométrie

Bestellnummer / Order No / No. de référence	1-LY13-3/350
Typ / Type / Type	3/350 LY13
Widerstand / Resistance / Résistance	350 Ω ±0.35 %
Stückzahl / Contents / Quantité	10
k-Faktor / Gage factor / Facteur k	2.06 ±1.0 %
Temperaturkoeffizient des k-Faktors / Temperature coefficient of gage factor / Coefficient de température du facteur k	101 ±10 [10^{-6} / K] (-10°C ... +45°C)
Querempfindlichkeit / Transverse sensitivity / Sensibilité transverse	-0.8 %
Folienlos / Foil lot / Lot de la feuille	A409/10
Herstellungslos / Production batch / Lot de fabrication	812083438
Temperaturkompensation: Aluminium mit / Temperature compensation: aluminium with / Compensation de température: aluminium avec	α = 23.0 [10^{-6} / K]
Max. effekt. Brückenspeisespannung / max. rms bridge excitation voltage / tension d'alim. de pont maxi eff.	14.5 V

Daten / Data / Données

RoHS

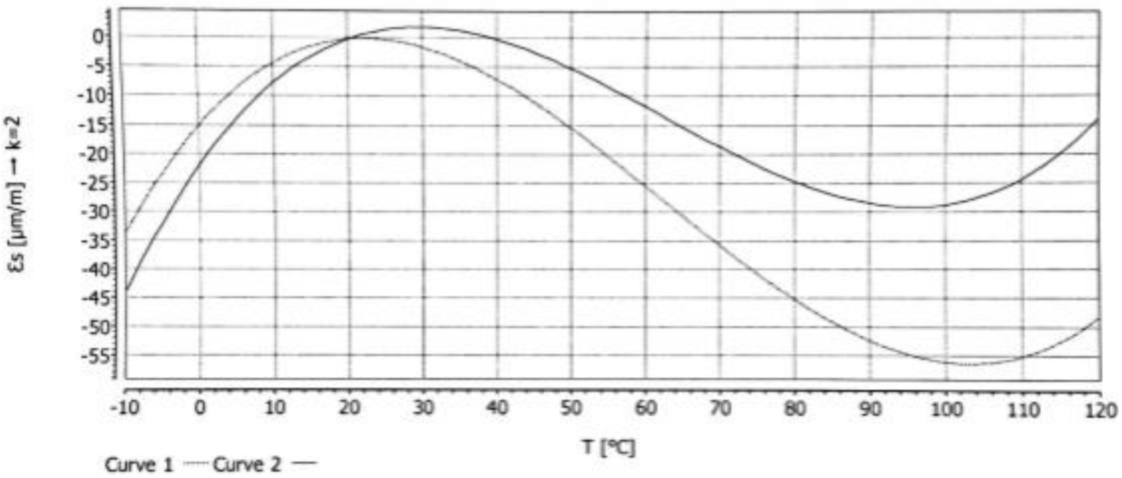

$$\varepsilon_S(T) = -15.13 + 1.45 \cdot T - 3.97E\text{-}02 \cdot T^2 + 2.11E\text{-}04 \cdot T^3 \pm (T-20) \cdot 0.30\ [\mu m/m] + 0.01140 \cdot L \cdot (T-20)\ [\mu m/m]$$

Alle technischen Daten nach VDI/VDE 2635. Geben Sie bei Rückfragen bitte Bestellnummer und Herstellungslos an.

All specifications in accordance with VDI/VDE 2635. In case of further inquiries please indicate order no. and production batch number.

Toutes les caractéristiques techniques selon la norme VDI/VDE 2635. Dans toutes communications, prière d'indiquer le numéro de commande et le numéro du lot de production.

Temperaturgang der Dehnungsmessstreifen bei Applikationen mit oben angegebenen Wärmeausdehnungskoeffizienten α. Gemessen bei kontinuierlicher Temperaturänderung.

Kennlinie 1: DMS ohne Anschlussbändchen.

Kennlinie 2: DMS mit Anschlussbändchen (30mm einfache Bändchenlänge). Bei gekürzten Bändchen liegt der Temperaturgang zwischen Kennlinie 1 und 2. Die numerische Darstellung erlaubt, den Temperaturgang für jede Bändchenlänge exakt zu errechnen.
T = Temperatur in °C L = einfache Bändchenlänge in mm (dimensionslos)

Réponse en température des jauges d'extensométrie appliquées sur des matériaux dont des coefficients de dilatation termique α sont indiqués. Mesurée à variation continue de la température.

Courbe 1: Jauges sans pattes de raccordement.

Courbe 2: Jauges avec pattes de raccordement (longueur unitaire de la patte de 30 mm). Lorsque les pattes sont plus courtes, la réponse en température se trouvera entre les deux courbes 1 et 2. La représentation numérique permet de calculer exactement la réponse en température pour chaque longueur de patte.
T = température en °C L = longueur unitaire de la patte en mm (sans dimension)

The temperature response refers to strain gages bonded to materials with specified coefficients of thermal expansion α. Values are measured with continuous temperature variation.

Curve 1: Strain gages without leads.

Curve 2: Strain gages with leads (simple lead length of 30 mm). If the leads are shorter, the temperature response lies between curve 1 and 2. The numeric representation allows exact calculation of the temperature response for any lead length.
T = temperature in °C L = simple lead length in mm (dimensionless)

Kopfdaten / Header / Titre

A point (".") is used as decimal separator in data, the separator needs to be configured accordingly for import into Excel.

Appendix C – Instrumented Pedals Device

Appendix C.1 – Foot Interface Solidworks Solid Mesh Convergence

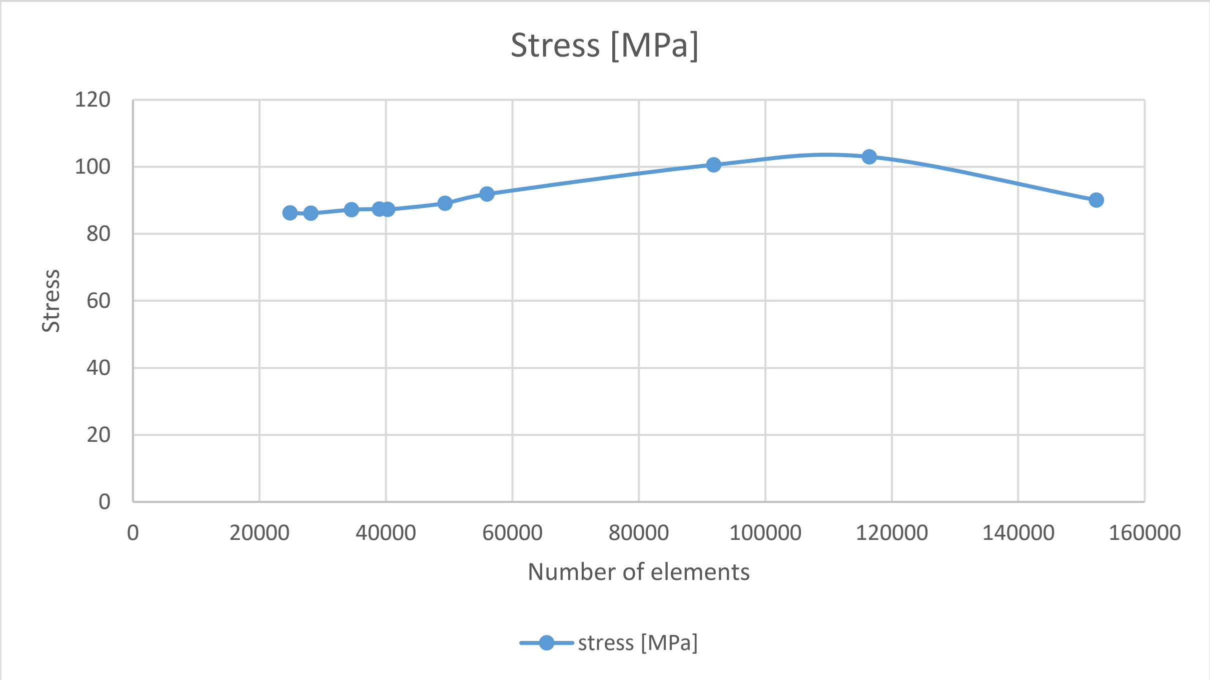

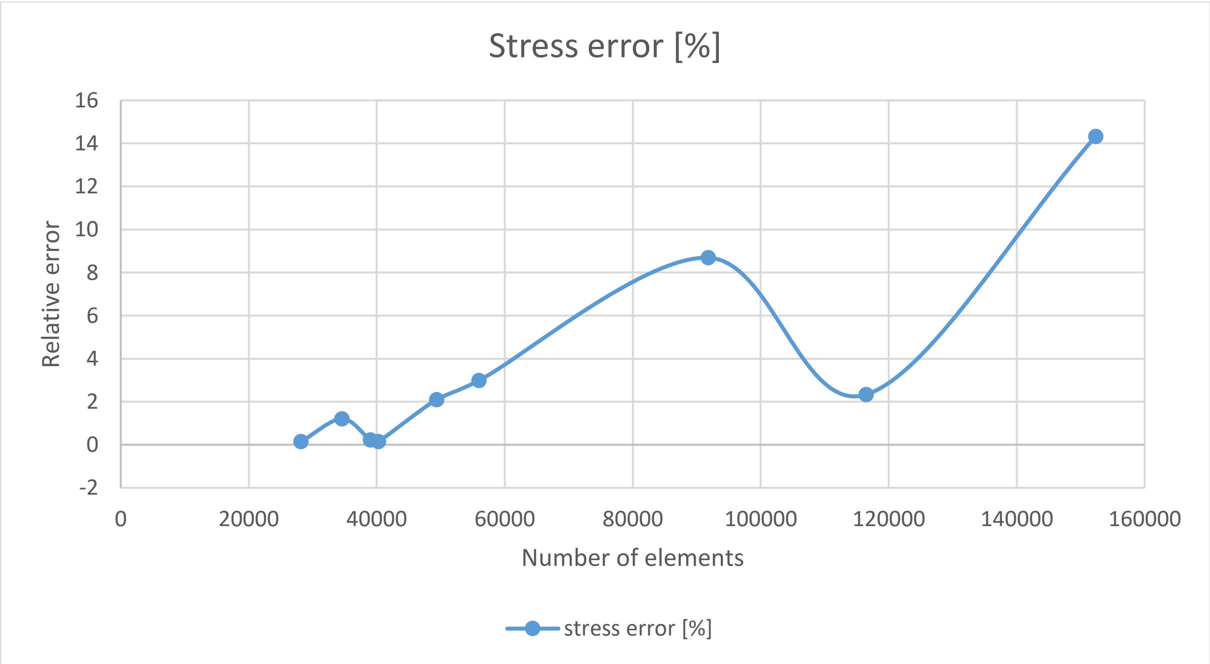

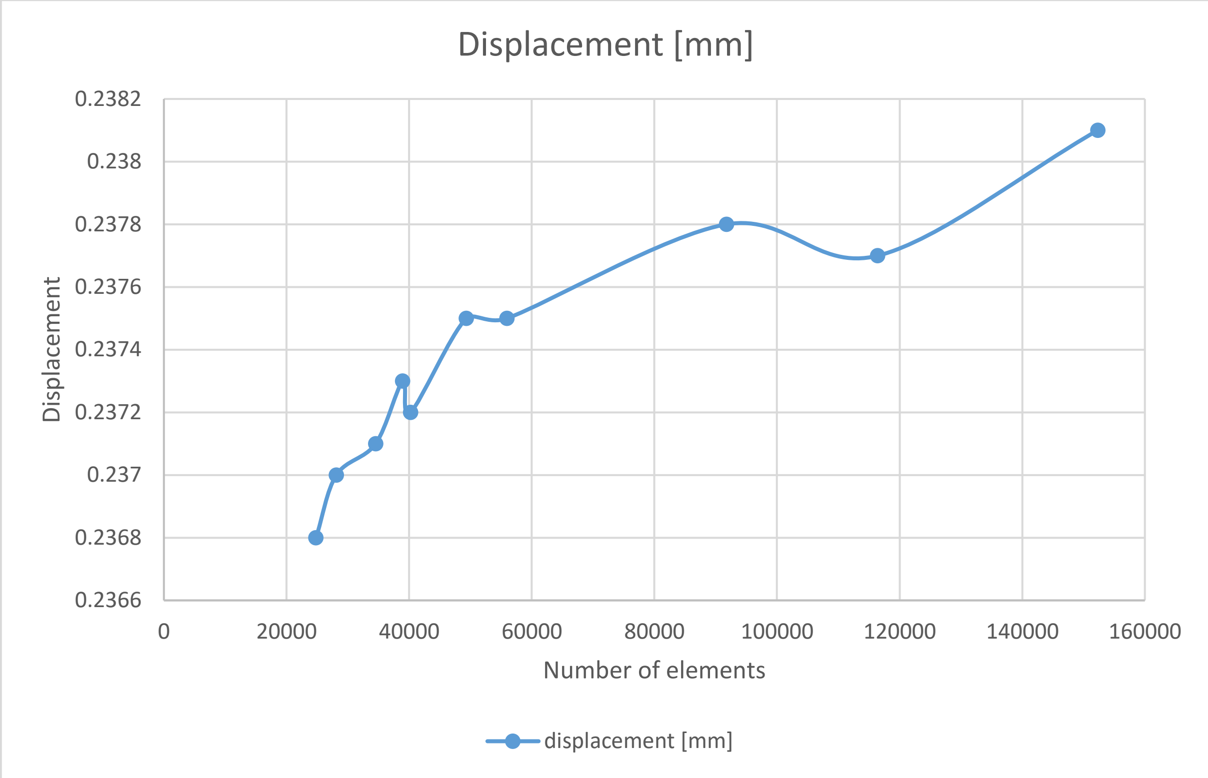

Displacement [mm]
0.2382
0.238
0.2378
0.2376
0.2374
0.2372
0.237
0.2368
0.2366
Displacement
0
20000
40000
60000
80000
100000
120000
140000
160000
Number of elements
displacement [mm]

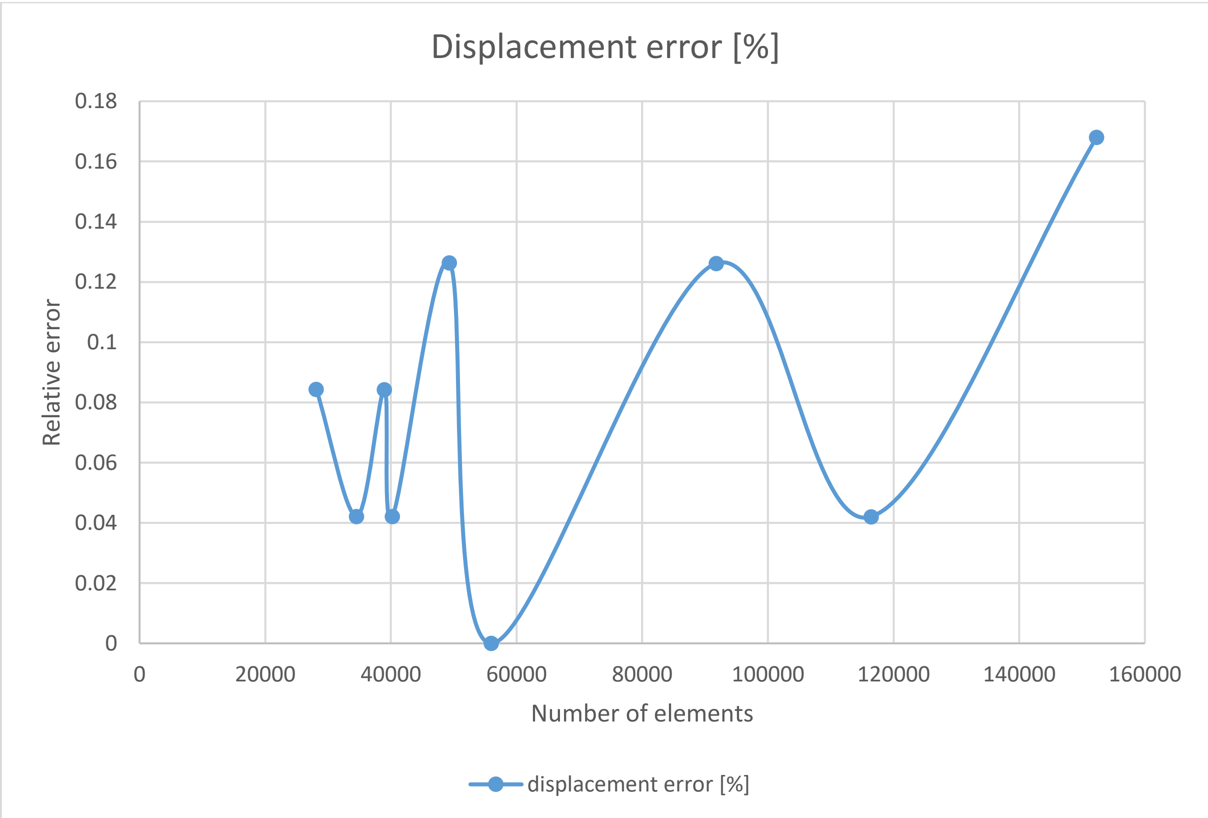

Displacement error [%]
0.18
0.16
0.14
0.12
0.1
0.08
0.06
0.04
0.02
0
Relative error
0
20000
40000
60000
80000
100000
120000
140000
160000
Number of elements
displacement error [%]

Appendix C.2 – Cleat Interface Solidworks Solid Mesh Convergence

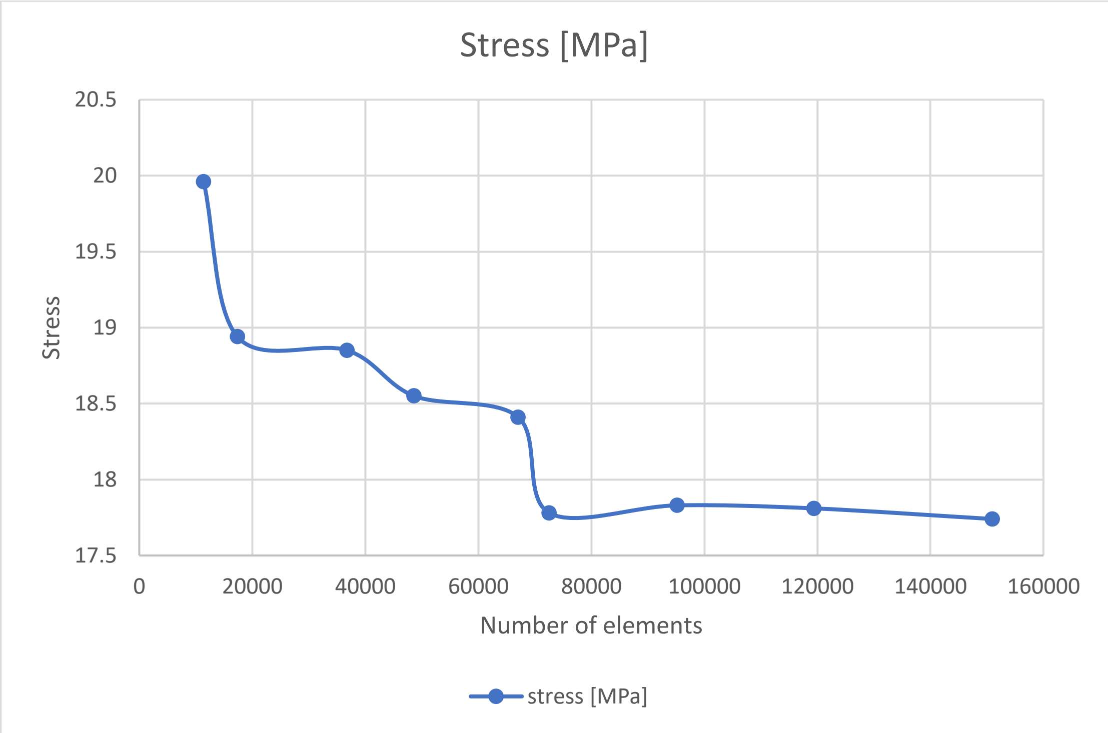

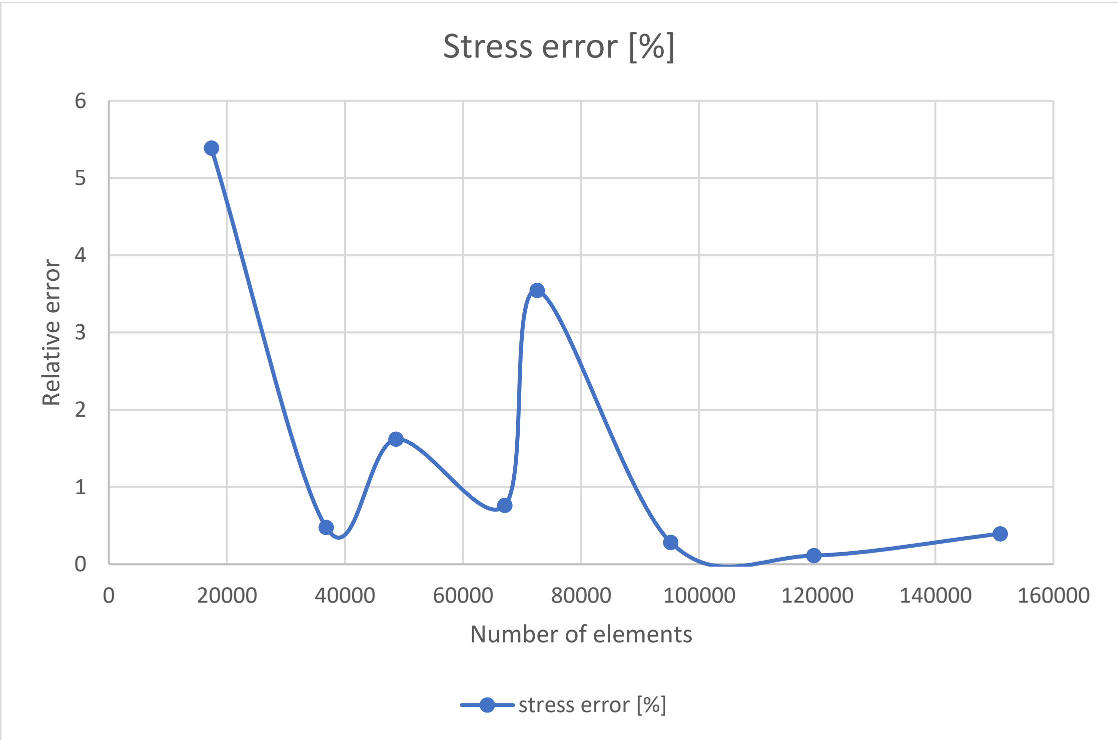

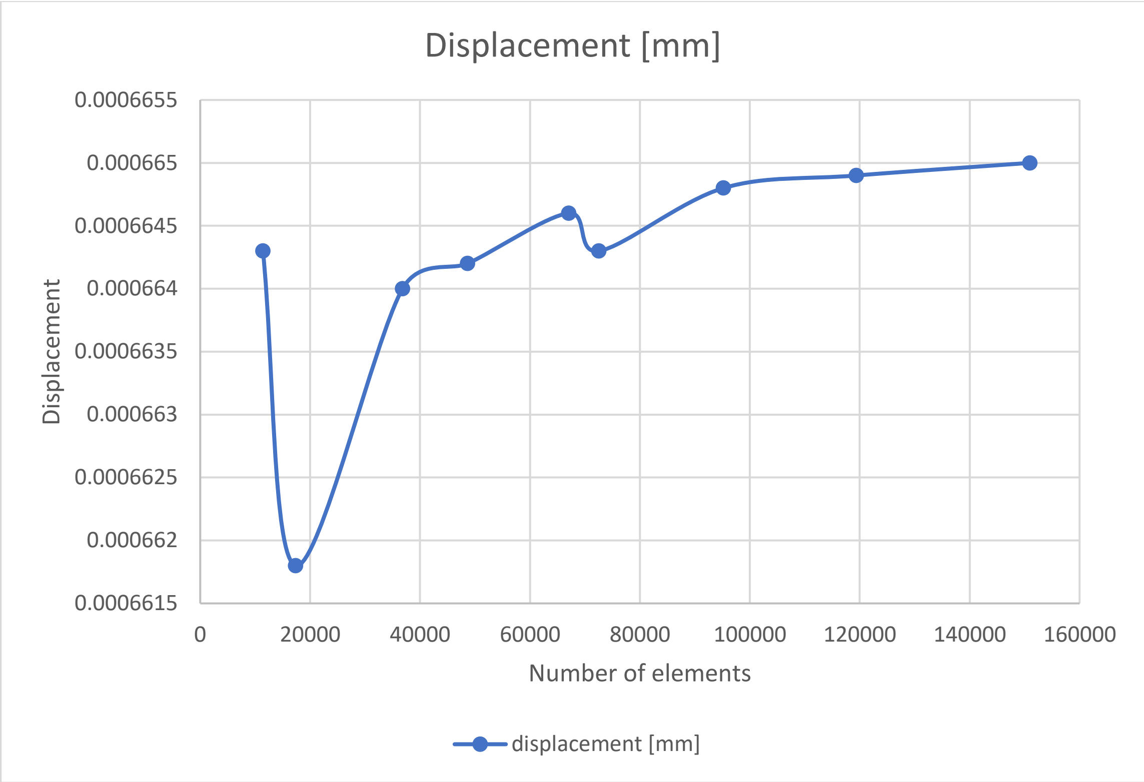
Displacement [mm]
0.0006655
0.000665
0.0006645
0.000664
0.0006635
0.000663
0.0006625
0.000662
0.0006615
Displacement
0
20000
40000
60000
80000
100000
120000
140000
160000
Number of elements
displacement [mm]

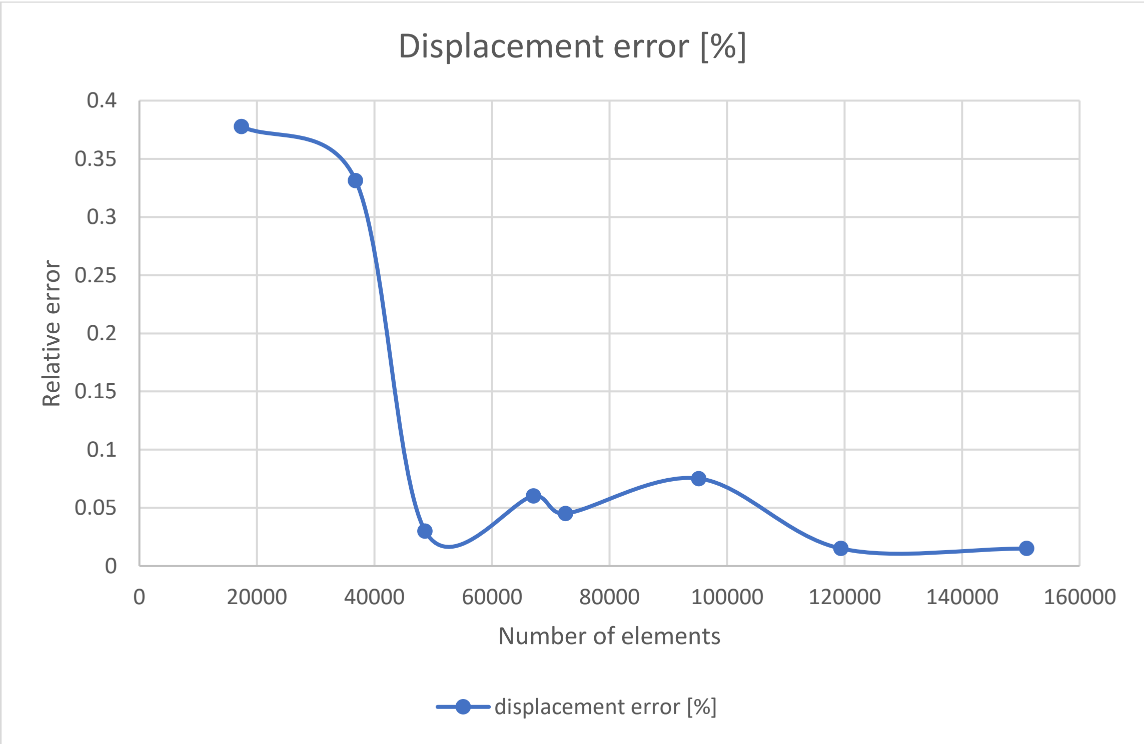
Displacement error [%]
0.4
0.35
0.3
0.25
0.2
0.15
0.1
0.05
0
Relative error
0
20000
40000
60000
80000
100000
120000
140000
160000
Number of elements
displacement error [%]

Appendix C.3 – Foot Interface MSC Nastran/Patran Solid Mesh Convergence

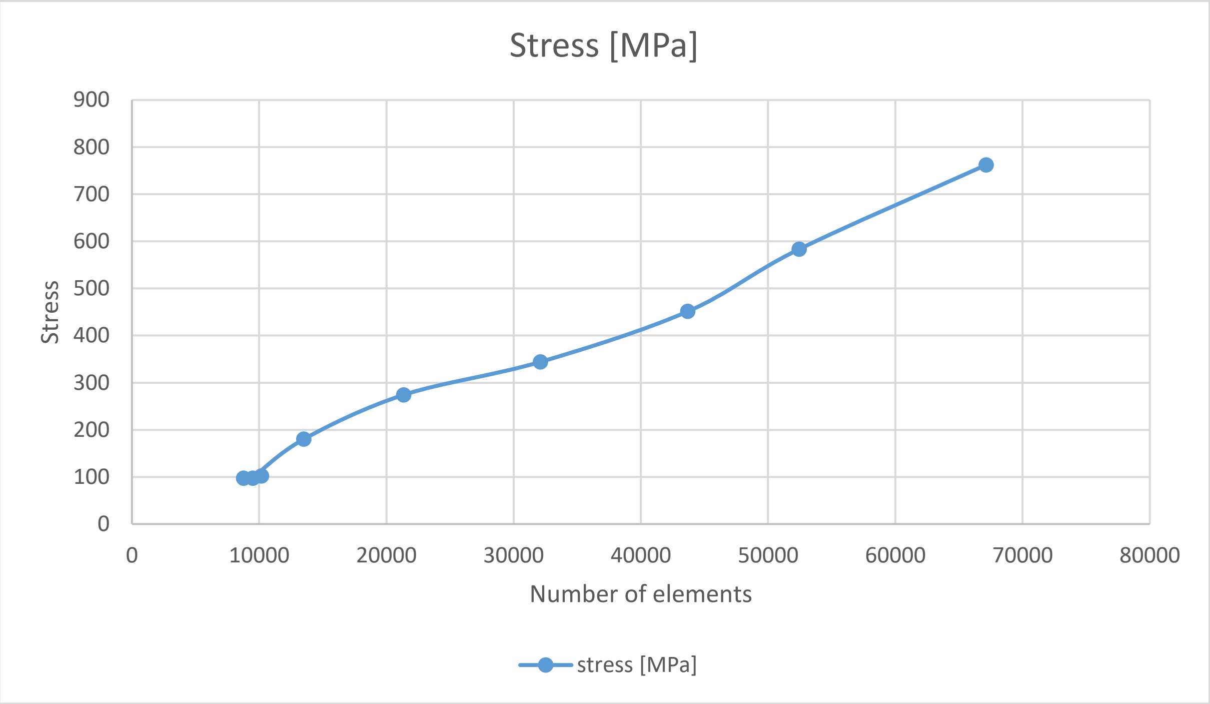

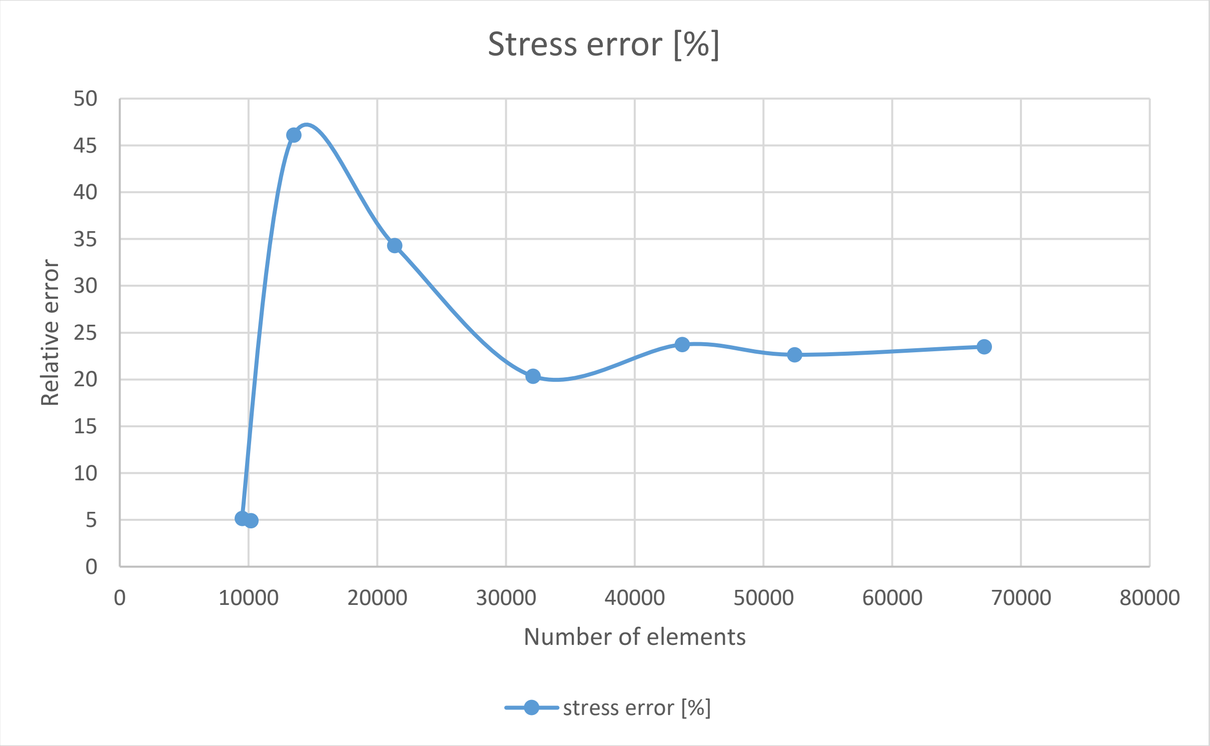

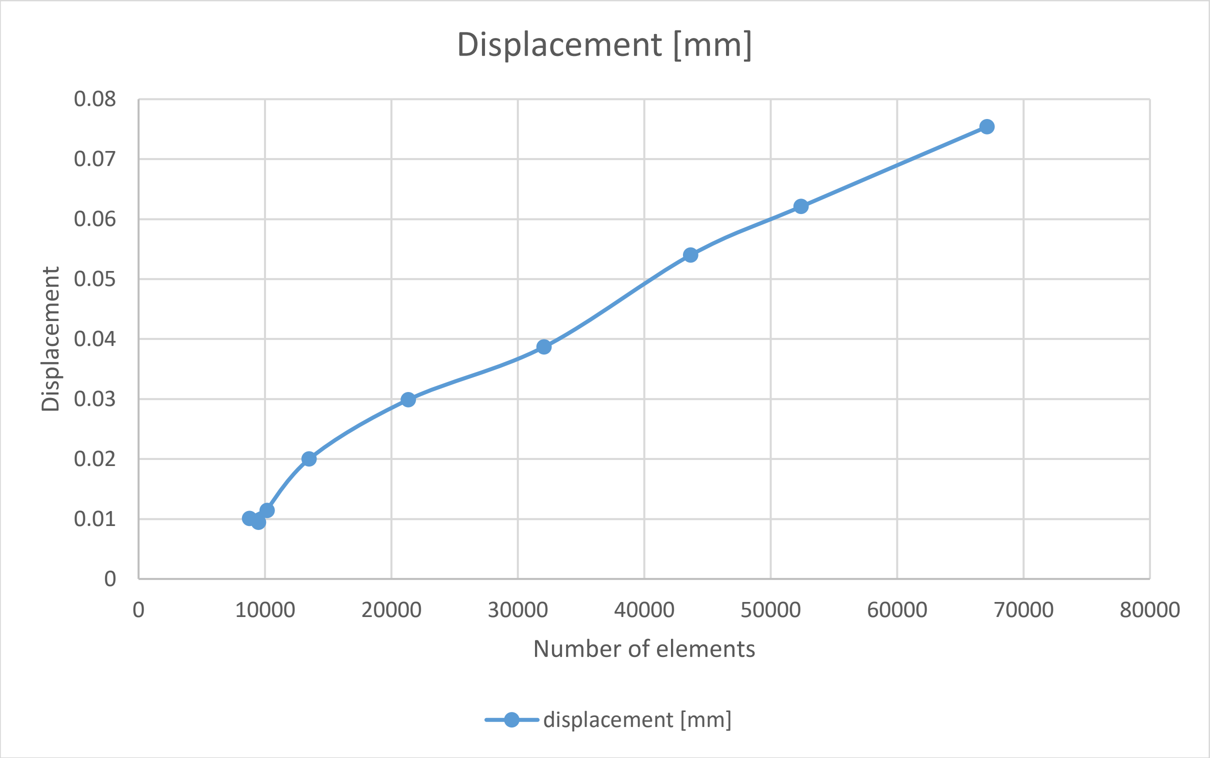
Displacement [mm]
0.08
0.07
0.06
0.05
0.04
0.03
0.02
0.01
0
Displacement
0
10000
20000
30000
40000
50000
60000
70000
80000
Number of elements
displacement [mm]

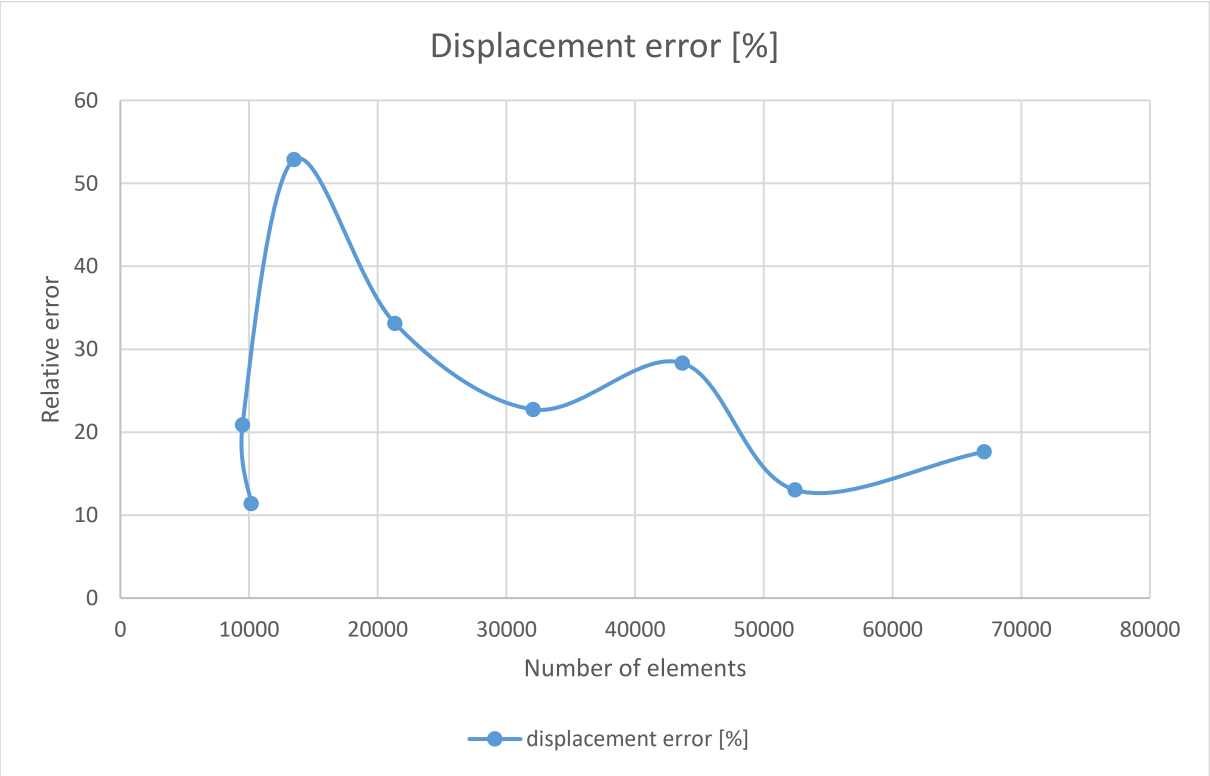
Displacement error [%]
60
50
40
30
20
10
0
Relative error
0
10000
20000
30000
40000
50000
60000
70000
80000
Number of elements
displacement error [%]

Appendix C.4 – Cleat Interface MSC Nastran/Patran Solid Mesh Convergence

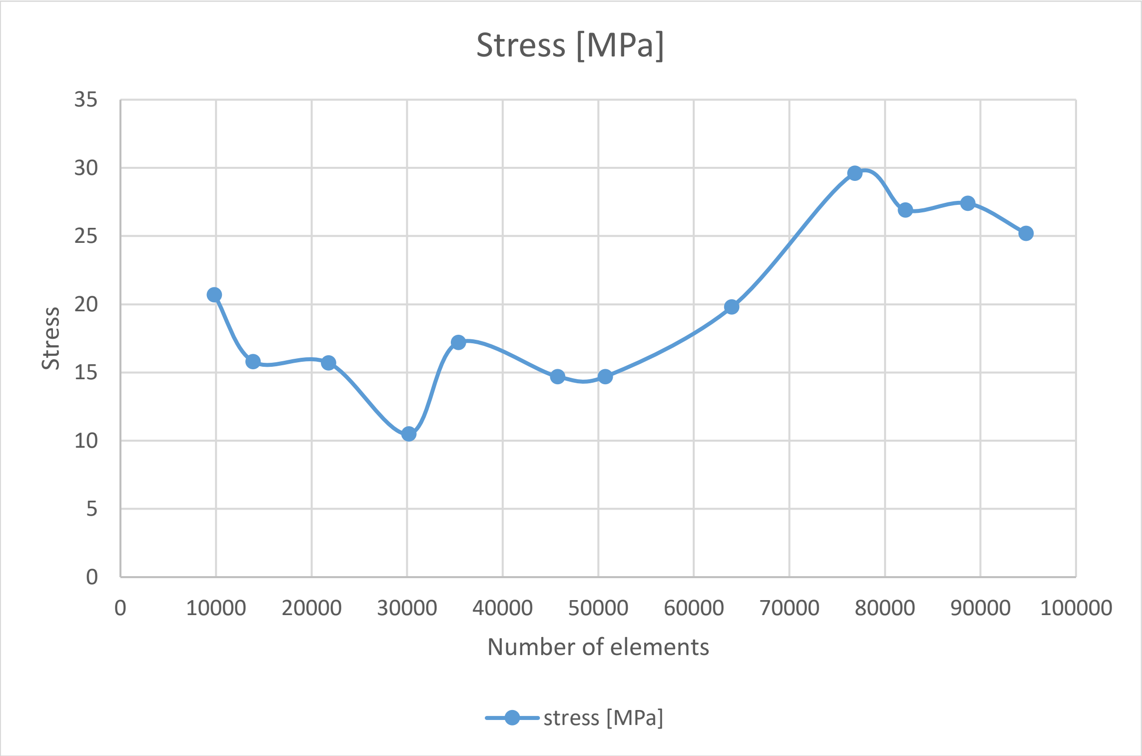

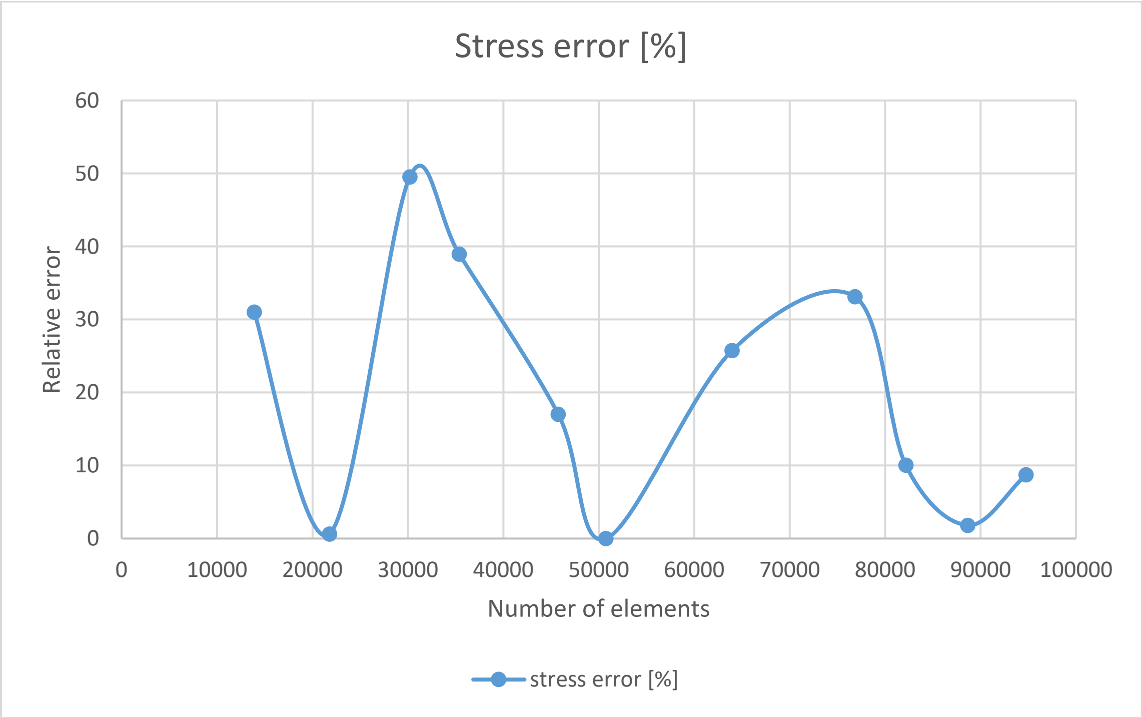

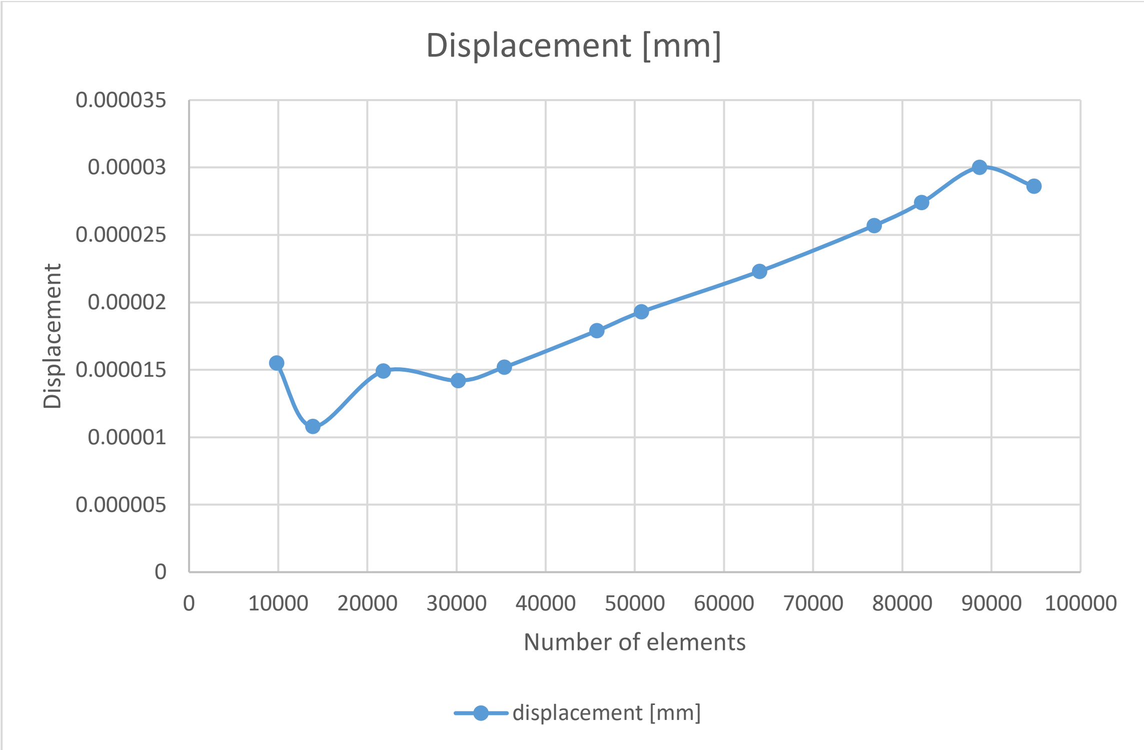
Displacement [mm]
Displacement
0.000035
0.00003
0.000025
0.00002
0.000015
0.00001
0.000005
0
0
10000
20000
30000
40000
50000
60000
70000
80000
90000
100000
Number of elements
displacement [mm]

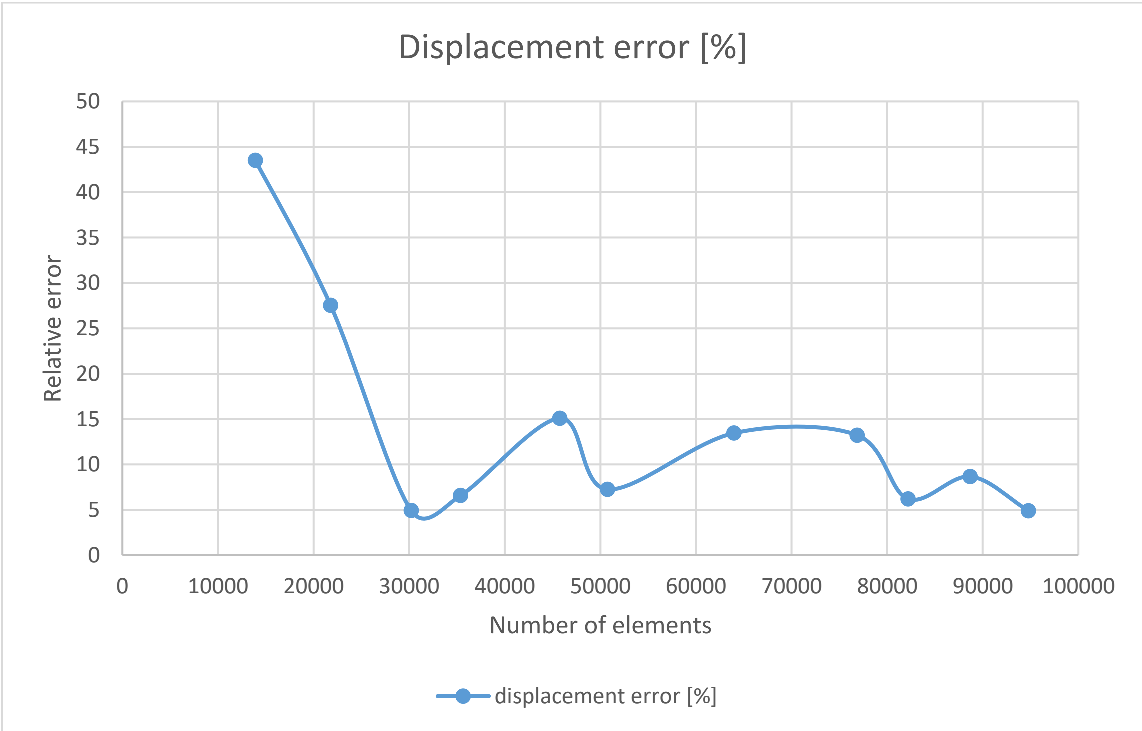
Displacement error [%]
Relative error
50
45
40
35
30
25
20
15
10
5
0
0
10000
20000
30000
40000
50000
60000
70000
80000
90000
100000
Number of elements
displacement error [%]

Appendix C.5 – Pedals Loadcell Datasheet

LOAD CELL CALIBRATION CERTIFICATE

Model: 202WA — Max.Cap.（Emax）: 200lb

Part#: 202WA-200lb — S/N : 1218006094

Output Sensitivity	mV/V/KΩ	0.90000	
Non-linearity	%FS	<0.017	
Hysteresis	%FS	<0.017	
Repeatability	%FS	<0.017	
Zero Balance	μV	±200	
Creep(30min)	%FS/30min	<0.030	
Zero Temp.Coefficient	%FS/10℃	<0.030	
Rated Output Temp.Coefficient	%FS/10℃	<0.010	
Input Resistance	Ω	1204±10	
Output Resistance	Ω	1000±10	
Insulation Resistance	MΩ	≥3000[50VDC]	
Safe Overload	%FS	150	
Minimum Dead Load	lb	0	
Compensated Temp.Range	℃[℉]	-10~+40[14~+104]	
Recommended Supply Voltage	V	5～12(DC/AC)	
4-Core shielded cable 0.27 m	Input	E+: Red	E－: Black
	Output	S+: Green	S－: White
	Shield	Bare	

Appendix C.6 – Loadcell Calibration

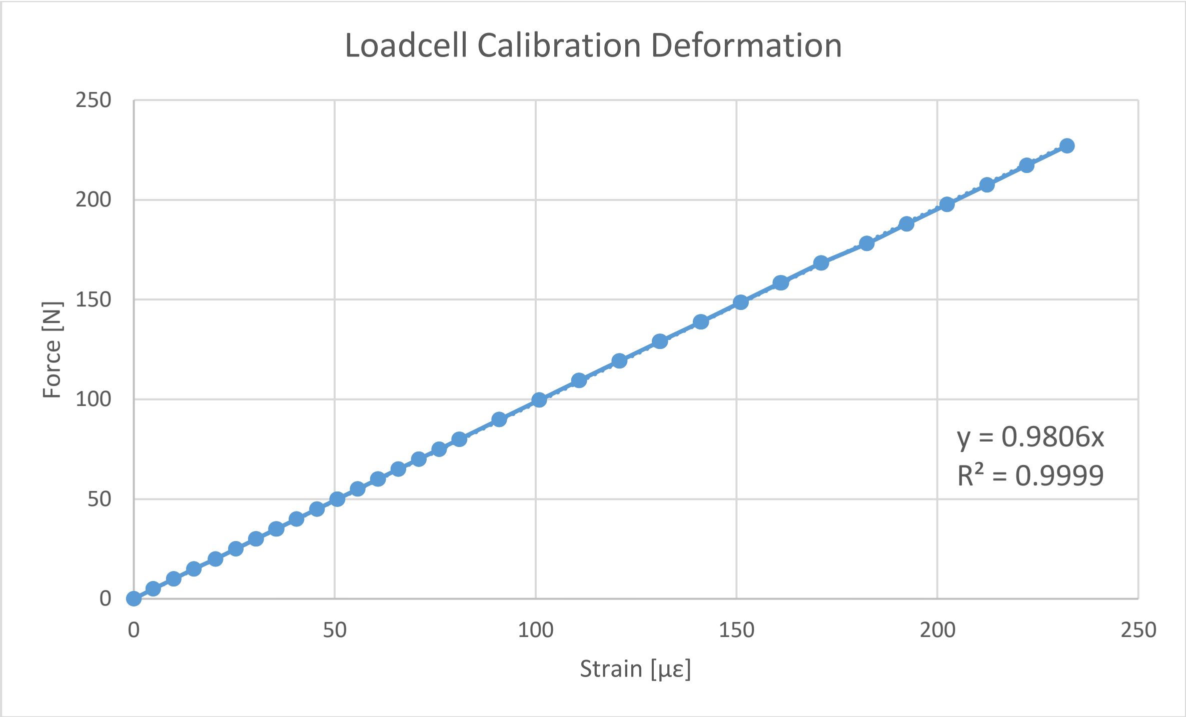

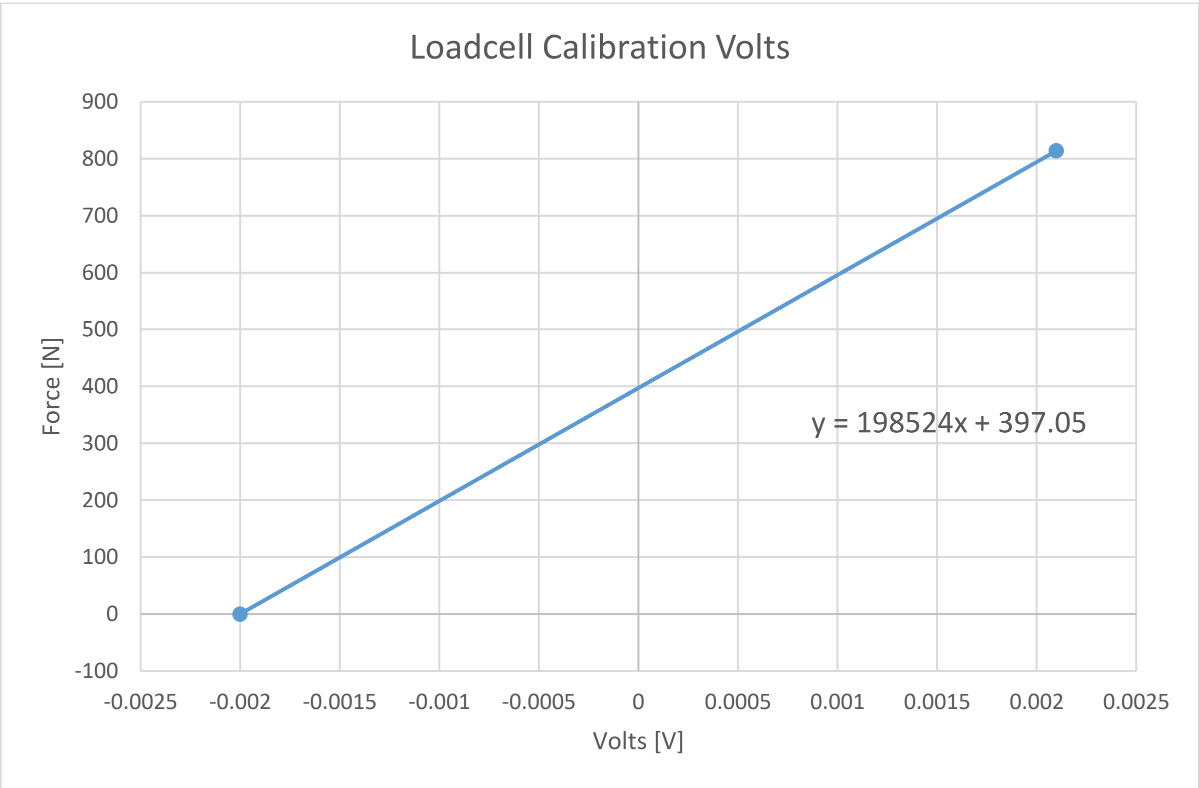

Appendix D – Instrumented Grip Device

Appendix D.1 – Instrumented Rods Dimensioning

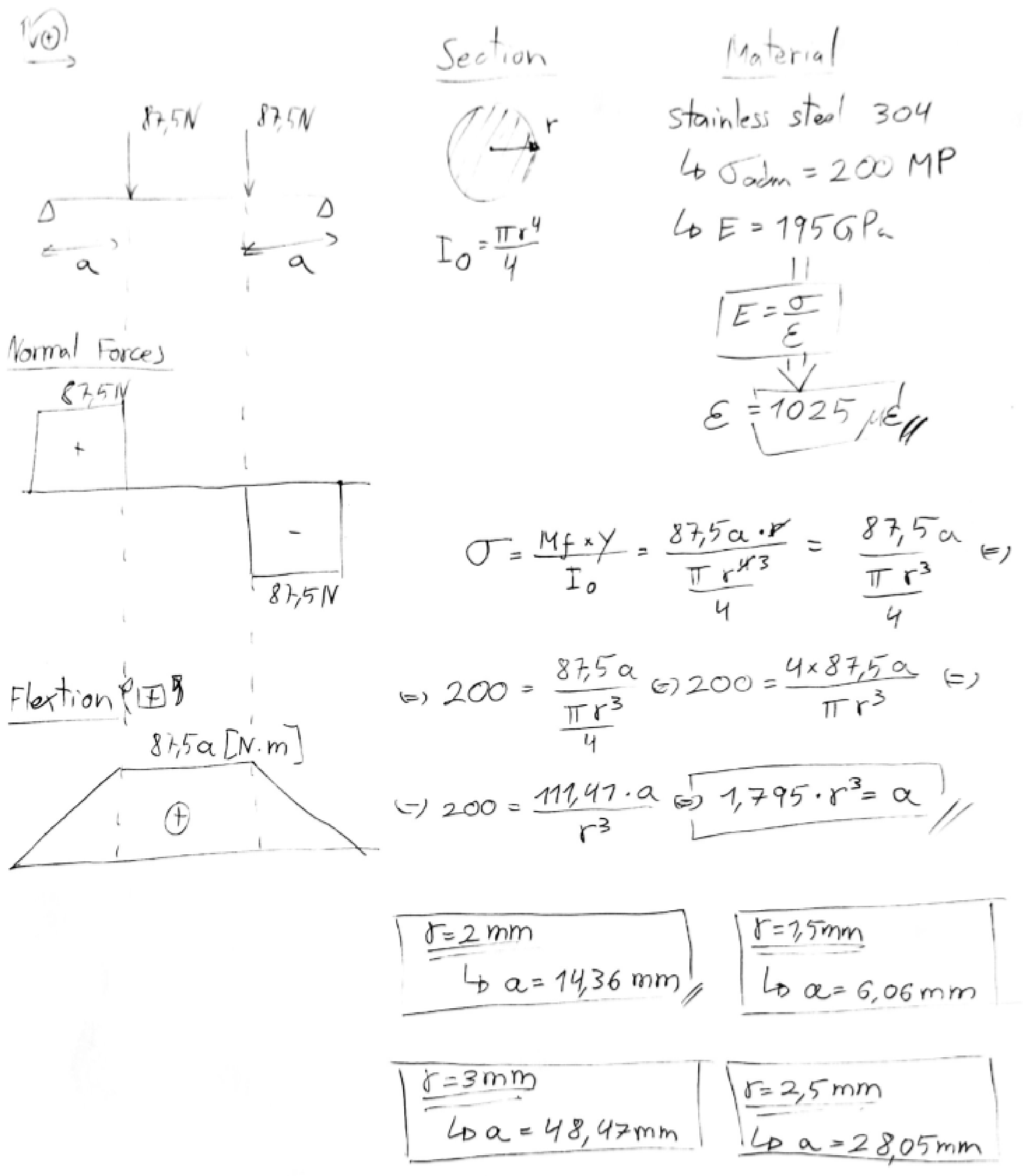

Appendix D.2 – Solidworks Solid Mesh Convergence

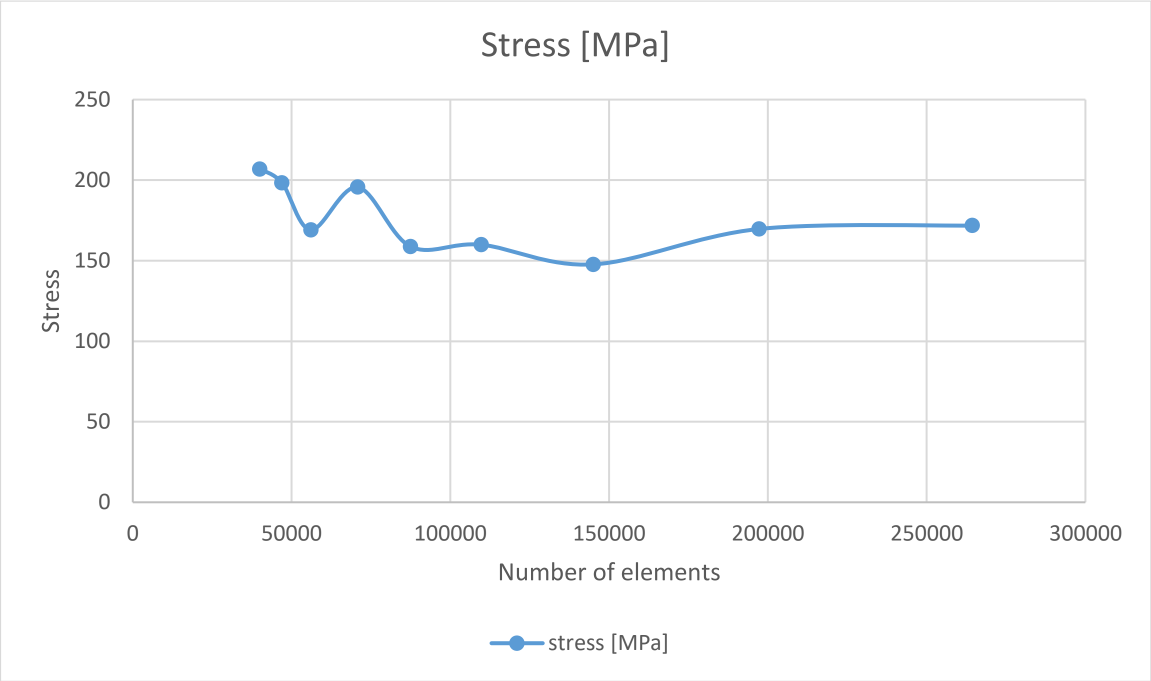

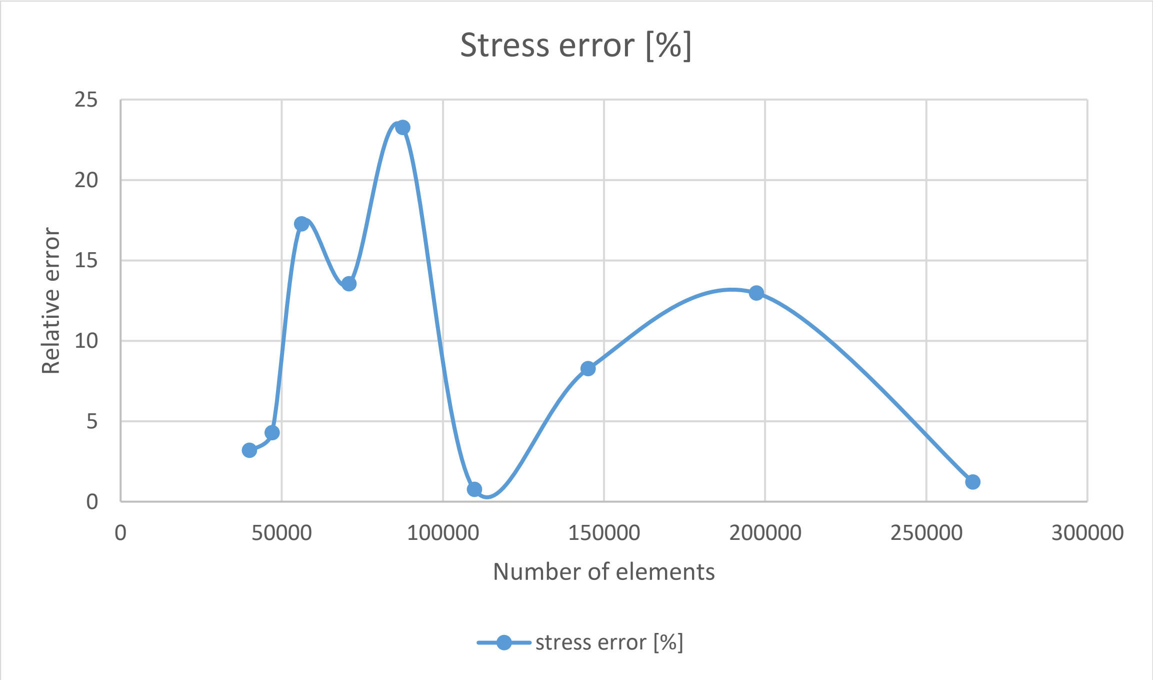

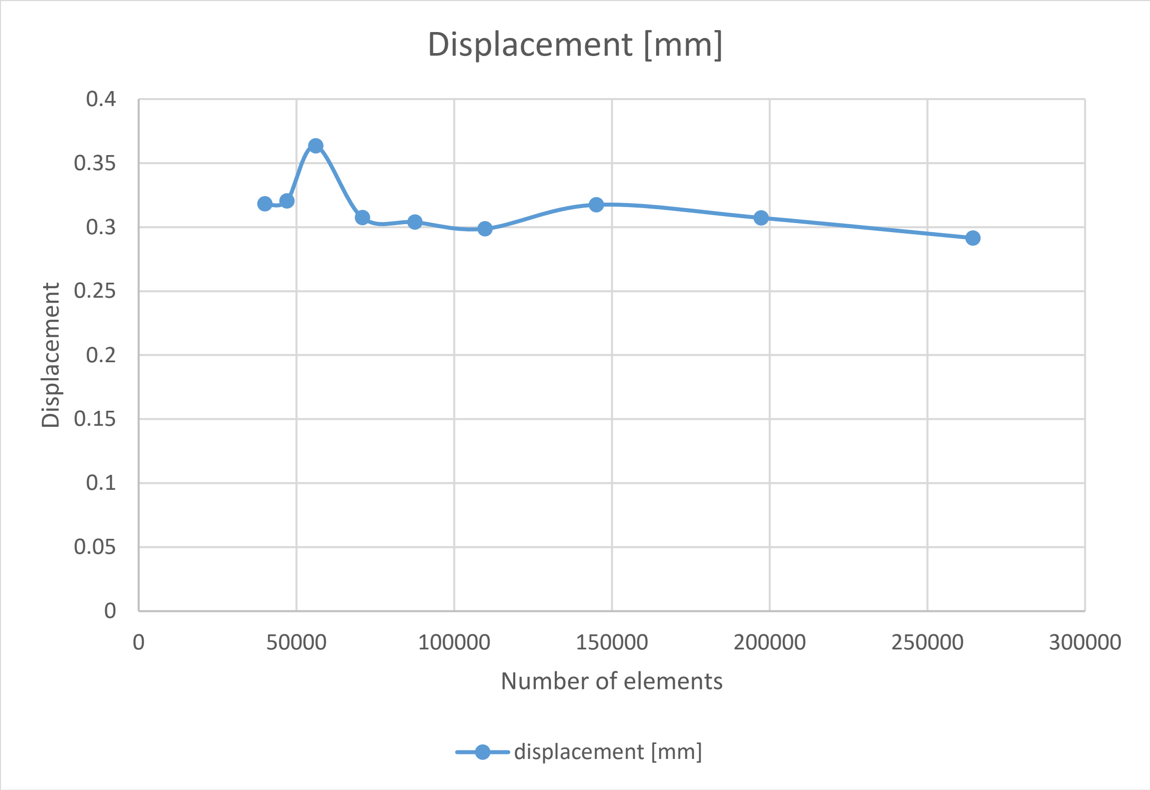

Displacement [mm]
0.4
0.35
0.3
0.25
0.2
0.15
0.1
0.05
0
Displacement
0
50000
100000
150000
200000
250000
300000
Number of elements
displacement [mm]

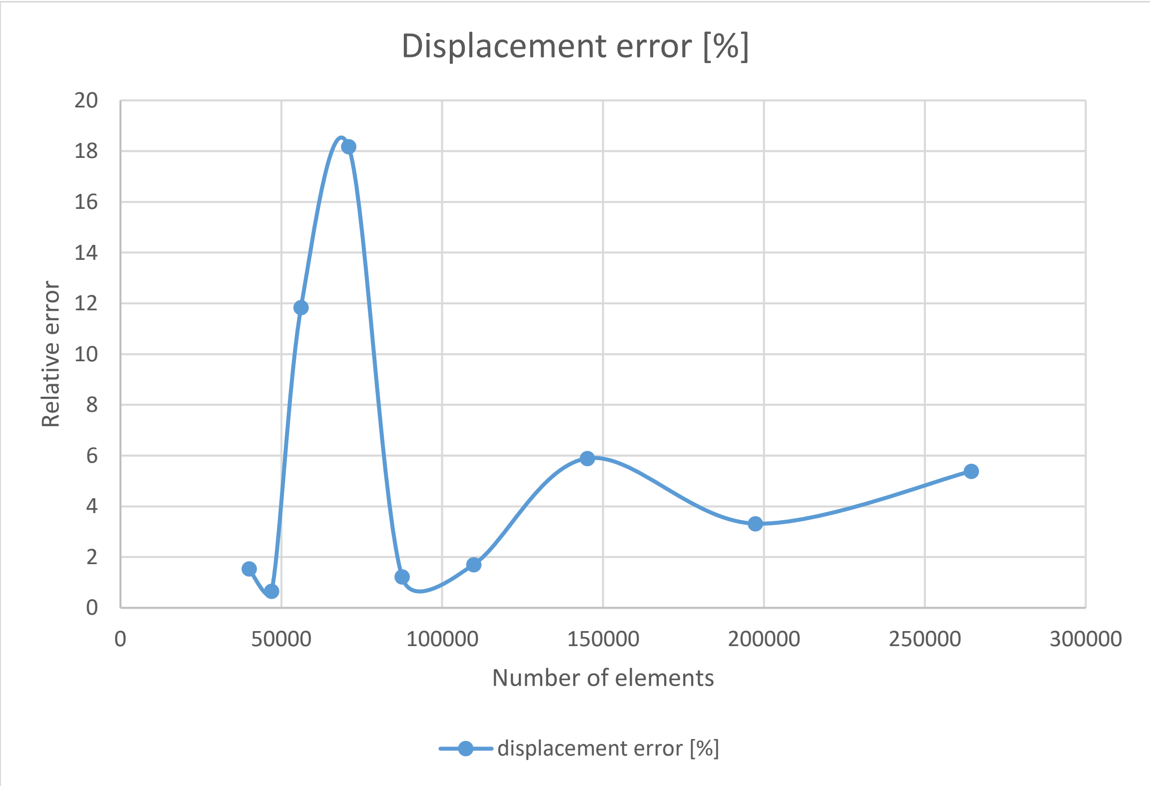

Displacement error [%]
20
18
16
14
12
10
8
6
4
2
0
Relative error
0
50000
100000
150000
200000
250000
300000
Number of elements
displacement error [%]

Appendix D.3 – MSC Nastran/Patran Solid Mesh Convergence

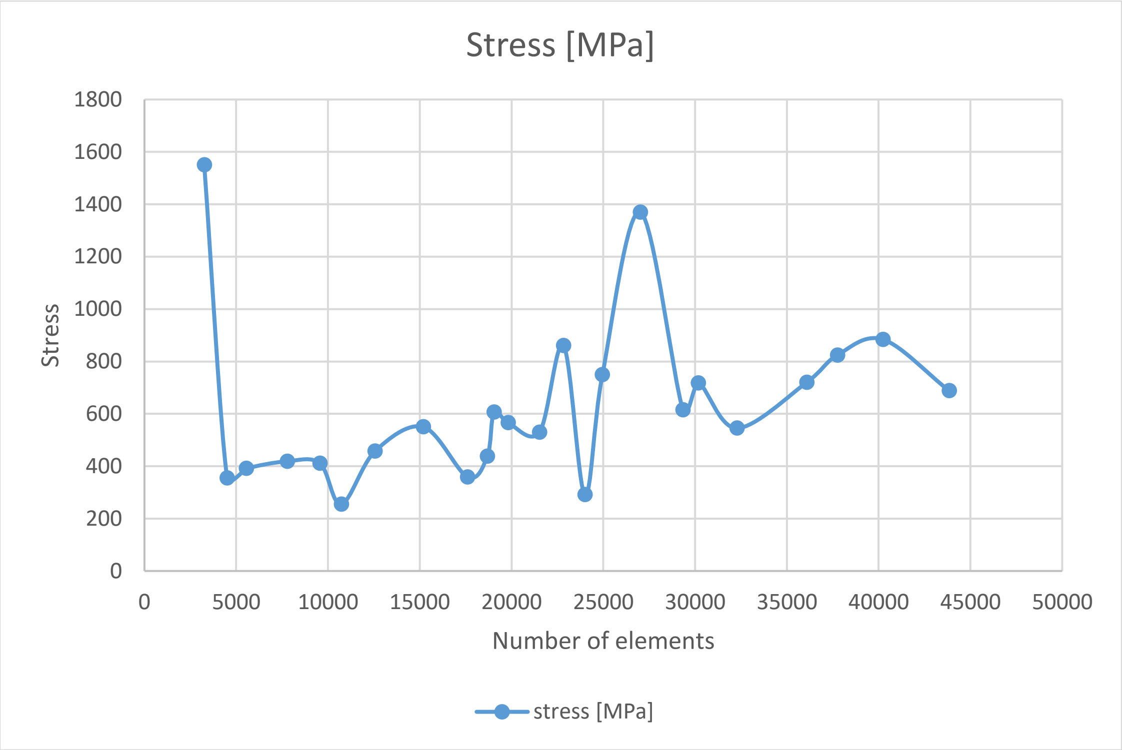

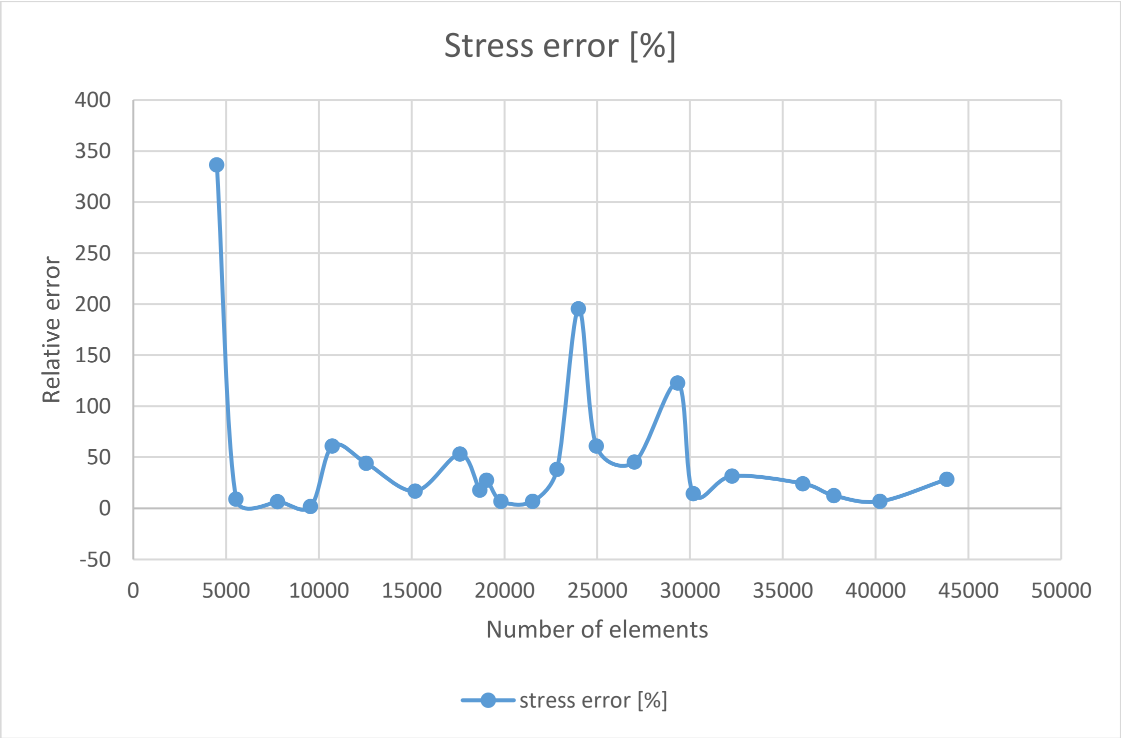

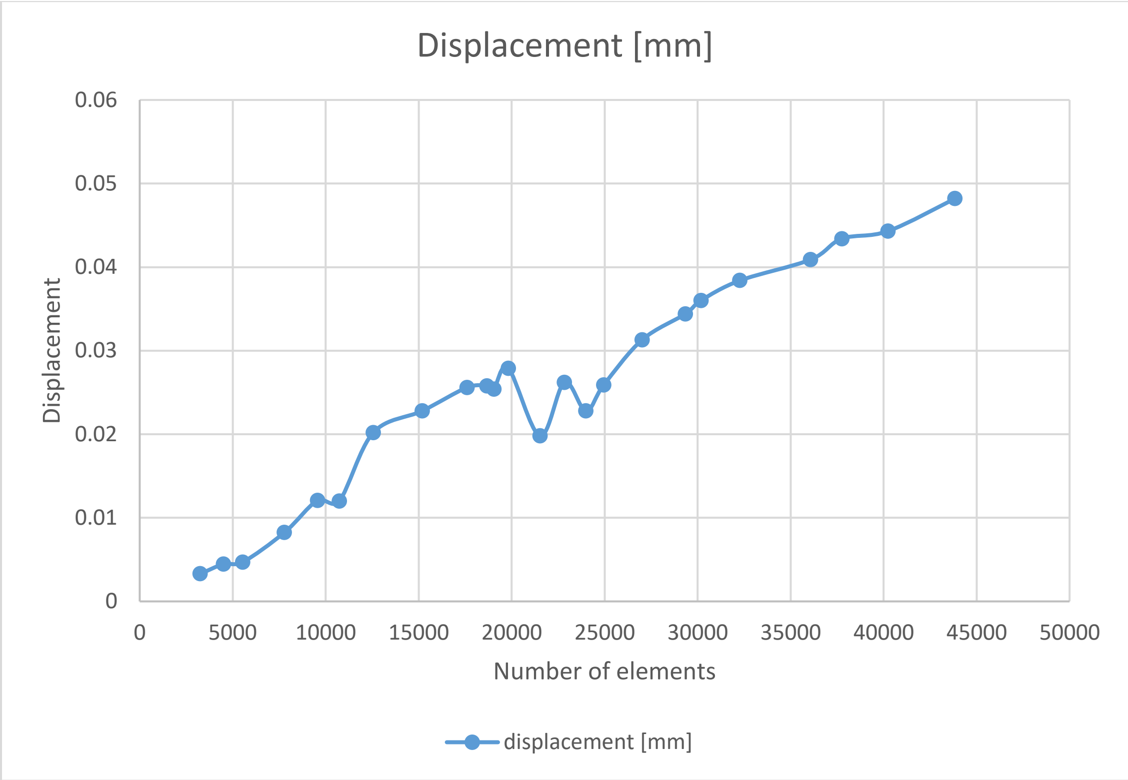
Displacement [mm]
0.06
0.05
0.04
0.03
0.02
0.01
0
Displacement
0
5000
10000
15000
20000
25000
30000
35000
40000
45000
50000
Number of elements
displacement [mm]

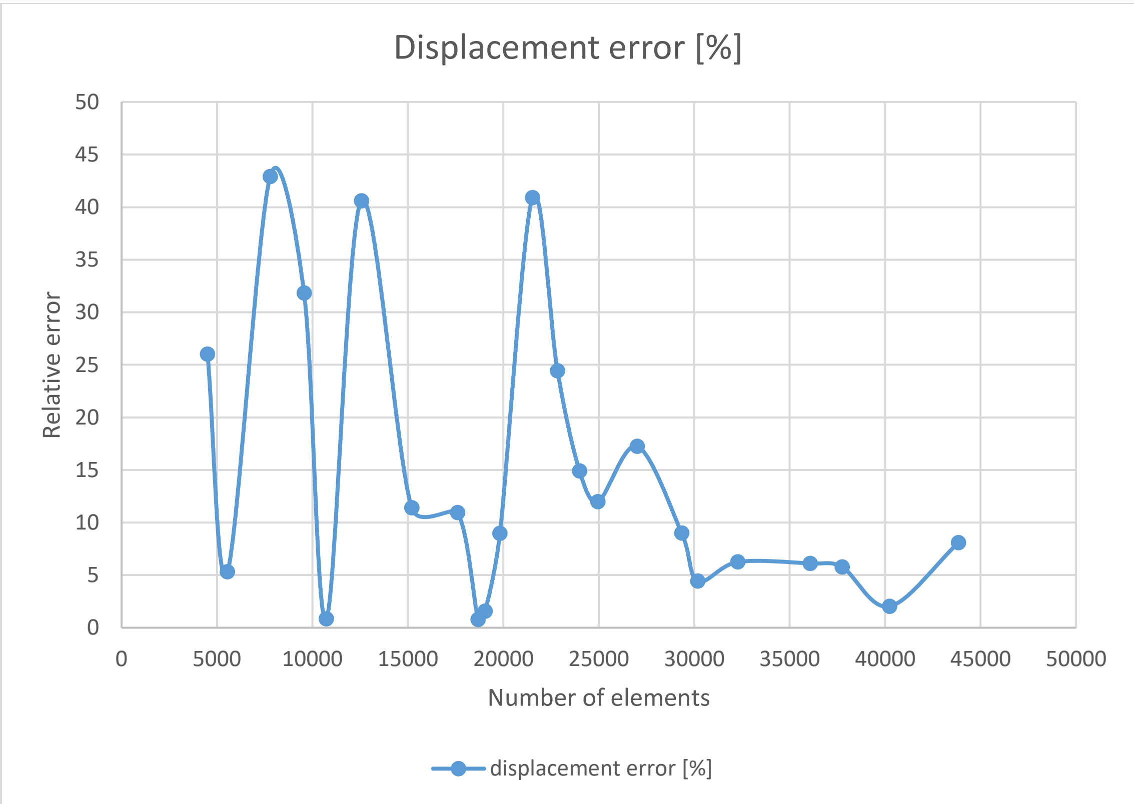
Displacement error [%]
50
45
40
35
30
25
20
15
10
5
0
Relative error
0
5000
10000
15000
20000
25000
30000
35000
40000
45000
50000
Number of elements
displacement error [%]

Appendix E – Functional Tests

Appendix E.1 – Preliminary Instrumented Saddle Device Tests

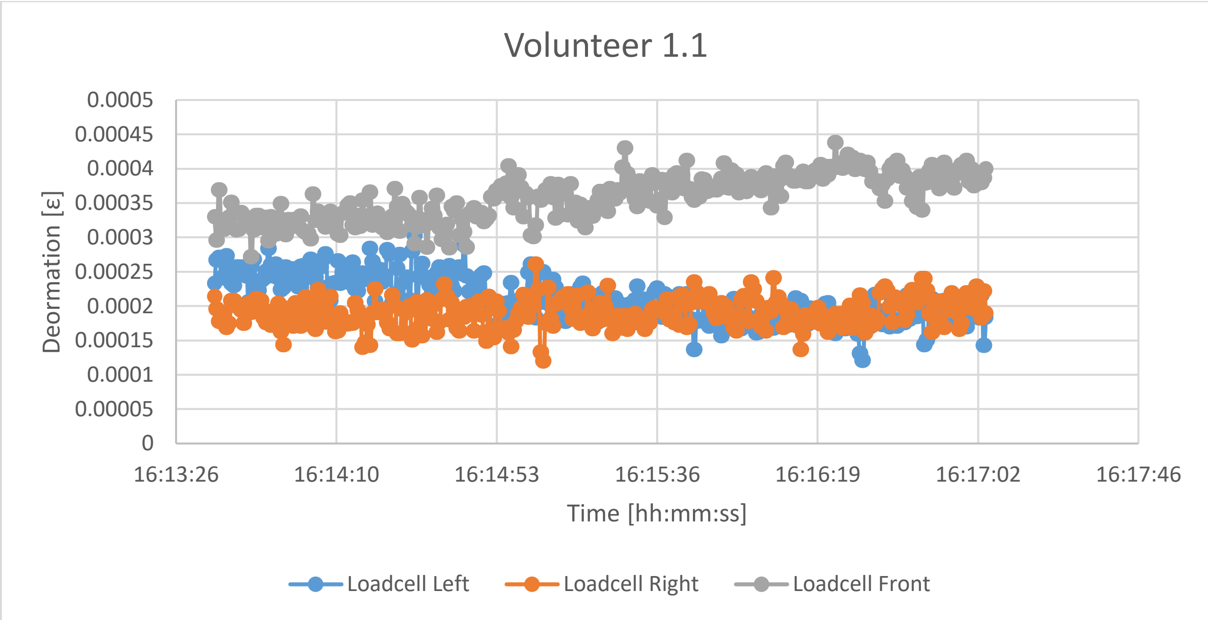

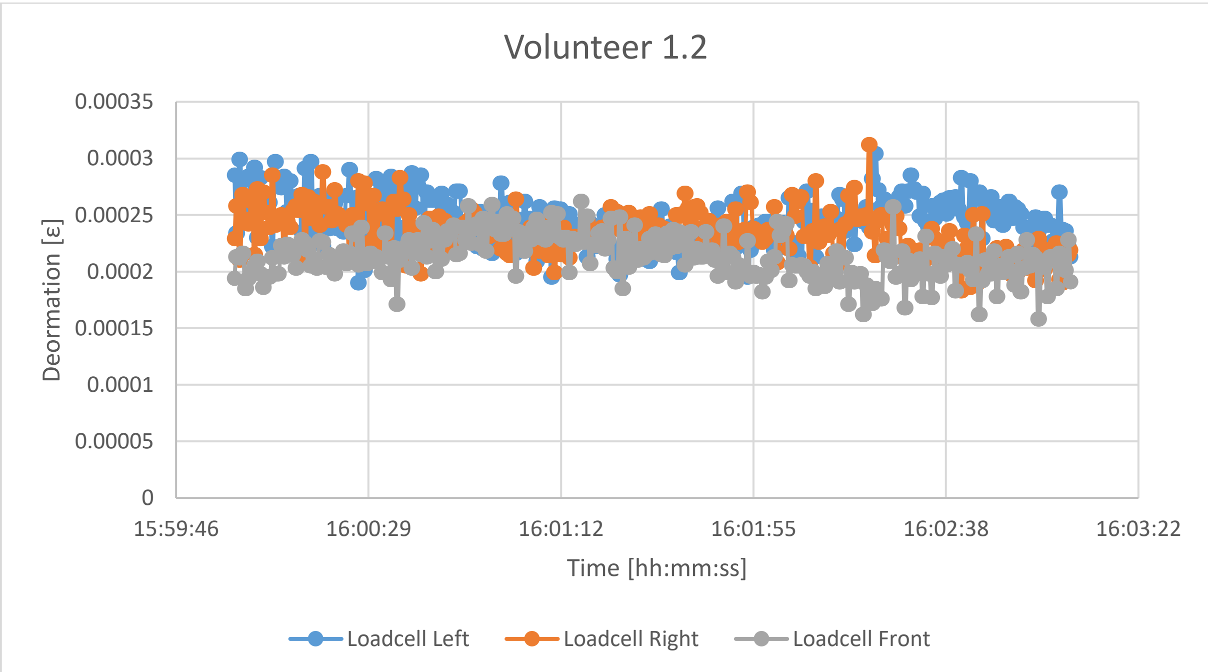

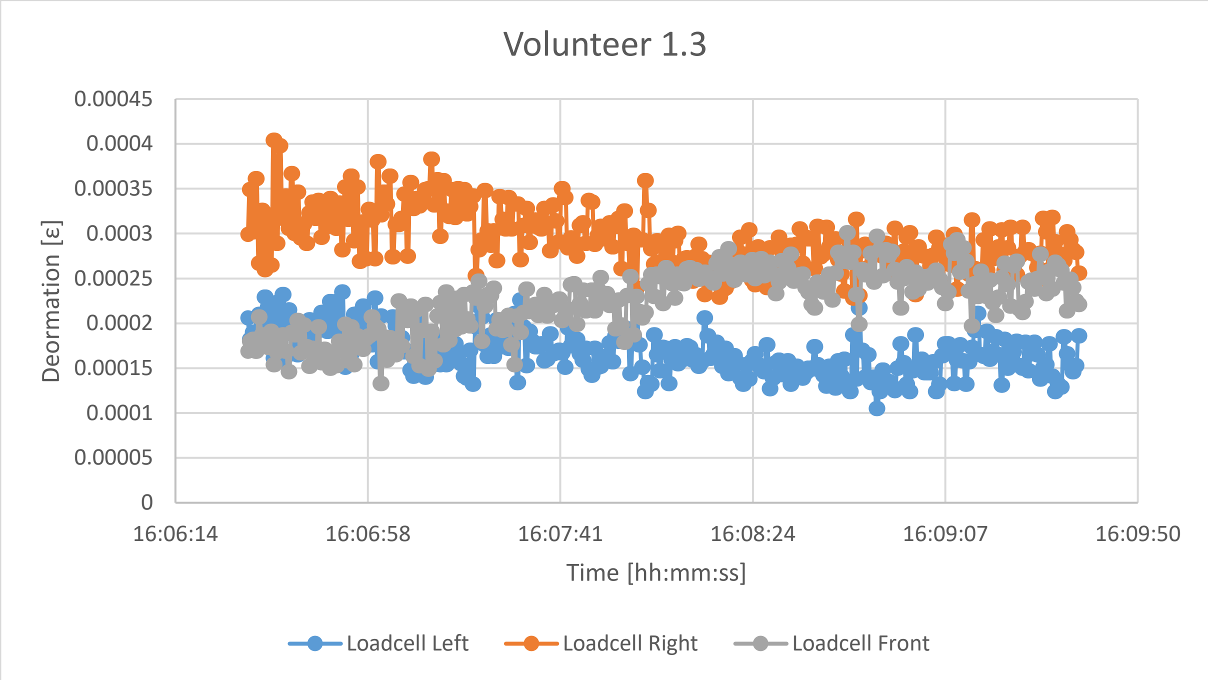
Volunteer 1.3
0.00045
0.0004
0.00035
0.0003
0.00025
0.0002
0.00015
0.0001
0.00005
0
Deormation [ε]
16:06:14
16:06:58
16:07:41
16:08:24
16:09:07
16:09:50
Time [hh:mm:ss]
Loadcell Left
Loadcell Right
Loadcell Front

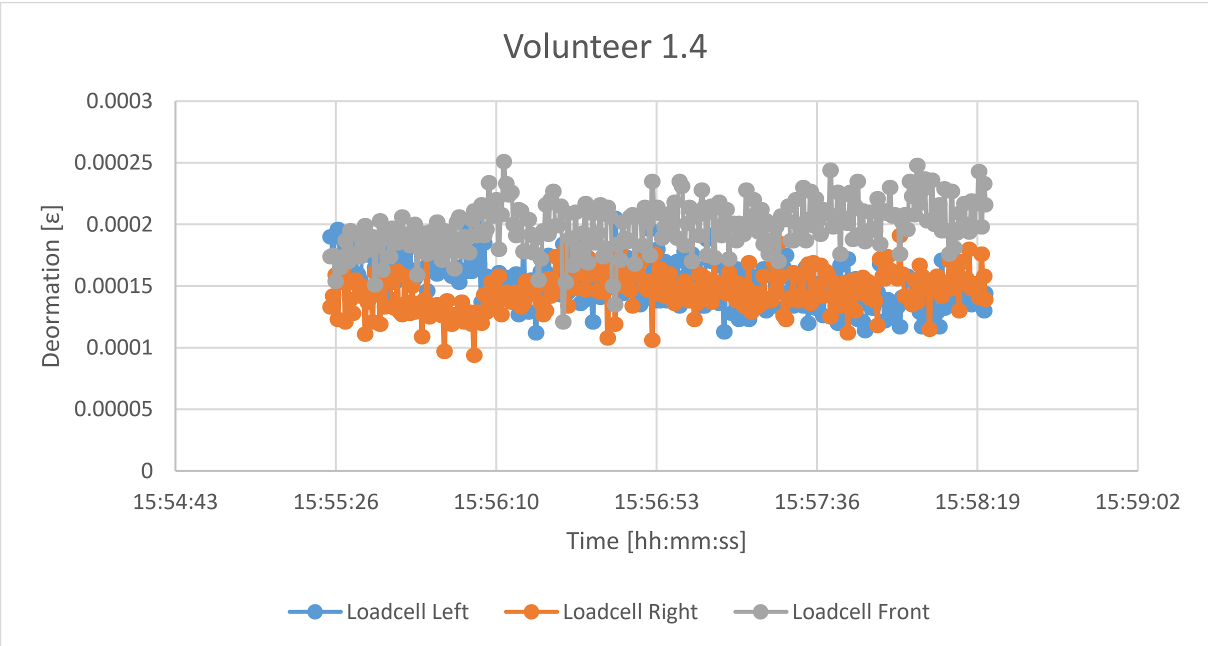
Volunteer 1.4
0.0003
0.00025
0.0002
0.00015
0.0001
0.00005
0
Deormation [ε]
15:54:43
15:55:26
15:56:10
15:56:53
15:57:36
15:58:19
15:59:02
Time [hh:mm:ss]
Loadcell Left
Loadcell Right
Loadcell Front

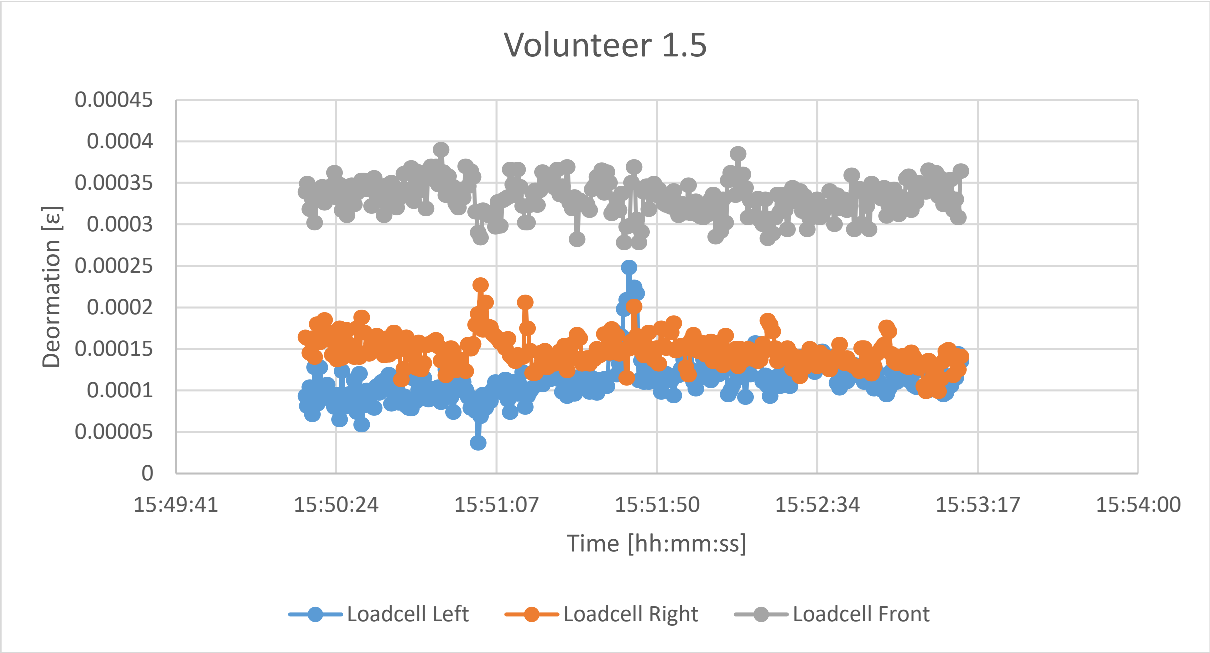
Volunteer 1.5
0.00045
0.0004
0.00035
0.0003
0.00025
0.0002
0.00015
0.0001
0.00005
0
Deormation [ε]
15:49:41
15:50:24
15:51:07
15:51:50
15:52:34
15:53:17
15:54:00
Time [hh:mm:ss]
Loadcell Left
Loadcell Right
Loadcell Front

Appendix E.2 – Preliminary Instrumented Handlebar Device Tests

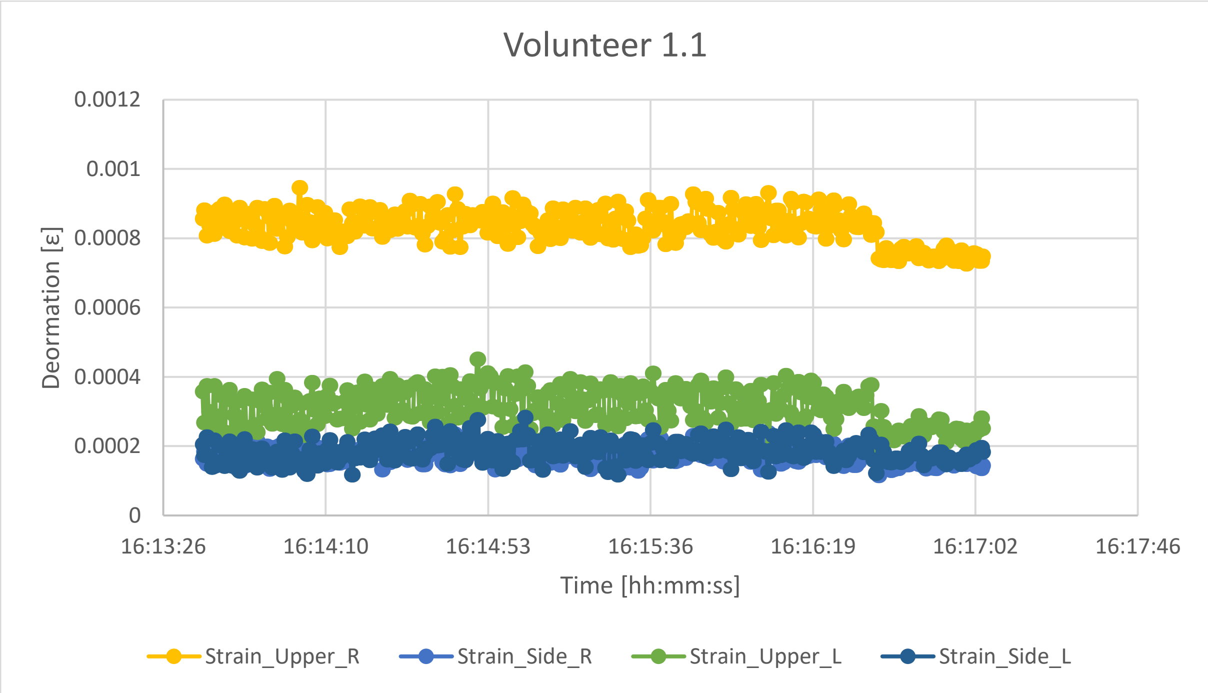

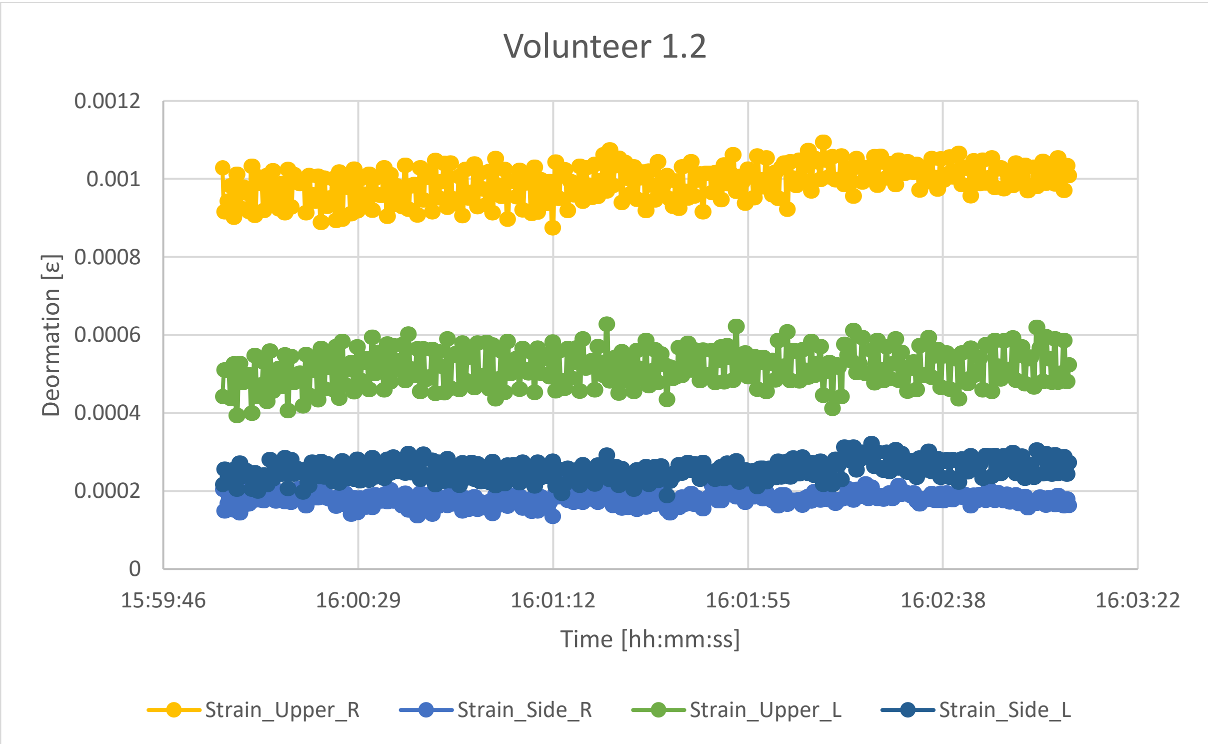

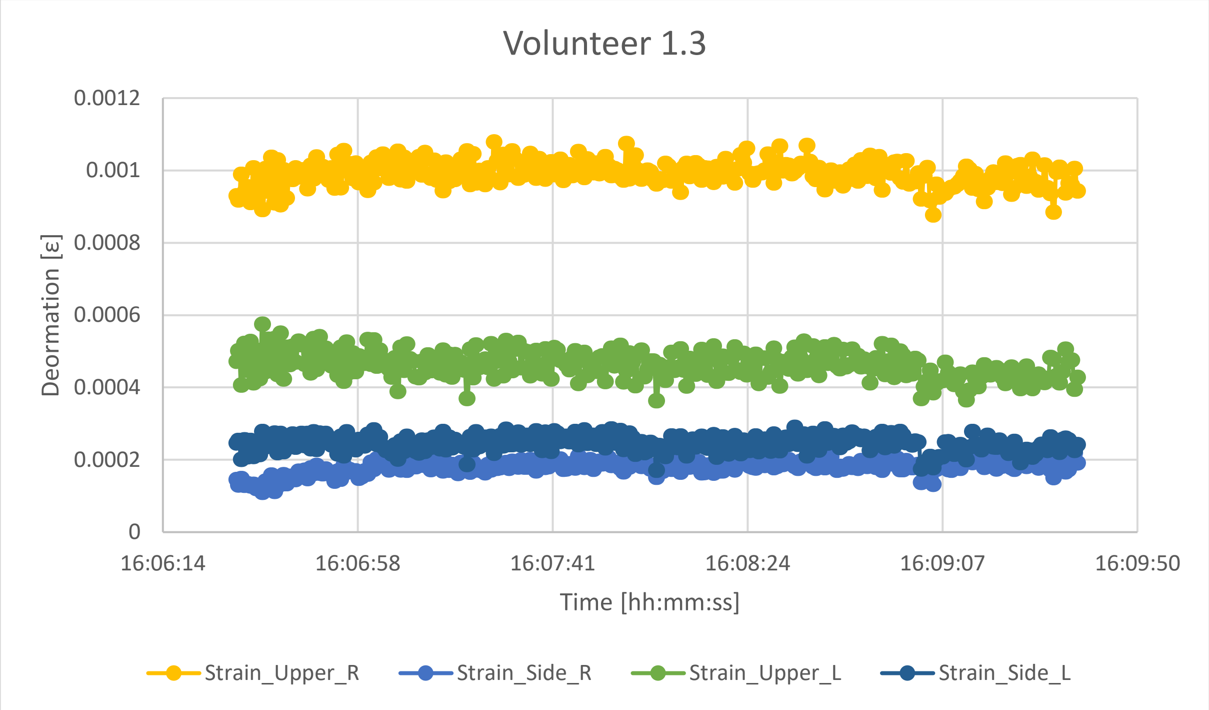

Volunteer 1.3
0.0012
0.001
0.0008
0.0006
0.0004
0.0002
0
Deormation [ε]
16:06:14
16:06:58
16:07:41
16:08:24
16:09:07
16:09:50
Time [hh:mm:ss]
Strain_Upper_R
Strain_Side_R
Strain_Upper_L
Strain_Side_L

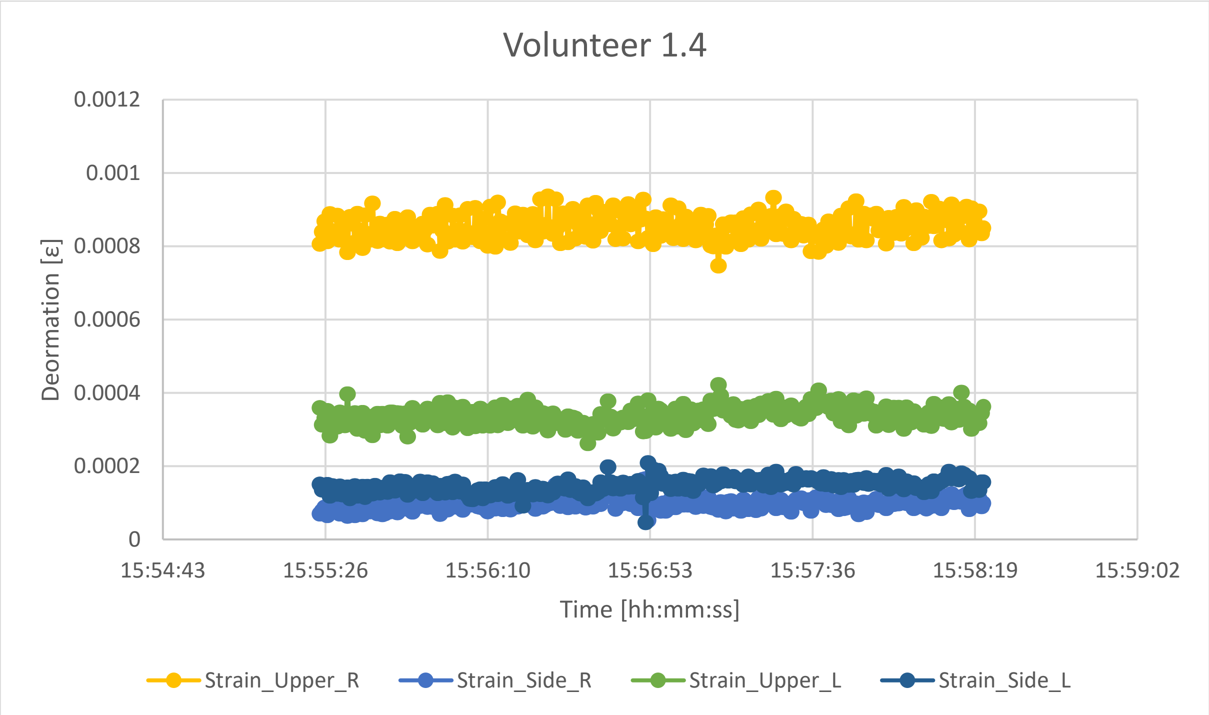

Volunteer 1.4
0.0012
0.001
0.0008
0.0006
0.0004
0.0002
0
Deormation [ε]
15:54:43
15:55:26
15:56:10
15:56:53
15:57:36
15:58:19
15:59:02
Time [hh:mm:ss]
Strain_Upper_R
Strain_Side_R
Strain_Upper_L
Strain_Side_L

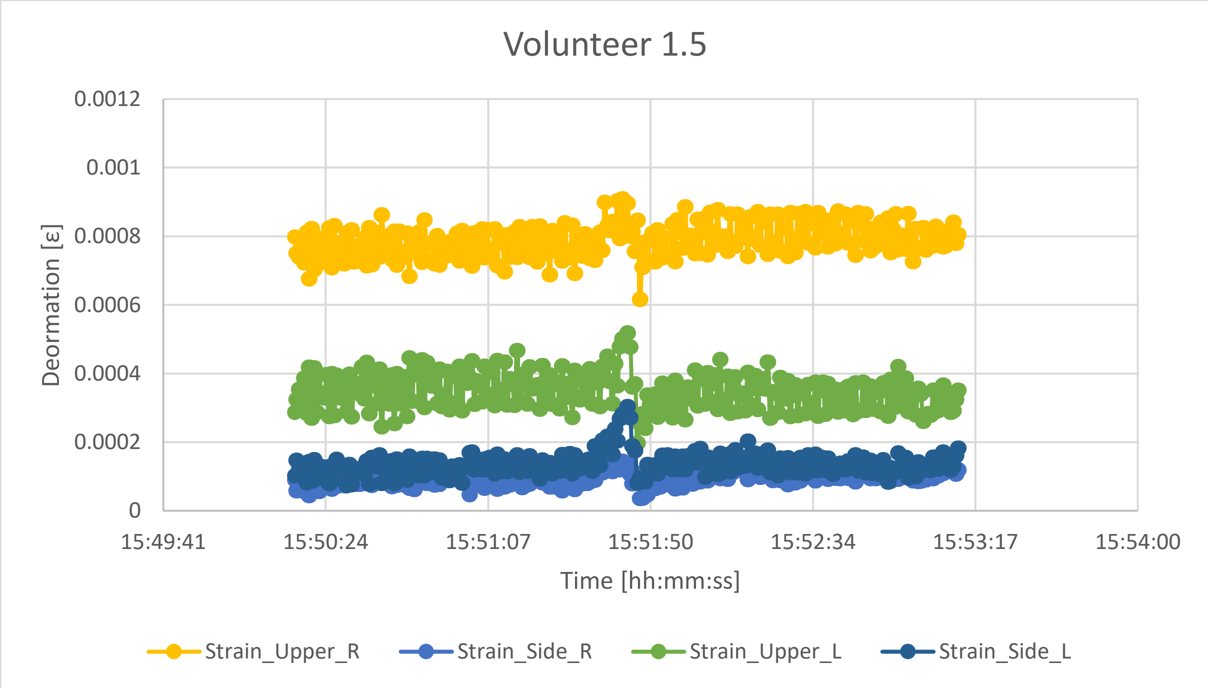
Volunteer 1.5
0.0012
0.001
0.0008
0.0006
0.0004
0.0002
0
Deormation [ε]
15:49:41
15:50:24
15:51:07
15:51:50
15:52:34
15:53:17
15:54:00
Time [hh:mm:ss]
Strain_Upper_R
Strain_Side_R
Strain_Upper_L
Strain_Side_L

Appendix E.3 – Preliminary Instrumented Pedals Device Tests

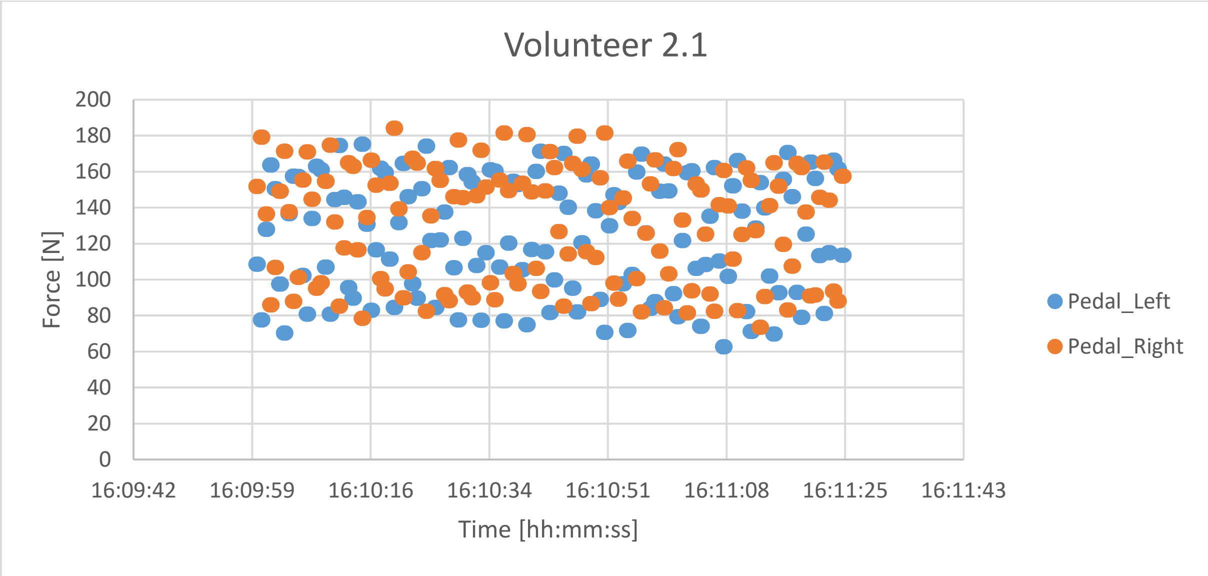

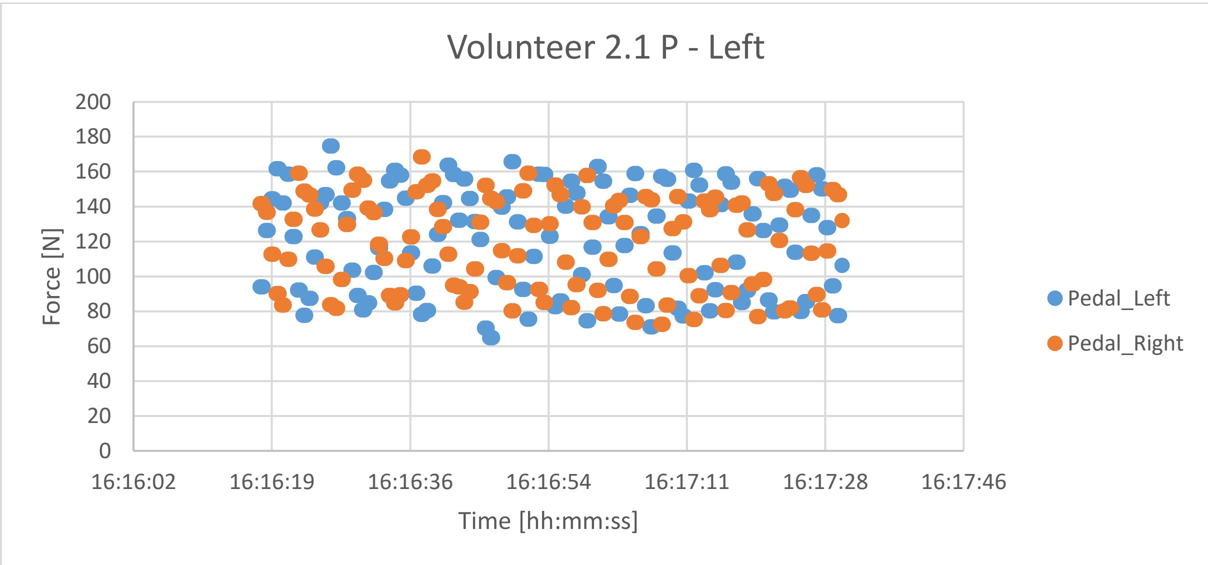

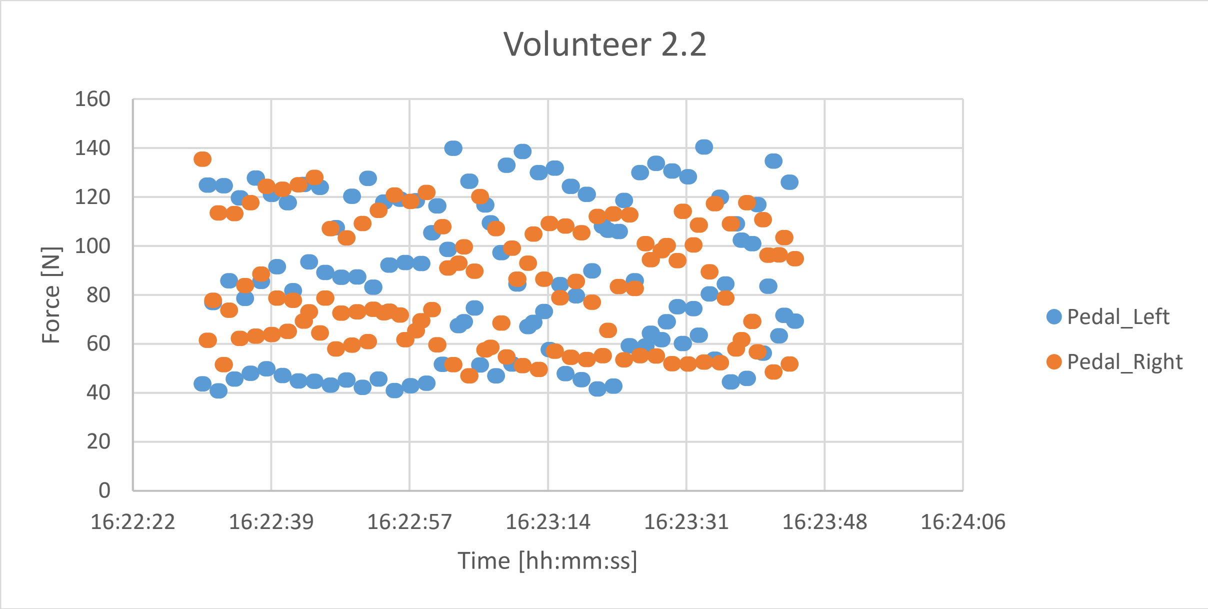
Volunteer 2.2
160
140
120
100
80
60
40
20
0
Force [N]
16:22:22
16:22:39
16:22:57
16:23:14
16:23:31
16:23:48
16:24:06
Time [hh:mm:ss]
Pedal_Left
Pedal_Right

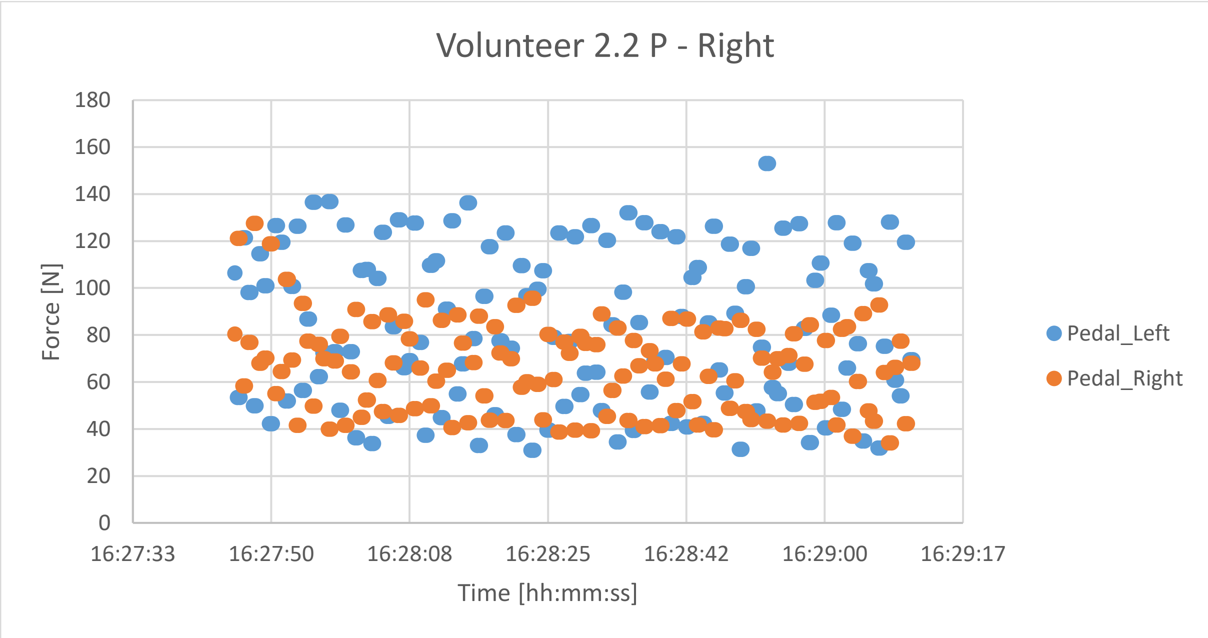
Volunteer 2.2 P - Right
180
160
140
120
100
80
60
40
20
0
Force [N]
16:27:33
16:27:50
16:28:08
16:28:25
16:28:42
16:29:00
16:29:17
Time [hh:mm:ss]
Pedal_Left
Pedal_Right

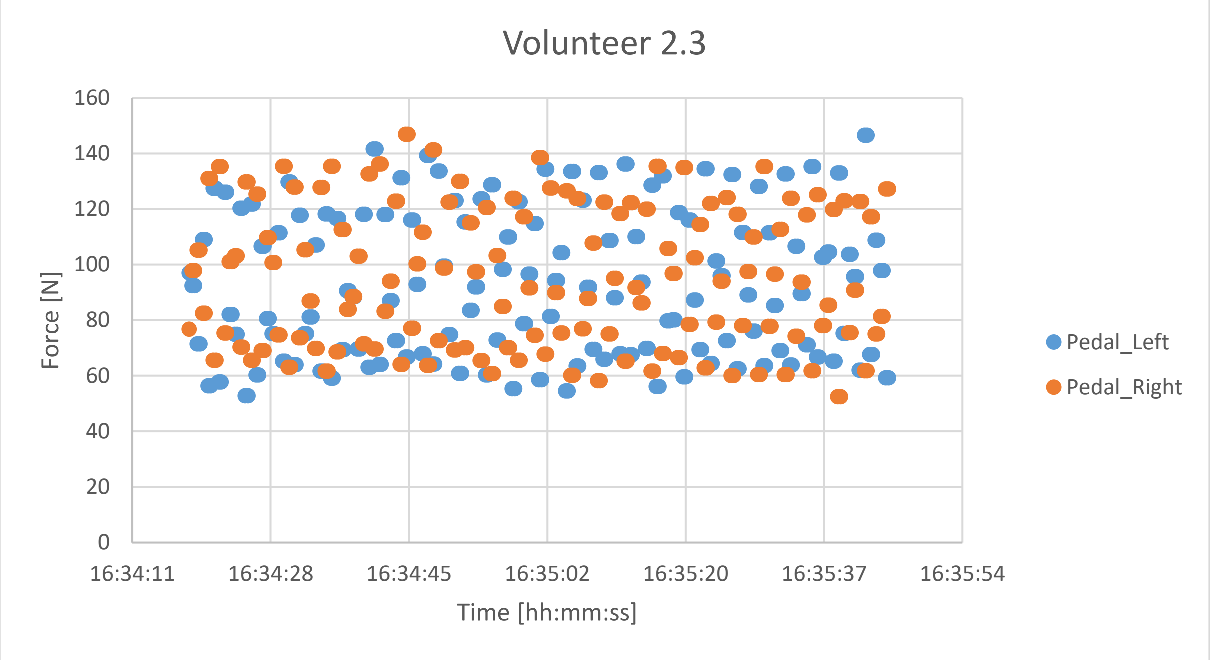

Volunteer 2.3
160
140
120
100
80
60
40
20
0
Force [N]
16:34:11
16:34:28
16:34:45
16:35:02
16:35:20
16:35:37
16:35:54
Time [hh:mm:ss]
Pedal_Left
Pedal_Right

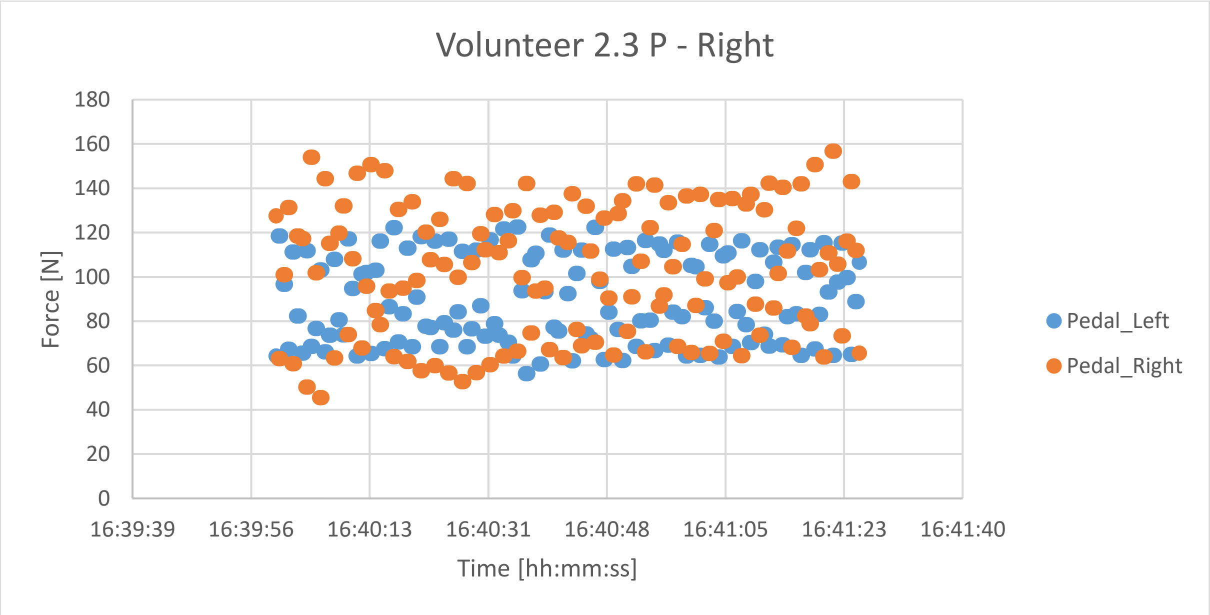

Volunteer 2.3 P - Right
180
160
140
120
100
80
60
40
20
0
Force [N]
16:39:39
16:39:56
16:40:13
16:40:31
16:40:48
16:41:05
16:41:23
16:41:40
Time [hh:mm:ss]
Pedal_Left
Pedal_Right

Appendix E.4 – Preliminary Instrumented Grip Device Test

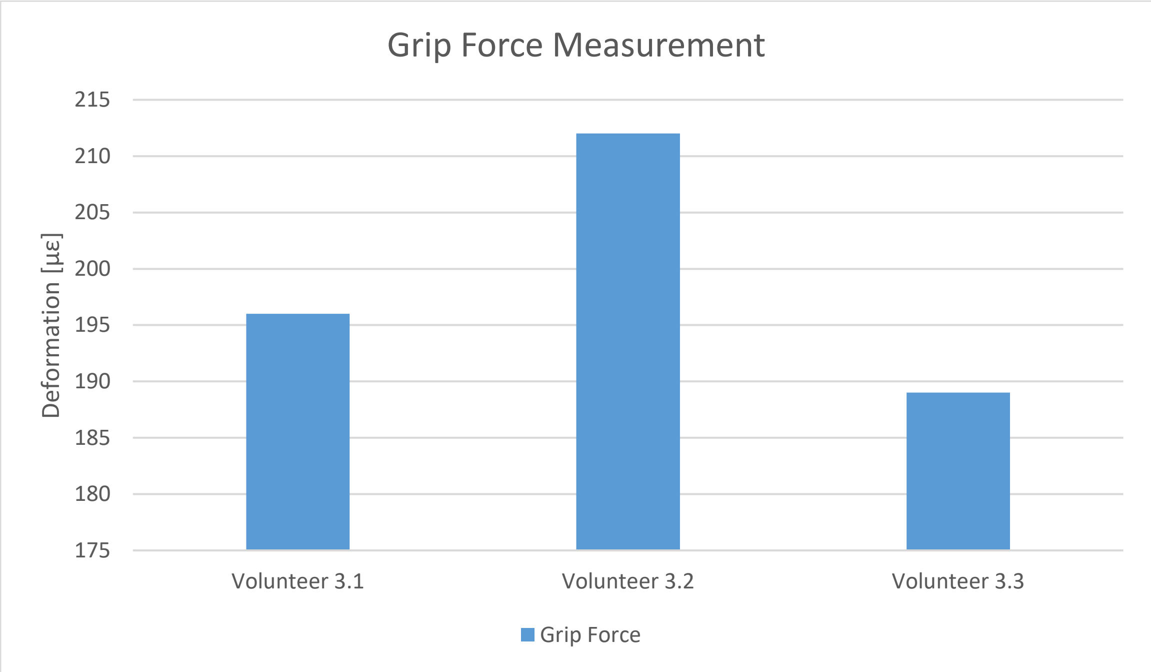

Appendix E.5 – Acquired Data From Volunteer PSG_25

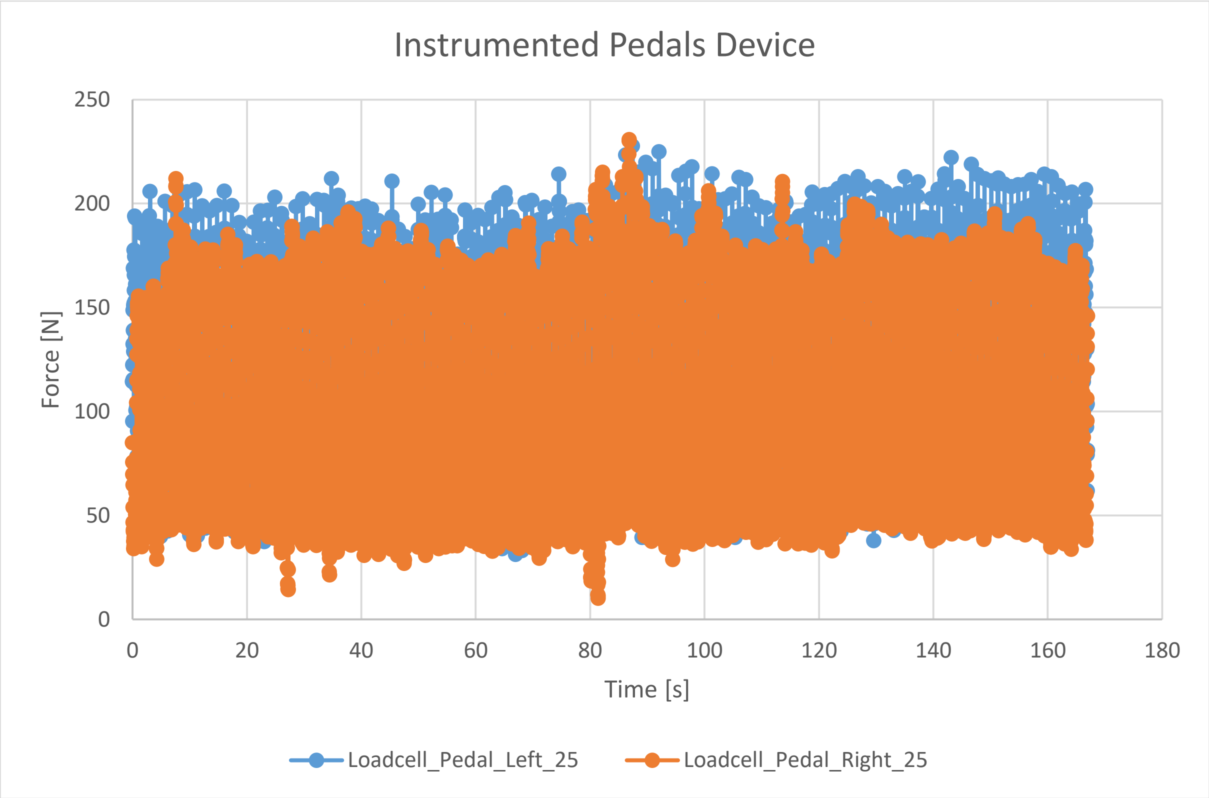

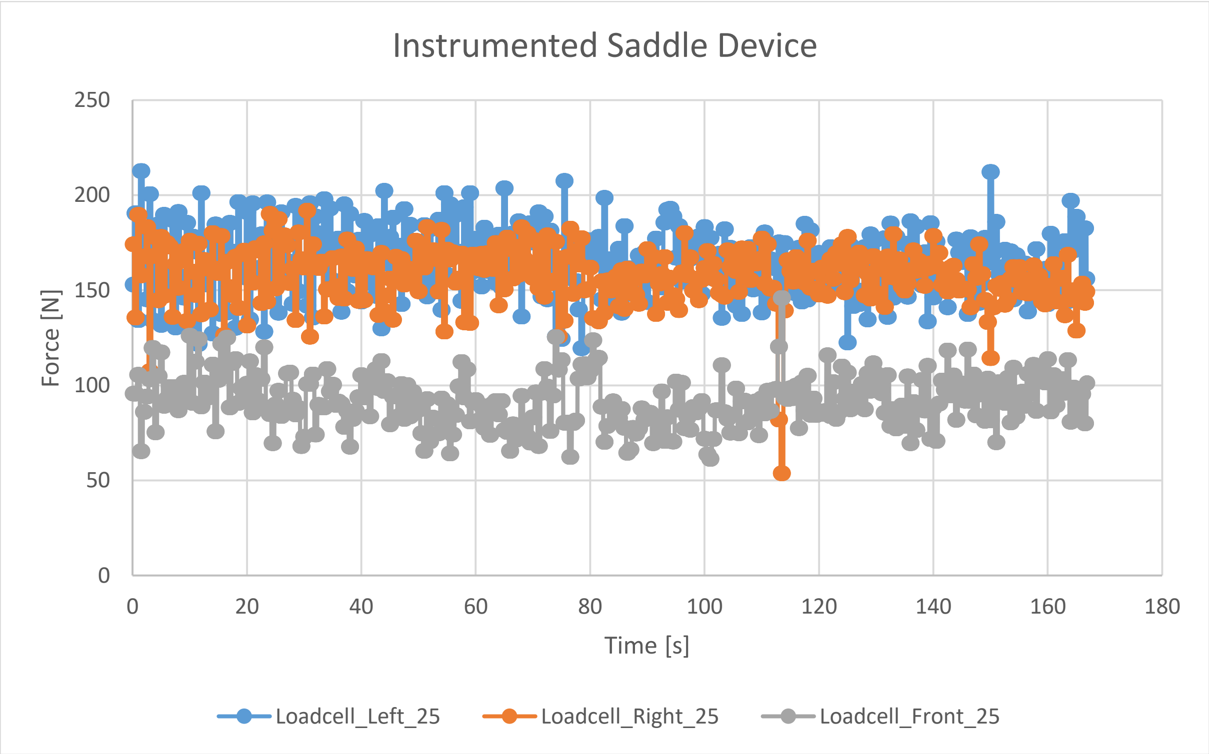

Appendix E.6 – Acquired Data From Volunteer PSG_02

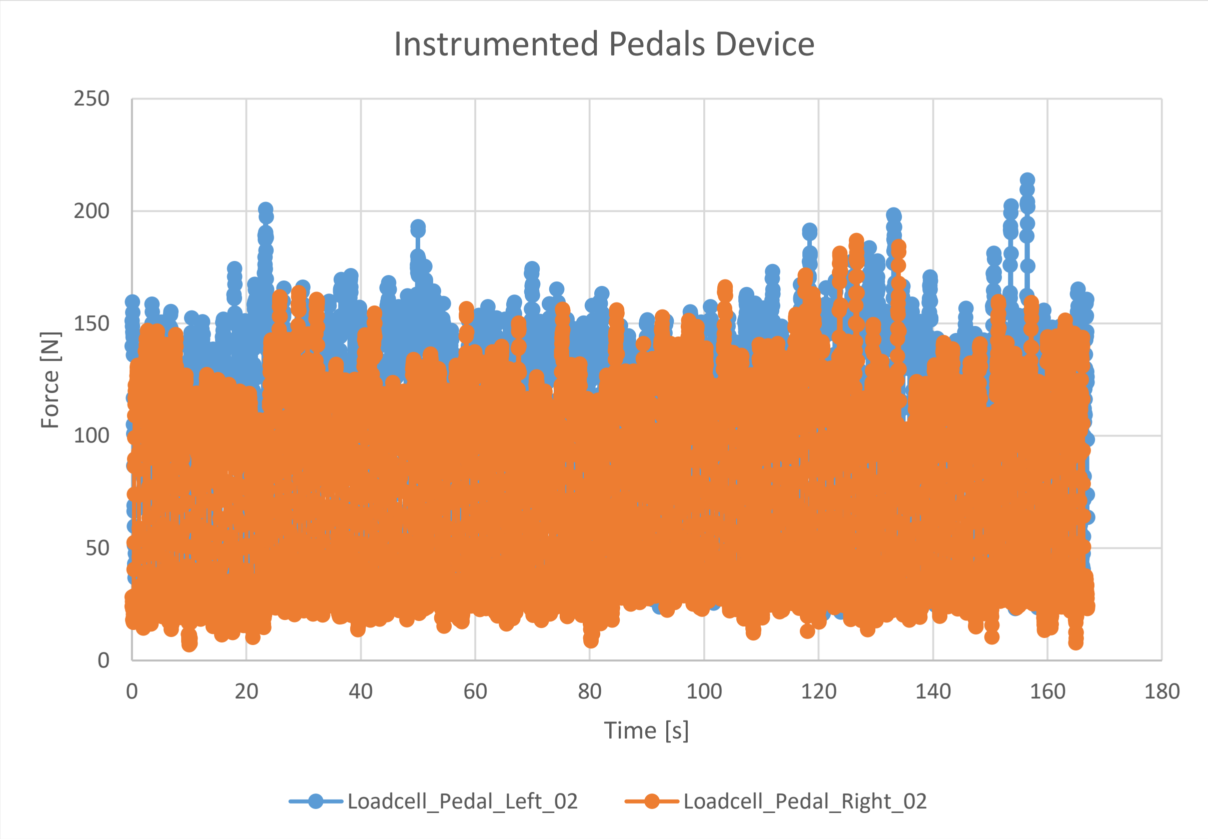

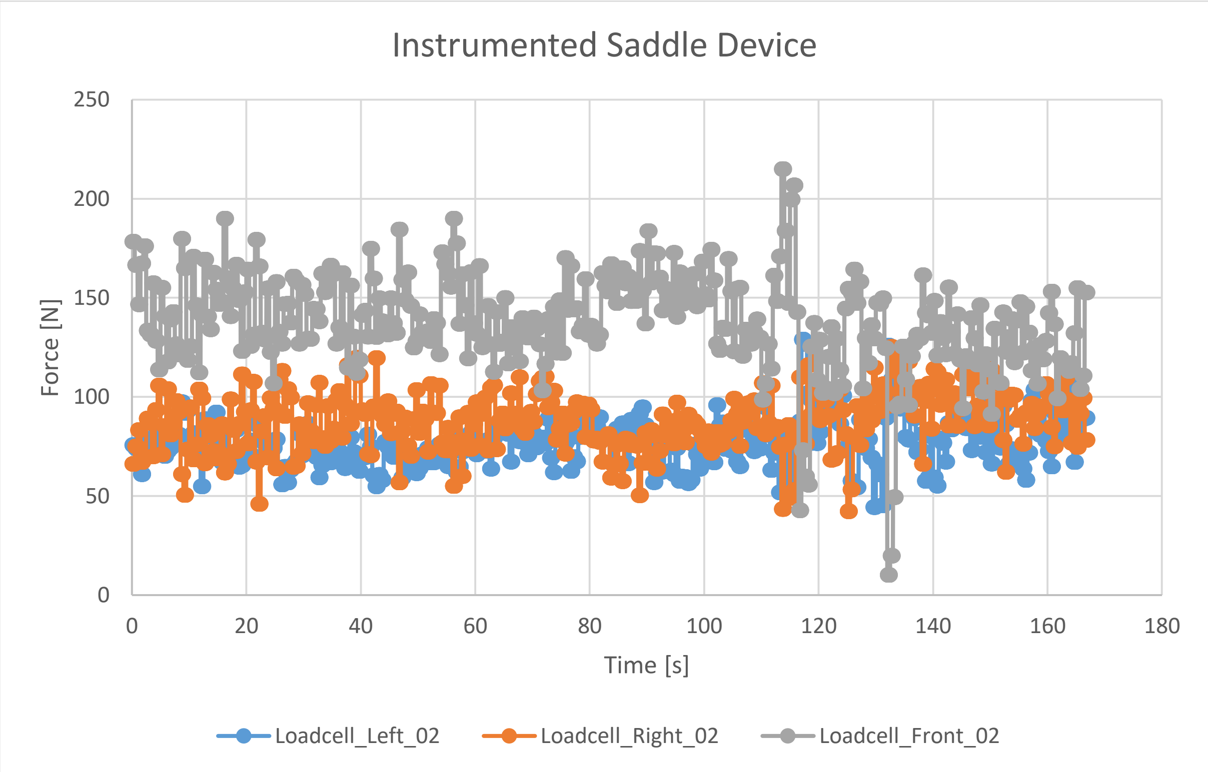

Appendix E.7 – Acquired Data From Volunteer PSG_19

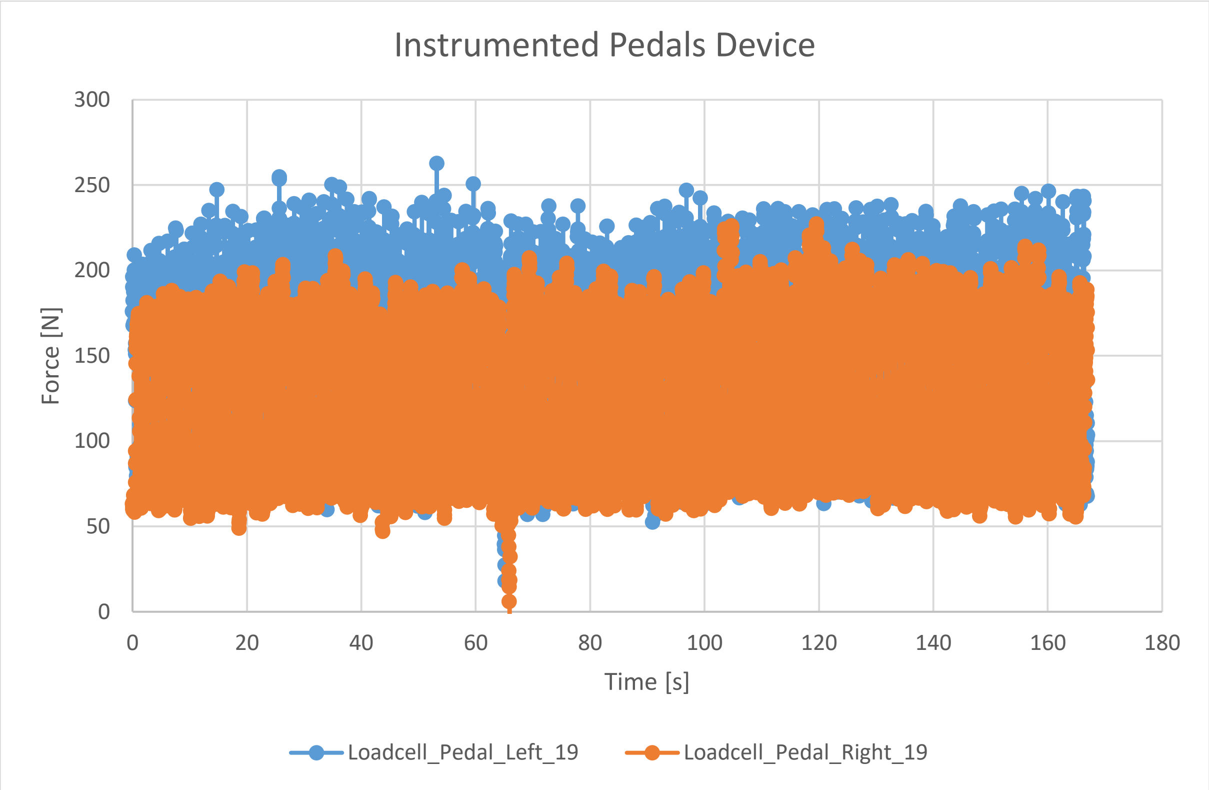

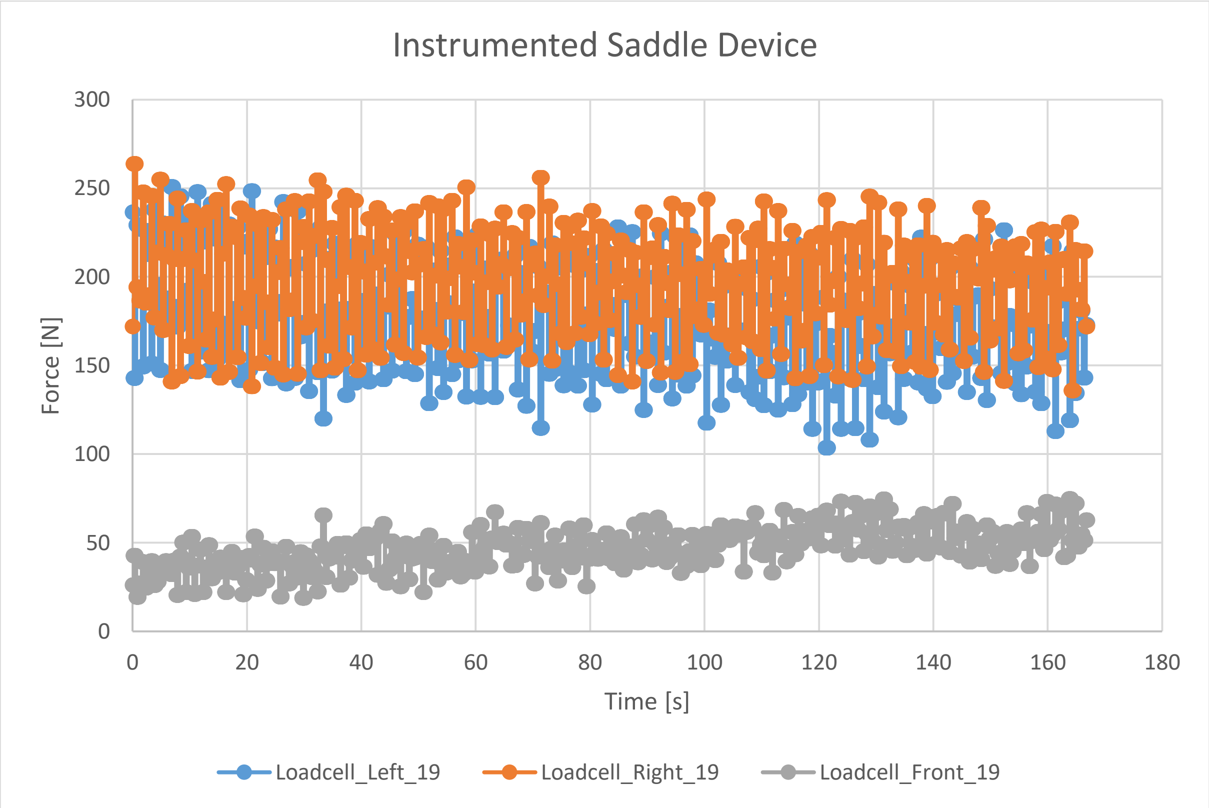

Appendix E.8 – Acquired Data From Volunteer PSG_12

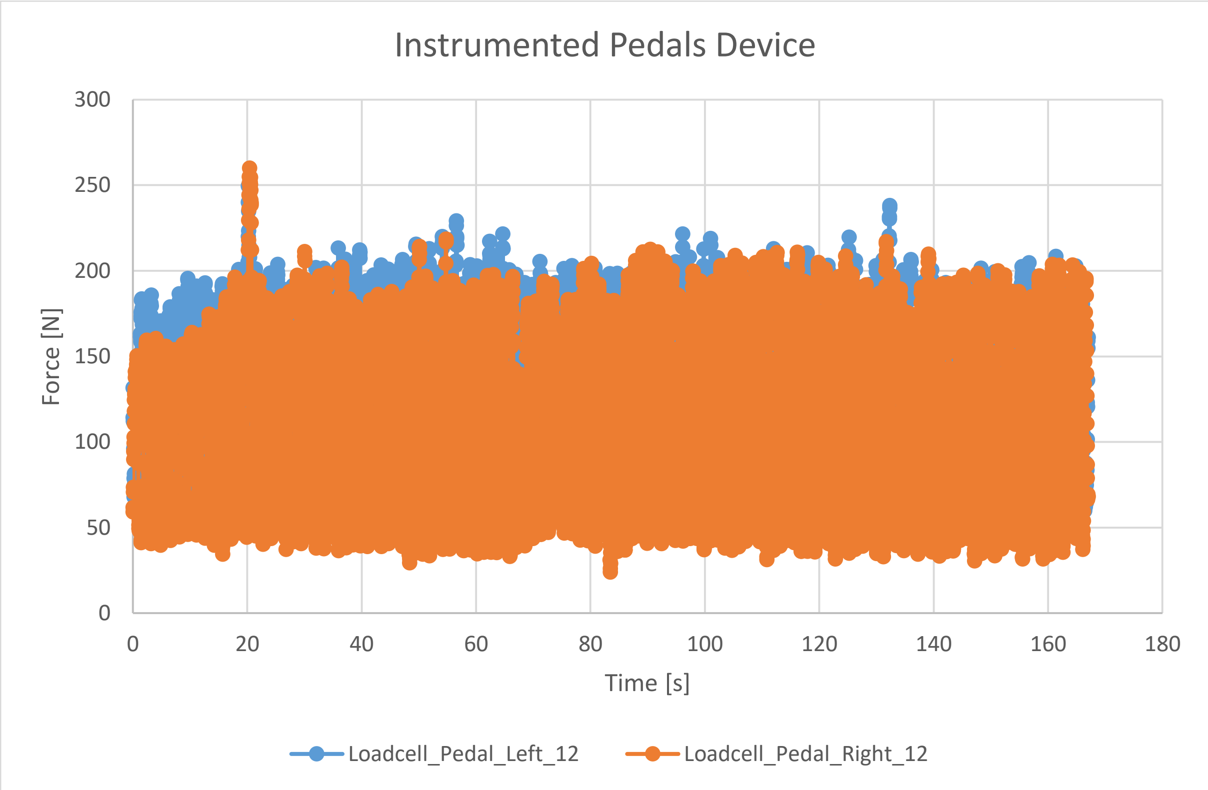

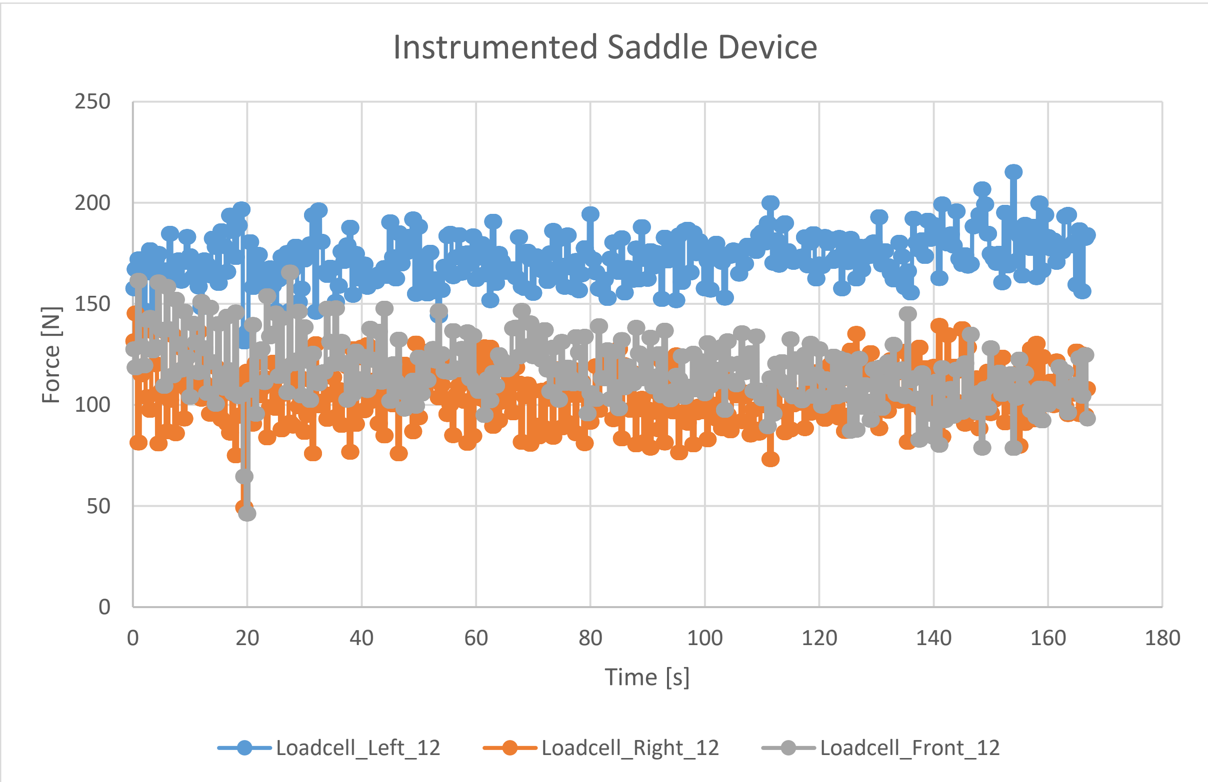

Appendix E.9 – Acquired Data From Volunteer PSG_01

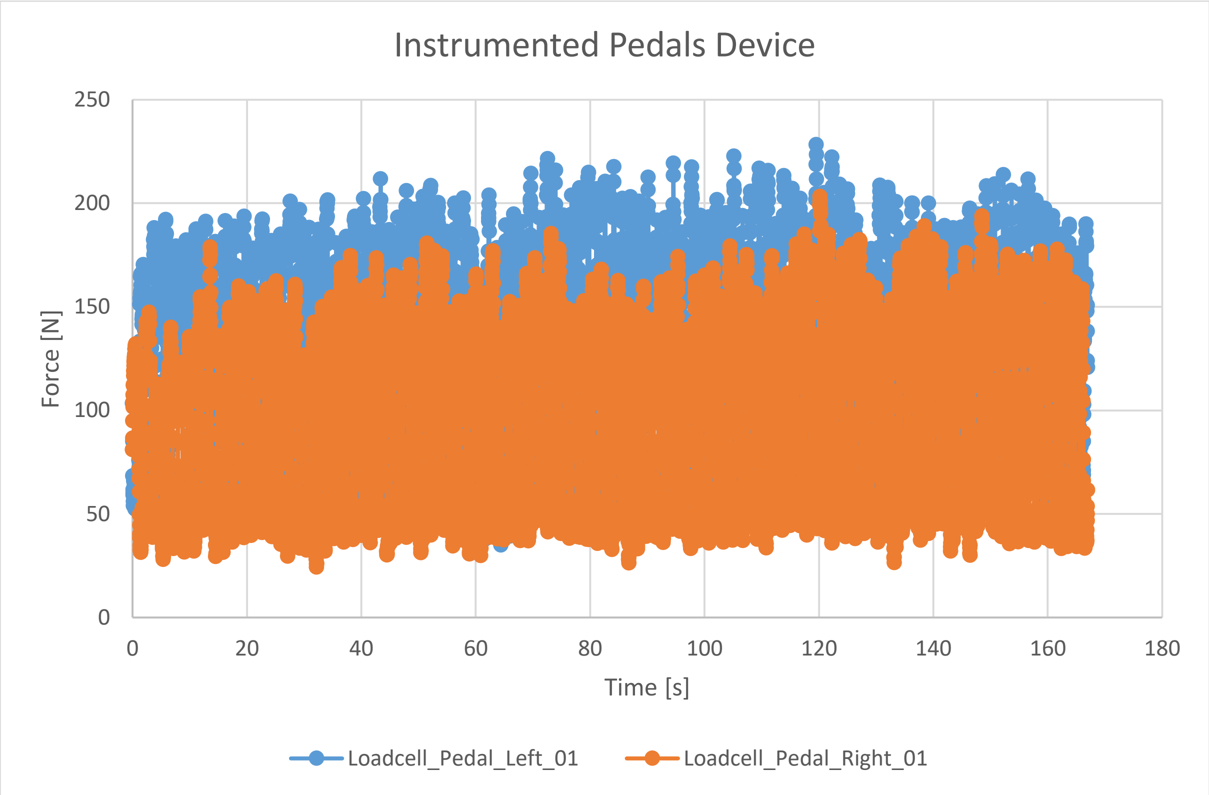

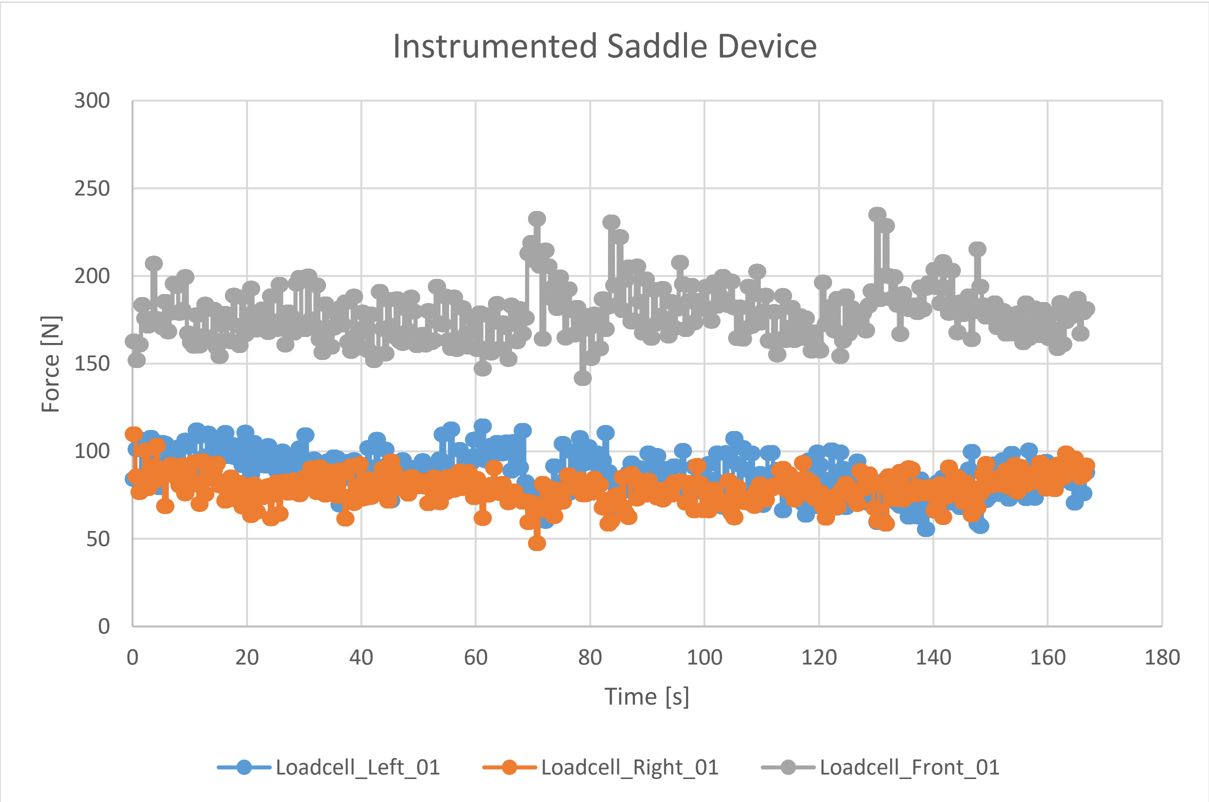

Appendix E.10 – Acquired Data From Volunteer PSG_08

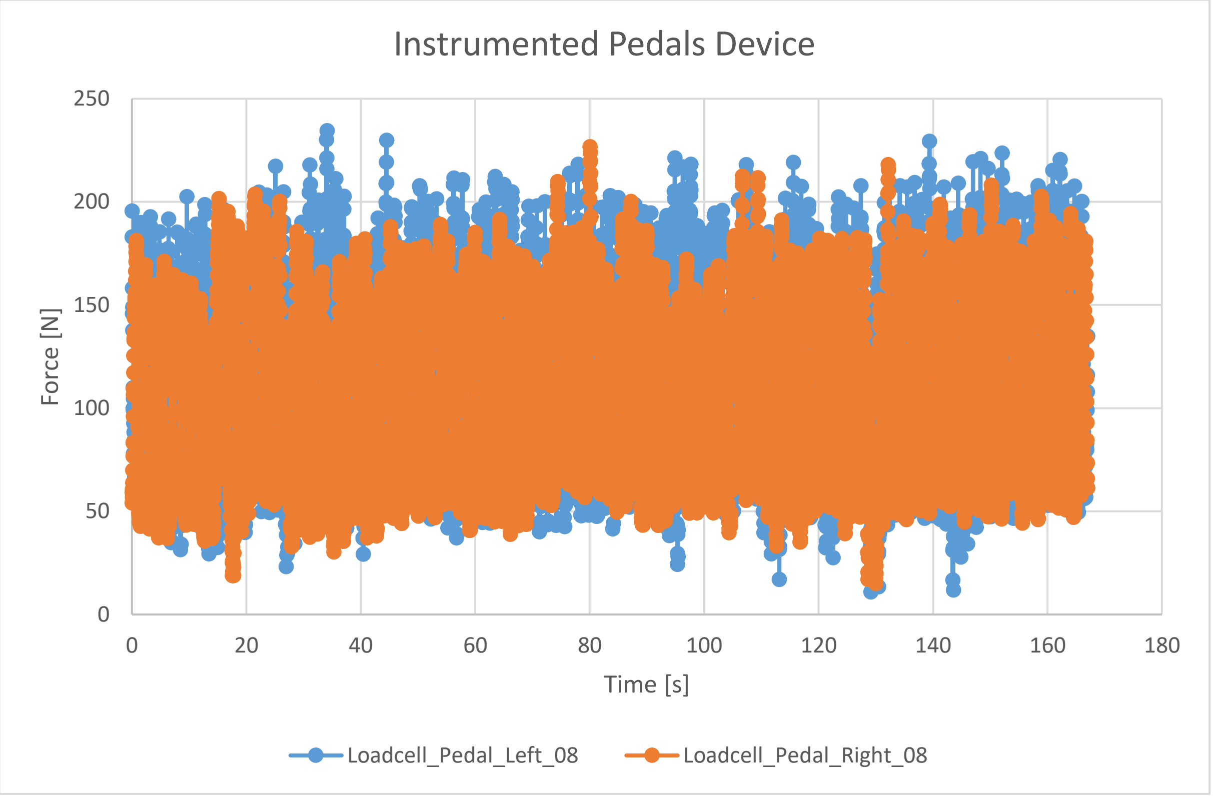

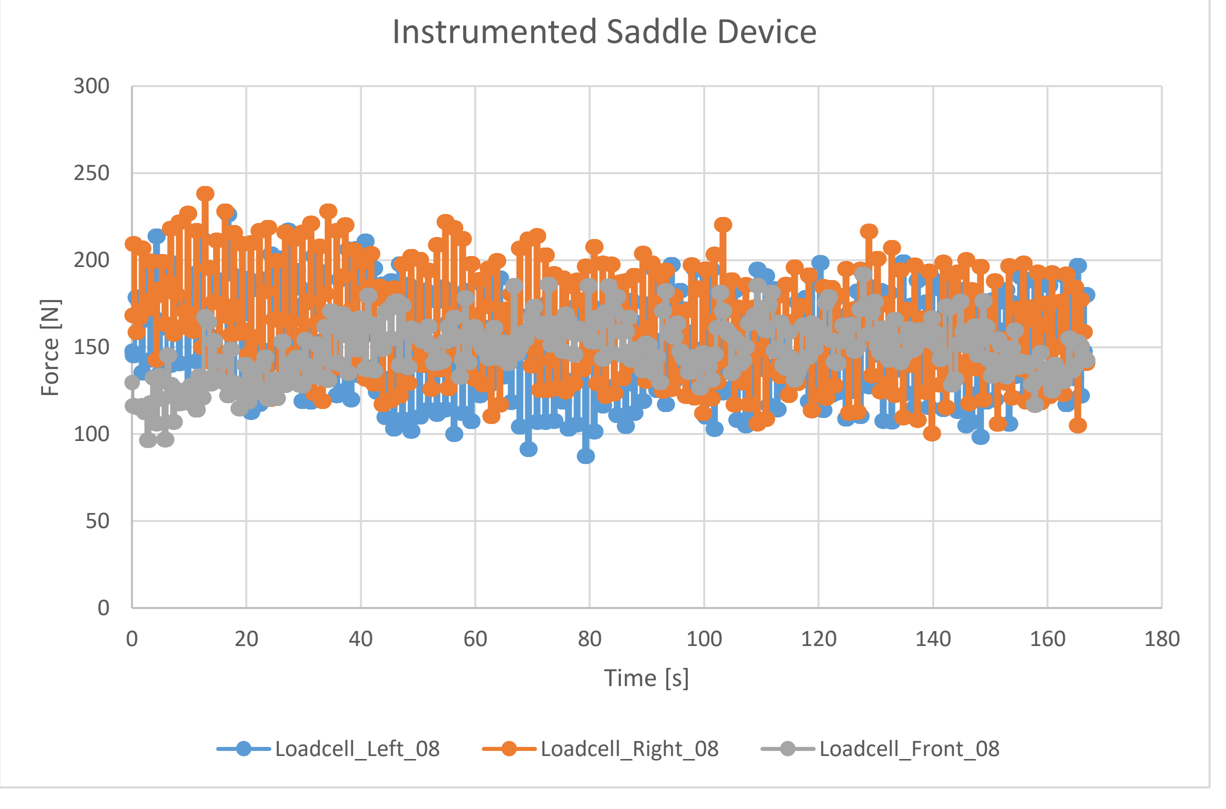

Appendix E.11 –Data From Volunteer PSG_08 vs PSG_08P